TECHNISCHE UNIVERSITÄT MÜNCHEN
Max-Planck-Institut für Biochemie
Abteilung Membran- und Neurophysik

GENETICALLY TARGETED N-PHOSPHONOOXYMETHYL HEMICYANINE PRODYES: VOLTAGE SENSITIVITY AND NEURAL CIRCUITRY LABELING

David Noel Hong Kian Ng

Vollständiger Abdruck der von der Fakultät für Chemie der Technischen Universität München zur Erlangung des akademischen Grades eines

Doktors der Naturwissenschaften
genehmigten Dissertation.

Vorsitzender:	Univ.-Prof. Dr. Chr. F.W. Becker
Prüfer der Dissertation:	1. Univ.-Prof. Dr. Dr. h.c. H. Kessler
	2. Hon.-Prof. Dr. P. Fromherz

Die Dissertation wurde am 25.05.2010 bei der Technischen Universität München eingereicht und durch die Fakultät für Chemie am 06.07.2010 angenommen.

ABSTRACT

Fast voltage sensitive dyes (VSDs) are fluorescent probes of transmembrane voltage, used to study the electrophysiology of the nervous system. The amphiphilicity critical in directing the insertion of the chromophore into the hydrophobic lipid bilayer is not cell-type specific, causing unwanted background staining and limiting the use of this technique. Chemically modifying the aliphatic tails of VSDs to introduce an N-phosphonooxymethyl quaternary amine salt yielded water soluble, non-binding prodyes. These compounds were shown to be substrates for cell-surface bound placental alkaline phosphatase (PLAP), and undergo a two-step bioreversion to yield the desired amphiphilic dyes, which subsequently binds to the plasma membrane. One newly synthesized prodye, di-1,8P6-ANEPPS, showed excellent selectivity, and the enzymatically activated dye was shown to exhibit voltage sensitivity comparable to the most widely used VSDs. This technique has the potential label the fine structure of individual neurons, and monitor their local electrophysiology. This technique may be extended beyond the labeling of single neurons to interconnected neural networks.

Current neuronal circuits mapping techniques use trans-synaptic tracer molecules; these compounds label a single nerve cell, then migrate to functionally connected neurons. As only a small fraction of tracer material is transported across each synapse, current techniques falter due to greatly reduced signals from each successive neuron in the circuit. A ‘gene switch’ that activates the expression of a marker protein in each neuron would eliminate the problem of decreasing signal strength; the P1 bacteriophage protein Cre could catalytically induce such an irreversible recombination event. This enzyme was thus fused to an atoxic, codon-optimized version of the Tetanus neurotoxin, a protein known to both undergo trans-synaptic retrograde transport, and deliver proteins into the cytosol of targeted neurons. The hybrid fusion protein was then tested in a simple model system and shown to retain recombinase activity, and is therefore now ready for direct testing in brain tissue.

TABLE OF CONTENTS

1 INTRODUCTION

The elucidation of the processes that collectively form the human mind is one of the foremost endeavors in modern science. Understanding the biological basis of consciousness and the mechanisms by which we perceive, learn, and act provide some of the most captivating questions for humanity. The field of neuroscience, research focused on the nervous system, utilizes techniques derived from many branches of science to study the molecular, developmental, structural, functional, and computational aspects of the brain. The goal of this project is to develop new techniques with which to study the central nervous system.

The complex electrophysiology of the brain is one of its defining characteristics; the ability to monitor any selected individual neuron's electrophysiology with the necessary spatial and temporal resolution needed to capture the form and progression of a single action potential is a principal goal in neuroscience. A second defining characteristic of the brain is its extreme complexity; neurons are massively interconnected, forming intricate networks that process and store information. Unraveling this structural organization is the key to mapping and understanding functional neuronal circuits.

Neuroscientists already have a wide range of tools at their disposal to elucidate the structural and functional organization of the brain. These techniques utilize a wide range of physical mechanisms, and cover a broad range of targets at the molecular, synaptic, cellular, circuit and whole brain level. These techniques must cover an extraordinarily challenging 6-orders of spatial, and 11-orders of temporal resolution or experimental duration [1]. The most established methods are the patch-clamp technique, positron emission tomography, electroencephalography, functional magnetic resonance imaging, and the optical techniques [2], with the limits of their resolution shown in Figure 1-1. However, it is the development of new techniques that is a fundamental to the progress of neuroscience.

1.1 Optical Sensors of Electrophysiology

Compared to the other existing techniques, the optical methods have the widest spatiotemporal range for observing the electrophysiology of the brain. Optical probes use a variety of mechanisms to report the transmembrane voltage of neurons, in order to capture the electrical information by which neurons communicate [3]. Some of these mechanisms include: Förster Resonance Energy Transfer (FRET), between fluorescent protein or dye pairs, whose relative positions are influenced by transmembrane voltage [4]; fluorescence activation or modulation via calcium binding, with either a Genetically EnCoded Indicator

(GECI) [5], or a Calcium-chelating small molecule indicator [6], that reports the calcium influxes into the neuron; or most directly with small-molecule, membrane-binding probes, whose fluorescent signal varies with transmembrane voltage [7].

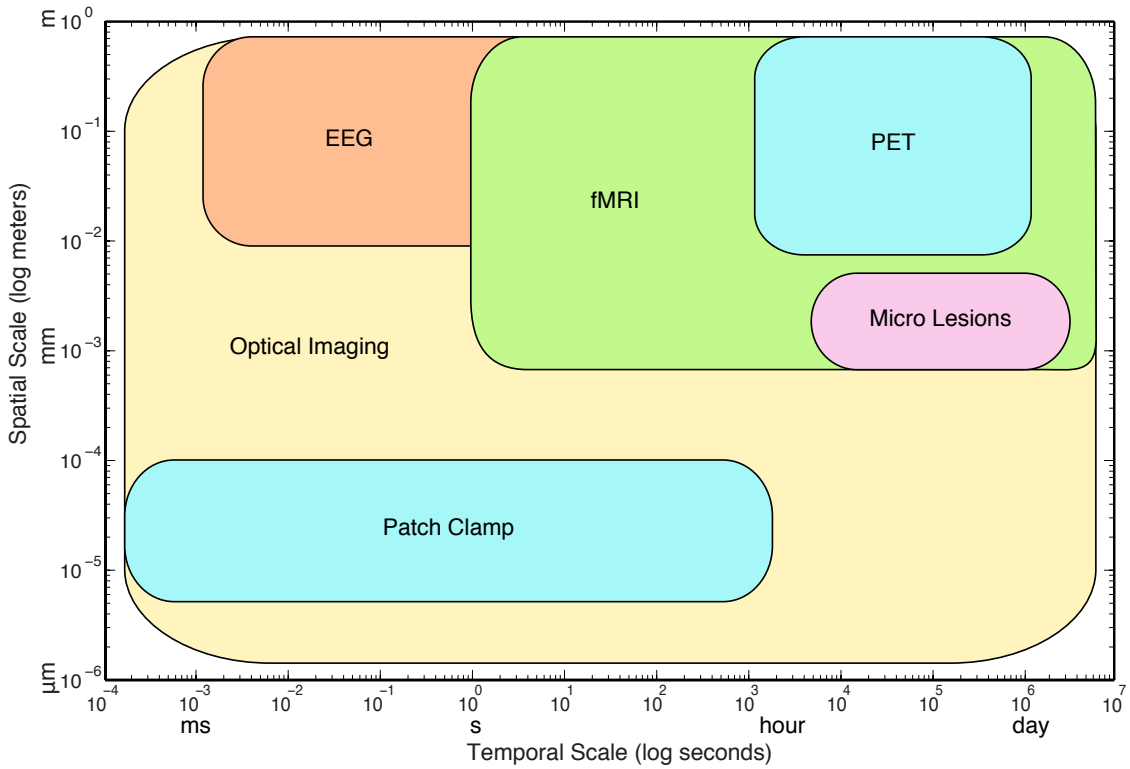

Figure 1-1 The approximate spatiotemporal capabilities of the most commonly used techniques in neuroscience.

This last class of probe, the fast Voltage Sensitive Dye (VSD), is a promising tool for elucidating electrophysiological information. These amphiphilic molecules bind into neuronal cell membrane, where they exhibit a change in fluorescence intensity reflecting changes in local membrane potential. As the effects are local, this technique offers excellent spatial localization, including the capability of tracing the progression of a single action potential thorough the dendrites of a neuron [8-10]. The spatiotemporal resolution achievable with voltage-sensitive dyes is limited only by the resolution and sensitivity of the dyes, optics and recording equipment.

However, the amphiphilicity critical in directing the insertion of the chromophore into the hydrophobic lipid bilayer core is not neuron specific. Thus, unavoidable staining of the cells adjacent to target neurons precludes the measurement of voltage transients in the neuron's finely ramified structures. Although intracellular loading of the dye alleviates these problems, it requires demanding laboratory procedures and physical access to individual neurons, severely limiting its application.

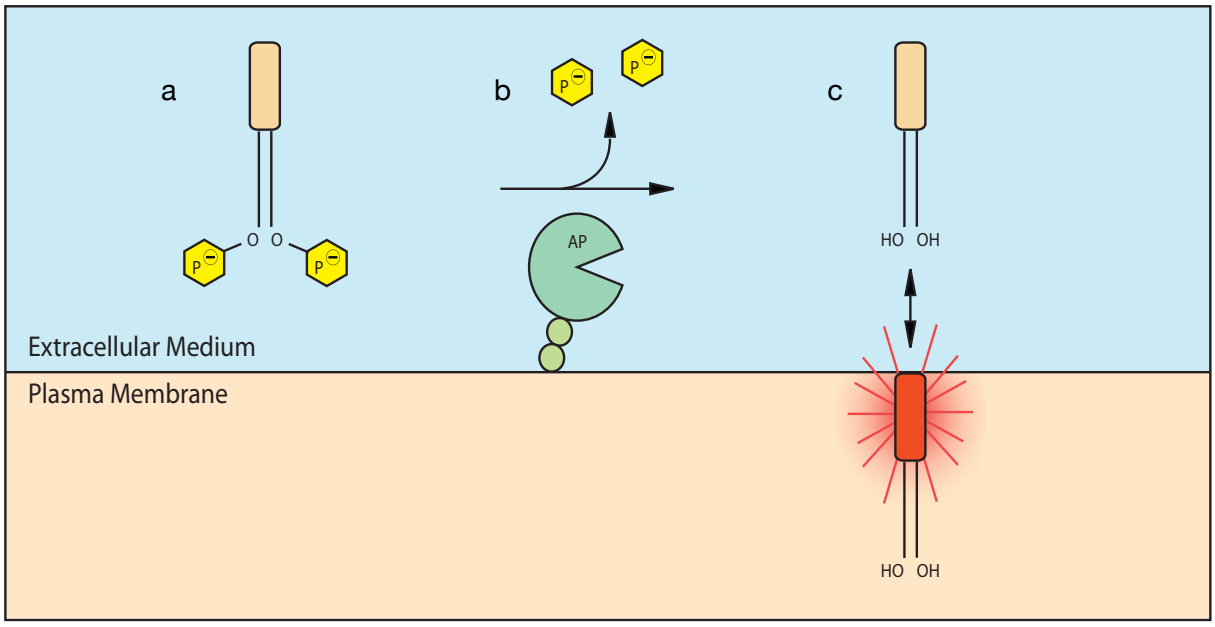

Figure 1-2 The mechanism for the genetically-targeted, selective staining of cell membrane via enzymatic activation; a) water-soluble prodye encounters a membrane-bound alkaline phosphatase, b) which catalyses the cleavage of the charged phosphate groups, c) leading to the insertion of the amphiphilic dye into the cell membrane.

A recently devised technique addresses the problems of unwanted background labeling inherent with conventional VSDs [11]. This new technique involves the enzymatic conversion of a water-soluble, non-binding 'prodye' into a membrane binding amphiphile. The model dye used in the method shows a negligible fluorescence in water, but greatly increased fluorescence upon transition into the hydrophobic interior of the plasma membrane, due to the large increase in quantum efficiency [11]. By attaching two enzymatically-cleavable phosphate groups at the dye's hydrocarbon tails, the membrane binding ability of the prodye was decreased by a factor of a thousand as compared to the processed dye. Using this prodye system, genetically specified HEK293 cells expressing membrane-bound phosphatase were selectively stained, as illustrated in Figure 1-2. This technique may have potential to label the fine dendritic structure of individual neurons, and monitor their local electrophysiology [12].

The system described above used the Amino Styryl Pyridinium (ASP) chromophore, which possesses minimal voltage sensitivity. It is also known that the orientation of the dye within the plasma membrane is a critical parameter for voltage sensitivity [13]. As the tails of the dye are modified to introduce primary-alcohol functional groups, it is important to test whether these polar groups disrupt the required perpendicular orientation of the dye in the cell membrane. Thus, the principal goals of this thesis are to synthesize a new set of prodyes incorporating a voltage sensitive chromophore; to show selective staining of genetically targeted cells; and to measure the activated dye's transmembrane voltage sensitivity.

1.2 Neuronal Circuit Mapping

The brain can be subdivided into interconnected groups of neural circuits, with various regions of the brain used to interpret, store and process different kinds of sensory data. The analysis of these circuits is hindered by the fact that the connectivity within these networks is difficult to obtain. The field of neuroanatomical tracing began with the manual analysis of histochemically labeled neurons; they were assumed to be connected when their stained neuronal processes appeared to be joined together [14]. This was improved with the discovery of marker compounds that are actively transported through neurons; these materials are either transported in the anterograde direction, from the cell body towards the periphery of the neuron, or the reverse retrograde direction, back towards the cell body. Some of these new markers were found to have the ability to pass across the trans-synaptic cleft between two neurons, and hence show the presence of functionally connected circuits [15].

However, the detection of these trans-synaptic tracers remains a significant problem. As the signal strength drops dramatically upon crossing the trans-synaptic cleft, the mapping of circuits beyond fourth order neurons is not possible [16] even with the use of sensitive *in situ* antibody labeling. In order to overcome this limitation, viral vectors that target the central nervous system have been utilized to amplify the signal in connected neurons. Both the pseudo-rabies virus [17] and herpes virus [18] have been genetically engineered to include protein marker genes. These viruses exploit natural retrograde transport systems to infect directly connected neurons. Upon infection, high levels of marker protein such as GFP or ß-galactosidase are expressed, together with new viral particles that go on to infect further connected neurons. Unfortunately, these viruses are highly toxic to the neurons, with the high production of new viral particles leading to altered cell function and eventual cell death.

What is required is a new system, one that has the benefits of signal amplification inherent in the viral techniques, but without the toxicity and experimental restrictions involved with using live viruses. This project will outline a possible new technique to map functionally connected neural circuits, using a fusion protein that activates DNA sequences already present in the genome of target organisms. Like a viral system, the fusion protein would ‘jump’ from neuron to neuron, but once inside an interconnected neuron, it would only activate the transcription of a marker gene, yielding normal levels of protein expressions so as not to impair the function of the cell. This method of gene activation, typically performed with a recombinase enzyme, is widely used in molecular biology. Fusing such a recombinase to the Tetanus neurotoxin, a bacterial protein known to undergo retrograde trans-synaptic transport as well as able to carry a variety of cargo proteins into the cytosol of target neurons, would allow targeted delivery of the enzyme, thus yielding the desired system.

1.3 Thesis Overview

This project aims to develop a technique for the selective staining of genetically targeted individual neurons in brain slices with a voltage sensitive dye. This will require the development of a new family of genetically targetable voltage sensitive dyes, and the design and construction of the materials and apparatus required to test their properties. In parallel, the foundations for a new technique to label individual neuronal circuits will be described. The long-term objective of this project is to combine these two new techniques: to genetically label functionally connected neural circuits with alkaline phosphatase, and selectively stain these neurons with a targeted voltage sensitive dye. The amalgamation of these two new methods would allow the first exploration into the high-resolution spatiotemporal electrophysiology of neural circuits.

Chapter 2 deals with the synthesis of these genetically targetable phosphate prodyes. It describes the required physicochemical properties and the planned synthetic routes to the various compounds that were constructed. It also describes the design and successful synthesis of a new family of N-phosphonooxymethyl based prodyes, based on recent developments in the field of medicinal prodrugs.

Chapter 3 describes the generation of new genetic tools and cell-lines designed for the rapid testing of the prodyes. All of the newly synthesized prodyes were then shown to be alkaline phosphatase substrates, and all were found to selectively stain the plasma membrane of cells that expressed placental alkaline phosphatase on the cell-surface.

In Chapter 4, the design and construction of an apparatus to measure the voltage sensitivity of the targeted dye is described, together with the results for the selective staining of the new cell line with the best of the new prodyes. This prodye, di-1,8P6-ANEPPS, shows excellent membrane targeting, and was found to possess a transmembrane voltage sensitivity similar to the widely used di-4-ANEPPS dye from which it is derived.

Chapter 5 discusses the current tools used for the tracing of neural circuits, and introduces a new, hybrid system that is designed to overcome the numerous limitations of the currently used methods. It describes the design and gene-synthesis of a new and novel family of fusion proteins based on a non-toxic adaptation of the Tetanus neurotoxin, and shows that the fundamental requirements for this new tool are met.

Finally, Chapter 6 concludes with a summary of the new developments achieved in this project. The Appendices will cover the abbreviations, equipment, plasmid maps, and protocols referenced during this work, together with sequence data for the newly synthesized gene construct.

2 VOLTAGE SENSITIVE DYE SYNTHESIS

In this chapter, the design and planning of the voltage sensitive dyes will be discussed, in regards to the desired physicochemical properties of the dyes and prodyes, such as solubility, membrane binding, voltage sensitivity, toxicity, and phosphatase activity. A literature review of the current generation of phosphatase-based prodrugs shows a variety of new prospective mechanisms for selective staining, with the N-phosphonooxymethyl prodrugs offering excellent potential mechanism for prodye use. Following this analysis, the synthesis of the two classes prodyes will be described and discussed, along with a brief analysis of their physical properties.

2.1 Structural Strategy

The goal of selectively labeling *in vivo* neurons with a voltage sensitive dye that can be used to monitor the electrophysiology of the brain requires the successful fulfillment of several criteria. The dye must be able to reach the site of activation, be a good enzymatic substrate, show strong cell membrane binding only after such enzymatic activation, show good voltage sensitivity, and be relatively non-toxic.

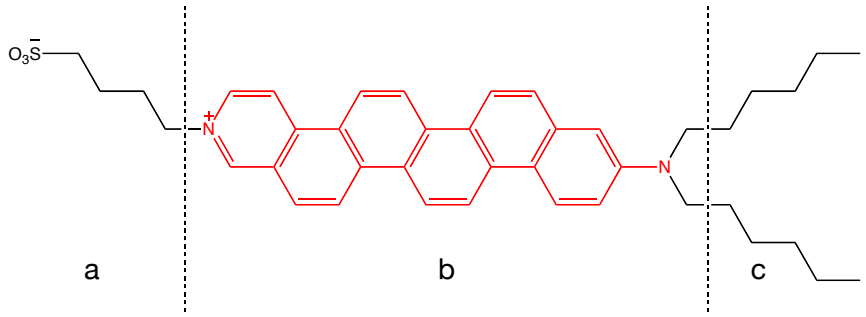

Figure 2-1 The structure of a fast voltage sensitive dye, ANNINE-6. a) The charged headgroup, b) voltage sensitive chromophore, c) and the aliphatic tail.

The structure of "Fast" voltage sensitive dyes can be compartmentalized into three distinct functional sections, as shown with the example of ANNINE-6 in Figure 2-1. When the dye is bound within a lipid bilayer, a charged head group region remains in the aqueous phase; the chromophore and tail lie embedded in the hydrophobic domain of the cell membrane. For the dye di-8-ANEPPS bound to the plasma membrane model palmitoyl-oleoyl-phosphatidyl-choline (POPC), it lies at an angle of 37.8° from perpendicular, as determined by fluorescence

interferometry [13]. By altering each of these three regions separately, the solubility, sensitivity, and binding strength of the dyes can be altered relatively independently.

2.1.1 Chromophore Selection

There are a wide variety of synthesized voltage sensitive dyes. These vary in their sensitivity, fluorescence spectra, quantum efficiency and stability. The most widely used chromophore is that from the dye di-4-ANEP-BS (Amino Naphthyl Ethenyl Pyridinium - Butane Sulfonato), [19,20], which was first reported together with the synthesis of 33 other voltage sensitive dyes. There have been over a hundred voltage sensitive dyes developed [21-24], and it is in the chromophore that the greatest variation between the dyes is apparent. Figure 2-2 shows a few of these structures, which are believed to derive their voltage sensitivity from a combination of the intramolecular Stark effect, photoisomerism and photorotamerism, and solvatochromism [25]. The elimination of the last two effects, with the construction of a rigid, fully-anellated aromatic chromophore, has yielded the ANNINE series of dyes [7,23].

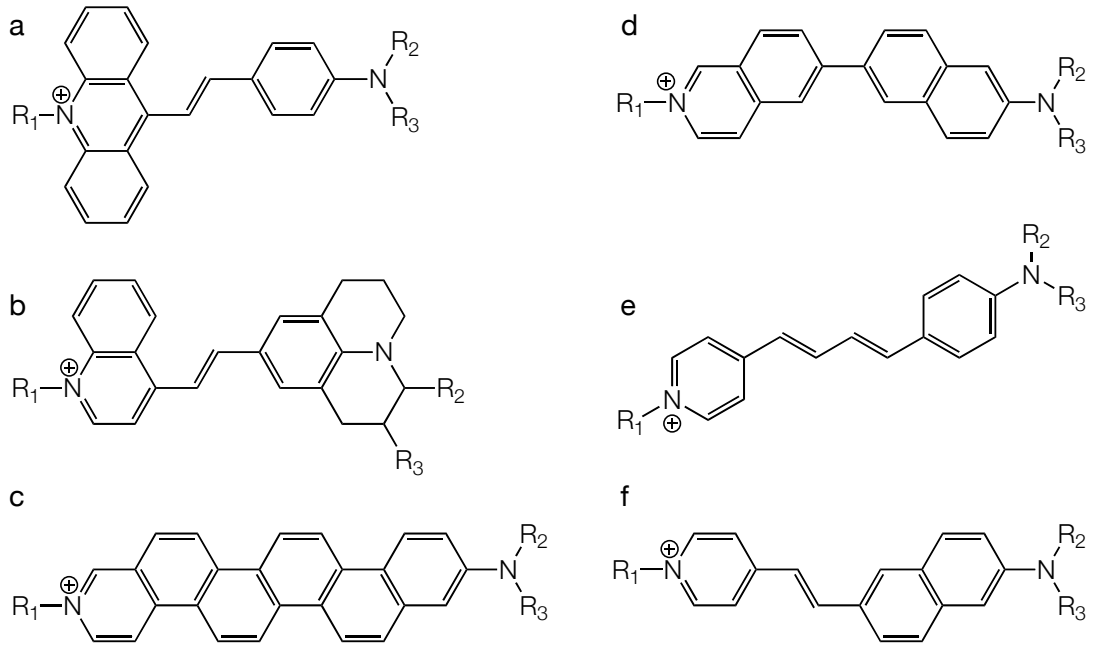

Figure 2-2 Examples from the various chromophores developed for voltage sensitive dyes; a) DB1-195, b) DB2-039, c) ANNINE-6, d) BNBIQ, e) di-4-APPPS, f) di-4-ANEPPS [19,21,23].

This family of chromophores has been demonstrated to provide sensitivities in the range of ~70% per 100 mV at 1040 nm with two-photon excitation, far beyond the usually recorded 10-14% per 100 mV of widely used ANEP dyes [26]. As such, it would be the ideal candidate for a prodye used in the selective staining of cells. However, the difficulty in synthesizing the

anellated ring structure, with its concurrent low yields, leads us to the selection of the simpler ANEP structure for the development of targeted dyes, with the goal of replacing the chromophore for ANNINE system, once a working model has been demonstrated.

An important property of the ASP and ANEP hemicyanine dyes is the large enhancement in quantum fluorescence yield upon the transfer of the dye from an aqueous medium into the lipid bilayer [11]. This is a valuable property in the design of targetable voltage sensitive dyes, as the large increase in fluorescence together with well selected bandpass emission filters effectively allows the imaging of membrane-bound dye without background fluorescence from the aqueous prodye.

2.1.2 Head Group Selection

The overall solubility of the voltage sensitive dyes is strongly affected by the selection of the head group. This factor remains largely independent of the strength with which the dye binds to lipid membrane, as the head group is thought to remain in the aqueous media at the boundary of the lipid bilayer, with molecular modeling reaffirming experimental data [27,28]. Figure 2-3 shows some of the various head groups used in commercially available voltage sensitive dyes. The quaternary ammonium cationic head groups show much higher solubility than the sulfonato variants [27], however, negative physiological effects have been seen with the triethylammonium head group, with reports of arterial constriction [29].

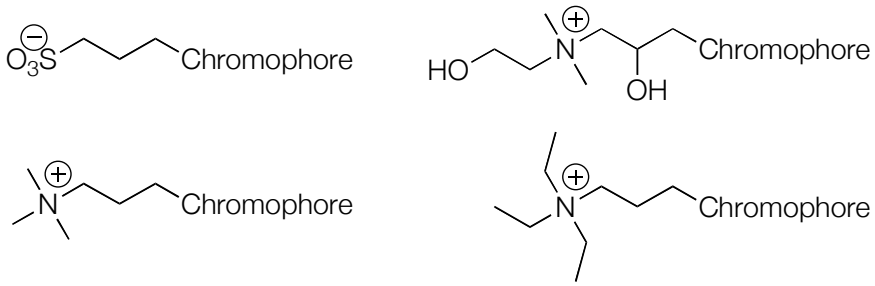

Figure 2-3 Common head groups utilized in voltage sensitive dyes, used to modify solubility and toxicity.

In this thesis, the initial synthetic target was the ANEP version of the ASPBS dyes, maintaining the choice of the sulfonato head group [11,12]. However, as high solubility is a desired property, aiding in the dye's ability to perfuse though tissue to the sites of enzymatic activation, the trimethylammonium head group was also selected as a potential target, avoiding the toxic triethylammonium version. During the dye synthesis, it was also found that head group induced solubility plays a key role in the selection of solvents and the yield for the production of the types of various dyes, and is discussed in detail below.

2.1.3 Tail Design

Together with the chromophore, the tail of the dye is embedded in the plasma membrane lipid bilayer during voltage sensitive recordings, due to lipophilic structure. The tail groups of most commercial voltage sensitive dyes consist of two 4-12 carbon aliphatic chains attached to the amino terminus of the chromophore. The selective staining system developed with alkaline phosphatase functions via the cleavage of charged, solubility-enhancing phosphate groups, leaving a more lipophilic tail that is better suited to embedding in the hydrophobic interior of the membrane, as shown in Figure 2-4 [12]. This system has been tested in lipid vesicles, HEK293, and MDCK cell lines, and is shown schematically in Figure 1-2.

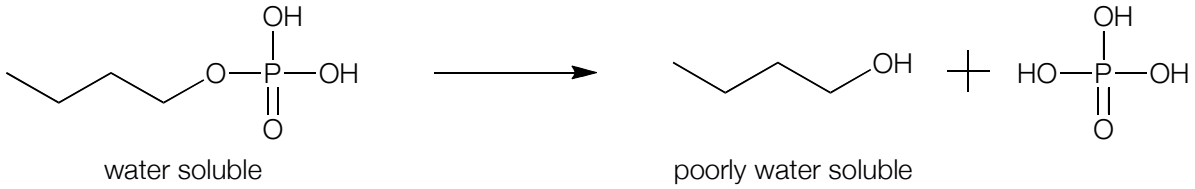

Figure 2-4 Enzymatic conversion of the prodye tail, increasing lipophilicity by the cleaving of a charged phosphate group.

However, in the initial studies assaying the binding of the dyes with lipid vesicles, the enzymatic conversion of the phosphorylated prodye into the activated alcohol dye showed only a 6-fold increase in fluorescence [11]. Tests involving the two cell lines *in vitro* produced even lower levels of selective staining, with 2:1 ratios of membrane fluorescence between phosphatase expressing cells and the control cells. To increase the difference in binding strength between dye and prodye, whilst maintaining the use of alkaline phosphatase as the activator of the prodye, the potential use of other functional group motifs used for increasing "prodrug" solubility were analyzed.

The delivery of active pharmaceutical compounds to their required destination depends on physical properties that may be antagonistic to their desired physiological properties. The *in vivo* delivery of large, poorly soluble compounds can be enhanced by bio-reversible chemical modification that produces more water-soluble derivatives. The technique of phosphorylation of alcohol groups to increase solubility that was utilized for the model prodyes, has also been used to increase the solubility of a large number of drugs [30-33], with Figure 2-5 showing a few examples of this kind of modification.

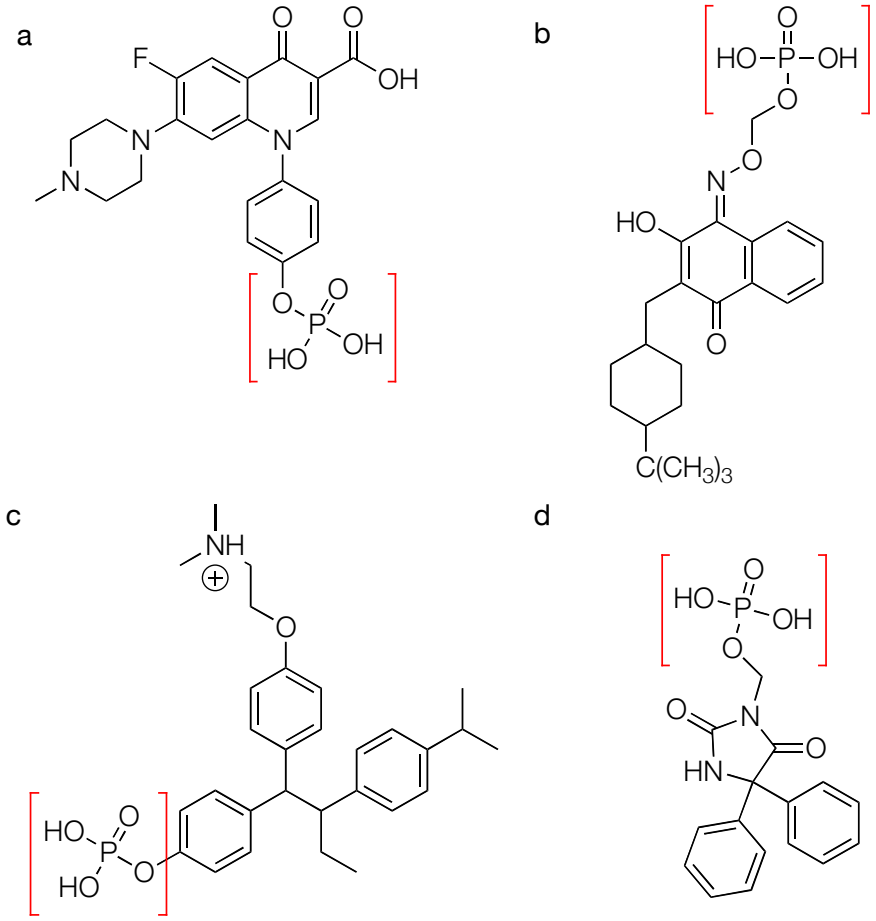

Figure 2-5 Phosphate-based prodrugs; a) PA2808, b) Bupuravaquone phosphate, c) Miproxifene phosphate, d) Fosphenytoin. The enzymatically cleavable phosphate is shown in red brackets.

There are a wide variety of other bioreversible chemical modifications that are used to create prodrugs [34], as shown in Figure 2-6. These prodrugs use *in vivo* processes such as peptidase cleavage or the breaking of the sulfenamide bond with cysteine, to convert the prodrug back to its active form. Of particular interest are the prodrugs based on N-phosphonooxymethylation of tertiary amines, shown in prodrugs such as Aminodarone disodium phosphate, displayed in Figure 2-6-d. In this technique, the tertiary amine is derivatized to a cationic quaternary amine salt, thus greatly increasing its solubility as compared to the phosphorylation of an alcohol functional group, as used is the previous prodye system [35]. In this strategy, bioconversion of the prodrug to its active conformation occurs in a two-stage process, as shown in Figure 2-7 and Figure 2-8.

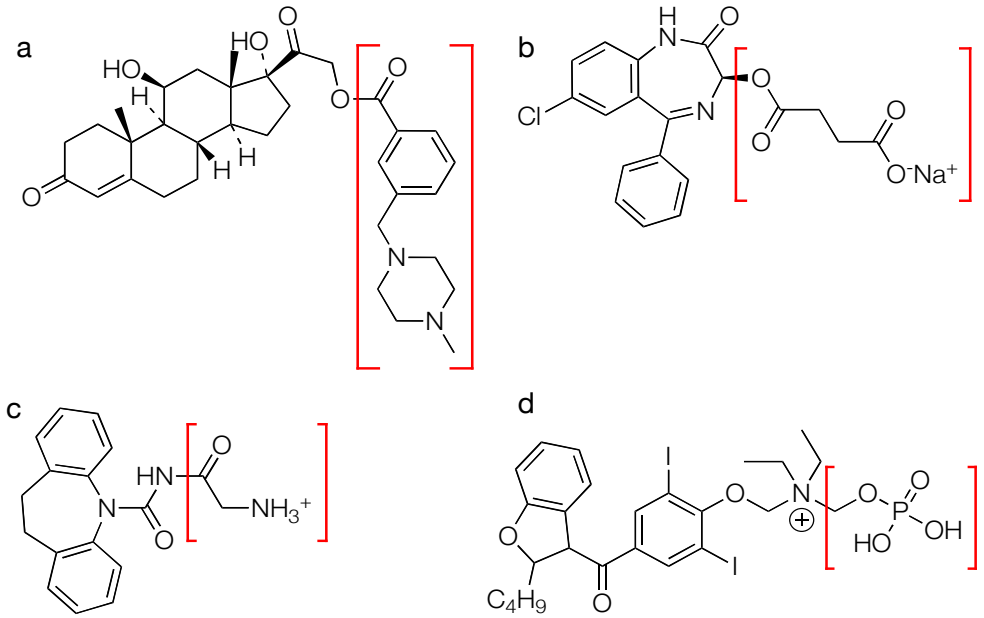

Figure 2-6 Bioreversible prodrugs; a) Hydrocortisone derivative b) Oxazepam sodium succinate c) N-glycyl Carbamazepine d) Aminodarone disodium phosphate. Chemical modifications to the original pharmaceutical compounds are shown in red brackets.

The prodrug first undergoes the enzymatic cleavage of its phosphate groups, yielding an unstable N-hydroxymethyl intermediate that spontaneously breaks down to produce the active drug and formaldehyde. The prodrug has been shown to be stable at physiological pH, and undergo rapid conversion *in vivo* with endogenous phosphatases, and increase the solubility of derivatized compounds by over 4 orders of magnitude [35-38].

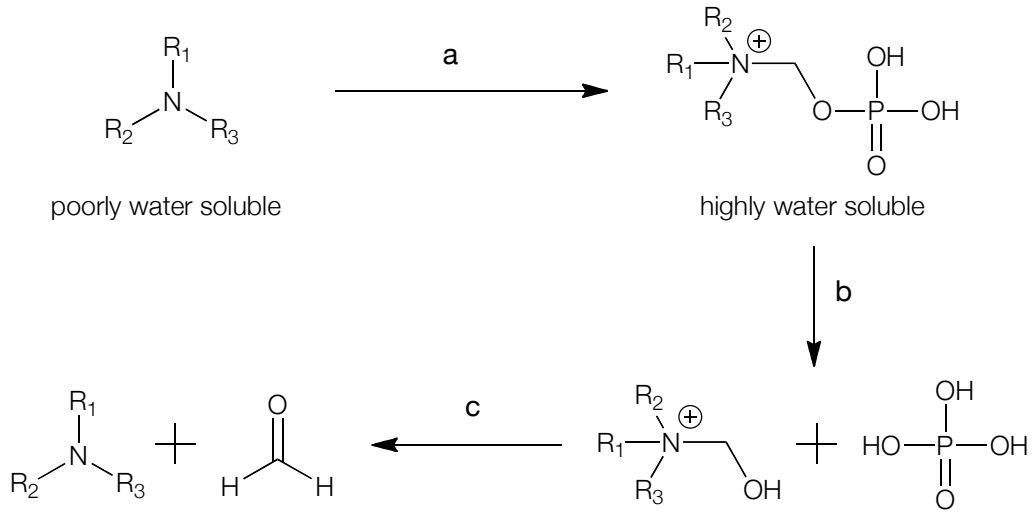

Figure 2-7 The mechanism of N-phosphonooxymethyl prodrug bioconversion; a) a poorly soluble, tertiary amine containing drug is chemically modified into a highly water soluble quaternary amine. b) *in vivo* endogenous phosphatases cleave off the phosphate group, leaving a highly unstable N-hydroxymethyl intermediate, which c) spontaneously breaks down to produce formaldehyde and the original drug.

2.1 STRUCTURAL STRATEGY

The oxymethyl linker, which extends the distance between the prodrug and the phosphate group, has also been shown to increase the substrates ability to undergo enzymatic activation [39,40]. This may be due to the greater ability of the phosphate group to enter the catalytic cleft of the membrane bound alkaline phosphatase.

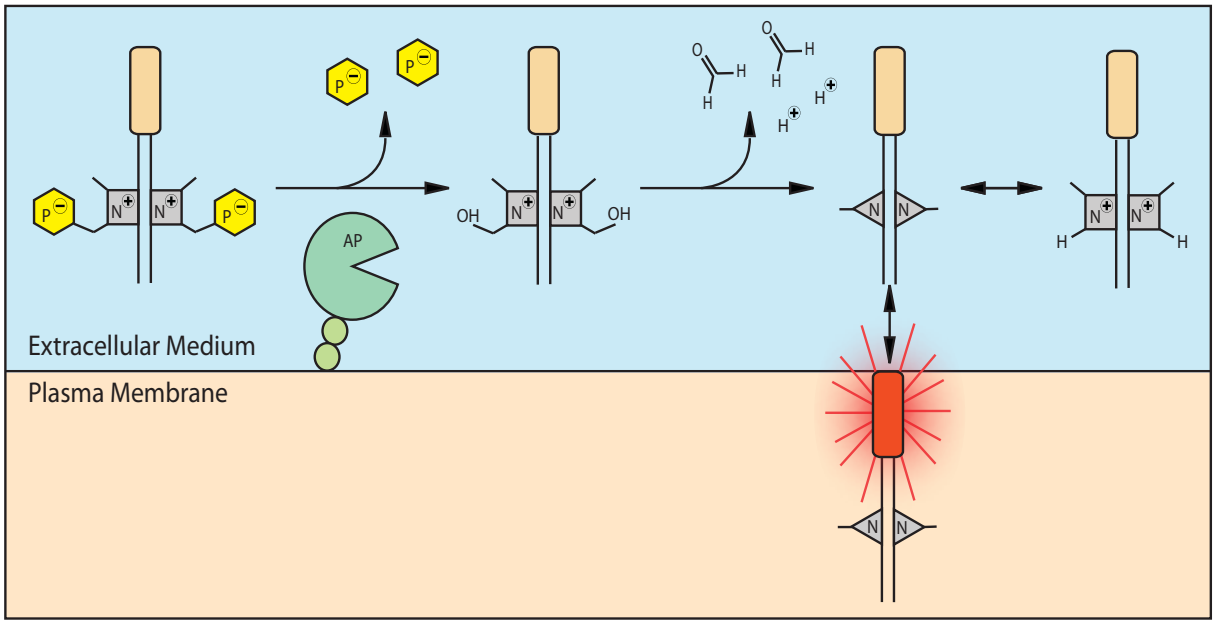

Figure 2-8 The mechanism for the selective staining of cell membrane via enzymatic activation of an N-phosphonooxymethyl prodye.

To test the feasibility of applying N-phosphonooxymethyl derivatization to voltage sensitive dyes, water/octanol distribution coefficients were calculated to give approximate binding coefficients for lipid membrane binding. This coefficient, the ratio of the sum of the concentrations of all forms of the compound (ionized plus un-ionized) in each of the two phases, is termed 'log D'. Software calculating the linear Gibbs energy relation with the Hammett and Taft equation [41], together with empirical data from a large library of organic molecules [42] including quaternary ammonium containing compounds [43], can be used to predict log D, traditionally performed via the shake-flask method at a buffered pH value [44]. The two most widely used online log D calculators were used to calculate the coefficients for model prodye and dye structures, for both the phosphate and N-phosphonooxymethyl derivative system, across a range of pH values, as shown in Figure 2-9. Both the Chemaxon Marvin package and the Advanced Chemistry Development Inc I-Lab online software package (www.chemaxon.com, www.acdlabs.com), showed very similar distribution profiles for pH 7.0 and above, the region of interest for physiological studies and the application of alkaline phosphatase.

The predicted results for both modeling system indicates that the tertiary amine dye is significantly more lipophilic than the alcohol dye from approximately pH 8.5 and higher, at which point the ratio of the deprotonated to the cationic form of the dye begins to increase, the uncharged form becoming the sole species over pH 11. For the prodyes, the quaternary N-phosphonooxymethyl form is significantly more water-soluble than the phosphorylated dye at all pH values. These computed results indicate that the N-phosphonooxymethyl prodye approach has the potential to outperform phosphorylated prodyes in selective staining. The high pKb of the aliphatic tertiary amine (~pH 10.3), would prevent the use of the dye at physiological pH, when the protonated, cationic form of the dye would overwhelmingly predominate, preventing binding in the lipophilic membrane core. However, the optimal pH of the alkaline phosphatase coincides at pH 9.6 [45]. Although this value is much higher than physiological pH, neurons can tolerate such high pH for long periods, where it has been demonstrated to protect cells from ischemia. Adult rat dorsal root ganglion (DRG) neurons kept at pH 9.3 at 37°C for 4 hours had a higher viability than those kept in the same conditions at pH 7.6 [46]. This higher pH could therefore be used for staining the cell membranes, followed by a return to a lower pH for measurement.

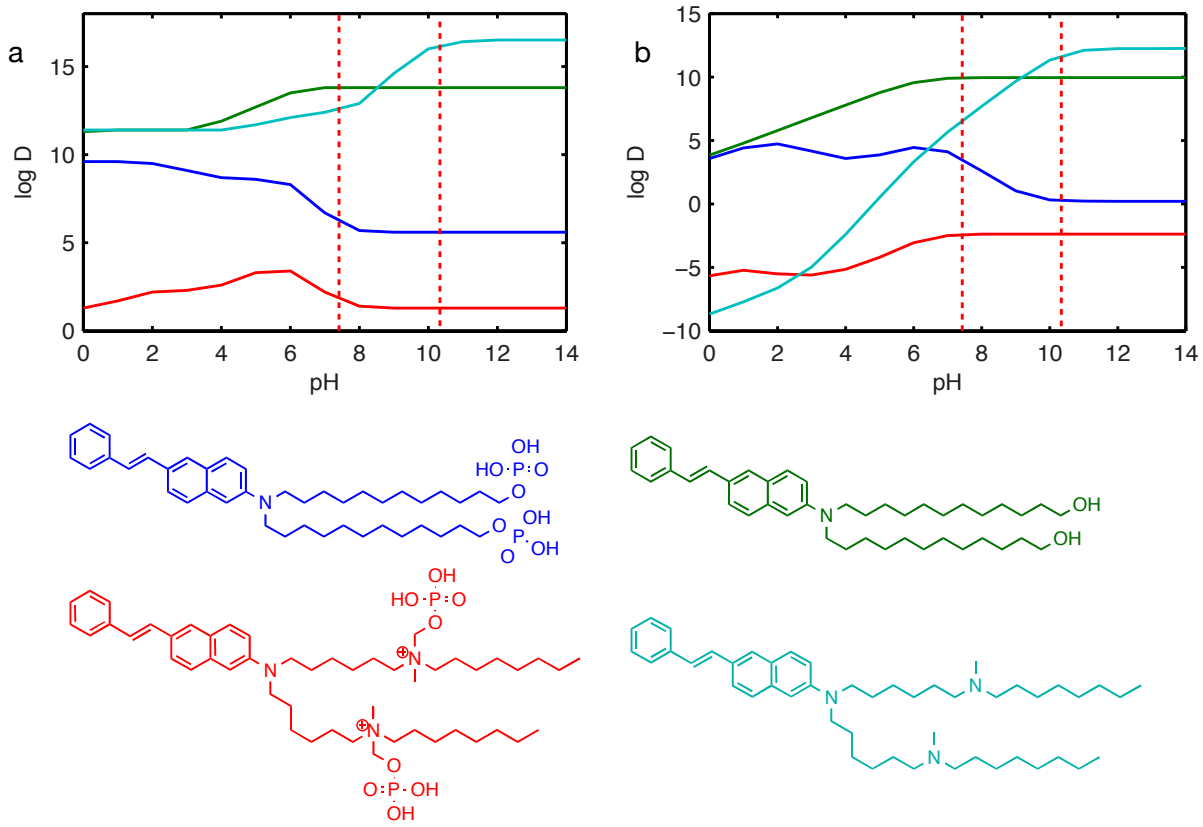

Figure 2-9 Predicted log D values for phosphate and phosphonooxymethyl dyes and prodyes; a) predicted values using the Chemaxon package, b) predicted values using the ACD Labs package, c) color-coded model compounds used for the analysis. The vertical dotted lines mark physiological pH and the pKb of aliphatic tertiary amine.

2.2 Synthesis of the Prodyes

The synthesis of the prodyes can be divided into two sections; the synthesis of the ANEP chromophore and head group, which is common for all prodyes in this project; and the synthesis of tail group, which is also divide into the phosphate and phosphonooxymethyl prodyes. The tail group in both cases is based on an aliphatic, terminal alcohol groups, that are either directly phosphorylated, or converted into a tertiary amine, for later N-phosphonooxymethylation.

2.2.1 Synthesis of the Chromophore and Head Group

The first route, describing the synthesize the di-4-ANEPPS chromophore, was used as published by Loew [20], and is shown in Figure 2-10-1. Starting with the easily obtainable 6-bromonaphthalen-2-ol, a functional group interconversion to the amine is performed with Bucherer reaction [47], Figure 2-10-1d, with a yield of ~80%. Alkylation of the newly created amine is performed with various iodinated aliphatic alcohols in nitromethane, varying in length from 6-12 carbons, Figure 2-10-1c. These themselves were synthesized from their corresponding bromides via the Finkelstein reaction, so as to increase their reactivity with the relatively unreactive aromatic amine. However, the yields for the alkylation of 6-bromonaphthalen-2-amine with any of these iodinated alkanes was found to be generally around 10%, rather than the reported 77% from the original literature, using 1-iodobutane. Also, the poor chromatographic separation between the once and twice alkylated products requires multiple rounds of purifications over silica.

The alkene bond was constructed with using vinyl pyridine, using the palladium catalyzed Mizoroki-Heck reaction [48], Figure 2-10-1b, which was chosen for its high yields in the desired *trans* selectivity. The yield published for this step is 77%, however, the actual yield obtained over the course of multiple reactions, under the same conditions, was an average of only approximately 35%.

The head group addition published by Loew, Figure 2-10-1a, uses the ring-opening of 1,3-propanesultone to form the cationic pyridinium betaine, however, the terminal alcohols required for the prodye would prohibit the use of this reagent without extra alcohol protection and deprotection steps, and so 3-bromopropane-1-sulfonic acid was used in its place. The formation of the dicationic dye utilized 3-Bromopropyltrimethylammonium bromide in an analogous reaction.

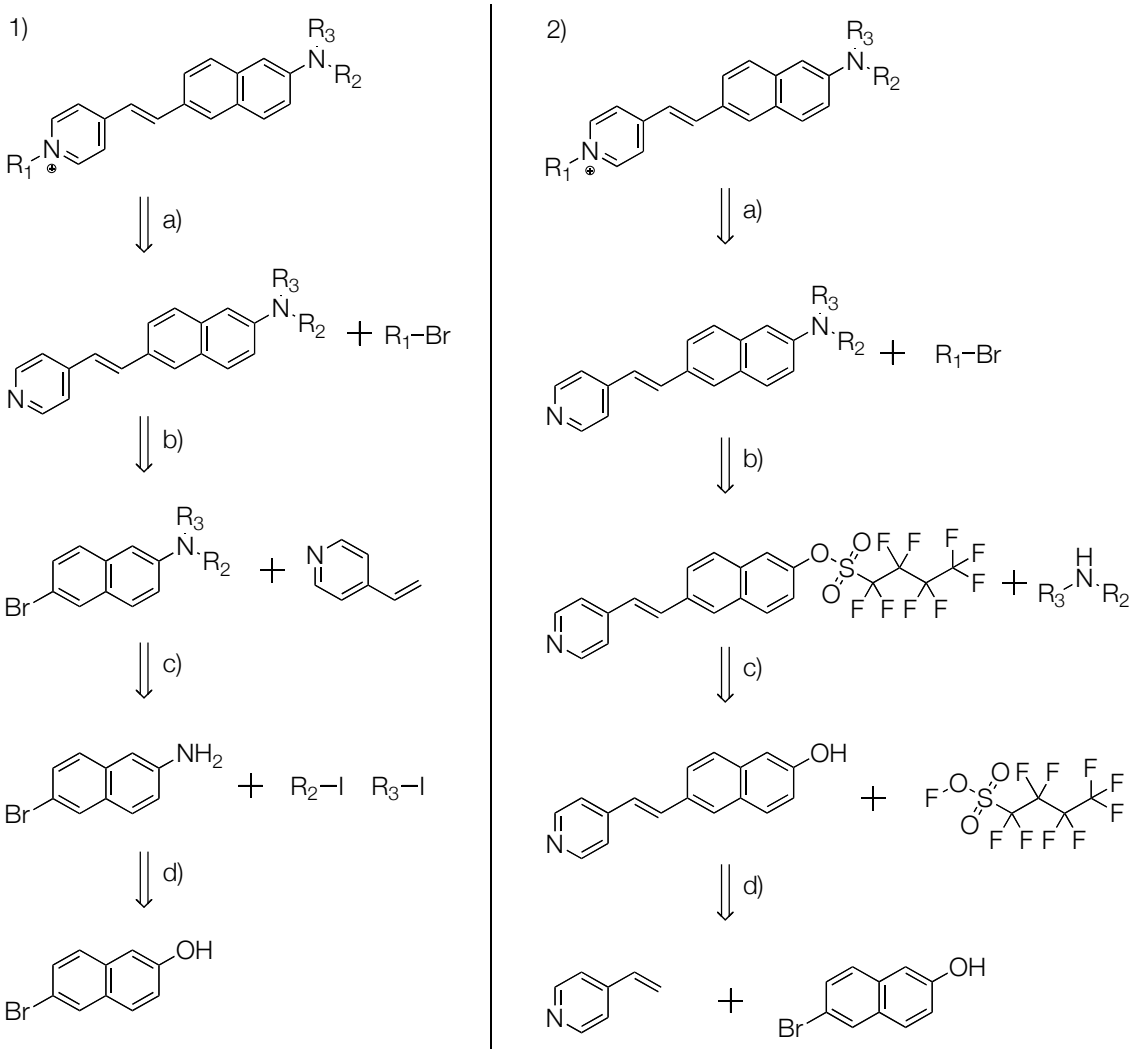

Figure 2-10 Retrosynthetic analysis of the chromophore structure; 1 a) N alkylation, b) Mizoroki-Heck reaction, c) N alkylation, d) Bucherer reaction. 2 a) N alkylation, b) Buchwald–Hartwig amination, c) Alcohol Nonaflation, d) Mizoroki-Heck reaction.

Due to the low yields for the subsequent phosphorylation step, we required large amounts of the alcohol dye, and so we formulated a new procedure for the chromophore synthesis, shown in Figure 2-10-2. In this scheme, the functional group interconversion is skipped, and the 6-bromonaphthalen-2-ol is used directly in the Mizoroki-Heck reaction, Figure 2-10-2d. The yield for this initial reaction was found to be extremely good, at ~90%, much better than the corresponding coupling reaction of 6-bromonaphthalen-2-amine at ~35%. The reaction also yielded an insoluble yellow product that was easily washed, and used directly in the next step without the need for column chromatography for purification.

The tail group is added after the formation of the *trans* bond, via the Palladium catalyzed Buchwald-Hartwig cross-coupling reaction [49-52], Figure 2-10-2b. Various combinations of catalysts, ligand and substrate were tested. For the substrate, the alcohol functional group

from the previous step was converted into either a triflate or nonaflate for amination, with triflic anhydride [49] or nonafluorobutane-1-sulfonyl fluoride [52] respectively, both of which gave near quantitative yields. The nonaflate used together with NaO*t*-Bu as the base, Pd_2dba_3 as the catalyst and 2-(Dicyclohexylphosphino) biphenyl as the ligand, and dibutyl amine gave a yield of 92%, with lower yield obtained from combinations using Cs_2CO_3, K_3PO_4 as the bases, or $Pd(OAc)_2$ as catalyst.

This brings the total yield to this point to ~70%, compared to the Loew scheme with ~3%. This new procedure both increases yields, and adds to the flexibility of the scheme, by allowing the length of the aliphatic tail group to be selected at a later stage in the synthesis. However, although the yield was significantly increased, the limited availability of secondary amine substrates for the aryl nonaflate amination meant that only di-(11-hydroxyundecane) amine was readily available (giving an amination yield of 62% with the above conditions). Although this was a useful product, there was not enough range to continue further research in this direction. However, this new reaction scheme is a very efficient method for the production of di-4-ANEPPS and di-4-ANEPBS, two of the most commonly used VSD's.

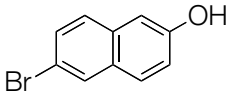

1

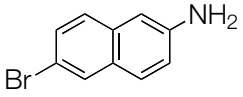

2

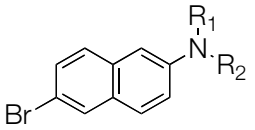

3a, $R_1 = (CH_2)_6OH$, $R_2 = (CH_2)_6OH$
b, $R_1 = (CH_2)_6OH$, $R_2 = (CH_2)_7CH_3$
c, $R_1 = (CH_2)_8OH$, $R_2 = (CH_2)_8OH$
d, $R_1 = (CH_2)_{10}OH$, $R_2 = (CH_2)_{10}OH$
e, $R_1 = (CH_2)_{12}OH$, $R_2 = (CH_2)_{12}OH$

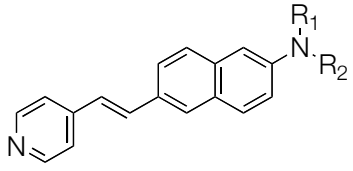

4a, $R_1 = (CH_2)_6OH$, $R_2 = (CH_2)_6OH$
b, $R_1 = (CH_2)_6OH$, $R_2 = (CH_2)_7CH_3$
c, $R_1 = (CH_2)_8OH$, $R_2 = (CH_2)_8OH$
d, $R_1 = (CH_2)_{10}OH$, $R_2 = (CH_2)_{10}OH$
e, $R_1 = (CH_2)_{12}OH$, $R_2 = (CH_2)_{12}OH$

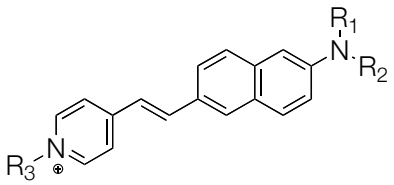

5a, $R_1 = (CH_2)_6OH$, $R_2 = (CH_2)_6OH$, $R_3 = (CH_2)_3SO_3^-$
b, $R_1 = (CH_2)_6OH$, $R_2 = (CH_2)_7CH_3$, $R_3 = (CH_2)_3SO_3^-$
c, $R_1 = (CH_2)_{10}OH$, $R_2 = (CH_2)_{10}OH$, $R_3 = (CH_2)_3SO_3^-$
d, $R_1 = (CH_2)_8OH$, $R_2 = (CH_2)_8OH$, $R_3 = (CH_2)_3N(CH_3)_3^+$
e, $R_1 = (CH_2)_{10}OH$, $R_2 = (CH_2)_{10}OH$, $R_3 = (CH_2)_3N(CH_3)_3^+$
f, $R_1 = (CH_2)_{12}OH$, $R_2 = (CH_2)_{12}OH$, $R_3 = (CH_2)_3N(CH_3)_3^+$

Figure 2-11 Intermediate products in the synthesis of the prodyes.

The ~3% yield of the Loew method was due to the low yield for the amine alkylation and Mizoroki-Heck reaction. Further research into the alkylation step found that the selection of solvent plays a strong role in overall yield [53], and that the change from nitromethane to t-butanol increased the yield from ~10% to 28%. Improvement in the yield of the Mizoroki-Heck reaction could also be obtained though the modification of reaction solvent. The need of a high-pressure 'bomb' as the reaction vessel was eliminated with the substitution of neat TEA with a 2:1 TEA:DMF solution [54], while also increasing the yield from 35% to 84%.

In summary, both reaction schemes were found to be viable, however, low yields for the original first scheme, and limited availability of reactants for the second necessitated the development of a third procedure, in which the low yielding steps published by Loew were optimized, giving rise to a yield of ~18%, from the initial ~3% yield. The second procedure shows promise due to the relative ease of secondary amine synthesis [55], but further development on this scheme lies beyond the scope of this thesis.

The optimized Loew scheme was used to synthesize all of the dyes used in this project. The only variations were in the length of the aliphatic tail chains, using either 6, 8 10 or 12-carbon primary alcohols, or a mixture of a 6-carbon alcohol and an 8-carbon alkane. This was produced by the re-alkylation of once alkylated hexanol intermediate with iodooctane. The following procedure for the synthesis for compound 5a was applied for the synthesis of all the other compounds.

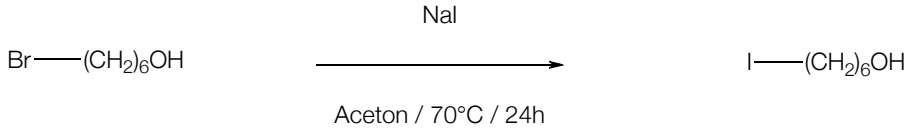

6-iodohexan-1-ol: 6-bromohexan-1-ol (100 g, 735 mmol), and NaI (121 g, 809 mmol) were refluxed in 250 ml ACE overnight, then cooled and filtrated. The ACE was removed under reduced pressure, and the mixture extracted with 3x 100 ml portions of EE, with the combined organic extracts dried over sodium sulfate, filtrated and concentrated in vacuo to yield a thick yellow oil (161 g, 96%).

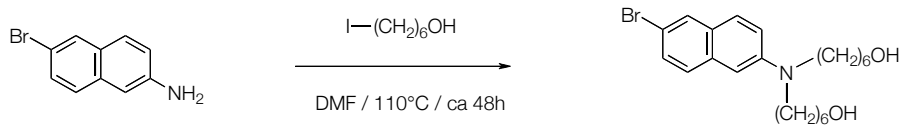

6-Bromo-2-(di-N-6-hydroxyhexylamino)naphthalene (**3a**): Into a 100 ml RBF containing 50 ml t-butanol, there was added 6-bromonaphthalen-2-amine (22.2 g, 0.1 mol), 6-iodohexan-1-ol (50 g, 0.22 mol), and K_2CO_3 (30.4 g, 0.22 mol). After 96 h reflux, the solution was filtrated

and the solvent removed under reduced pressure, and the crude product purified on SiO_2 1:1 EE/Heptane, to produce a pale brown oil (12 g, 28%).

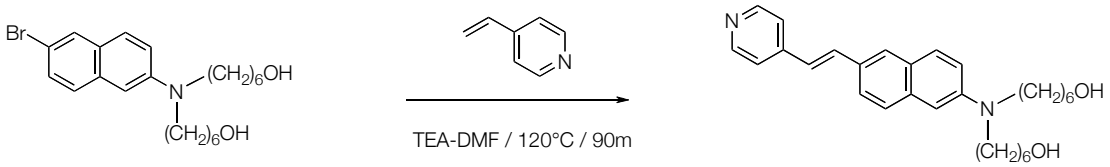

(E)-4-2-(6-(di-N-6-hydroxyhexylamino)naphthalen-2-yl)vinylpyridine (**4a**): To a solution of compound 4a, (3.4 g, 8 mmol) in 30 ml 2:1 TEA/DMF, there was added vinylpyridine (960 µl, 8.8 mmol), tris(o-tolyl)phosphine (3 mol %), and $Pd(OAc)_2$ (3 mol %), after which the flask was flushed with argon, and stirred at 120°C for 2 h. Upon cooling, the solution was filtrated, and the solvents removed in vacuo. The crude products was purified on SiO_2 10:1 EE/Heptane then MeOH, to yield red needle-like crystals (2.8 g, 84%). 1-H NMR (400 MHz; MeOD): δ 7.76 (t, J = 0.8, 2H), 7.58 (d, J = 9.1, 2H), 7.47 (d, J = 8.8, 2H), 7.32 (dd, J = 8.7, 2.0, 2H), 7.13-7.10 (m, 2H), 6.80 (d, J = 2.2, 2H), 3.56-3.35 (m, 26H), 1.65-1.25 (m, 40H), 0.90-0.87 (m, 7H).

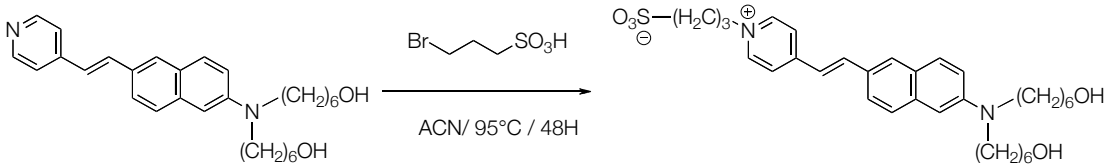

1-(4-Sulfonatobutyl)-4-[ß-[2-(di-N-6-hydroxyhexylamino)-6-naphthyl]vinyl] pyridinium betaine (**5a**): Compound 4a, (1.4 g, 3.13 mmol), together with 3-bromopropane-1-sulfonic acid (1.4 g, 6.27 mmol), was dissolved in 140 ml dry ACN, and heated to 95°C for 96 h under argon. The reaction mixture was cooled, and the solvent decanted off, then the remaining brown solid dissolved in MeOH, and precipitated with ether, sonicated and centrifuged. The red solid was washed 5 times with EE to remove the unreacted compound 2, and then the product was washed from the remaining 3-bromopropane-1-sulfonic acid with 5x 20 ml EtOH, the fractions pooled and the solvent removed under reduced pressure, yielding a black powder (765 mg, 43%).

3b *6-Bromo-2-(N-octyl,6-hydroxyhexylamino)naphthalen*: Thick brown oil, (2.8 g, 66%). 1-H NMR (400 MHz; MeOD): δ 7.75 (s, 1H), 7.58 (d, J = 8.9, 1H), 7.48 (d, J = 8.8, 1H), 7.33-7.31 (m, 1H), 7.12 (d, J= 2.31H), 6.80 (s, 1H), 3.54 (t, J = 6.4, 2H), 3.38-3.29 (m, 4H), 1.66-1.44 (m, 4H), 1.26-1.13 (m, 16H)

3c *6-Bromo-2-(di-N-8-hydroxyoctylamino)naphthalene*: Thick brown oil (2.7 g, 17.4%). 1-H NMR (400 MHz; CDCl3): δ 8.52-8.47 (m, 1H), 7.63-7.61 (m, 4H), 7.09 (s, 1H), 3.59-3.37 (m, 10H), 1.60-1.29 (m, 14H)

3d *6-Bromo-2-(di-N-10-hydroxydecanylamino)naphthalene*: Thick brown oil (6.5 g, 26%). 1-H NMR (400 MHz; CDCl3): δ 7.77 (s, 1H), 7.54 (dd, J = 8.9, 3.3, 1H), 7.44 (d, J = 5.8, 1H), 7.37-7.34 (m, 1H), 7.25 (s, 1H), 7.05-7.03 (m, 2H), 6.74 (s, 2H), 3.62 (t, J = 5.9, 11H), 3.38-3.29 (m, 10H), 2.03 (d, J = 1.5, 1H), 1.66-1.44 (m, 15H), 1.26-1.13 (m, 17H)

3e *6-Bromo-2-(di-N-12-hydroxydodecanylamino)naphthalene*: Thick brown oil (6.0 g, 24%). *1*-H NMR (400 MHz; CDCl3): δ 7.92-7.81 (m, 2H), 7.7 0-7.56 (m, 2H), 7.17-7.04 (m, 2H), 4.49-4.29 (m, 7H), 3.40-3.29 (m, 2H), 2.41-2.11 (m, 8H), 1.66-1.11 (m, 27H), 0.86-0.76 (m, 3H)

4b *(E)-4-2-(6-(N-octyl,6-hydroxyhexylamino)naphthalen-2-yl)vinylpyridine*: Dark red solid, (3.8 g, 86%). 1-H NMR (400 MHz; MeOD): δ 8.43 (d, J = 5.9, 2H), 7.76 (s, 1H), 7.68-7.64 (m, 2H), 7.58-7.55 (m, 4H), 7.14-7.10 (m, 2H), 6.83 (d, J = 1.5, 1H), 4.86 (s, 4H), 3.55 (t, J = 6.5, 2H), 3.41-3.38 (m, 5H), 3.30 (t, J = 1.4, 5H), 1.65 (dd, J = 3.5, 2.3, 3H), 1.64-1.62 (m, 2H), 1.55 (d, J = 6.5, 2H), 1.43 (s, 3H), 1.42-1.30 (m, 13H), 0.88 (d, J = 6.9, 3H)

4c *(E)-4-2-(6-(di-N-8-hydroxyoctylamino)naphthalen-2-yl)vinylpyridine*: Red waxy solid (1.37 g, 43%). 1-H NMR (400 MHz; MeOD): δ 8.43 (d, J = 6.0, 2H), 7.77 (s, 1H), 7.69-7.64 (m, 2H), 7.58-7.54 (m, 4H), 7.14-7.10 (m, 2H), 6.83 (s, 1H), 3.53 (d, J = 13.2, 5H), 3.41 (t, J = 7.5, 5H), 3.34 (s, 10H), 1.65-1.51 (m, 10H)

4d *(E)-4-2-(6-(di-N-10-hydroxydecylamino)naphthalen-2-yl)vinylpyridine*: Dark red solid (2.47 g, 67%). 1-H NMR (400 MHz; CDCl3): δ 8.54 (d, J = 6.0, 2H), 7.72 (s, 1H), 7.68-7.65 (m, 1H), 7.62-7.56 (m, 2H), 7.46-7.39 (m, 4H), 7.06-7.02 (m, 2H), 6.78-6.77 (m, 1H), 3.65-3.61 (m, 5H), 3.39-3.33 (m, 5H), 1.70-1.63 (m, 4H), 1.62-1.44 (m, 36H), 1.41-1.19 (m, 37H), 0.07 (s, 1H)

4e *(E)-4-2-(6-(di-N-12-hydroxydodecylamino)naphthalen-2-yl)vinylpyridine*: Dark red solid (1.94 g, 31%). 1-H NMR (400 MHz; CDCl3): δ 8.48-8.44 (m, 2H), 7.74-7.68 (m, 1H), 7.67-7.50 (m, 6H), 7.31-7.24 (m, 9H), 7.03-6.98 (m, 2H), 6.74-6.71 (m, 1H), 3.53-3.49 (m, 4H), 3.39-3.05 (m, 31H), 2.20-2.11 (m, 1H), 1.64-1.43 (m, 8H), 1.36-1.10 (m, 36H), 0.83-0.79 (m, 1H)

5b *1-(4-Sulfonatobutyl)-4-[ß-[2-(N-octyl,6-hydroxyhexylamino)-6-naphthyl]vinyl] pyridinium betaine*: Black waxy solid (695 mg, 15%). 1-H NMR (400 MHz; MeOD): δ 8.70 (t, J = 5.2, 2H), 8.12-7.93 (m, 4H), 7.75-7.72 (m, 2H), 7.62-7.60 (m, 1H), 7.37-7.32 (m, 1H), 7.17-7.14 (m, 1H), 6.89-6.87 (m, 1H), 4.85-4.77 (m, 22H), 4.71-4.65 (m, 2H), 3.52-3.43 (m, 4H), 3.27-3.23 (m, 42H), 3.20-2.96 (m, 8H), 2.86-2.81 (m, 2H), 2.72-2.67 (m, 3H), 2.46-2.38 (m, 2H), 1.75-1.62 (m, 6H), 1.52-1.21 (m, 23H), 0.93-0.86 (m, 3H)

5c *1-(4-Sulfonatobutyl)-4-[ß-[2-(di-N-10-hydroxydecylamino)-6-naphthyl]vinyl] pyridinium betaine*: Dark red solid (1.5 g, 60%). 1-H NMR (400 MHz; MeOD): δ 8.70 (d, J = 6.6, 2H), 8.09 (d, J =

6.6, 2H), 8.00 (d, J = 16.1, 1H), 7.73 (d, J = 9.0, 2H), 7.60 (d, J = 8.7, 1H), 7.33 (d, J = 16.0, 1H), 7.15-7.12 (m, 1H), 6.85 (s, 1H), 4.67 (t, J = 7.2, 2H), 3.65-3.54 (m, 16H), 3.44 (s, 4H), 3.34 (s, 9H), 2.89-2.84 (m, 17H), 2.42 (t, J = 7.0, 2H), 2.30 (d, J = 28.1, 14H), 1.67 (s, 2H), 1.67-1.58 (m, 4H), 1.55 (d, J = 6.3, 1H), 1.43-1.31 (m, 15H), 0.89 (t, J = 6.2, 3H)

5d *N-(3-trimethylammoniumpropyl)-4-[ß-[2-(di-N-8-hydroxyoctylamino)-6-naphthyl]vinyl] pyridinium dibromide*: Black powder (335 mg, 31%). 1-H NMR (400 MHz; MeOD): δ 8.75 (d, J = 6.8, 2H), 8.16 (d, J = 6.8, 2H), 7.94 (s, 1H), 7.74 (d, J = 8.9, 2H), 6.86 (d, J = 1.8, 1H), 4.75-4.73 (m, 10H), 4.59 (t, J = 7.6, 2H), 3.57-3.42 (m, 10H), 3.34-3.24 (m, 19H), 3.23-3.16 (m, 8H), 1.67 (t, J = 0.5, 2H), 1.67-1.64 (m, 2H), 1.54-1.47 (m, 4H), 1.47 (d, J = 2.8, 7H)

5e *N-(3-trimethylammoniumpropyl)-4-[ß-[2-(di-N-10-hydroxydecylamino)-6-naphthyl]vinyl] pyridinium dibromide*: Black solid (900 mg, 60%). 1-H NMR (400 MHz; CDCl3): δ 8.38-8.30 (m, 2H), 7.73-7.54 (m, 4H), 7.38-7.26 (m, 2H), 6.95-6.87 (m, 1H), 4.31-4.24 (m, 7H), 4.23-4.16 (m, 2H), 3.28-2.98 (m, 11H), 2.64-2.57 (m, 2H), 1.93-1.83 (m, 2H), 1.61-1.51 (m, 2H), 1.41-0.90 (m, 33H)

5f *N-(3-trimethylammoniumpropyl)-4-[ß-[2-(di-N-12-hydroxydodecylamino)-6-naphthyl] vinyl]pyridinium dibromide*: Black solid (1.02 g, 78%). 1-H NMR (400 MHz; MeOD): δ 8.79-8.76 (m, 2H), 8.16 (d, J = 6.8, 2H), 8.08-8.04 (m, 1H), 7.94 (s, 1H), 7.73 (d, J = 8.9, 2H), 7.61 (d, J = 8.7, 1H), 7.37 (d, J = 16.0, 1H), 7.16-7.13 (m, 1H), 6.86 (d, J = 1.3, 1H), 4.62-4.58 (m, 2H), 3.58-3.41 (m, 11H), 3.16-3.13 (m, 13H), 2.61-2.54 (m, 2H), 1.68-1.62 (m, 4H), 1.55-1.26 (m, 37H)

2.2.2 Synthesis of Phosphate Prodyes

The compounds 5c-f (Figure 2-11) represent the activated, amphiphilic dye that binds into the membrane core, whilst compounds 6 and 7a-c (Figure 2-12) are the desired prodyes. The strong amphiphilic character of the membrane-binding compounds, although a necessary trait, severely restricts the range of solvents that can be used during phosphorylation, and this in turn limits the type of reactions that can be performed. A variety of phosphorylation routes were tested on compound 6, starting with dimethyl chlorophosphate in pyridine , utilized for the synthesis of the first generation of prodyes [12], and regularly used for phosphorylation of long-chain terminal alcohols [56]. However the very poor solubility of compound 6 in pyridine resulted in no detectable product. Further phosphorylation methods were attempted, including phosphoryl chloride in pyridine and acetonitrile [57], tetramethylammonium di-tert-butylphosphate in 1,2-dimethoxyethane [58], and the conversion of the alcohol to the tosylate followed by treatment with tetra-N-butylammonium phosphate in acetonitrile or chloroform [59,60]. However, solubility issues precluded the successful synthesis of the prodyes based on compound 6.

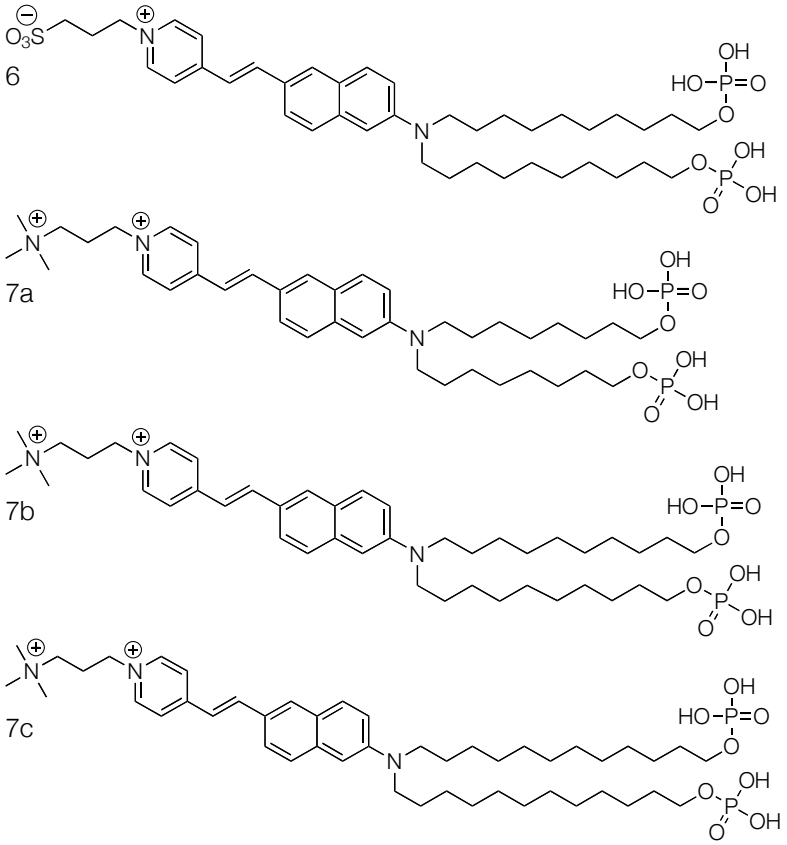

Figure 2-12 Phosphate prodyes with a range of tail lengths, which were the synthetic targets of this project.

2.2 SYNTHESIS OF THE PRODYES

Trialing the same phosphorylation techniques listed above with compound 7a resulted in success with the use of phosphoryl chloride in acetonitrile, a solvent in which the dicationic dye was partially soluble. Although the yield for the 8-carbon prodye was met with very low yields (~2%), the yield for the longer tailed reactants increased to ~3.6% for the 10-chain 5b compound, and 29% for the 12-chain 5c prodye. Compound 7c was synthesized in the following manner:

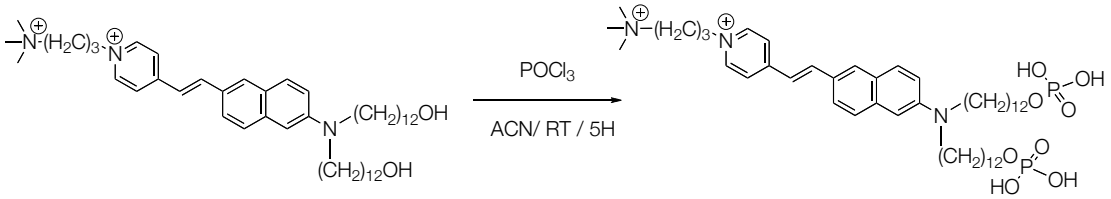

N-(3-trimethylammoniumpropyl)-4-[ß-[2-(di-N-12-phosphonooxydodecylamino)-6-naphthyl]vinyl]pyridinium dibromide (**7c**): Into 25 ml RBF containing a red solution of compound 5f (200 mg, 2.3 mmol) in 10 ml dry ACN, there was added $POCl_3$ (420 µl, 4 mmol), at which point the solution turned yellow, and the reaction vessel flushed with argon and stirred at RT for 5 h. At the end of this period, the yellow solution was added to 20 ml Et_2O, upon which a yellow oil precipitated. The oil was washed with 3x 10 ml Et_2O, and then dissolved in 5 ml H_2O. The addition of a small amount of 1 M HCl added dropwise caused the precipitation of a dark red solid that was washed and sonicated with 3x 10 ml n-propanol containing 3 drops conc. NH_3, and then washed once with 5 ml acetone, to yield a black solid (70 mg, 29%) 1-H NMR (400 MHz; D_2O): δ 8.90-8.73 (m, 2H), 8.03-7.83 (m, 2H), 7.82-7.63 (m, 2H), 7.63-7.43 (m, 2H), 7.39-7.25 (m, 1H), 4.91-4.49 (m, 25H), 3.78-3.40 (m, 6H), 3.30-3.03 (m, 10H), 3.03-2.71 (m, 4H), 2.61-2.40 (m, 2H), 1.49-1.27 (m, 5H), 1.25-0.39 (m, 35H).

7a *N-(3-trimethylammoniumpropyl)-4-[ß-[2-(di-N-8-phosphonooxyoctylamino)-6-naphthyl]vinyl]pyridinium dibromide*: Black solid, (12 mg, 1.2%), 1-H NMR (400 MHz; MeOD): δ 7.75 (d, J = 1.8, 1H), 7.57-7.44 (m, 3H), 7.32 (dd, J = 8.8, 2.0, 1H), 7.10 (dd, J = 9.1, 2.6, 1H), 6.80 (d, J = 2.2, 1H), 4.80 (s, 1H), 4.11-4.06 (m, 2H), 3.38-3.29 (m, 7H), 1.66-1.55 (m, 7H), 1.50-1.21 (m, 8H), 0.99-0.87 (m, 10H)

7b *N-(3-trimethylammoniumpropyl)-4-[ß-[2-(di-N-10-phosphonooxydecylamino)-6-naphthyl]vinyl]pyridinium dibromide*: Black solid, (22 mg, 3.6%), 1-H NMR (400 MHz; MeOD): δ 8.71-8.67 (m, 2H), 8.13-7.65 (m, 7H), 7.41-7.23 (m, 3H), 4.58-4.47 (m, 2H), 3.88-3.22 (m, 21H), 2.89-2.69 (m, 3H), 2.16-2.10 (m, 2H), 1.85-0.85 (m, 42H)

2.2.3 Synthesis of N-Phosphonooxymethyl Prodyes

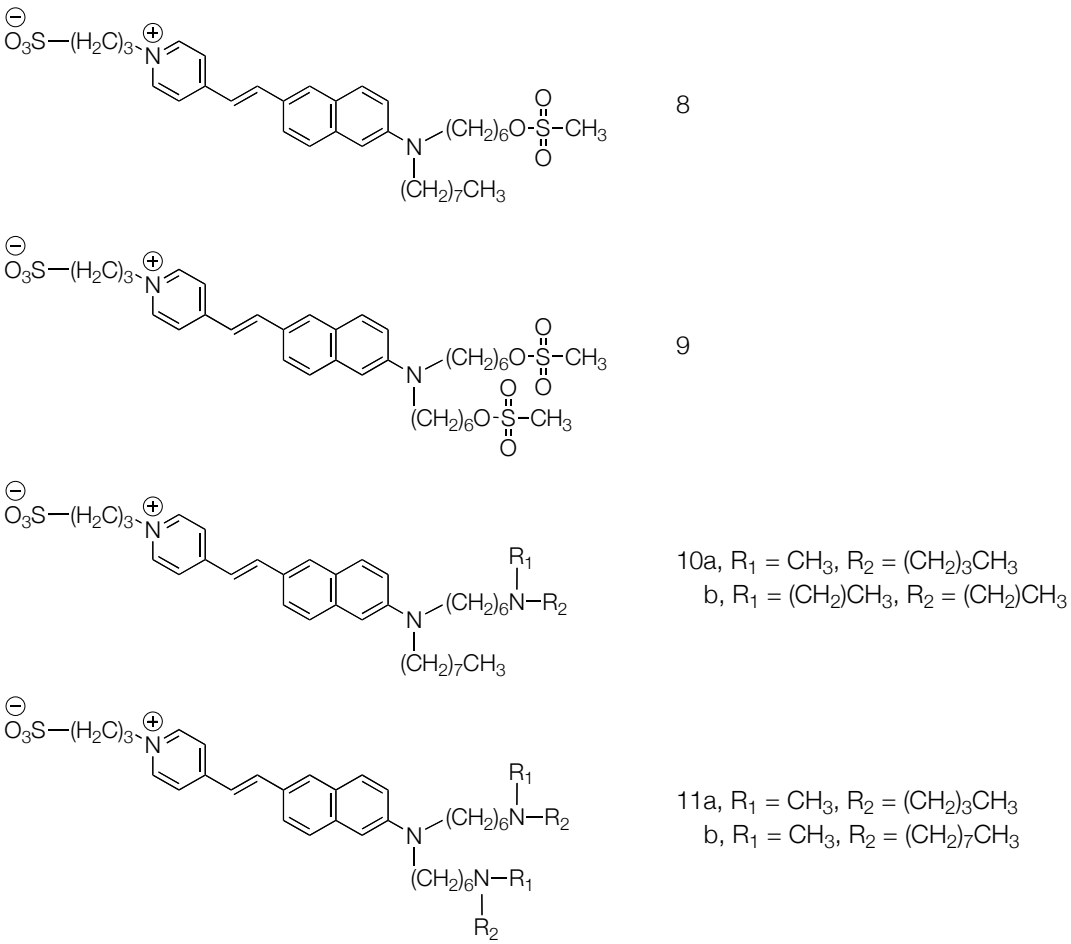

Figure 2-13 Intermediates in the synthesis of N-phosphonooxymethyl prodyes.

The synthesis of the N-phosphonooxymethyl prodyes required the conversion of the terminal alcohols to a good leaving group; unfortunately, the standard tosylation via tosyl chloride in either dichloromethane [61], pyridine [59] or acetonitrile [62] produced very low yields. Solvent-free mesylation, however yielded very good results, at around ~90% yield for all of the alcohol intermediates tested [63].

The mesylated intermediates were then used to alkylate various secondary amines, forming the target dyes that binds into the cell membrane. Methyl butylamine, and methyl octylamine formed the long-chain dyes. This selection places the quaternary amine's cationic charge near the middle of the lipophilic tail. This was chosen so as to prevent the aliphatic tail 'folding back' on itself, thereby hindering the insertion of the phosphorylated prodye into the membrane, Figure 2-14. This mechanism is suspected to be the cause of the poor selectivity of the preceding model prodyes [11].

2.2 SYNTHESIS OF THE PRODYES

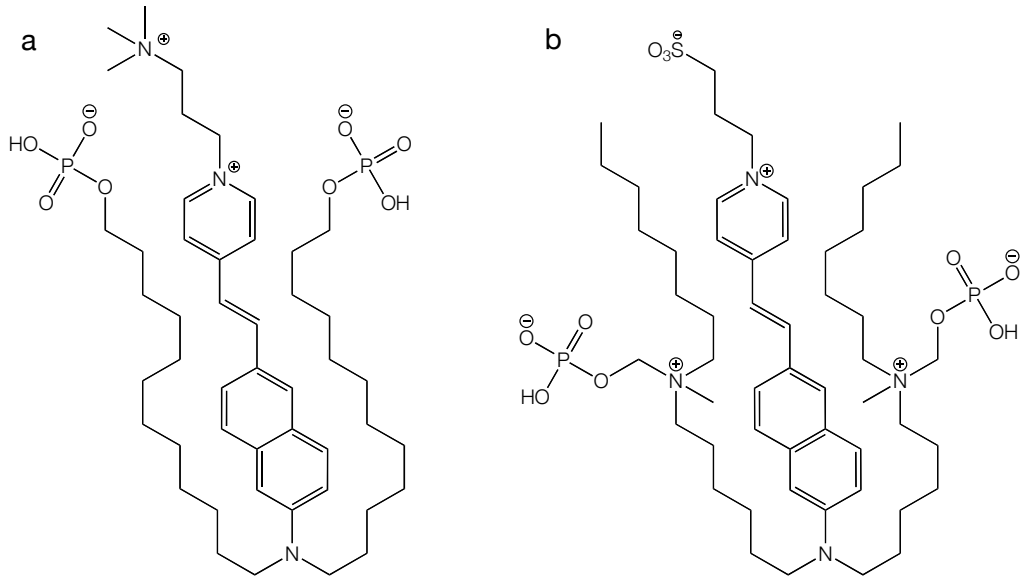

Figure 2-14 Prodye conformations; a) the phosphorylated prodye may still embed into the hydrophobic core of the lipid membrane, if the tails "fold-back", exposing the central lipophilic region of the prodye. b) The N-phosphonooxymethyl prodye cannot form such an amphiphilic conformation.

Dyes with a single modified tail based on diethylamine were synthesized in parallel, to determine the most efficient prodye, in terms of binding difference, solubility and substrate activity. The N-phosphonooxymethylation was performed with di-tert-butyl chloromethyl phosphate [35-37], in acetonitrile. The other aprotic solvents were tested for this reaction were dimethyl sulfoxide, dimethylformamide and tetrahydrofuran, however, only with acetonitrile was the correct product detected. The lack of solubility of the dicationic dyes prevented the synthesis of these corresponding series of prodyes.

The synthesis of di-tert-butyl chloromethyl phosphate was initially performed as described in the original paper [35], however low yields (~10%) of the material led us to use a second published procedure, (US Patent 6,362,172, Water Soluble Prodrugs of Azole Compounds), giving rise to yields of over 70%.

1-(4-Sulfonatobutyl)-4-[ß-[2-(di-N-(6-methylsulfonyloxy)hexylamino)-6-naphthyl]vinyl] pyridinium betaine (**9**): A flask containing compound 5a, (230 mg, 0.4 mmol), and methanesulfonyl anhydride (2.8 g, 16 mmol), was heated to 65°C, and stirred for 72 h. Upon cooling to room temperature, the mixture was dissolved in a minimal dry DCM, and mixed with 25 ml Et_2O. The suspended product was centrifuged down, and the pellet dissolved and purified with 50:20:4 $CHCl_3$/MeOH/H_2O on SiO_2, producing a black powder (180 mg, 62%).
1-H NMR (400 MHz; CDCl3): δ 9.52-9.42 (m, 4H), 8.03-7.93 (m, 2H), 7.88-7.84 (m, 1H), 7.83-7.52 (m, 8H), 7.38-7.29 (m, 6H), 7.07-7.04 (m, 1H), 4.04-4.00 (m, 2H), 3.64-3.31 (m, 7H), 3.04- 2.88 (m, 7H), 2.69 (s, 6H), 2.44-2.23 (m, 6H), 1.99-1.49 (m, 24H), 1.48-1.16 (m, 25H), 1.02-0.73 (m, 12H)

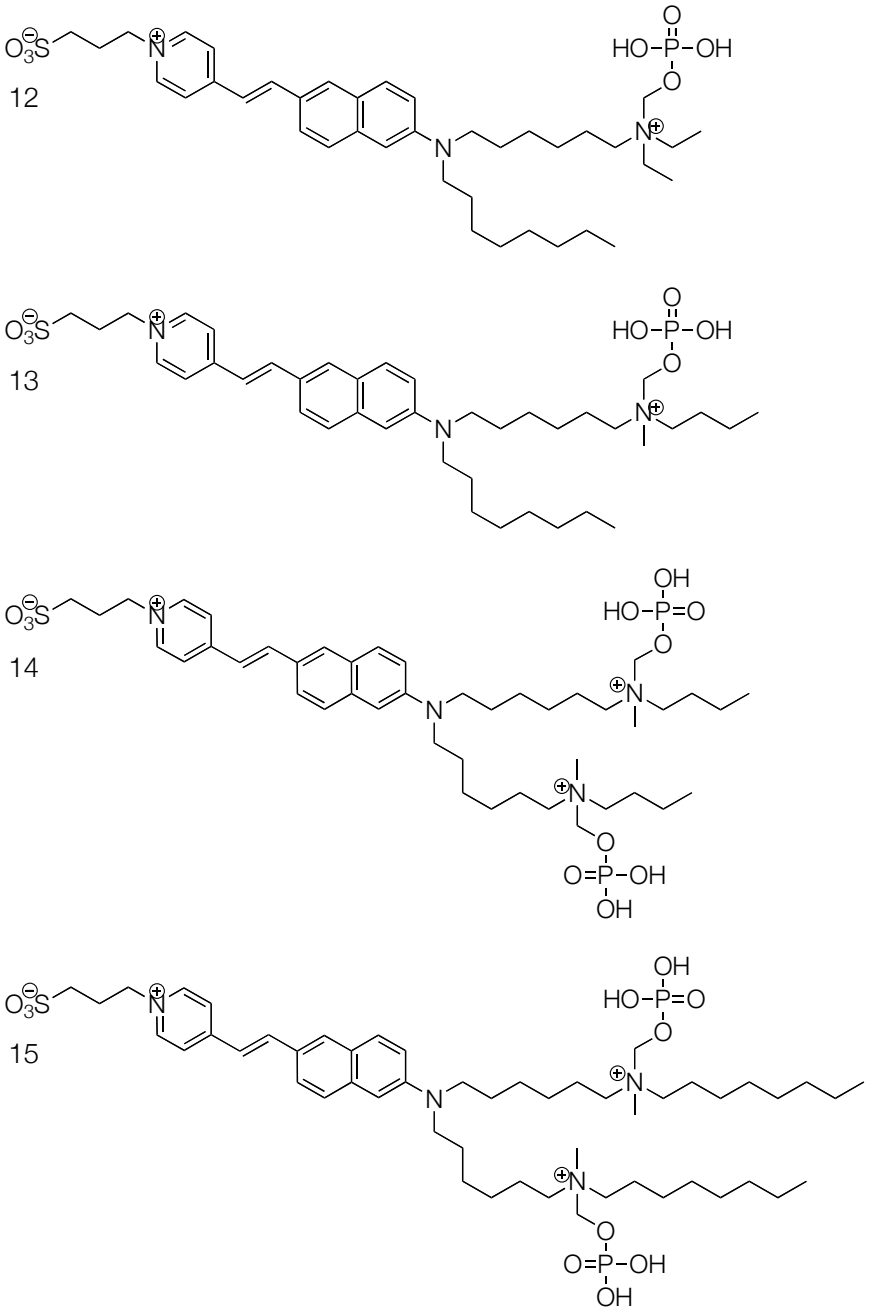

Figure 2-15 N-phosphonooxymethyl prodyes synthesized for this thesis.

1-(4-Sulfonatobutyl)-4-[ß-[2-(di-N-(6-(methyl(octyl)amino)hexyl)amino)-6-naphthyl]vinyl] pyridinium betaine (**11b**): Compound 9 (400 mg, 0.6 mmol), and N-methyloctan-1-amine (687 mg, 4.8 mmol), were dissolved in 10 ml ACN, the flask flushed with argon, and stirred at 50°C for 72 h. The solvent was decanted off, and the mixture dissolved and purified on SiO2 50:20:4 $CHCl_3$/MeOH/H_2O to yield a dark red tar (210 mg, 46.5 %). 1-H NMR (400 MHz; CDCl3): δ 8.82-8.81 (m, 1H), 7.82-7.74 (m, 2H), 7.65-7.62 (m, 1H), 7.50 (d, J = 0.4, 1H), 6.99-6.91 (m, 1H), 4.79 (d, J = 0.8, 1H), 3.32 (t, J = 0.3, 3H), 2.48-2.29 (m, 10H), 1.61-1.60 (m, 1H), 1.59-1.54 (m, 2H), 1.53-1.36 (m, 30H), 0.84 (s, 6H).

2.2 SYNTHESIS OF THE PRODYES

1-(4-Sulfonatobutyl)-4-[ß-[2-(di-N-(6-(methyl(octyl)(phosphonooxymethyl) ammonio)hexyl)amino)-6-naphthyl]vinyl] pyridinium betaine (**15**): A solution of compound 11b (89 mg, 0.11 mmol), together with di-tert-butyl chloromethyl phosphate (284 mg, 1.1 mmol), and 1,2,2,6,6-pentamethylpiperidine (198 µl, 1.1 mmol), in 2.3 ml ACN was stirred under argon at 50°C overnight. The solvents were removed under reduced pressure, and 1 ml 10% TFA in H2O was added, and the mixture stirred for 24 h. The TFA was removed under reduced pressure, and the mixture basified with 3 drops of 8% NH_3, changing the solution from a pale orange to a dark red color. The product was purified on a Prontosil 120-20-C18-AQ (Bischoff) column with a 10 mmol ammonium acetate/ACN gradient, and lyophilized to yield a dark red powder (4 mg, 3.5%, 2 steps). 1-H NMR (400 MHz; MeOD): δ 8.55 (dd, J = 7.2, 4.6, 1H), 7.84-7.76 (m, 1H), 7.61-7.47 (m, 2H), 7.37-7.29 (m, 5H), 7.05-6.95 (m, 1H), 6.68 (dd, J = 1.0, 0.5), 4.77-4.66 (m, 2H), 3.91-3.77 (m, 24H), 3.38-3.30 (m, 3H), 3.28-3.20 (m, 6H), 3.16-3.12 (m, 2H), 3.09-3.04 (m, 2H), 2.88-2.81 (m, 3H), 2.76-2.71 (m, 1H), 2.34-2.26 (m, 1H), 1.96-1.84 (m, 2H), 1.63-1.56 (m, 6H), 1.39-1.32 (m, 7H), 1.22-1.13 (m, 18H), 0.77-0.72 (m, 4H)

8 *1-(4-Sulfonatobutyl)-4-[ß-[2-(N-octyl,(6-methylsulfonyloxyhexyl)amino)-6-naphthyl]vinyl] pyridinium betaine*: Dark red solid (477 mg, 80%). 1-H NMR (400 MHz; MeOD): δ 7.90 (s, 5H), 7.69-7.59 (m, 3H), 7.58 (d, J = 7.3, 1H), 7.22 (d, J = 15.9, 2H), 7.10 (d, J = 0.4, 1H), 6.81 (t, J = 0.5, 1H), 4.59 (d, J = 13.5, 2H), 4.21 (d, J = 12.5, 2H), 2.38 (d, J = 13.6, 2H), 1.74-1.52 (m, 7H), 1.20-1.19 (m, 18H), 1.18-1.05 (m, 2H), 1.04-0.79 (m, 6H)

10a *1-(4-Sulfonatobutyl)-4-[ß-[2-(N-(6-(butyl(methyl)amino)hexyl)(octyl)amino)-6-naphthyl] vinyl] pyridinium betaine*: Dark red solid (144 mg, 74%). 1-H NMR (400 MHz; MeOD): δ 8.63 (d, J = 6.3, 2H), 8.03-7.89 (m, 4H), 7.66 (dd, J = 47.4, 9.0, 3H), 7.29 (d, J = 16.1, 1H), 7.15 (dd, J = 9.1, 1.8, 1H), 6.87 (s, 1H), 4.59 (t, J = 7.1, 2H), 3.50-3.43 (m, 4H), 3.08 (dt, J = 15.4, 7.5, 4H), 2.91-2.76 (m, 8H), 2.38 (quintet, J = 6.9, 2H), 1.69 (dd, J = 15.3, 7.2, 9H), 1.48-1.25 (m, 21H), 1.00-0.87 (m, 7H)

10b *1-(4-Sulfonatobutyl)-4-[ß-[2-(N-(6-(diethylamino)hexyl)(octyl)amino)-6-naphthyl]vinyl] pyridinium betaine*: Dark red solid (190mg, 99%). 1-H NMR (400 MHz; MeOD): δ 8.68-8.60 (m, 2H), 8.09-7.58 (m, 7H), 7.30-7.14 (m, 2H), 6.87 (s, 1H), 4.88-4.81 (m, 3H), 4.58 (t, J = 7.2, 2H), 3.47 (dt, J = 10.7, 7.5, 3H), 3.34-3.29 (m, 2H), 3.13 (dq, J = 41.7, 8.1, 5H), 2.90-2.81 (m, 1H), 2.37 (quintet, J = 6.9, 2H), 1.87-1.66 (m, 4H), 1.48-1.22 (m, 19H), 0.96-0.87 (m, 3H)

11a *1-(4-Sulfonatobutyl)-4-[ß-[2-(di-N-(6-(methyl(butyl)amino)hexyl)amino)-6-naphthyl] vinyl]pyridinium betaine*: Dark red solid 943 mg, 24%). 1-H NMR (400 MHz; MeOD): δ 7.58 (d, J = 6.3, 2H), 7.00-6.96 (m, 2H), 6.95-6.89 (m, 2H), 6.77-6.72 (m, 2H), 6.66-6.64 (m, 1H), 6.26-6.19 (m, 2H), 5.91 (d, J = 0.4, 1H), 3.90-3.82 (m, 5H), 3.57-3.53 (m, 2H), 3.31 (q, J = 6.4, 2H), 2.57-2.49 (m, 5H), 2.38 (dd, J = 15.3, 2.2, 4H), 2.25-2.18 (m, 2H), 2.16-2.08 (m, 5H), 1.93-1.83 (m, 6H), 1.83-1.74 (m, 4H), 1.44-1.41 (m, 1H),

1.40-1.37 (m, 1H), 0.85-0.81 (m, 4H), 0.80-0.69 (m, 9H), 0.61-0.46 (m, 12H), 0.45-0.41 (m, 1H), 0.36-0.32 (m, 1H), 0.08-0.01 (m, 4H)

12 *1-(4-Sulfonatobutyl)-4-[ß-[2-(6-((6-(diethyl(phosphonooxymethyl)ammonio)hexyl)(octyl) amino)-6-naphthyl]vinyl] pyridinium betaine*: Black powder (6 mg, 3%). 1-H NMR (400 MHz; MeOD): δ 8.72-8.63 (m, 2H), 8.07 (d, J = 6.0, 2H), 7.74-7.67 (m, 3H), 7.65-7.60 (m, 1H), 7.33 (d, J = 16.0, 1H), 7.20-7.13 (m, 1H), 4.89-4.88 (m, 7H), 4.66-4.60 (m, 1H), 4.28-4.20 (m, 1H), 3.49 (t, J = 6.0, 1H), 3.47-3.44 (m, 2H), 3.35 (d, J = 7.7, 7H), 3.17 (td, J = 15.0, 8.2, 4H), 3.07 (t, J = 6.8, 1H), 2.85 (q, J = 6.8, 7H), 2.41 (q, J = 6.7, 1H), 1.93-1.87 (m, 2H), 1.82-1.56 (m, 9H), 1.55-1.19 (m, 35H), 1.02-0.81 (m, 8H)

13 *1-(4-Sulfonatobutyl)-4-[ß-[2-(6-((6-(butyl(methyl)(phosphonooxymethyl)ammonio)hexyl) (octyl)amino)-6-naphthyl]vinyl] pyridinium betaine*: Black powder (67 mg, 66%). 1-H NMR (400 MHz; MeOD): δ 8.71 (d, J = 6.7, 2H), 8.13-8.00 (m, 3H), 7.94-7.93 (m, 1H), 7.74 (dd, J = 8.8, 6.4, 2H), 7.62 (d, J = 8.8, 1H), 7.35 (d, J = 16.0, 1H), 7.17-7.14 (m, 1H), 6.88 (t, J = 3.1, 1H), 4.94-4.74 (m, 32H), 4.73-4.65 (m, 3H), 3.52-3.18 (m, 62H), 3.05-2.94 (m, 5H), 2.91-2.83 (m, 3H), 2.47-2.38 (m, 3H), 1.81-1.62 (m, 10H), 1.53-1.24 (m, 21H), 1.03-0.87 (m, 7H)

14 *1-(4-Sulfonatobutyl)-4-[ß-[2-(di-N-(6-(butyl(methyl)(phosphonooxymethyl)ammonio) hexyl)amino)-6-naphthyl]vinyl] pyridinium betaine*: Black solid (4 mg, 2.6 %) 1-H NMR (400 MHz; MeOD): δ 8.62 (s, 2H), 8.02-7.88 (m, 4H), 7.72-7.70 (m, 2H), 7.60 (d, J = 8.5, 1H), 7.28 (d, J = 15.9, 1H), 7.15 (d, J = 8.7, 1H), 6.87 (s, 1H), 4.59 (d, J = 5.6, 2H), 3.47 (t, J = 7.0, 4H), 3.34-3.29 (m, 4H), 2.84-2.66 (m, 10H), 2.45-2.44 (m, 6H), 2.44-2.36 (m, 3H), 1.69-1.51 (m, 12H), 1.43-1.23 (m, 15H), 0.96-0.90 (m, 6H)

2.2.4 Naming Convention

Taking direction from Loew and Hinner [12,19], the synthesized voltage sensitive dyes have been named with the following convention: The tail of the dye is first referenced by the chain length and a single letter representing the functional group, followed by the chromophore and then head group, which are formed by an acronym that has been used to describe the Amino Naphthyl (vinyl in *Entgegen*) Pyridinium chromophores (ANEP), with both the dicationic Propane Quaternary amine (PQ) or Propane Sulfonato (PS) head group.

Compound	Dye Name	Compound	Prodye Name
5d	Di-8A-ANEPPQ	7a	Di-8P-ANEPPQ
5e	Di-10A-ANEPPQ	7b	Di-10P-ANEPPQ
5f	Di-12A-ANEPPQ	7c	Di-12P-ANEPPQ
10a	8-2,2N6-ANEPPS	12	8-2,2P6-ANEPPS
10b	8-1,4N6-ANEPPS	13	8-1,4P6-ANEPPS
11a	Di-1,4N6-ANEPPS	14	Di-1,4P6-ANEPPS
11b	Di-1,8N6-ANEPPS	15	Di-1,8P6-ANEPPS

Table 1 Abbreviated dye and prodye names used in this thesis

2.2.5 Aqueous Solubility

Due to the very low amounts of the prodyes produced, measuring accurate aqueous solubilities of the various compounds was not undertaken. However, both the phosphate and alcohol dyes have demonstrated low solubility in water. In order to bring the phosphate prodyes into aqueous solution, it was necessary to first dissolve the prodyes in minimal 2.5% aqueous ammonia (~2 µl/mg), before preparing buffered stock solutions for cell staining.

All four N-phosphonooxymethyl prodyes were extremely soluble in water, and were also found to be slightly hygroscopic. The precursor amine dyes, on the other hand, were found to be highly insoluble in water. These very strong differences in solubility indicate good potential for selective cell staining, as the solubility differences are due solely to differences in the chemistry of tail region of the prodye and dye.

2.3 Future Directions

At the time of the writing of this thesis, two new versions of the N-phosphonooxymethyl dyes are being synthesized, in order to modify of the pH range at which the dye can bind, as discussed in Chapter 3. The pKb of a tertiary aliphatic amine is in the range of pH 9.8 to 10.5, depending on the substituents, with a pH of approximately 10.05 for the methyl octylamine version of the dye synthesized in this project. This value is above the physiological pH of the central nervous systems; using an appropriate biological pH would also lead to the protonated form of the amine dye being the dominant species, preventing correct membrane insertion.

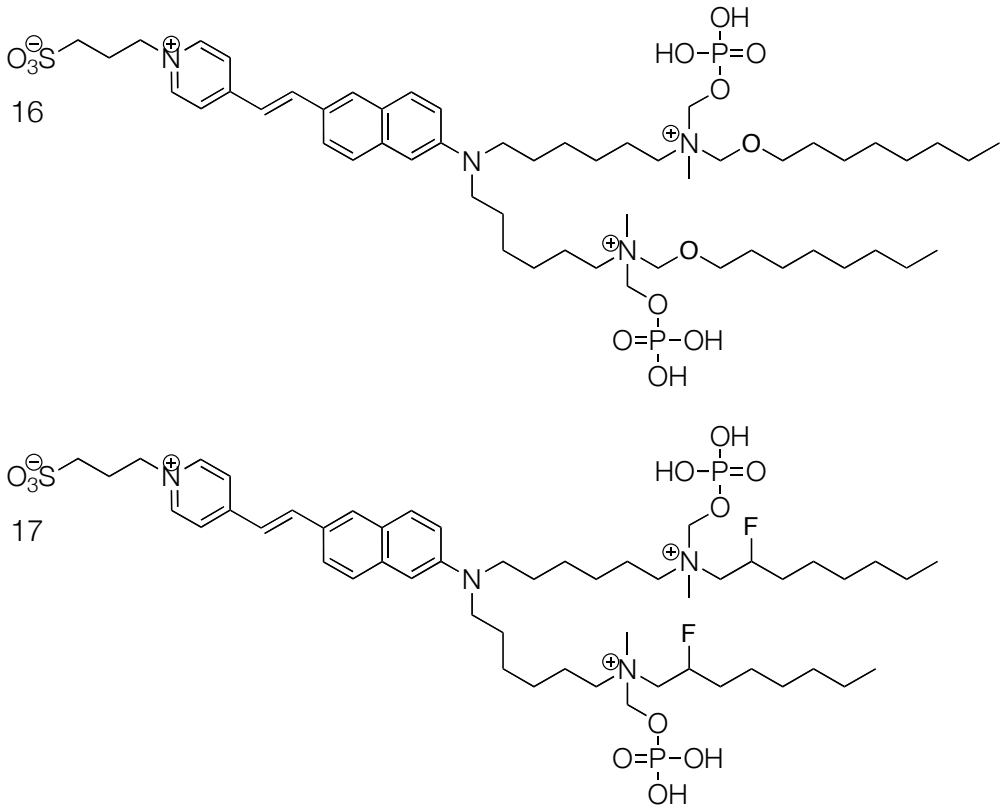

Figure 2-16 Modified dyes designed to bind to lipid membrane at a lower pH.

In order to overcome this, strategies to lower the pKb were attempted, as shown in Figure 2-16, with compound 16 containing an ether bridge, and compound 17 being the fluorinated version of the dye. In both cases, the calculated pKb of the resulting tertiary amine was found to be ~pH 7.5. Compound 17 has been prepared via the ring-opening of the of an epoxide [64], to form the correct fluorinated secondary amine, that was then used in the same manner as the synthesis of Di-1,8P6-ANEPPS. This new material will be used for further studies into selective membrane staining at physiological pH.

2.3 FUTURE DIRECTIONS

The replacement of the prodye's chromophore could yield a more sensitive system; the ANNINE dyes have been show to give a -ΔF/F of up to 70%/100 mV with 2-photon excitation [26]. The ANEPPS chromophore was used in this project due to its ease of synthesis, and parallel to this project, initial modification to the ANNINE synthesis to allow tail modifications have begun. However, modifications to the ANNINE chromophore itself might lead to an even more desirable targetable dye. Commonly used VSD chromophores have been systematically modified [21], giving general rules on emission and excitation spectra modification. The modification of the ANNINE6 chromophore to increase the emission and excitation wavelength towards the red would improve its *in vivo* application, as longer wavelength light is better able to penetrate tissue, suffering from less scattering.

Further work on the head-group of the dye is also justified; charge modification is known to influence dye toxicity and the ability of the compound to diffuse into tissue. The synthesis of a dicationic head-group prodye would increase the solubility of the prodye without affecting the binding ability of the activated dye [27]. This target compound was not produced, due to the low-solubility of the precursor in acetonitrile, the solvent best suited for the N-phosphonooxymethylation step. Further experimentation with other solvents, or the modification of the reaction scheme, so as to add the head-group after tail modification may allow for the successful synthesis of this prodye.

3 PHOSPHATASE EXPRESSION SYSTEM

In order to utilize the synthesized water-soluble prodyes for the selective staining of genetically specified cells, it is necessary to express an active phosphatase on the surface of the plasma membrane in this defined population of cells. The phosphatase should be nontoxic, and not affect the development or function of neurons, and show strong de-phosphorylation activity towards the prodye under acceptable physiological conditions. It is also important to be able to identify phosphatase-expressing cells in the presence of non-transfected cells in mixed cell cultures, in order to easily analyze the levels of unspecific cell membrane staining. Such a cell marker must not interfere with the expression or activity of the phosphatase, should not affect the binding or measurement of the voltage sensitive dye, and must also be tightly correlated to the expression level of the phosphatase. Finally, the ability to exchange the type of phosphatase enzyme expressed, without varying the expression levels or cell type in stably transfected cells, would allow a direct comparison of enzyme activity. This chapter describes the development of a system that satisfies all of the criteria listed above, and demonstrates its successful use in the selective staining of mammalian cells.

3.1 System Components

3.1.1 Alkaline Phosphatase

Alkaline phosphatase (AP), is a type of hydrolase enzyme which cleaves the phosphate groups from a wide variety of substrates, such as nucleotides, proteins and alkaloids, in a process termed ‘dephosphorylation’, described by Enzyme Commission number EC 3.1.3.1. These enzymes are most active at high pH, most often between 8.0 and 9.0, and require Zinc or Magnesium as a cofactor, where the metal ion forms the site of catalytic activity.

There are a number of uses for alkaline phosphatases in research; such as antibody labeling in *E*nzyme-*L*inked *I*mmunosorbant *A*ssays (ELISA); and as a tool in molecular biology, where it is used to remove the 5’ phosphate from linear DNA to prevent unwanted ligation or for later replacement with radioactive phosphate groups for radiolabeling. Standard laboratory protocols make use of the following four enzymes: *B*acterial *A*lkaline *P*hosphatase (BAP), from *Escherichia coli* C4 cells; *S*hrimp *A*lkaline *P*hosphatase (SAP), from the arctic shrimp *Pandalus borealis*; *C*alf *I*ntestinal alkaline *P*hosphatase (CIP), and human *PL*acental *A*lkaline *P*hosphatase (PLAP) and its C terminally truncated version, lacking the last 24 amino acids that contain its glycosyl-phosphatidylinositol anchor, *SE*creted *A*lkaline *P*hosphatase (SEAP).

These different phosphatases are selected for their various properties, the most important being their denaturation temperature, optimal pH and cellular location. Of these four, all are globular secreted proteins, with the exception of PLAP, which is bound to the plasma membrane, and was therefore selected for use in this project.

Human PLAP is a commonly used marker for the genetic labeling of cells for histochemical analysis. Together with GFP and ß-lactamase, it is one of the key marker genes in current molecular biology. PLAP is a 1611 bp gene, first cloned and expressed in mammalian cells in 1987 [65]. It is a Glycosylphosphatidylinositol (GPI) anchored enzyme, located on the outer plasma membrane [66-68]. It has been used to mark cell lineages in mouse retinal neurons [69-71], where it was found to be non-toxic, and localized to the surface of the neurons. In the brain, PLAP expressing neurons show enzymatic activity along the length of unmyelinated and myelinated axons, as well as dendritic arborization [71]. This localization ensures that prodye activation would occur at the entire surface of the genetically specified neuron, a strong requirement for the project, as voltage sensitive dyes are thought not to diffuse laterally though the plasma membrane [72]. Stable long-term expression of PLAP has also been shown in neurons transplanted into the CNS from transgenic rats [73], further demonstrating its lack of toxicity. Furthermore, ubiquitous expression of human PLAP in mice showed no adverse effects on mouse development or viability [74]; due to the high pH required by this enzyme, there is no appreciable activity at physiological pH.

PLAP accepts a wide range of mono- or polyphosphorylated substrates [75]. Alkaline phosphatase histochemistry has four commonly used techniques; the Gomori method, BCIP/NBT, ELF-97 phosphate, naphthol AS-MX phosphate coupled with Fast Blue BB (colored) and Fast Red TR (fluorescent) diazonium salts [76]. Each of there techniques involves the formation of a colored or fluorescent precipitate at the site of the substrate de-phosphorylation, unlike the targeted staining of cells with membrane-binding amphiphilic dye [11,12]. Both BCIP/NBT and ELF-97 phosphate were also used in this project as controls, for determining the correct expression of PLAP in genetically targeted cells. BCIP (5-*B*romo-4-*C*hloro-3-*I*ndolyl-*P*hosphate), and NBT (*N*itro-*B*lue *T*etrazolium Chloride), are used together as purple chromogenic mixture used for in situ labeling of fixed tissue, where the precipitate-forming phosphatase substrate BCIP work in conjunction with NBT as an electron acceptor. For more sensitive detection of PLAP, the fluorogenic substrate ELF-97 phosphate was used. The conversion to ELF-97 alcohol by PLAP yields a bright yellow-green fluorescent precipitate at the site of enzymatic activity, visible by fluorescence microscopy [76], and more photostable than fluorescein.

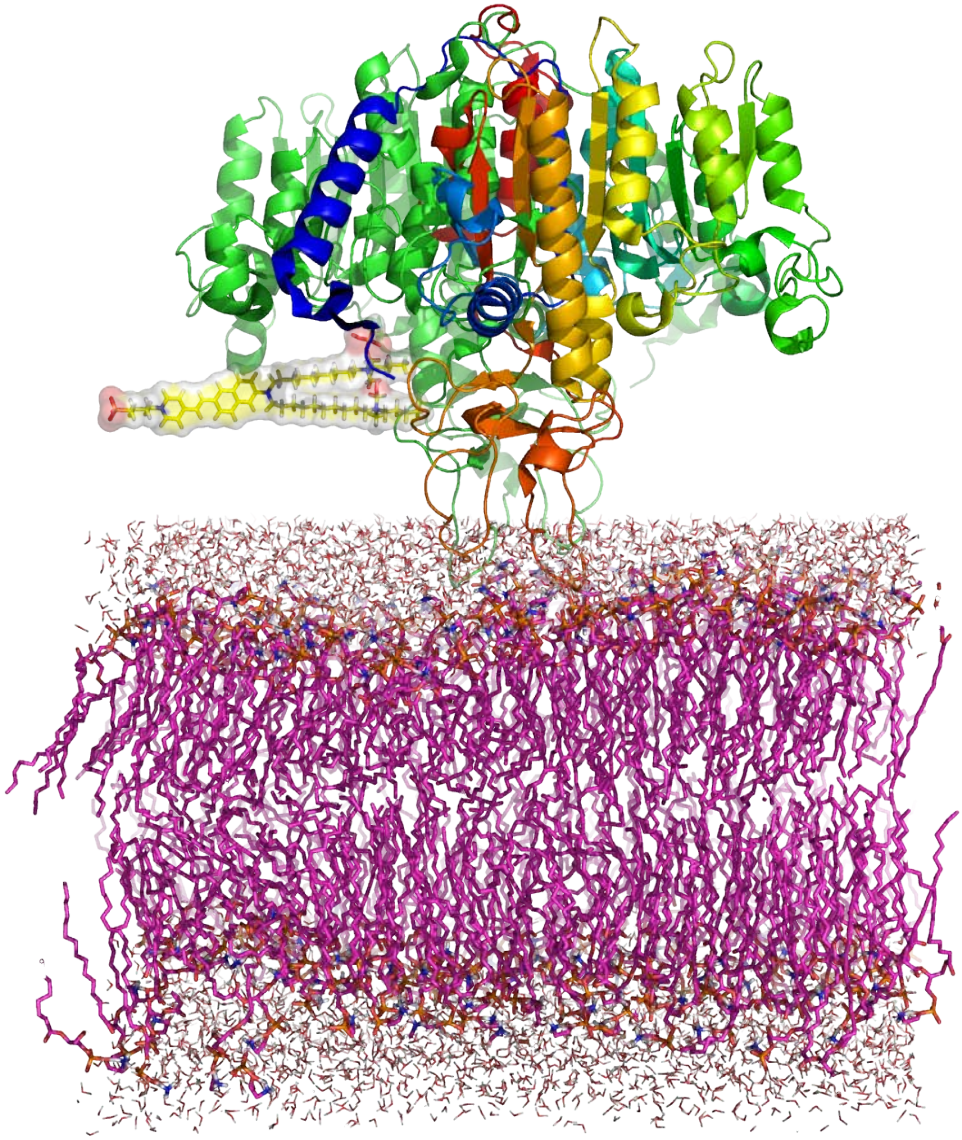

Figure 3-1 Illustration of the structure of human PLAP, bound to the plasma membrane via its GPI anchors. Di-1,4P6-ANEPPS is shown with its phosphate group entering the site of catalytic activity. Rendering of the water molecules has been restricted to the surface of plasma membrane for clarity.

The structure of PLAP is a dimer, with each monomer containing 479 residues, together with 4 metal atoms. Two disulfide bridges can be found in each monomer; one is close to the first glycosylation site, where it may serve to support the loop that carries this carbohydrate chain. The second is located near to Asp-481, where the GPI anchor is attached, where it is thought to stabilize the orientation of PLAP relative to the lipid bilayer [77]. The catalytic site contains three of the metal ion binding sites, two for zinc and one for magnesium, and a catalytic serine. The upper side of the catalytic cavity, that furthest from the plasma membrane, contains a large number of basic residues, whilst the lower side has a hydrophobic

character [78]. The GPI anchor is a post-translational modification, conferred on the newly translated protein due to its C-terminal hydrophobic attachment sequence [79].

-TACDLAPPAGTT**D** AAHPGRSVVPALLPLLAGTLLLLETATAP

The terminal 42 aa from PLAP are shown above; the hydrophobic domain in blue, and the cleavage site in red, with the C-terminal Asp-481 underlined, the GPI attachment point [68].
A second alkaline phosphatase was used in this project, a modified version of PLAP with the C-terminal GPI modification sequence replaced with an *Art*ificial *Plas*ma *M*embrane *A*nchor (APMA) [12]. It contains a transmembrane localization and binding domain, consisting of 22 hydrophobic Leucine residues [80], preceded by four positively charged Lysine residues, orienting the transmembrane domain according to the "positive-inside rule" [81], which leads to the N-terminus being cytoplasmic, making APMA a type II membrane anchor. The anchor was encoded in an expression vector, so as to be utilized by other types of enzymes, such as ß-galactosidase, for other prodye activation schemes. The anchor has the benefit of being impervious to phosphatidylinositol-specific phospholipase C induced cleavage and release, which can occur with GPI anchored PLAP, but has not been reported for neurons. The APMA anchor, as an N-terminal modification, reverses the orientation of the enzyme with respect to the plasma membrane, potentially altering its activity by interfering with the formation of the dimer pair, or from allosteric interactions due to the orientation of the new membrane-spanning domain. Both alkaline phosphatases were compared directly after transient transfection, with the best performing to be chosen for further research.

3.1.2 Fluorescent Marker

There are a variety of cellular marker systems available for identifying which cells express PLAP, which itself is a common marker gene. However, fluorescent proteins have the advantage of being directly observable without the use of a reactive substrate, such as for X-gal for ß-galactosidase marker gene. There are a wide variety of fluorescent proteins available, ranging in emission spectra from blue to near infrared. These fluorescent proteins are derived from a number of sources, one of the earliest being that of *G*reen *F*luorescent *P*rotein (avGFP), from *Aequorea Victoria*, and later the first Red fluorescent protein, DsRed (or drFP583), from *Discosoma sp*. Subsequent mutations and refinements have removed the need for protein oligomerization, whilst improving fluorescence quantum yield and photostability. This work was carried out both via rational design with the use of crystal structures of the proteins [82], and also via evolutionary pressure on randomly mutated

versions of GFP, that were selected for beneficial mutations with flow cytometry using Fluorescence-Activated Cell Sorting (FACS) [83,84]. The emission and excitation spectra have also been broadened; the emission maxima of the original GFP has been mutated from 509 nm towards the blue, with a maximum for the evolved protein mBFP now at 440 nm; DsRed has been red shifted from 586 nm to the far-red mutant mPlum at 649 nm [85-88]. A wide variety of yellow, orange and cyan fluorescent proteins lie between these two spectra [85,89], as shown in Table 2.

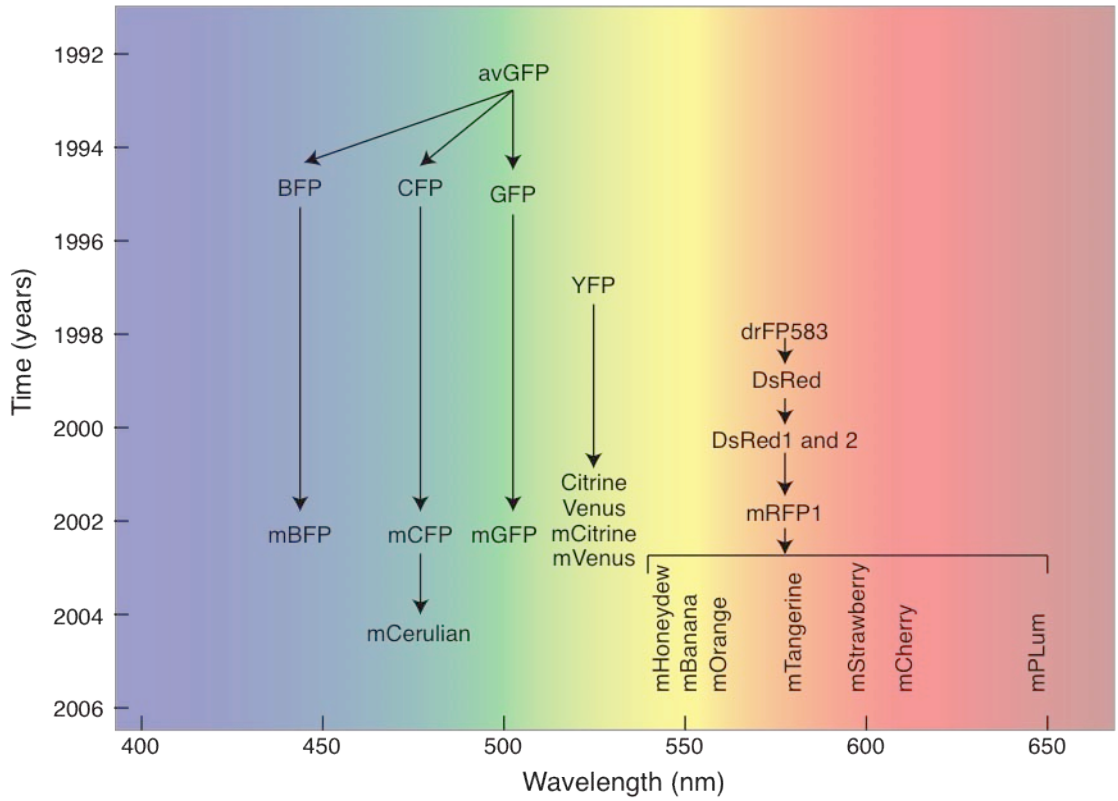

Figure 3-2 The development of the wide variety of currently used fluorescent proteins, from the original avGFP and DsRed.

The selection of a fluorescent marker for the identification of cells co-expressing alkaline phosphatase is dependent on its excitation and emission spectral overlap with that of the dye chromophore. During the selective staining of cells [12], the initial staining was difficult to quantitatively analyze, as the faint fluorescence of the activated and membrane-bound dye was overwhelmed by fluorescence originating from closely packed cells expressing GFP. As shown in Figure 3-3, non-selective staining was not measurable, as the GFP fluorescence in the cytosol of these cells extends to the plasma membrane, masking the unspecific staining signal. This prevented the quantitative analysis of the effectiveness of the first generation prodyes.

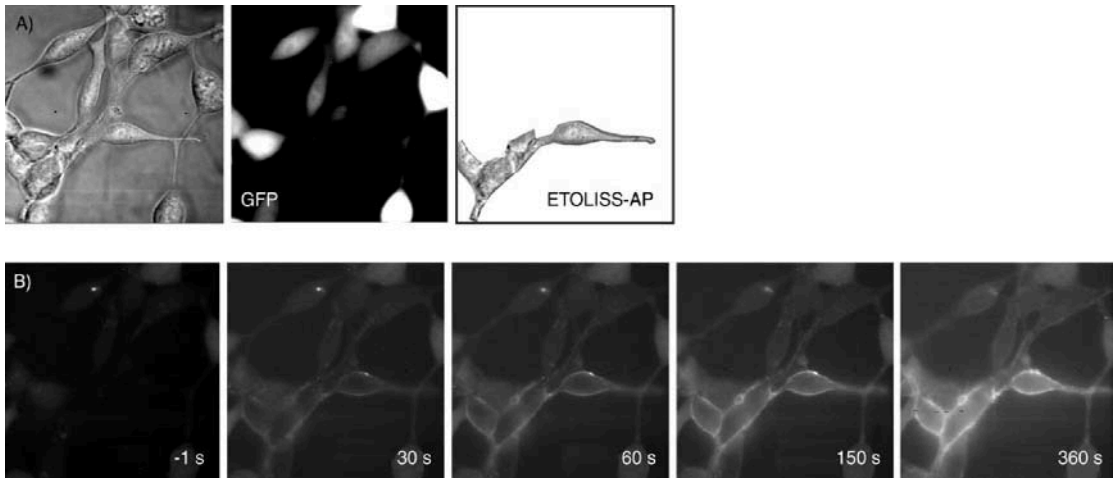

Figure 3-3 The selective staining of a mixed population of stably transfected cells as taken from [12]; a) bright-field image of cells expressing GFP and ETOLISS-AP respectively, b) the selective staining of the ETOLISS-AP cells.

Both the ASP chromophore used by Hinner [12], and the ANEP chromophore share an emission maximum in lipid membrane at 610 nm. The spectra of the orange and red fluorescent proteins overlap that of the dye, such that bandpass filters used to block the emission spectra of the fluorescent protein would severely reduce the measurable signal from the dye. This restricts the selection of the fluorescent marker to one with an emission maximum wavelength shorter than 550 nm, due to the broad emission profiles of fluorescent proteins. The high intensity light used to measure voltage sensitivity also causes increased bleaching, and so high photostability is also necessary. Of the remaining fluorescent proteins, GFP matches both requirements, as shown in Table 2, and was therefore selected as the marker for this project. A long-pass filter at 590 nm was used to record the progression of selective staining of the cells with the prodye. Although the fluorescence emission spectrum of GFP has a maximum at 488 nm, some of the emitted light is at 590 nm and longer. Using a longer wavelength long-pass filter would only slightly reduce this overlap, whilst greatly reducing the captured dye fluorescence.

Confining the expression of GFP away from the plasma membrane would further reduce the unwanted GFP signal overlap. There have been many GFP-fusion proteins created to track the location and lifespan of proteins, labeling the C or N terminal of cellular components, including the ribosome, cytoskeleton and histone bodies [90,91]. This last type of fusion, of GFP with histone 2B (H2BGFP), has been shown to be confined to the cell nucleus, where it forms histone bodies that tightly bind DNA [92]. As such, their restricted distribution in the cell separates the emission profile spatially, leaving cell membrane staining free from overlap. This fluorescent fusion protein was thus selected as the marker for this project.

Class	Protein	Ex (nm)	Em (nm)	Brightness	Photostability
Far-red	mPlum	590	649	4.1	53
Red	mCherry	587	610	16	96
	tdTomato	554	581	95	98
	mStrawberry	574	596	26	15
	J-Red	584	610	8.8	13
	DsRed-monomer	556	586	3.5	16
Orange	mOrange	548	562	49	9
	mKO	548	559	31	122
Yellow	mCitrine	516	529	59	49
	Venus	515	528	53	15
	YPet	517	530	80	49
	EYFP	514	527	51	60
Green	Emerald	487	509	39	0.69
	GFP	488	507	34	174
Cyan	CyPet	435	477	18	59
	mCFPm	433	475	13	64
	Cerulean	433	475	27	36

Table 2 The current generation of fluorescent proteins, taken from [88]. Brightness is the product of extinction coefficient and quantum yield at pH 7.4, and photostability is the bleaching time from an initial emission rate of 1,000 photons/s down to 500 photons/s.

3.1.3 Phosphatase Expression Analysis

At this stage of the project, experiments were performed to test the expression and activity of the alkaline phosphatase and fluorescent marker gene, using plasmids for either pcDNA3.1-ETOLLIS-AP or pORF-PLAP, together with the plasmid encoding the marker H2BGFP (pBOS-H2BGFP). The tests were performed on transiently transfected cells, using Lipofectamine 2000, a transfection agent used for its high efficiency, Appendix 7.4.4.2. It is also used for the transfection of primary cell lines such as neurons, which show high mortality rates with most other transfection agents that also have overall low transfection rates (~25% for dissociated hippocampal neurons compared to 80% for HEK293) [93,94], and was used under standard protocol described in Appendix 7.4.5. Images were recorded with an iXonEM+ camera, mounted on an Axiovert 135TV microscope, with a Plan-NEOFLUAR 40x/1.30 oil-immersion objective. Fluorescence images were illuminated with Luxeon LEDs; GFP images used the Luxeon V LXHL-LB5C (peak 470 nm), with an excitation bandpass filter (470/40 nm), and an emission filter (535/50 nm).

Cells were analyzed for expression after 24, 48 and 72 hours, with cells at 72 hours showing the highest levels of marker expression, and this length of post-transfection time was used for

all further experiments. Figure 3-4 shows the testing of the phosphatase activity. BCIP/NBT staining is exclusively targeted to cells co-expressing H2BGFP for both encoded phosphatases, according to the protocol described in Appendix 7.4.6. The fluorescent nucleus of the cell is well separated from the plasma membrane in HEK293 cells, and the cells show strong expression of the fluorescent protein. The levels of expression of both proteins can be seen to vary in HEK293 cells, with some cells clearly brighter than others in GFP fluorescence. The difference in phosphatase expression is difficult to quantify with bright-field microscopy, but nonetheless, some cells appear to show stronger BCIP/NBT precipitation than others. Examination with bright-field microscopy showed no morphological differences between transfected and un-transfected cells.

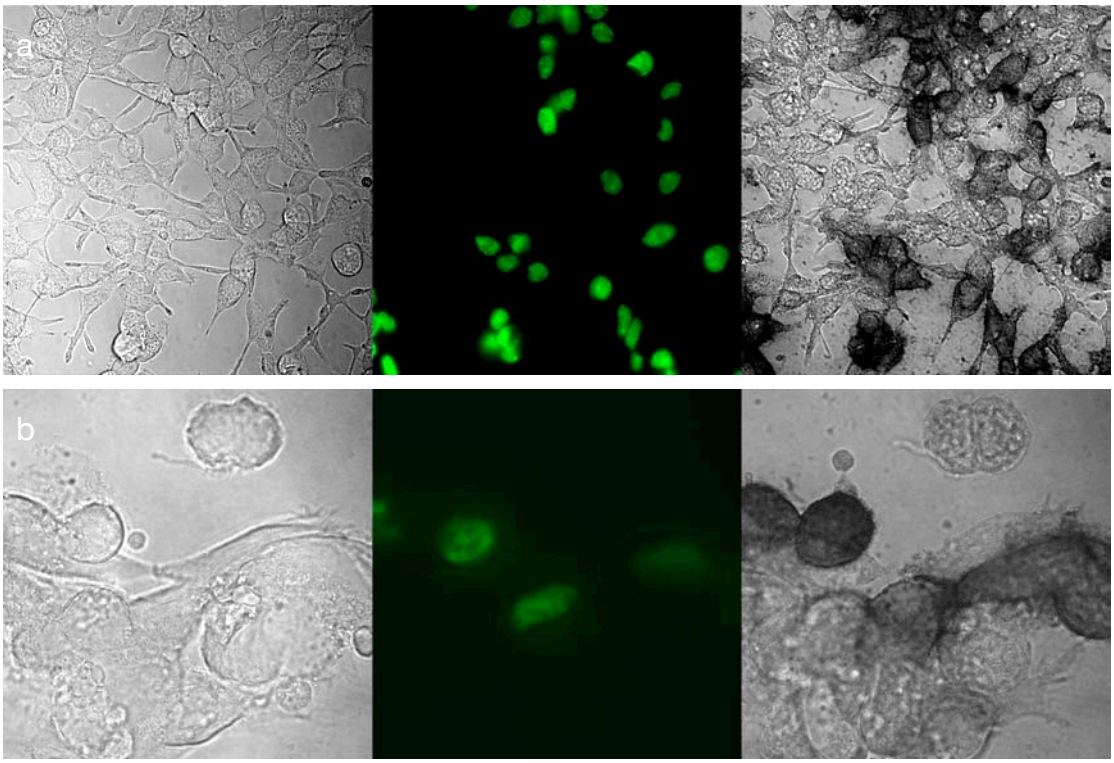

Figure 3-4 Transient dual transfection of HEK293 cells; a) pORF-PLAP and pBOS-H2BGFP, b) cropped ETOLISS-AP and pBOS-H2BGFP image. Bright-field, GFP fluorescence imaging and BCIP/NBT staining respectively.

Dissociated rat E18 hippocampal neurons were also tested for correct expression of both phosphatases, with the method described in Appendix 7.4.5. As with the HEK293 cells, the expression of the phosphatase and H2BGFP were found exclusively together in the same cells. BCIP/NBT staining demonstrated the expression of both alkaline phosphatases on the surface of the cell bodies, axons and dendritic trees. The borders of the cell nucleus, as seen with GFP expression, are separated from the cell membrane.

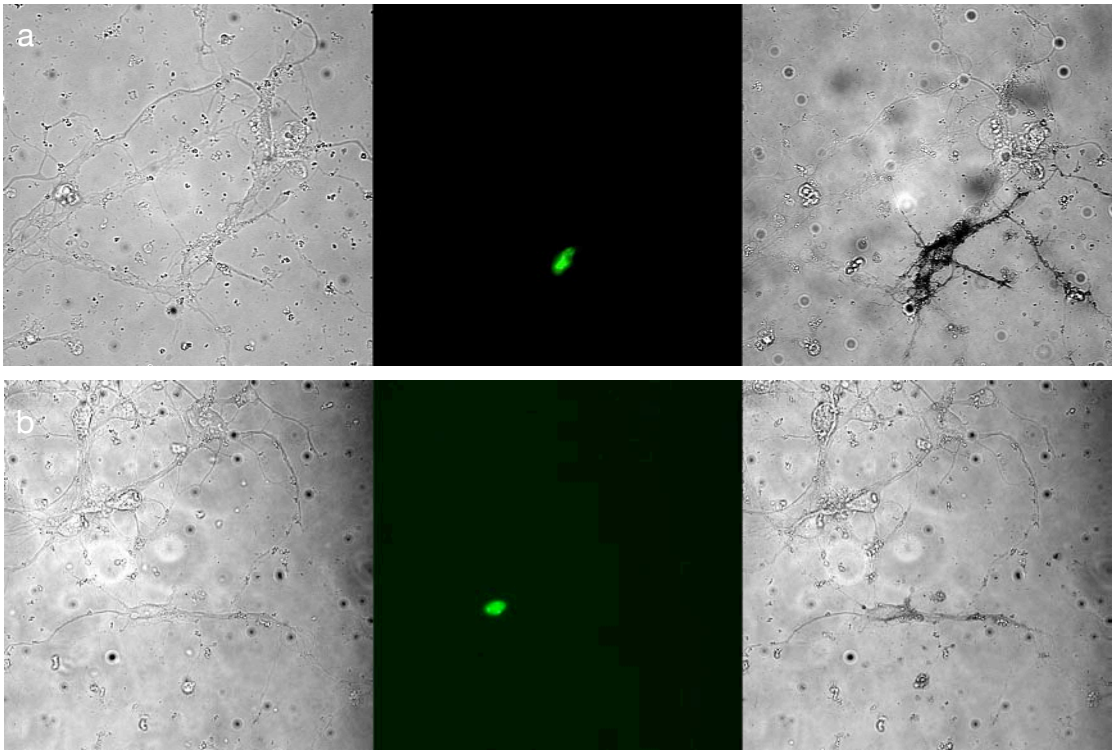

Figure 3-5 Transient dual transfection of dissociated E18 rat hippocampal neurons; a) pORF-PLAP and pBOS-H2BGFP, b) ETOLISS-AP and pBOS-H2BGFP. Bright-field, GFP fluorescence imaging and BCIP/NBT staining respectively.

3.1.4 Bicistronic Gene Expression

Whilst the H2BGFP marker unambiguously identifies cells expressing both proteins, under normal co-transfection protocols, there is little correlation between the expression levels of both markers. This is because the number of copies of each of the plasmids that have entered the nucleus can vary significantly in each transfected cell. This lack of correlation precludes the selection of strongly expressing PLAP cells by direct visual analysis of GFP fluorescence, for stable cell line generation.

In order to link the expression of two proteins in a mammalian biological system, it is necessary to generate a polycistronic mRNA, such that it contains the required coding to recruit the ribosomal translation machinery to a second translational initiation site [95]. This kind of polycistronic system is common in bacteria and archaea, and is usually found to group functionally related proteins together under the control of a regulatory protein, in a system termed an operon [96]. Although such operons are primarily found in prokaryotes, examples can sometimes be found in eukaryotes, including nematodes [97]. However, such systems are rarely found in higher organisms, with just one example found for mammalian systems [98].

Eukaryotes are generally thought to initiate mRNA translation via a cap-binding then scanning mechanism, although in some cases mRNA lacking a free 5' end of cap structure are still efficiently translated [99,100]. These cap-free mRNA's contain sequences that can directly recruit the translation machinery via their RNA secondary structure [95]. These *I*nternal *R*ibosome *E*ntry *S*ite (IRES) sequences, when present in the intercistronic region of dicistronic mRNA, can direct translation of a second protein independently of the first cistron. The sequence structure of the Antennapedia IRES has been tested via deletion analysis, but distinct boundaries have been difficult to determine, with small 55 bp fragments still demonstrated to show some translational initiation activity [101]. RNA folding analyses have suggested that IRES elements form a Y-type stem-loop structure immediately upstream of the initiation codon, although there is no obvious sequence similarity between cellular or viral IRES elements. This structure is believed to bind factors leading to the cap-independent recruitment of the 40S ribosome in mammalian cells [102].

During viral infection, proteases encoded by the virus can cleave the mRNA cap-structure translation initiation factors, shutting down the host's ability to manufacture defensive proteins. Viral mRNA is then translated via IRES elements, avoiding the need for the normal ribosomal apparatus [96]. Comparisons between viral and eukaryotic IRES elements indicate that the latter are generally less efficient in their activity, and can also be of limited cell-type specificity [103]; these two factors have led to the use of viral IRES element in molecular biology.

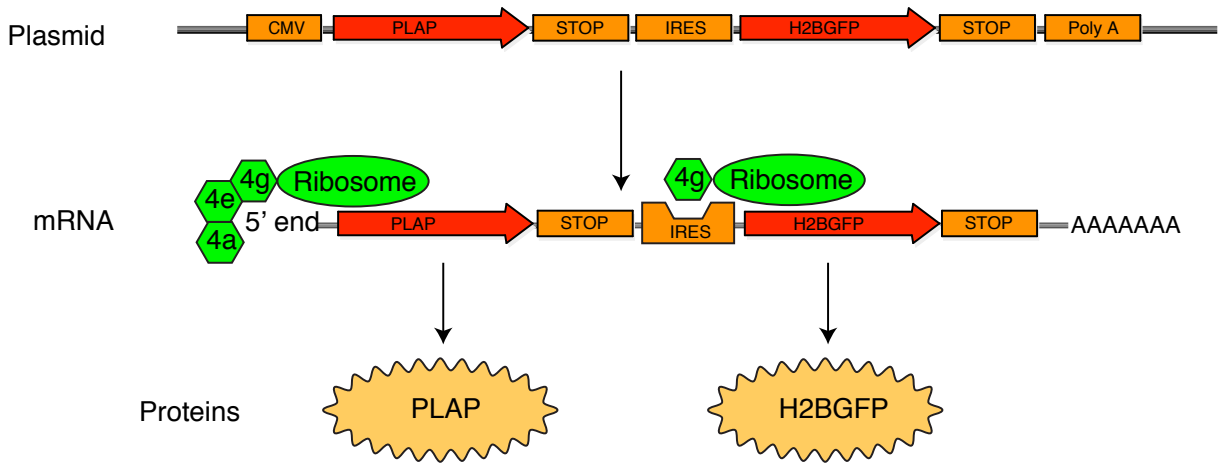

Figure 3-6 Diagram of bicistronic IRES containing plasmid producing two proteins, PLAP and H2BGFP via the recruitment of the ribosomal machinery to the eIF4G subunit directly bound to mRNA, due to the loop containing secondary structure present in the IRES domain.

The IRES selected to drive the expression of H2BGFP in this project was derived from the encephalomyocarditis virus (EMCV) from the family Picornaviridae, a non-enveloped, positive-stranded RNA virus with an icosahedral capsid [104]. These viral elements show strong IRES activity in a wide variety of cells, and have been used in a wide variety of experiments [105-107]. A highly conserved region found in several IRES elements, including this EMCV IRES, contain an eukaryotic initiation factor (eIF) binding site for a protein that acts as a bridge between mRNA and the small ribosomal subunit. The three eIF's, 4A, 4E, and 4G form a complex together, and make up the cap at the 5' end of the most mRNA for translational machinery recruitment. The 450 nt long conserved binding site forms a series of RNA loops that recruits the eIF4G without the involvement of eIF4E [108].

3.1.5 Stable Gene Expression

To directly compare the phosphatase activity between PLAP and APMA-AP expressed in cell culture, it is necessary to have identical levels of mRNA transcription. This is not possible with transient transfection, where the plasmid copy number varies between cells, and changes with time. The use of selection agents to generate stable cell lines, although producing isogenic cells, cannot be used to compare different cell lines, as transcription rates are dependent upon the integration site in the host genome, and copy number.

The use of site-specific recombinase integration overcomes this problem. By utilizing a recombinase recognition site stably transfected into a cell line, genetic information can be inserted precisely and reliably via enzymatic recombination. The FLP-In system was used in this project to generate two cell lines, for the PLAP and APMA-AP H2BGFP operon system described above.

The FLP-In system uses the *Saccharomyces cerevisiae*-derived DNA recombination system together with three vectors to generate these stable cell lines. The first vector, pFRT/*lac*Zeo, is used to stably transfect new cell lines, with the use of the selection agent Zeocin [109]. This new cell line expresses the lacZ-Zeocin gene under the control of the SV40 early promoter. An FRT site that acts as the binding and cleavage site for Flp recombinase is inserted directly downstream of the ATG initiation codon, as shown in Figure 3-7-a. The integration is random, however, the zeocin selection agent and ß-galactosidase activity can be used to select highly expressing clones, and then screened to identify those clones containing a single FRT site. A stable human embryonic kidney (HEK293) cell line transfected with this vector was purchased from Invitrogen, as Flp-In-293 cells.

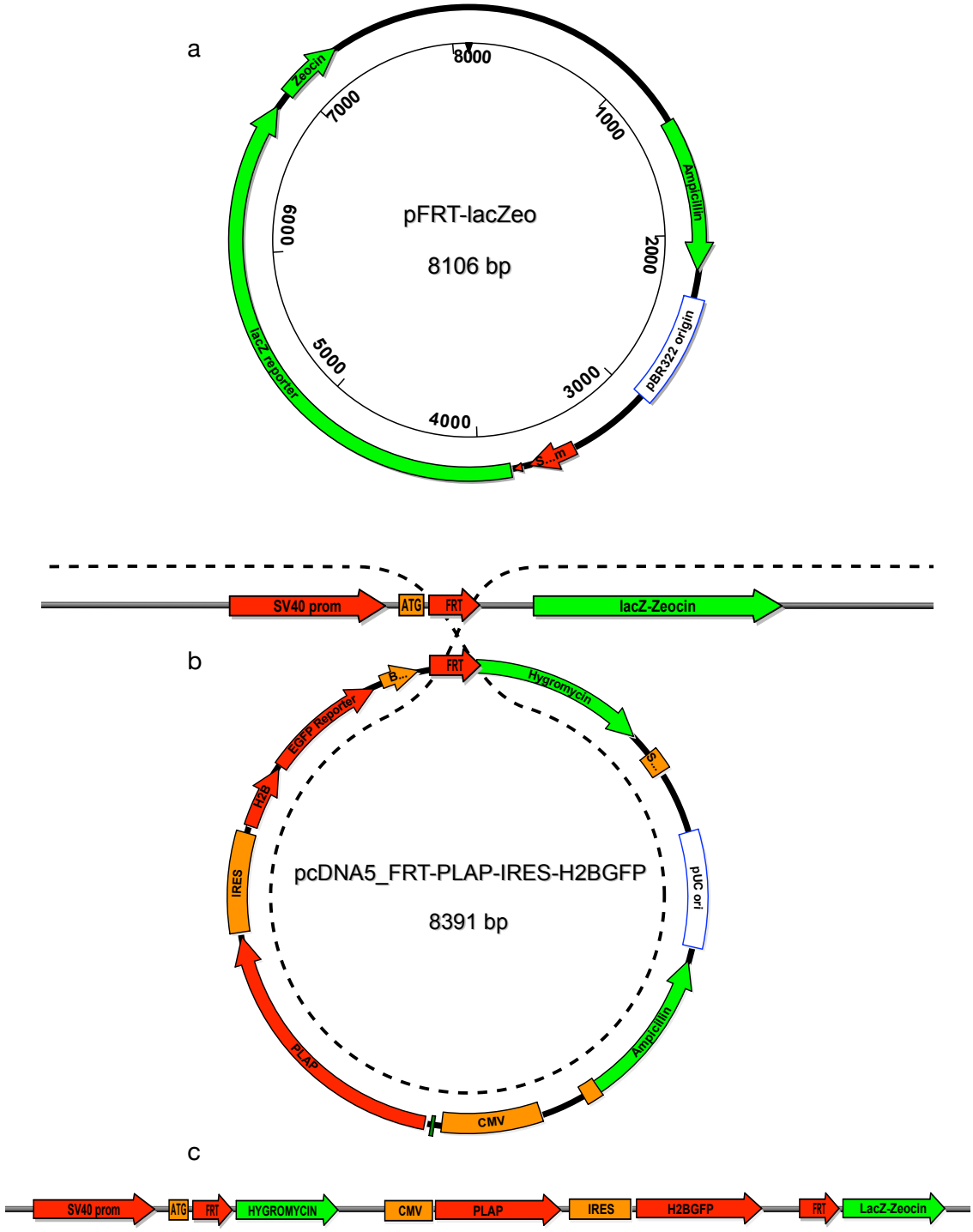

Figure 3-7 The generation of the stably integrated double reported plasmid pcDNA5_FRT-PLAP-IRES-H2BGFP via Flp induced recombination; a) Vector map of the pFRT-lacZeo plasmid that is stably integrated in the genome via standard selection, b) the Frt catalyzed integration of pcDNA5_FRT-PLAP-IRES-H2BGFP, c) the integrated sequence now expressing hygromycin resistance and no longer expressing zeocin resistance.

Vectors constructed from the pcDNA5/FRT vector contain the gene of interest, together with the Hygromycin resistance gene, located downstream of a FRT site, lacking however a promoter and ATG initiation codon. In this project, the PLAP and APMA-AP H2BGFP operon system were cloned into pcDNA5/FRT, under the control of the cytomegalovirus (CMV) immediate-early enhancer-promoter Figure 3-7-b. When this vector is co-transfected with the Flp recombinase encoding pOG44 plasmid, Flp mediates a homologous recombination between the FRT site in the pcDNA5/FRT plasmid and the FRT site of the stably transfected pFRT/*lac*Zeo, causing the integration of the new plasmid into the genome, whilst transferring the SV40 promoter and ATG codon from the Zeocin to Hygromycin resistance gene [110], as shown in Figure 3-7-c. Thus, the new cell line can now be selected for Hygromycin resistance, Zeocin sensitivity, lack of ß-galactosidase activity, and expression of the recombinant protein of interest.

3.2 System Construction

3.2.1 Vector Synthesis

The PCR and cloning protocols are described in the Appendix 7.4.1 and 7.4.3.

The alkaline phosphatase gene, PLAP, was obtained from pORF14-PLAP (InvivoGen, San Diego, CA, USA), and amplified out via PCR using the primer pair 5'-TTGACCTCGAGATGATTCTGGGGCCCTGCA-3' and 5'-TTACGACGCGTTCAGGGA-GCAGTGGCCGTCTC-3', to incorporate the restriction sites XhoI and MluI (highlighted in red). The fragment was cleaned up via gel electrophoresis, and ligated into the pre-cut and cleaned pIRES vector (BD Biosciences Pharmingen, San Diego, USA), to produce the vector pIRES-PLAP, as shown in Figure 3-8-a. The vector was amplified in transformed One Shot Top10 *E coli* cells (Invitrogen, Karlsruhe, Germany), as with the standard procedure outlined in Appendix 7.4.3.

The H2BGFP gene from pBOS-H2BGFP (BD Biosciences) was then cut, purified by gel electrophoresis, and cloned into this new plasmid, using the restriction enzymes SalI and NotI, to give pIRES-PLAP-H2BGFP (Figure 3-8-b), and amplified in Top10 cells. The expression vector was tested in the HEK293 cell line for GFP expression and for surface phosphatase activity, using the chromogenic NBT/BCIP Reagent Kit (Invitrogen), testing positive for both markers.

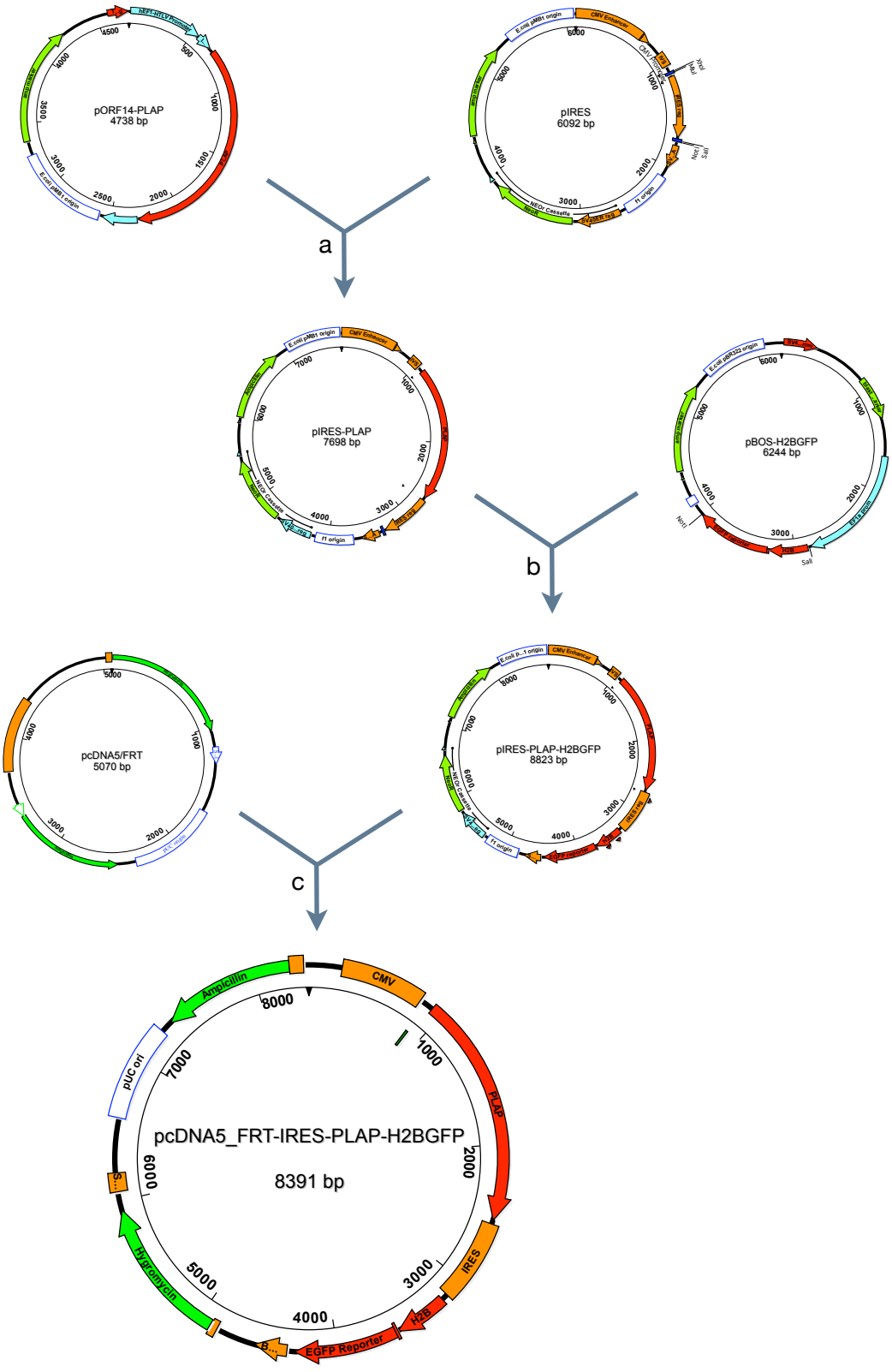

Figure 3-8 The construction of pcDNA5_FRT-IRES-PLAP-H2BGFP. The construction used the plasmids described in Appendix 7.7.1.1, 7.7.1.2, 7.7.1.3 and 7.7.1.5

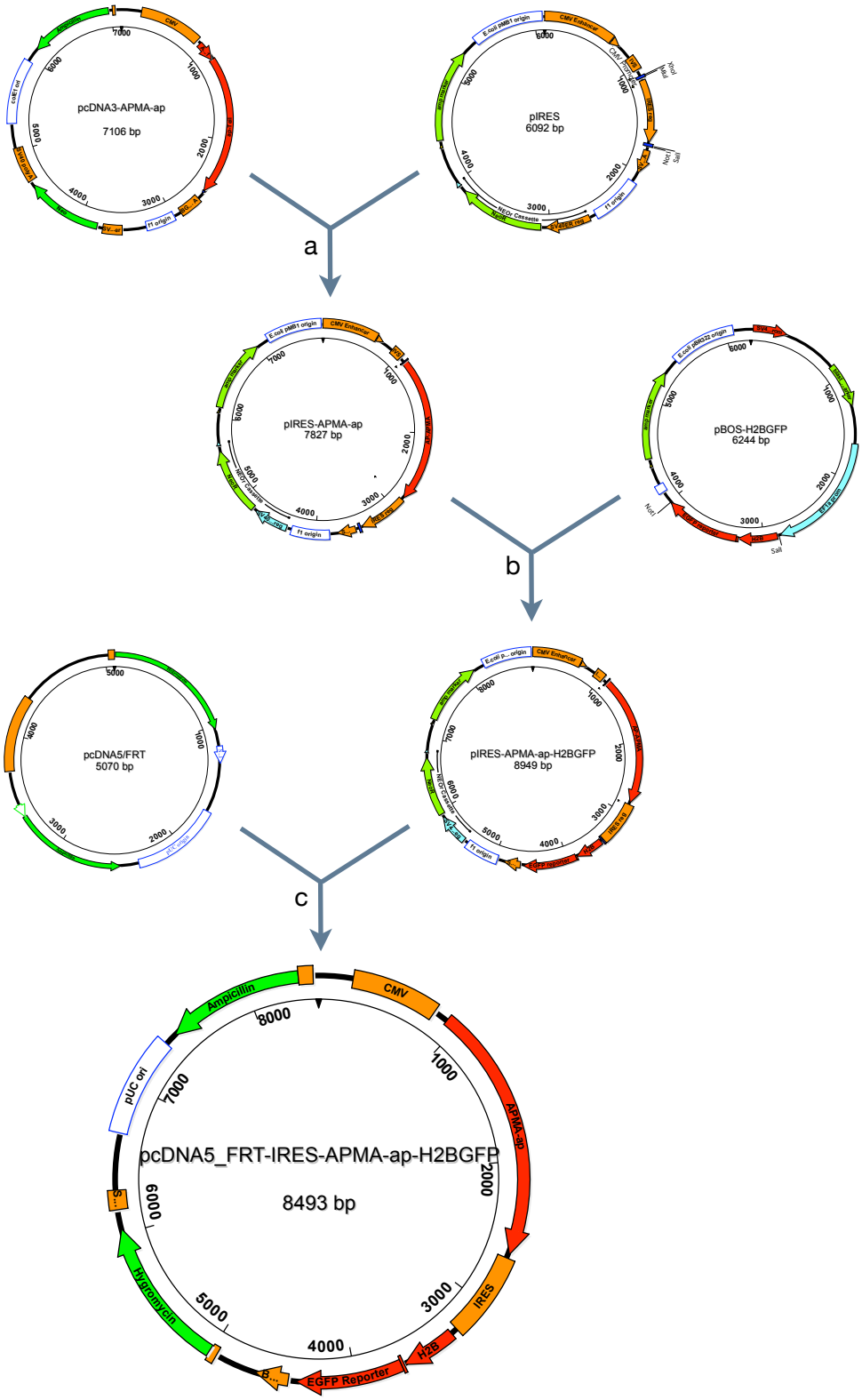

Figure 3-9 The construction of pcDNA5_FRT-IRES-APMA-ap-H2BGFP. The construction used the plasmids described in Appendix 7.7.1.1, 7.7.1.4, 7.7.1.2, 7.7.1.3 and 7.7.1.6.

The functional PLAP-IRES-H2BGFP operon sequence was amplified using the primers 5'-TCTACTTAAGGCCACCATGATTCTGGGGCCCTGC-3' and 5'-CTGCTCGAAGCATTA-ACCCTCAC-3', introducing the AflI site at the 5' end (highlighted in red), and cloned into the pre-cut vector pcDNA5/FRT (Invitrogen) with AflI and NotI, producing pcDNA5_FRT-IRES-PLAP-H2BGFP, Figure 3-9-c. This vector was used for both transient transfection, and site-specific stable transfection in conjunction with pOGG44.

In a similar manner, the APMA-AP version of this vector was constructed by excising the alkaline phosphatase from pcDNA3-APMA-AP with the primer pair 5'-TTGACCTCGAG-ATGGGCCACCATCACCACCATC-3' and 5'-TTACGACGCGTTATTATCACAGGTCCT-CCTCGC-3' (introducing the restriction sites XhoI and MluI, highlighted in red), Figure 3-9-a. This fragment was cloned into pIRES, in the 5' multiple cloning site, and after amplification, followed by H2BGFP which was cloned with SalI and NotI into the second multiple cloning site Figure 3-9-b. The APMA-AP-IRES-H2BGFP fragment was amplified using the primers 5'-TCTACTTAAGGCCACCATGGGCCACCATCACCAC-3' and 5'-CTGCTCGAAGCATTAACCCTCAC-3', adding the AflI restriction site to the 5' end of the fragment, and ligated into pcDNA5/FRT cut previously with AflI and NotI Figure 3-9-c. The ligated plasmid was amplified to give the vector pcDNA5_FRT-IRES-APMA-ap-H2BGFP.

3.2.2 Stable Cell Line Generation

Flp-In-293 cells (Invitrogen), were cultured using standard protocols in 35 mm polypropylene culture dishes (BD Biosciences), containing a culture medium of DMEM (high glucose), 10% FBS, 2 mM L-glutamine, 1% Penicillin/Streptomycin and 100 µg/ml Zeocin, at 37.0°C with 5% CO_2. One day prior to transfection, the culture medium was replaced with an equivalent medium lacking Zeocin.

Transfection was performed with Lipofectamine 2000, under standard protocols (Appendix 7.4.3) with a 9:1 ratio of pOG44:pcDNA5_FRT-IRES-PLAP-H2BGFP or pOG44:pcDNA5_FRT-IRES-APMA-ap-H2BGFP plasmid DNA. After 24 hours, the culture medium was replaced with one containing DMEM (high glucose), 10% FBS, 2 mM L-glutamine, 1% Penicillin/Streptomycin and 50 µg/ml Hygromycin, and cultured at 37.0°C with 5% CO_2. The selection process was performed over 2 weeks, and the surviving cells assayed for phosphatase activity with BCIP/NBT and GFP fluorescence; both cells lines testing positive. All cells were cultured using standard laboratory procedures, and split at ~90% confluency twice weekly.

3.3 Selective Staining

For selective staining experiment, each phosphatase expressing cell line was split 1:20 together with untransfected Flp-In-293 cells split 1:20, into 35 mm culture dishes containing an uncoated, ⌀ 30 mm, #1-thickness glass coverslip (Thermo Scientific, Waltham, USA), using the described cell culture media without selection agents, and grown to 40% confluency over 24 hours.

Before selective staining, the culture medium was removed, and the cells gently washed in their 35 mm culture dishes with buffer (100 mM NaCl, 70 mM D-Glucose, 20 mM AMPD, pH 8.6). The moist coverslip glass (Figure 3-10-e) was mounted into a custom Perspex chamber (Figure 3-10-f), and a watertight seal was provided by a silicon ring, pressed in place by a hollow threaded mounting ring Figure 3-10-d,c), allowing access to the cells from above.

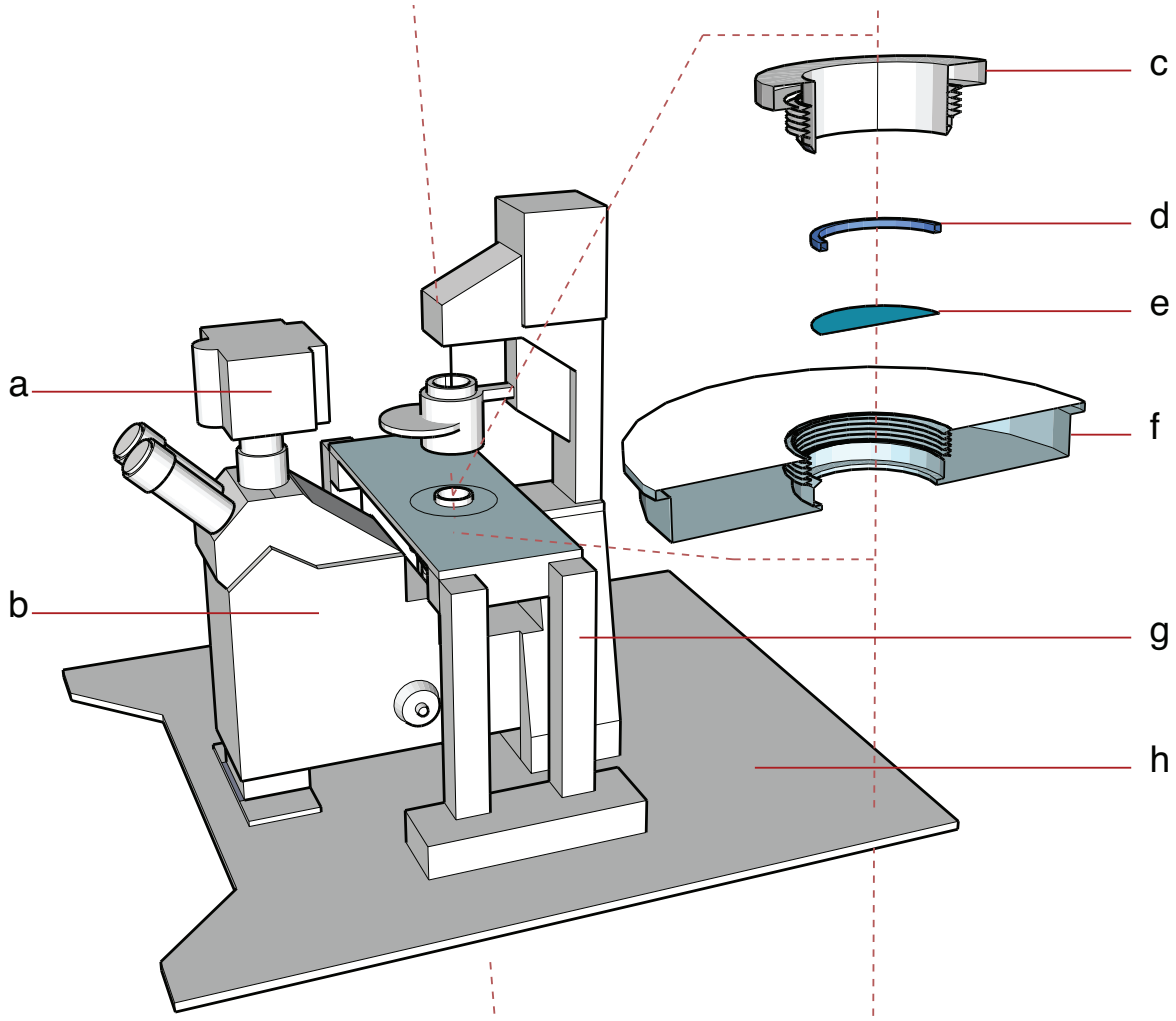

Figure 3-10 Selective staining experimental apparatus; a) iXon camera system, b) Axiovert inverted microscope, c,d,e,f) magnified view of the custom cell chamber, g) custom supporting framework and h) vibration-dampened table.

Images were taken with an iXonEM+ DU885KCS camera system, shown in Figure 3-10-a, mounted on an Axiovert 135TV microscope (Figure 3-10-b), with a Plan-NEOFLUAR 40x/1.30 oil-immersion objective, all mounted to a vibration-dampened table (Figure 3-10-h). LED illumination was chosen for this apparatus, as a previous major limitation in the use of voltage sensitive dyes was the lack of high-intensity light sources. The lack of a spectral line at the red-edge of the excitation for VSD's results in the use of a narrow spectral band from an arc or incandescent bulb, as laser excitation has the problem of speckling [26]. The development of high-intensity LED has overcome these problems, and LED's are now available with emission profiles suitable for voltage sensitive measurements, and will be further discussed in Chapter 4.

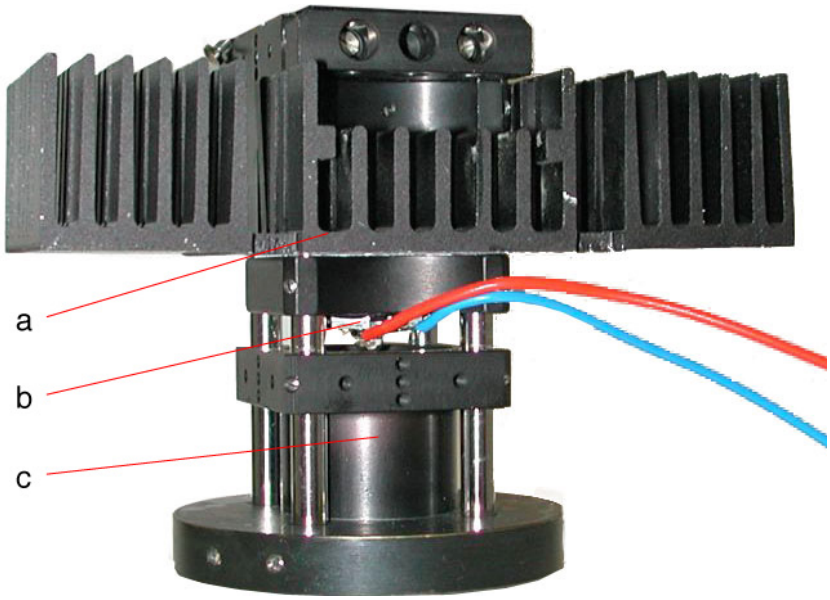

Figure 3-11 LED illumination apparatus; a) Heatsink, b) replaceable LED module on adjustable rails, c) collimating lens.

GFP fluorescence images were illuminated with a Luxeon V LXHL-LB5C LED (peak 470 nm) build into a custom mounting system, Figure 3-11 and Figure 3-12-b, and used with an excitation bandpass filter (470/40 nm), and an emission filter (535/50 nm). Voltage sensitive dye staining sequences used the same LED and excitation filter, but with an emission long pass filter of 590 nm. LED illumination was synchronized to camera acquisition timing to reduce bleaching, via the opto-isolated circuit, Figure 3-12-c.

3.3 SELECTIVE STAINING

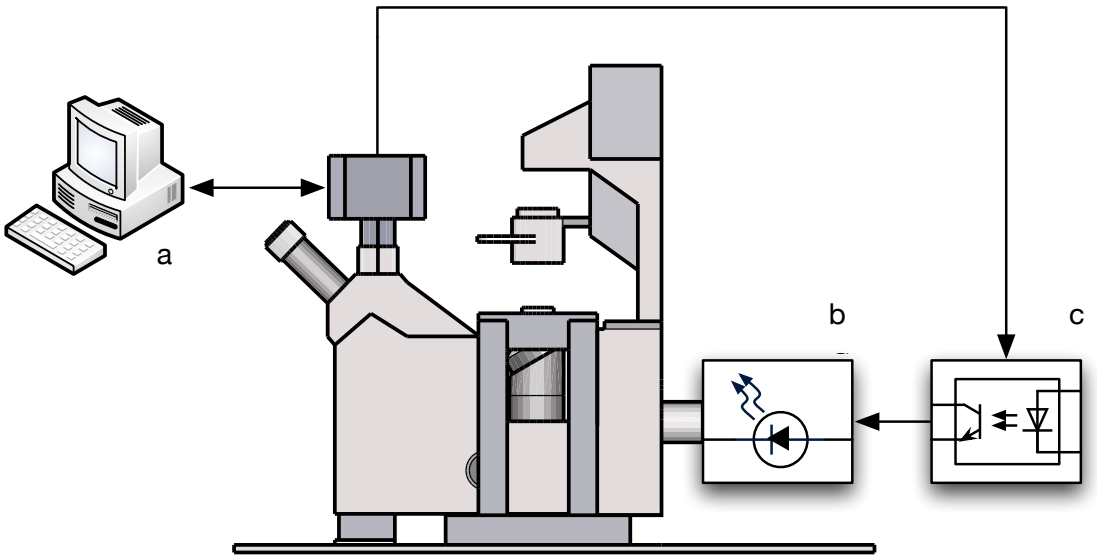

Figure 3-12 Selective staining experimental apparatus; a) PC controlling the camera apparatus, b) high-intensity LED, c) opto-isolator controlled by the camera system.

Cells were brought into focus and imaged under bright field illumination, and again for GFP fluorescence with LED illumination. The Solis software package (Andor Technology PLC), was used to control the camera system, Figure 3-12-a. Images were taken at 1004x1002 pixels, with a 100 ms exposure for 100 frames at 1 Hz. The acquisition sequence was started, and after 5 seconds, 2 ml of dye staining solution was added to the chamber (1 μM voltage sensitive dye, 100 mM NaCl, 70 mM D-Glucose, 20 mM AMPD, pH 8.6).

Buffer	Useful pH Range	pKa (at 25)
HEPES	6.8–8.2	7.48
TEA	7.3–8.3	7.80
Tris	7.5-9.0	8.06
HEPBS	7.6–9.0	8.30
TAPS	7.7-9.1	8.40
AMPD	7.8–9.7	8.80
AMPSO	8.3–9.7	9.00

Table 3 Biological buffers applicable for selective staining method.

The pH of the buffer used in the work of Hinner [12] was pH 8.1, selected on the basis that the optimum for PLAP is pH 9.6 [111], and that higher pH might negatively affect the cultured cells. However, neurons have been shown to be able to tolerate much higher alkalinity, such as pH 9.3 in the work of [46]. Also, the aliphatic tertiary-amine containing dye tails have a pKb ~10.3, and protonation of this amine functionality at lower pH values may diminish the membrane-binding capability of the dye. Thus, a wider range of pH buffer

was tested to optimize the experiment. Table 3 shows the standard biological buffers used in cell biology; Hinner [11,12] utilized Tris buffer for selective staining experiments, with a usable pH range of 7.5-9.0.

Initial testing of the apparatus was performed with Di-1,4P6-ANEPPS, in TRIS buffers prepared from pH 8.0 to 9.0, with bright-field and fluorescent images recorded after 60 seconds of staining. At pH values between 8.0-8.4, the dye showed no evidence of plasma membrane staining, either selectively or unselectively, as shown in Figure 3-13. However, the dye selectively stained dead cells, identified by their shrunken and granular appearance with bright field imaging. This is surmised to arise from the transport of the cationic prodye through the porous cell membrane of the dead cells, where it could bind to the densely packed lipid membranes of the endoplasmic reticulum. This conjecture is supported by the fact that there is no evidence of plasma membrane staining, and that dye fluorescence requires a hydrophobic chemical environment. The very low membrane-binding ability of the prodye would be offset by the high concentration of lipid material in the dead cell.

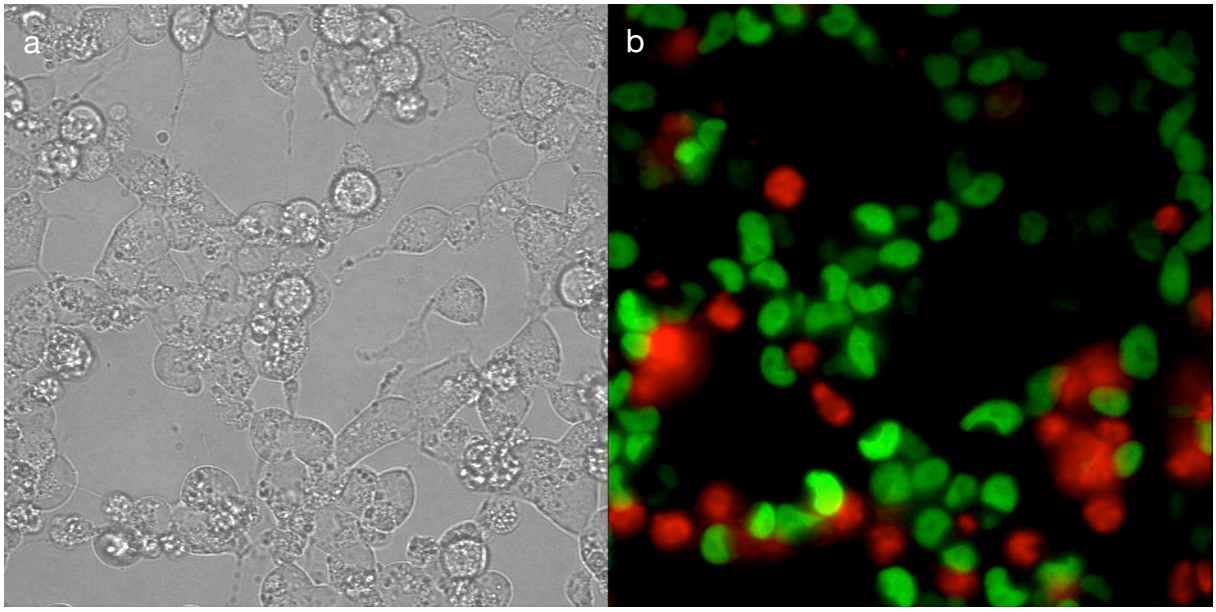

Figure 3-13 1 μM Di-1,4P6-ANEPPS at pH 8.1, 60 seconds of staining; a) bright field image of a mixed population of transfected and untransfected HEK293 cells, b) overlaid GFP and Di-1,4P6-ANEPPS fluorescence images, showing no overlap between cells expressing GFP and red dye fluorescence.

With buffers ranging from pH 8.5-9.0, selective staining was accomplished with Di-1,4P6-ANEPPS, as shown in Figure 3-14. GFP fluorescence is confined to the cell nucleus, and shows good co-localization to cells that show plasma membrane staining with the dye. At higher pH values, from 8.8 and above, HEK293 cells change in morphology after ~4-5

minutes in the buffer, taking on a rounded appearance and detaching from the glass coverslip. At pH 8.6, good selective staining was observed, and cells maintained a healthy morphology for >10 minutes; this pH value was used for all further experiment.

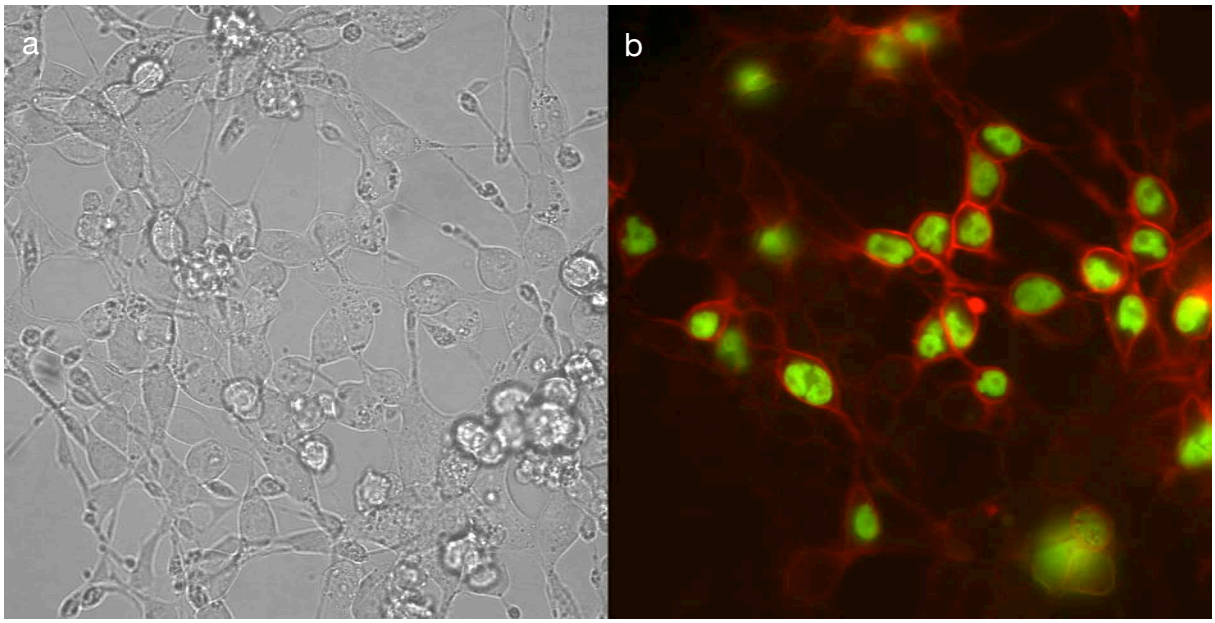

Figure 3-14 1 µM Di-1,4P6-ANEPPS at pH 8.6, 60 seconds of staining; a) bright field image of a mixed population of transfected and untransfected HEK293 cells, b) overlaid GFP and Di-1,4P6-ANEPPS fluorescence images, demonstrating a good correlation between GFP expression and plasma membrane staining.

The buffer 2-amino-methyl-1,3-propanediol (AMPD) has a higher pH range, (7.8-9.7), and has been shown to improve alkaline phosphatase enzyme activity when compared to Tris [45]. It has a pKa of 8.8, the closest to pH 8.6 from the commonly used biological buffers (Table 3), and after testing well at pH 8.6, this buffer was chosen to replace Tris in the project.

The seven prodyes listed in Table 1 were used to create buffered 1 µM voltage sensitive dye staining solutions, using the method described above. The results of the imaging are shown and described in Figures 3-15 to 3-21. The images shown are the bright field, GFP fluorescence, dye fluorescence, and merged images, with the dye image being the last from the 100-image sequence.

Each of the prodyes tested shows selective staining to some degree, with cells expressing GFP and PLAP undergoing more plasma membrane staining than the untransfected cells. The effect is subtler for the phosphate prodyes, and more pronounced for the N-phosphono-oxymethyl prodyes. One prodye in particular, Di-1,8P6-ANEPPS, shows excellent selective staining, with very low levels of non-specific cell labeling or background staining.

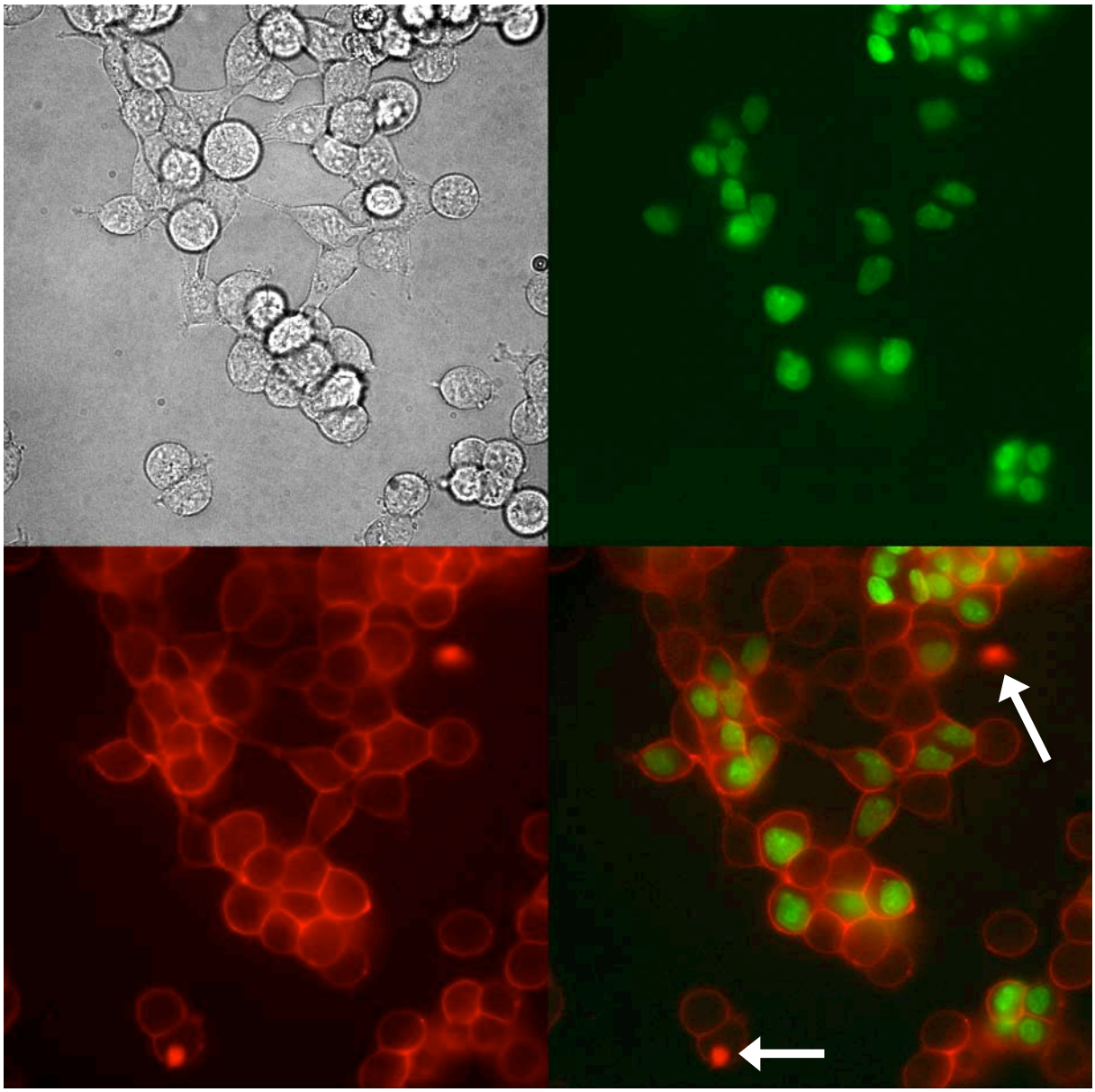

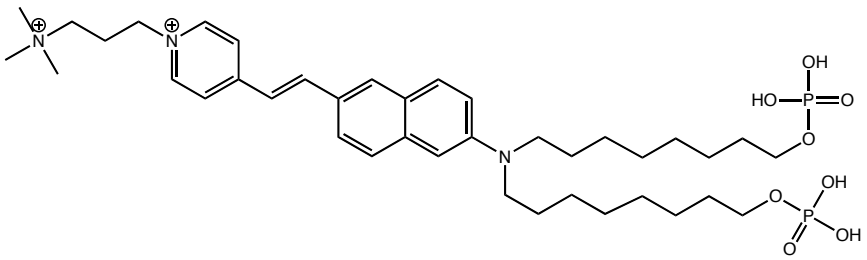

Figure 3-15 1 µM Di-8P-ANEPPQ. The selective staining of phosphatase expressing HEK293 cells is visibly higher than that of the control cells. Dead cells appear to be stained in some cases, with their locations indicated by the arrows.

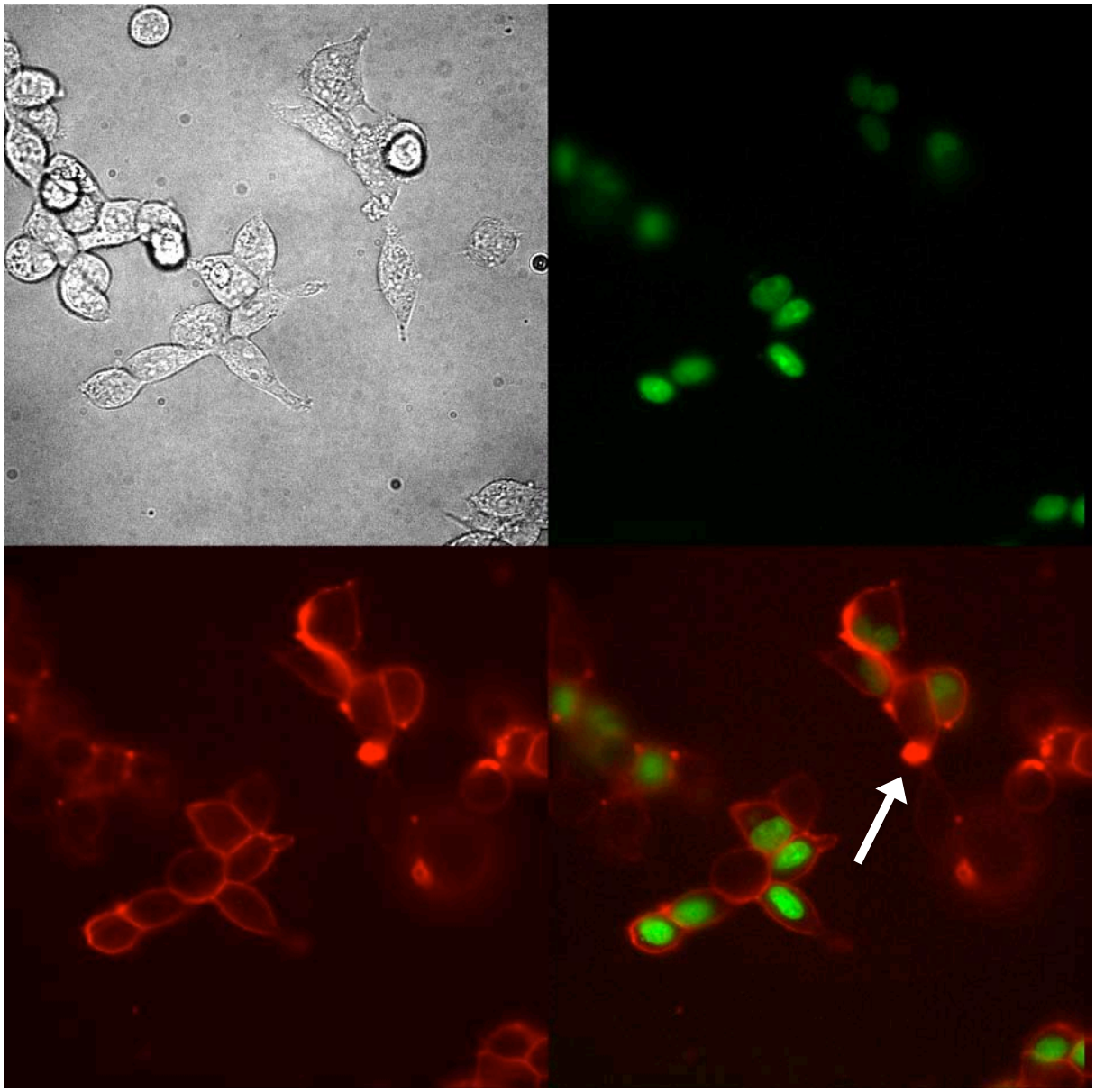

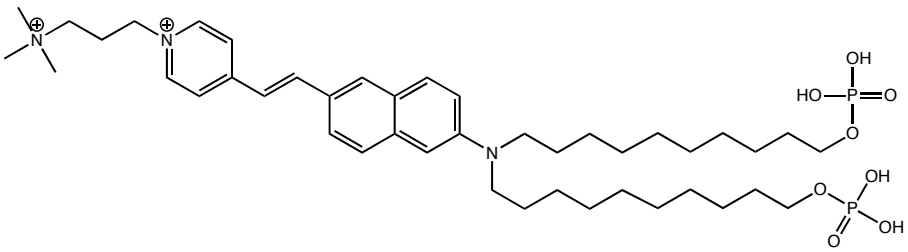

Figure 3-16 1 μM Di-10P-ANEPPQ. Selective staining is again higher for PLAP expressing cells than the control cells, and also appears to be slightly better than Di-8P-ANEPPQ. Dead cells are stained, as indicated by the arrows.

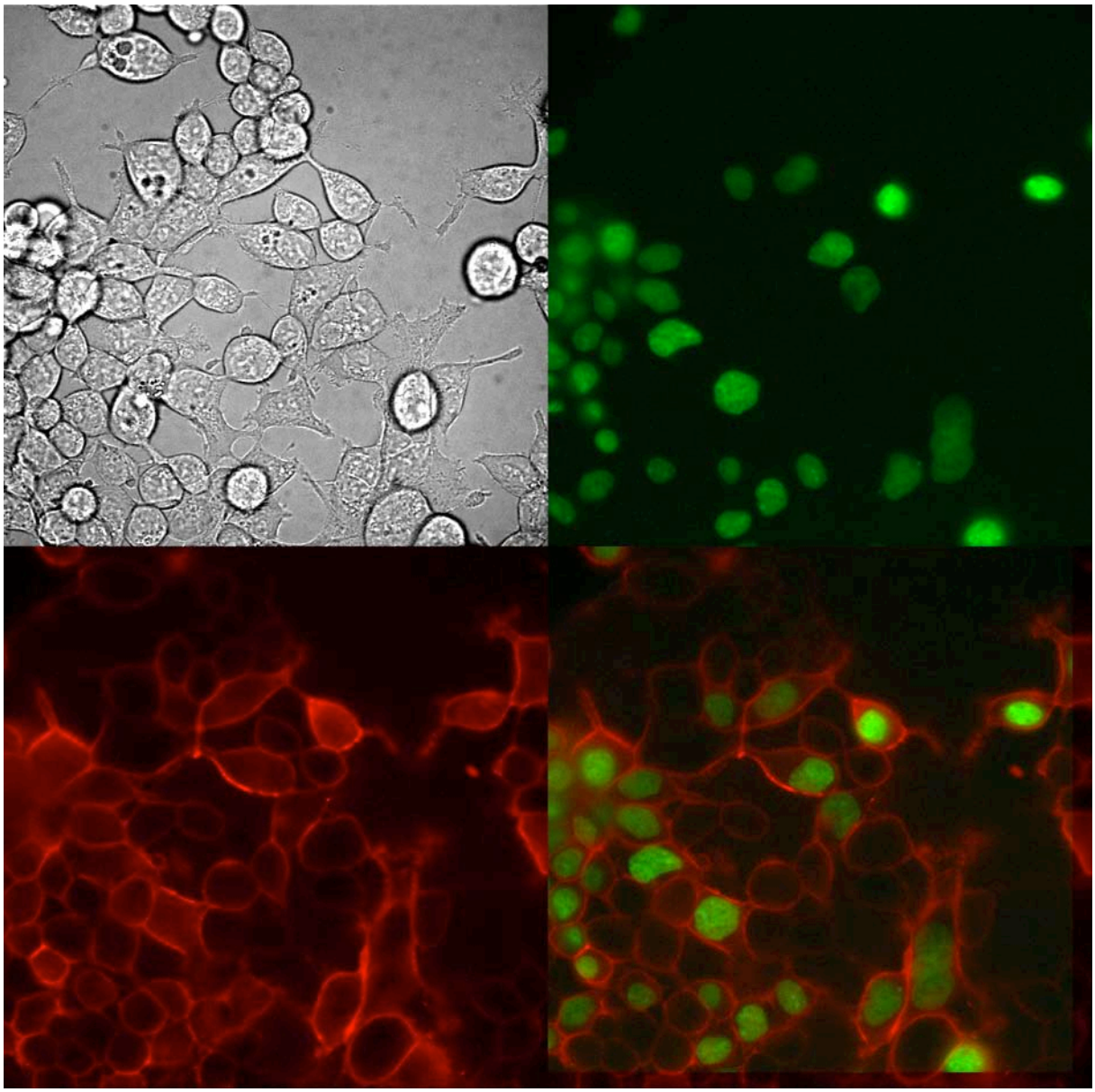

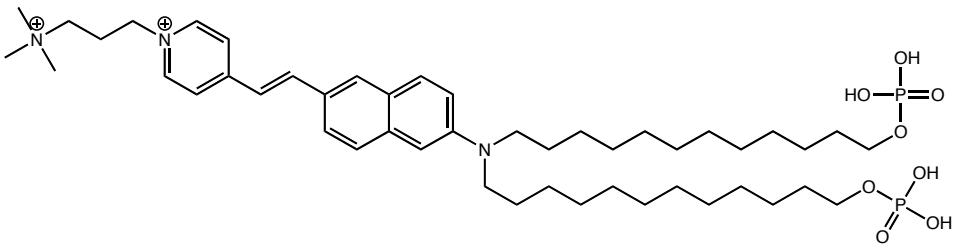

Figure 3-17 1 μM Di-12P-ANEPPQ. Selective staining is higher for the transfected cells than for the control cells. The level of selectivity appears to be similar to that of Di-8P-ANEPPQ.

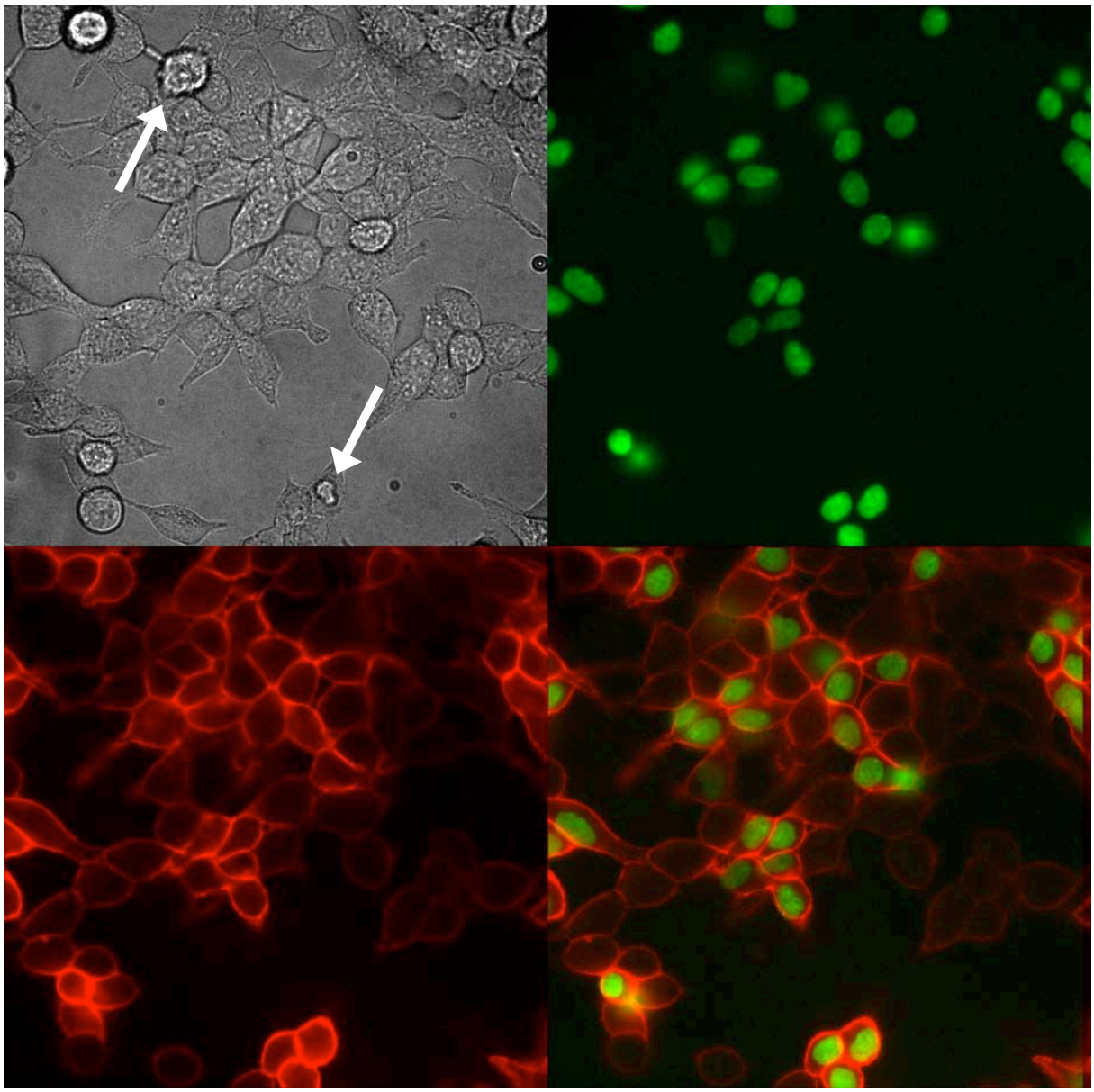

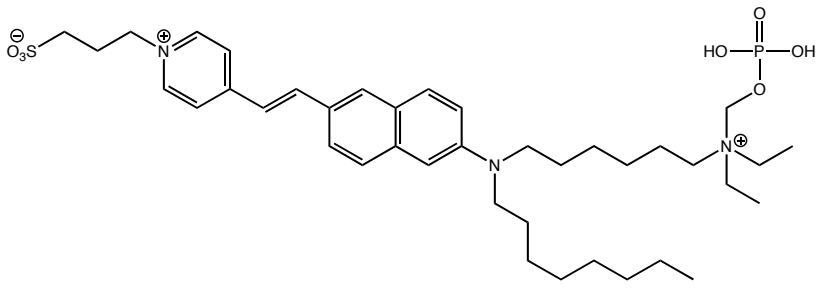

Figure 3-18 1 μM 8-2,2P6-ANEPPS. The pattern of cell staining is similar to the previously described family of phosphate prodyes, although discernibly better. Also, dead cells do not show non-specific staining, as indicated by the arrows.

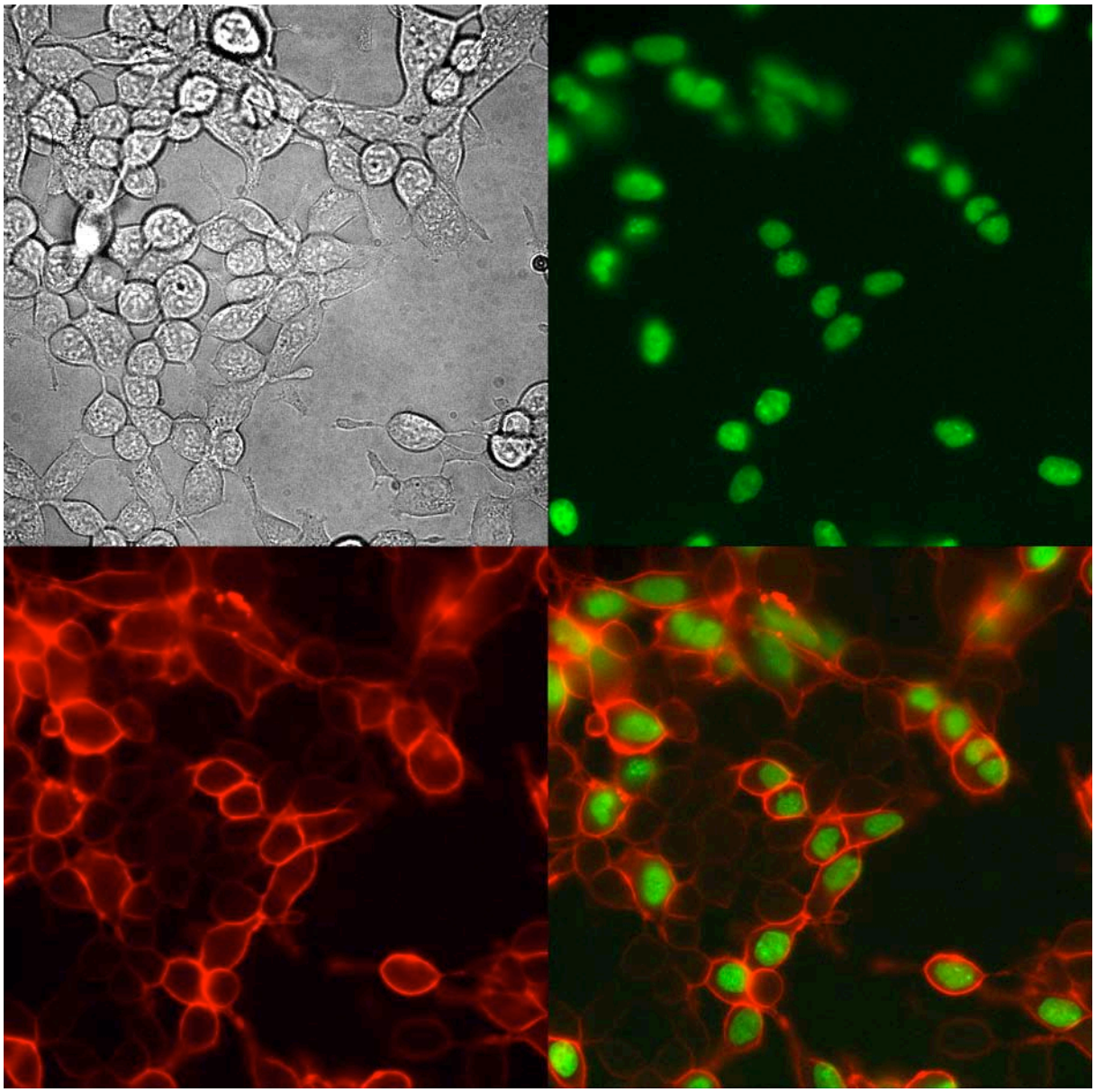

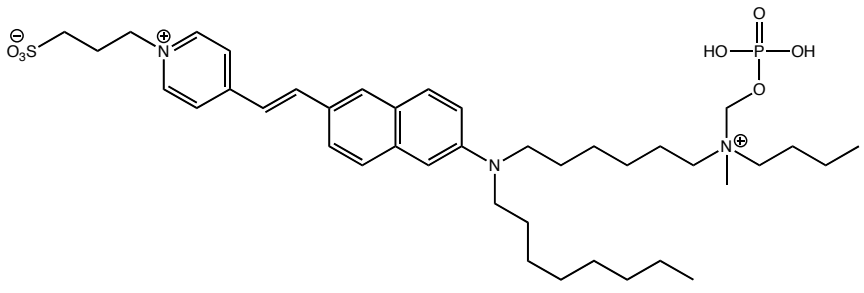

Figure 3-19 1 µM 8-1,4P6-ANEPPS. The level of selective staining for this prodye is clearly much higher than that of any of the terminal-phosphate class of prodyes. Non-specific staining of the control HEK293 cells is highest in cell membrane directly adjacent to transfected cells. Control cells up to two cell-lengths away from transfected cells show light staining.

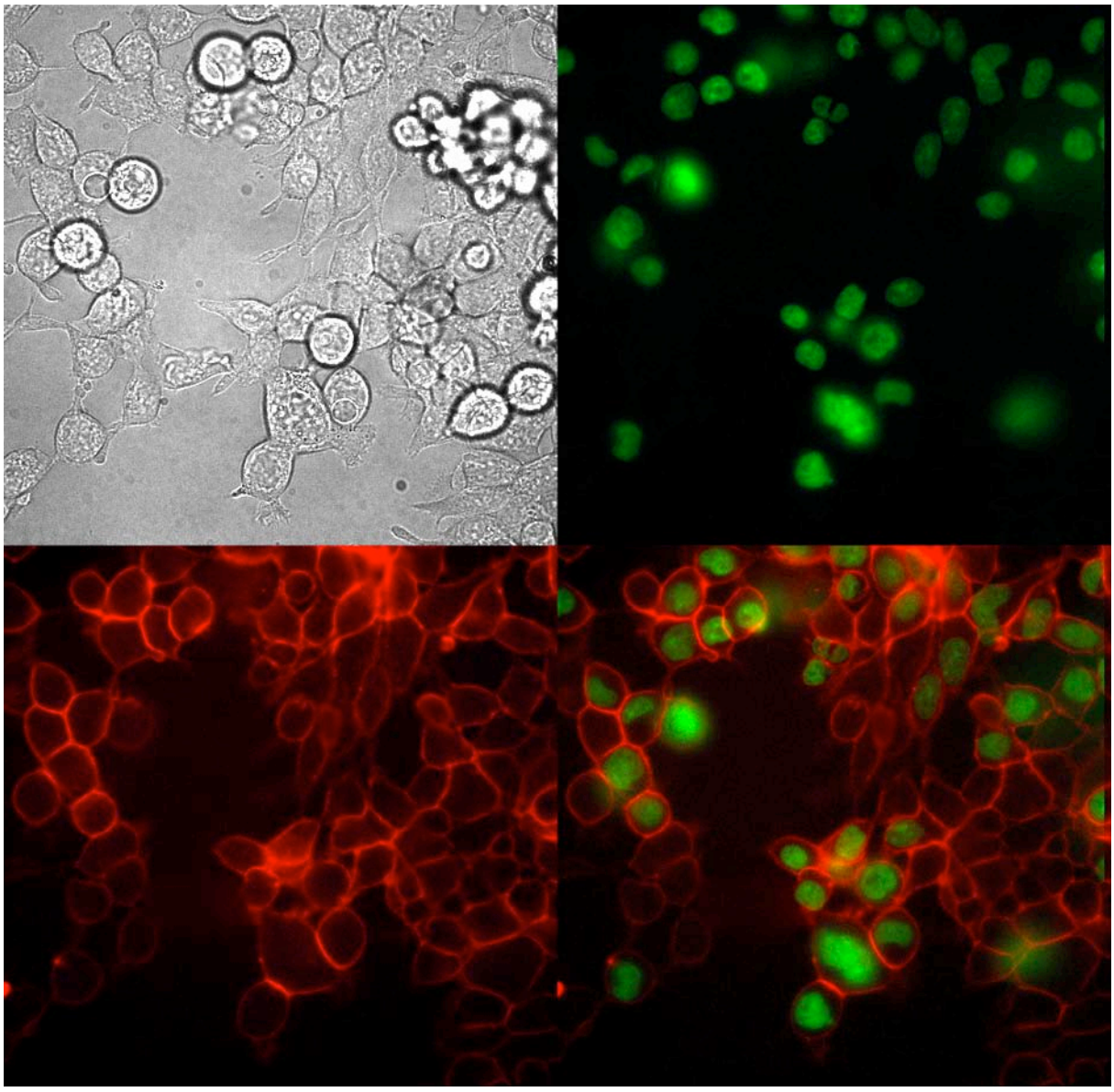

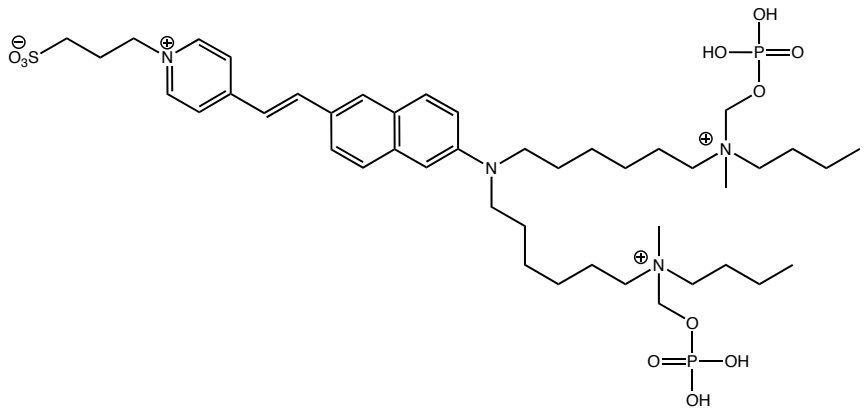

Figure 3-20 1 µM Di-1,4P6-ANEPPS. Although similar in structure to the prodye 8-1,4P6-ANEPPS, this prodye performs notably worse than the other N-phosphonooxymethyl prodyes, with selective staining at level similar to the phosphate prodyes observed.

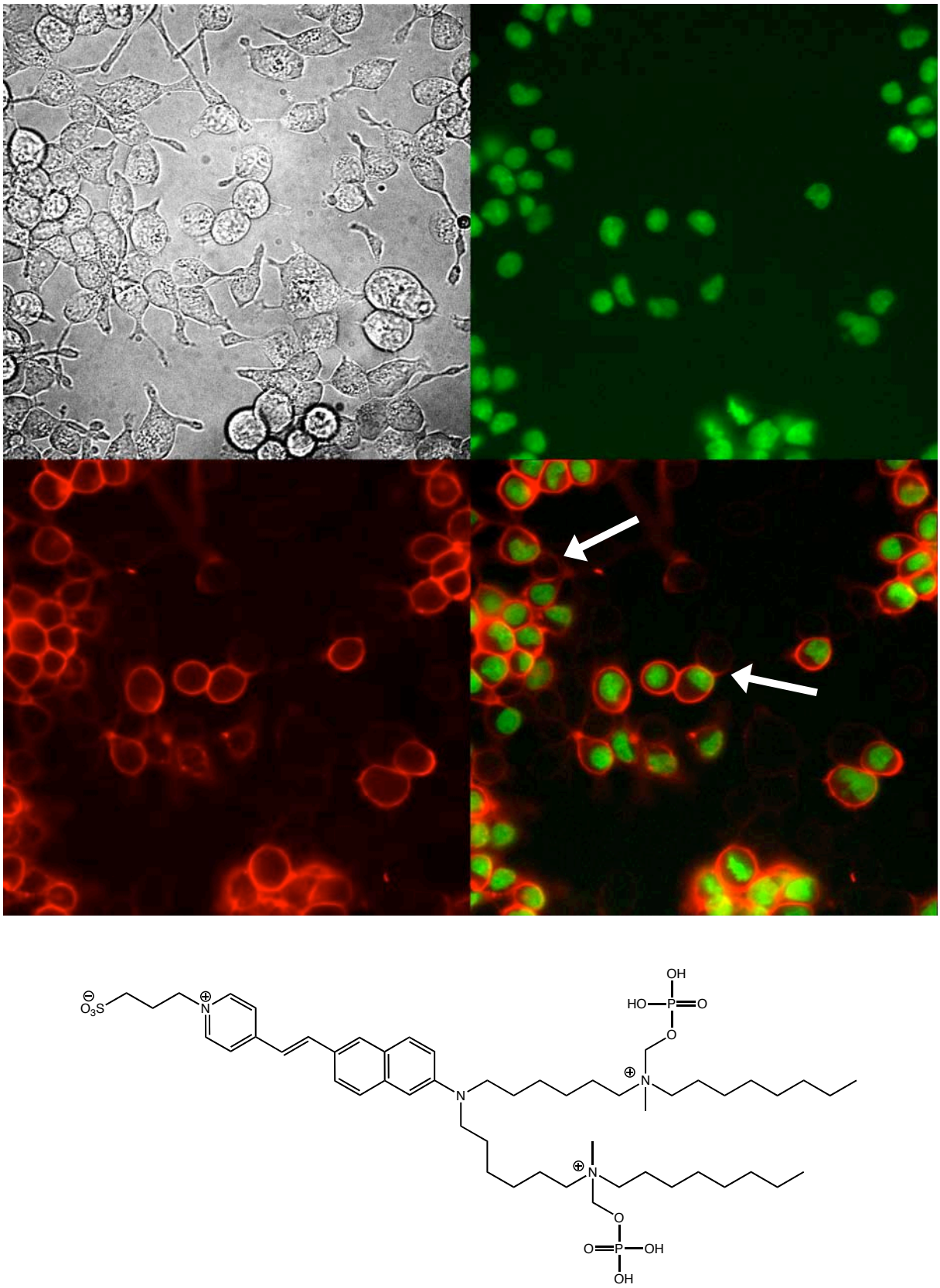

Figure 3-21 1 µM Di-1,8P6-ANEPPS. Excellent results are obtained with this prodye. High levels of plasma membrane staining are observed exclusively on HEK293 cells co-expressing H2BGFP and PLAP, with very slight membrane staining of control cells directly in contact with the targeted cells, as shown by the arrows.

3.3 SELECTIVE STAINING

In order to quantitatively measure the performance of the prodyes, the image sequences for each experiment were analyzed to determine the rate of uptake of dye into the cell membranes. The image stack was imported into Matlab, and the images aligned with a 2D translation image registration algorithm [112], based on discrete Fourier transforms for phase retrieval [113]. From the aligned stack, regions of interest were marked over patches of selectively stained plasma membrane; patches of membrane from control cells located 1 cell-width from a transfected cell (~15-20 μm); and from areas on the coverslip glass free from cells. The photon count for 2D patches was averaged and plotted, shown in Figure 3-23.

Subtracting the background fluorescence from the targeted and unspecific staining time-courses allowed the fitting of the exponential function:

$$\Delta F = \Delta F_{\infty}\left[1-\exp\left(-t/\tau_{stain}\right)\right]$$

This function was found to match the time-course empirically, as shown in Figures 3-24 to 3-30, and discussed further in Section 3.3.1. The fit for Di-1,8P6-ANEPPS appears almost linear, due to the time constant for staining τ_{stain} being much greater than the staining time.

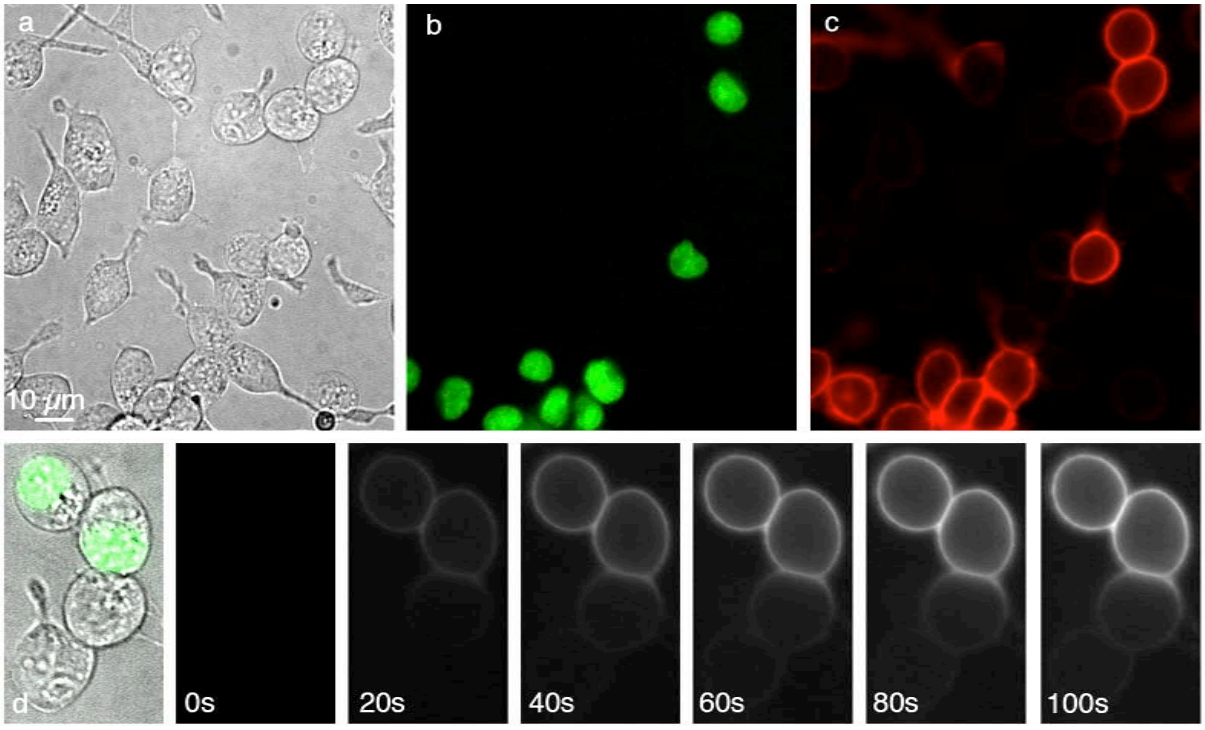

Figure 3-22 The progression of selective staining with 1 μM Di-1,8P6-ANEPPS; a) the bright field view of a mixture of transfected and control HEK293 cells, b) green fluorescence from the H2BGFP construct, c) the staining pattern of the cells after 100 seconds, d) a magnified and rotated view of top right of image (a), followed by images taken at 20 second intervals during the staining procedure.

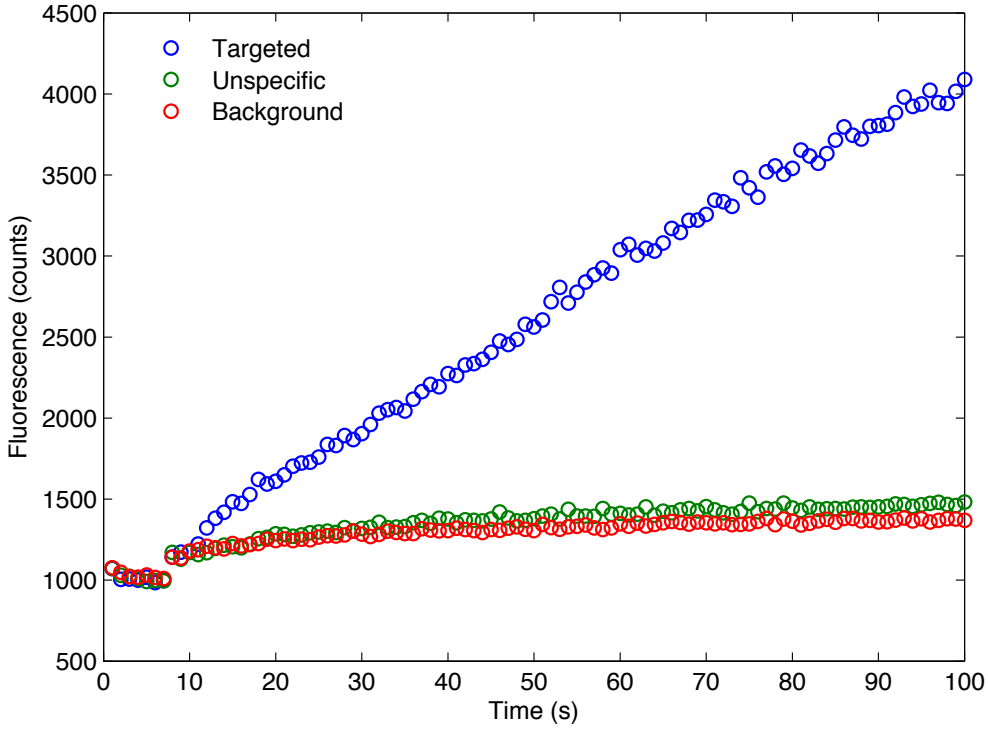

Figure 3-23 Di-1,8P6-ANEPPS staining progression.

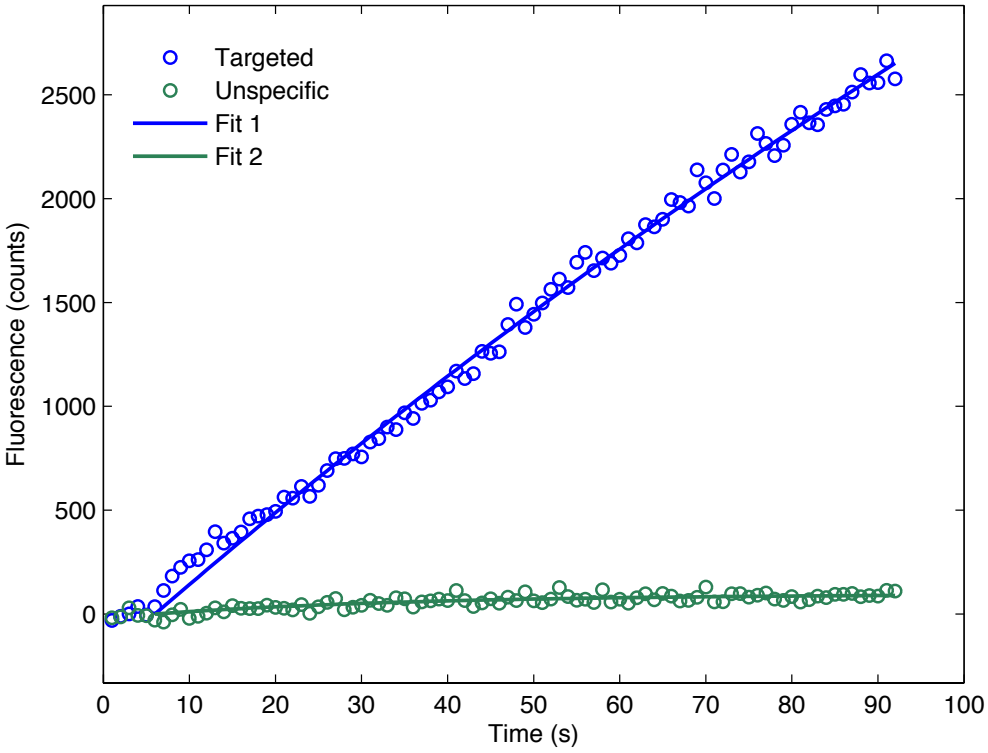

Figure 3-24 Di-1,8P6-ANEPPS corrected and fitted to an exponential function.

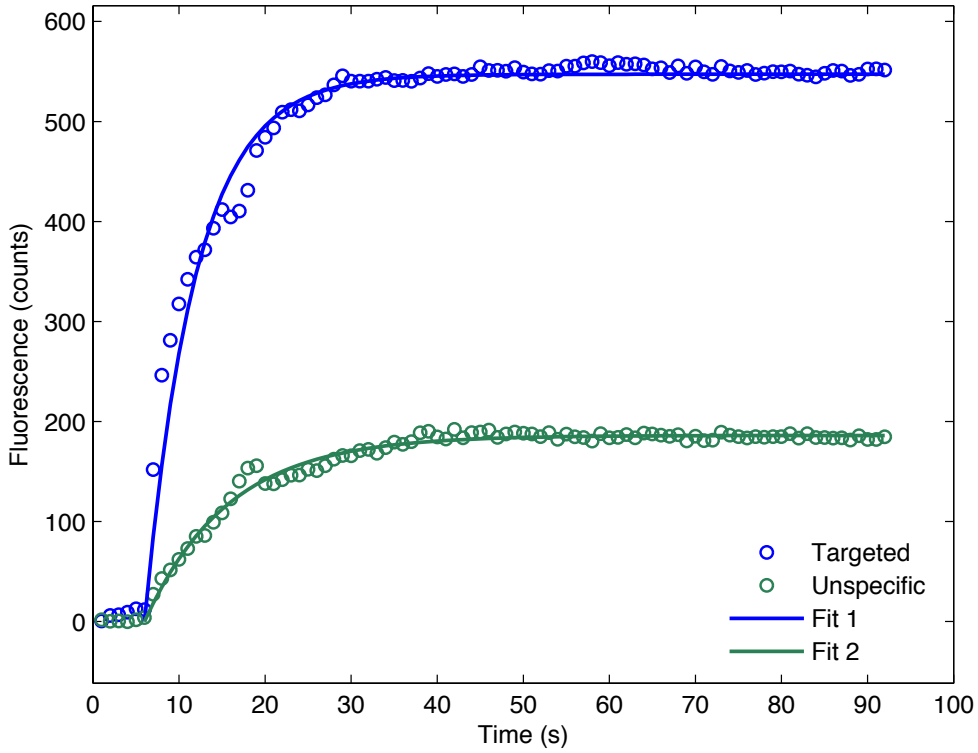

Figure 3-25 Di-8P-ANEPPQ corrected and fitted to an exponential function.

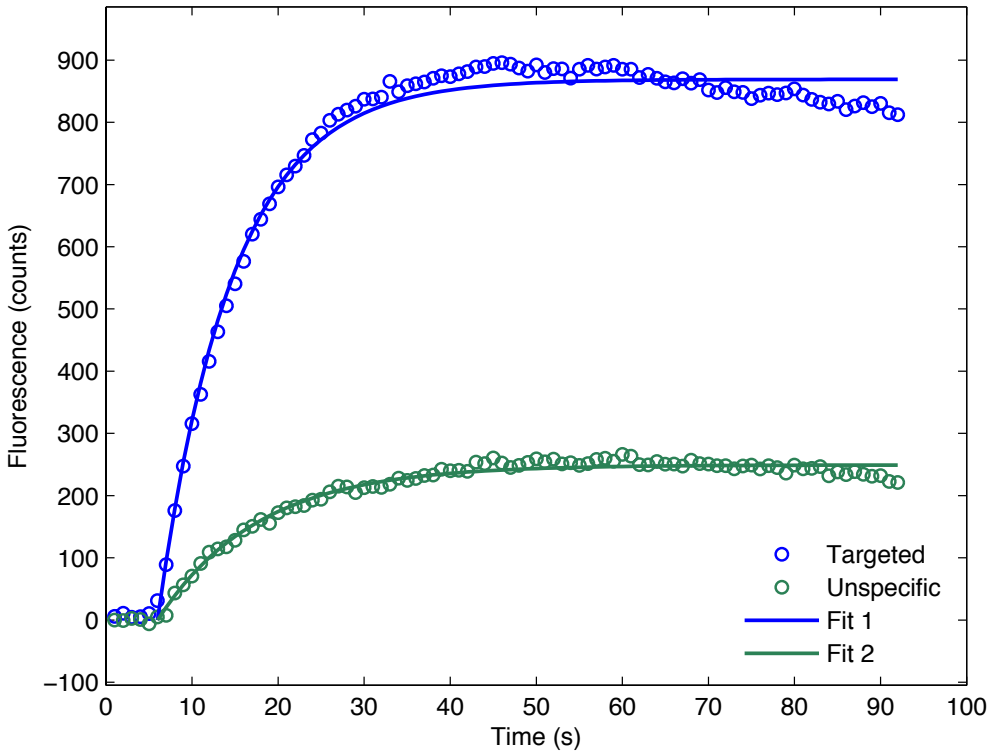

Figure 3-26 Di-10P-ANEPPQ corrected and fitted to an exponential function.

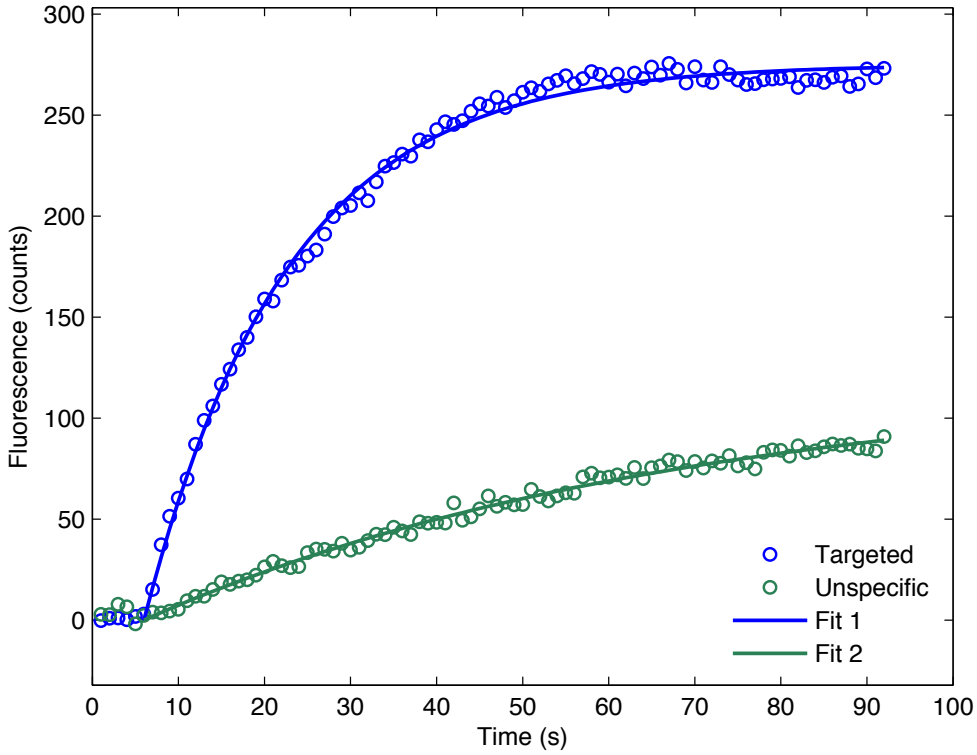

Figure 3-27 Di-12P-ANEPPQ corrected and fitted to an exponential function.

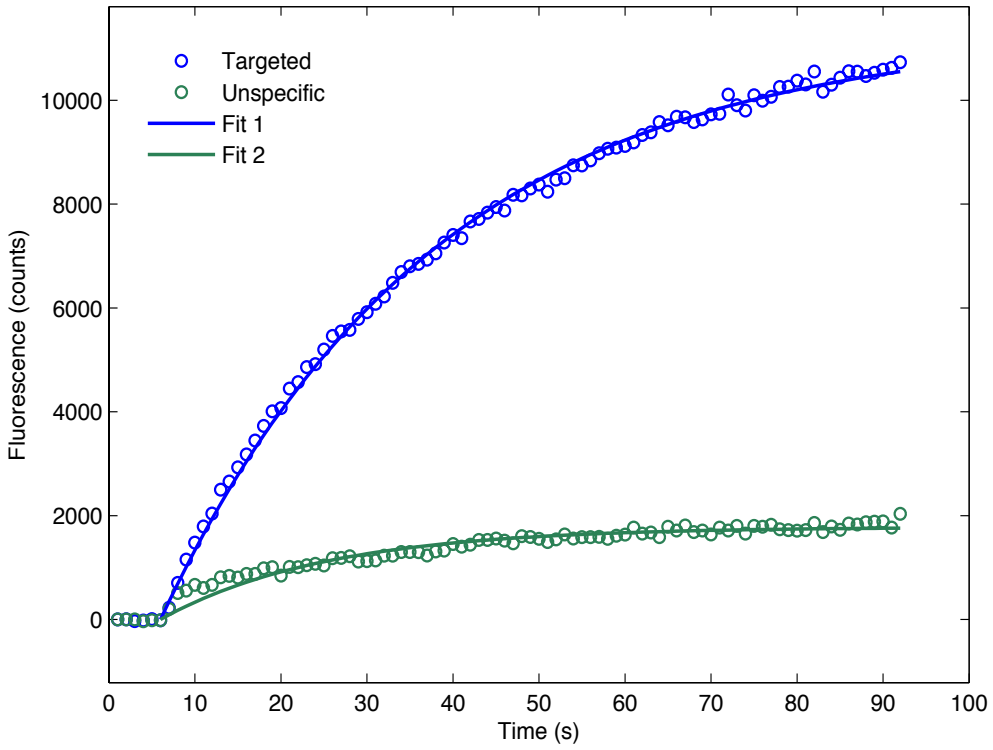

Figure 3-28 8-2,2P6-ANEPPS corrected and fitted to an exponential function.

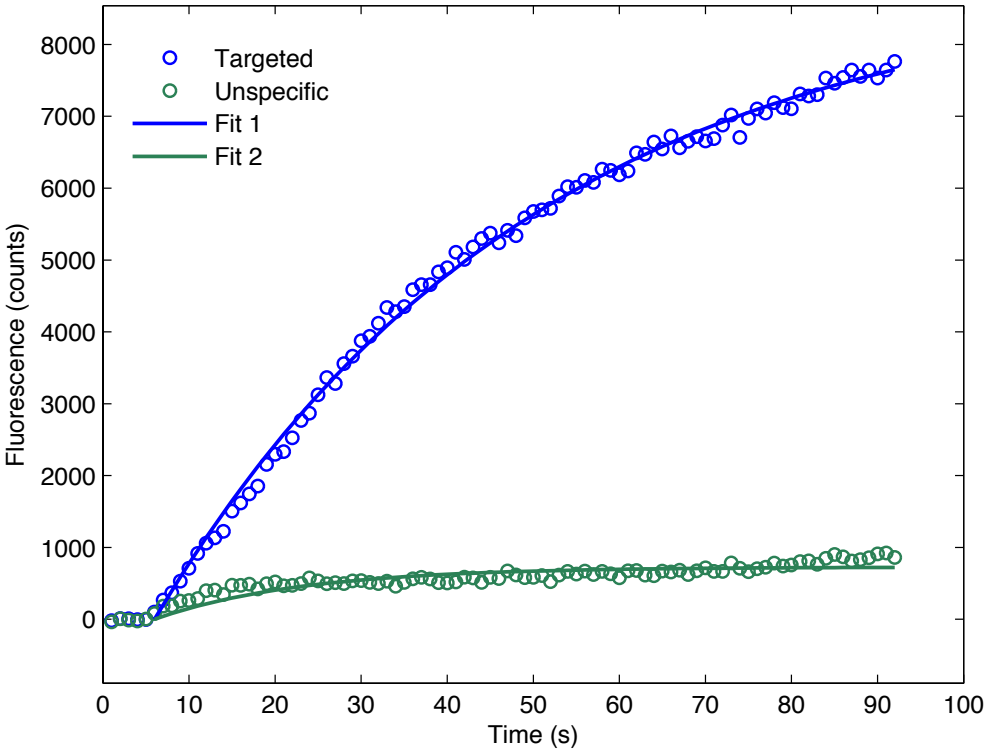

Figure 3-29 8-1,4P6-ANEPPS corrected and fitted to an exponential function.

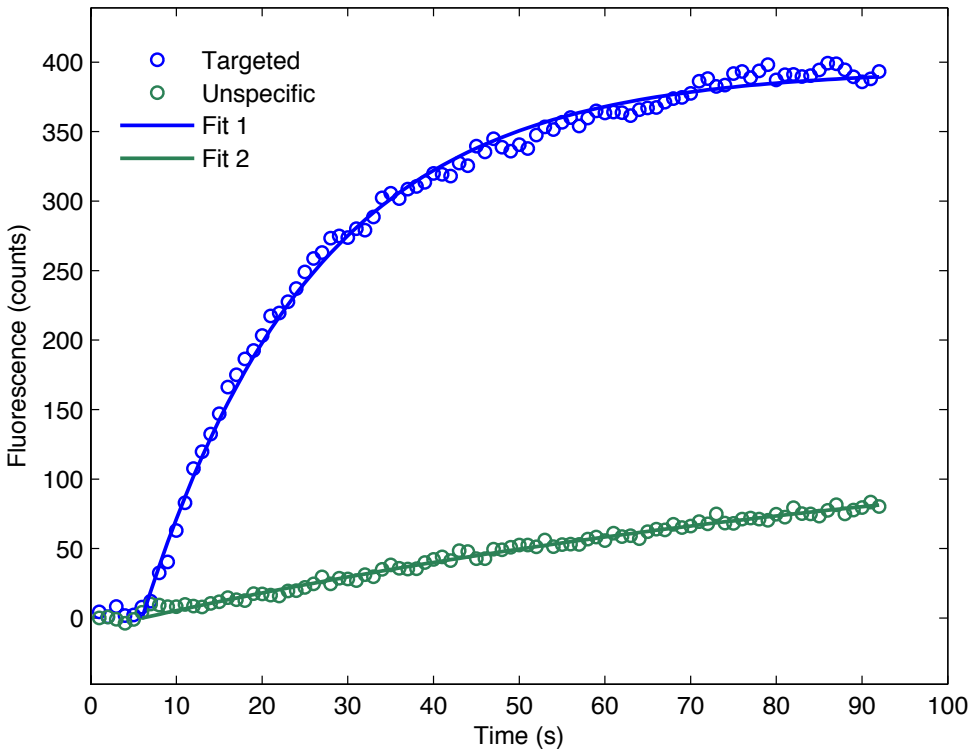

Figure 3-30 Di-8-1,4P6-ANEPPS corrected and fitted to an exponential function.

Prodye	Targeted Staining			Unspecific Staining		
	ΔF_∞	95% bounds		ΔF_∞	95% bounds	
Di-8P-ANEPPQ	547.3	557	537.5	186.1	187.8	184.5
Di-10P-ANEPPQ	868.9	876.3	861.6	249.3	252.1	246.5
Di-12P-ANEPPQ	275.1	277.1	273.2	119.2	127	111.5
8-2,2P6-ANEPPS	11300	11400	11200	1780	1831	1730
8-1,4P6-ANEPPS	8912	9073	8751	726.4	762.8	690
Di-1,4P6-ANEPPS	394.9	398	391.8	147.9	165.7	130.1
Di-1,8P6-ANEPPS	10200	12600	7749	95.61	110.4	80.85

Table 4 The estimated ΔF_∞ values for the voltage sensitive dyes, as determined by fitting with an exponential function.

Prodye	Targeted Staining			Unspecific Staining		
	τ (s)	95% bounds		τ (s)	95% bounds	
Di-8P-ANEPPQ	5.937	6.517	5.357	9.734	10.2	9.269
Di-10P-ANEPPQ	8.66	9.084	8.237	11.65	12.29	11
Di-12P-ANEPPQ	16.62	17.08	16.17	62.64	69.34	55.93
8-2,2P6-ANEPPS	31.94	32.62	31.25	19.38	21.28	17.48
8-1,4P6-ANEPPS	44.03	45.6	42.45	17.2	20.41	13.98
Di-1,4P6-ANEPPS	20.11	20.65	19.58	107.7	125.2	90.29
Di-1,8P6-ANEPPS	284.8	360.8	208.8	31.4	43.42	19.39

Table 5 The estimated time constant (τ) values for the voltage sensitive dyes, as determined by fitting with an exponential function.

The results of the fitting analysis are shown in Table 4, giving the estimated final levels of targeted and unspecific staining, and Table 5, with the estimated time constants. A comparison of the staining capability of the dyes, based on the ratio of targeted-to-unspecific cell membrane fluorescence and shown in Figure 3-31, demonstrates that all of the synthesized dyes show selective staining capabilities, but that the phosphate dyes give poor results. This is in line with the results for the ASP- based dyes [11,12], where the ratio of targeted to unspecific staining were around 2-6, compared to the values of 2.3-3.5 for the new ANEPPS-based prodyes.

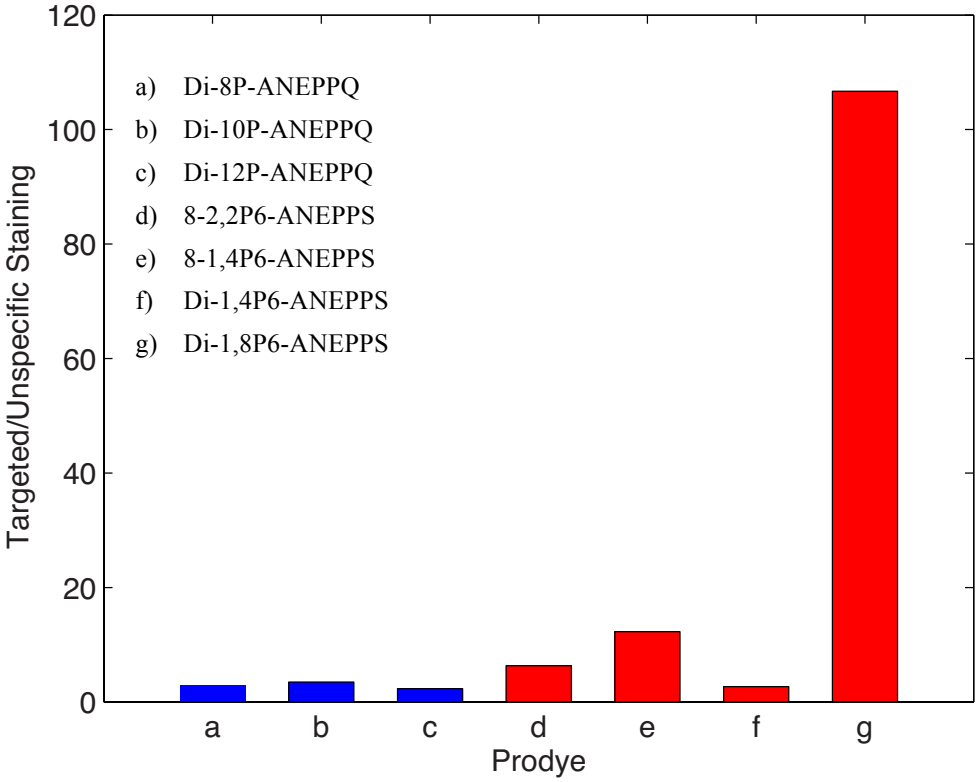

Figure 3-31 Prodye staining capacity, showing the ratio of targeted-to-unspecific cell membrane fluorescence. Phosphate prodyes are shown in blue, and N-phosphonooxymethyl prodyes in red.

The results for the N-phosphonooxymethyl prodyes show considerable variability, with the prodye di-1,8P6-ANEPPS clearly showing excellent selectivity. Surprisingly, the largest variation was found between the dyes that contain two functionally modified tails. This suggests that it requires a large amount of aliphatic carbons to offset the polar tertiary amine in the tail of the activated dye.

Without an estimation of the binding coefficients, a more detailed analysis of the effects of dye tail composition on membrane binding cannot be undertaken, and as discussed in Chapter 2, the very low solubility of the activated dye and very weak binding of the prodye to lipid vesicles prohibits the binding-assays used for the ASP-based dyes.

3.3.1 Modelling the Kinetics of Selective Staining

To interpret the graphs of staining of the cell membranes expressing PLAP, we must first build a model for selective staining. To do so, we divide the immediate area around the site of dye activation into three regions that each contain a certain concentration of activated dye: The cell membrane, an unstirred Nernst layer of thickness δ_W in which the dye is formed, and a bulk aqueous phase above that into which dye can diffuse.

The production of dye by the enzymatic activation of the prodye by membrane bound alkaline phosphatase occurs with a rate of j_E per unit area of accessible cell surface. Dye produced in this Nernst layer can either bind to the membrane, giving a density of σ_M, or diffuse into the bulk media according to the diffusion coefficient D_W, and is described by Eq. 1.

$$\delta_W \frac{dc_W}{dt} = j_E - \frac{D_W}{\delta_W} c_W - \frac{d\sigma_M}{dt} \qquad (1)$$

The kinetics of dye membrane binding depend on the relative association and dissociation constants, k_{ass} and k_{diss} respectively, Eq. 2.

$$\frac{d\sigma_M}{dt} = k_{ass} c_W - k_{diss} \sigma_M \qquad (2)$$

As the concentration of the hydrophobic dye always remains very low, we introduce the quasi-stationary Bodenstein condition $dc_W/dt = 0$ for the concentration of activated dye in the Nernst layer. This simplifies Eq. 1, giving rise to an overall staining equation, Eq. 3.

$$c_W = \frac{\delta_W}{D_W} \left(j_E - \frac{d\sigma_M}{dt} \right) \qquad (3)$$

The insertion of Eq. 3 into Eq. 2, and solving for $d\sigma_M/dt$ produces Eq. 4:

$$\left(\frac{k_{ass}\delta_W}{k_{diss} D_W} + \frac{1}{k_{diss}} \right) \frac{d\sigma_M}{dt} = \frac{k_{ass}\delta_W}{k_{diss} D_W} j_E - \sigma_M \qquad (4)$$

The kinetic equilibrium relation $\gamma_{MW} = k_{ass}/k_{diss}$, together with Eq. 4 describes the dynamics of staining, and if we defined τ_{MW} as the time constant for staining, and stationary staining $\bar{\sigma}_M$, we derive Equation 5.

$$\tau_{MW} \frac{d\sigma_M}{dt} = \bar{\sigma}_M - \sigma_M \qquad (5)$$

$$\tau_{MW} = \frac{\gamma_{MW} d_W}{D_W} + \frac{1}{k_{diss}}, \quad \bar{\sigma}_M = \frac{\gamma_{MW}\delta_W}{D_W} j_E$$

3.3 SELECTIVE STAINING

To model the staining of cells from the moment of prodye addition, we integrate Eq. 5 to produce Eq. 6.

$$\sigma_M = \sigma_M \left[1 - \exp\left(-t/\tau\right)\right] \qquad (6)$$

This simple kinetic model fits the measured data very accurately. It explains the linear increase in staining seen during the initial phase, followed by an exponential transition to stationary staining. The unspecific staining in the non-targeted cells cannot be explained so easily, as the staining may be due to a combination of prodye binding, low levels of intrinsic phosphatase activity and diffusion of the activated dye. Although these factors are also present in the targeted cells, the high rate of dye production at the cell surface masks the progression of these minor processes.

If we assume that δ_W and D_W, the thickness of the unstirred Nernst layer and the diffusion coefficient both remain constant, and that the association constant k_{ass}, among the different dyes also remains steady, then we can derive the relationship between the time constant for staining and stationary staining by rearranging Eq. 5 to give Eq. 7. The second requirement, that of identical association constants, is suggested by experiments on the partitioning coefficients and rates of dissociation between fatty acids and lipid vesicles, from which we can estimate that the rate constant of association is independent of the length of the hydrocarbon chain [114,115].

$$\bar{\sigma}_M = \tau_{MW} j_E - \frac{j_E}{k_{diss}} \qquad (7)$$

This would imply a linear relationship between τ_{MW} and $\bar{\sigma}_M$, modulated by the varying values of k_{diss} between the dyes. As $\bar{\sigma}_M$ itself is hard to measure, masked by the combination of selective and non-selective staining, we instead use the more easily measured staining capacity, the ratio of stationary selective staining to non-target cell unspecific staining. Plotting these calculated values against the measured time constant τ_{MW}, we generate Figure 3-32 and Figure 3-33 for the phosphate and N-phosphonooxymethyl prodyes respectively. The later prodyes show a linear relationship between staining capacity and the time constant. As the staining capability of the prodyes is calculated from the unspecific staining, and this in turn is a function of the k_{diss}, this model is plausible. The lack of a linear relationship for phosphate prodyes may be due to the 'fold-back' model described in Figure 2-14, as the increase in unspecific staining is independent of k_{diss}.

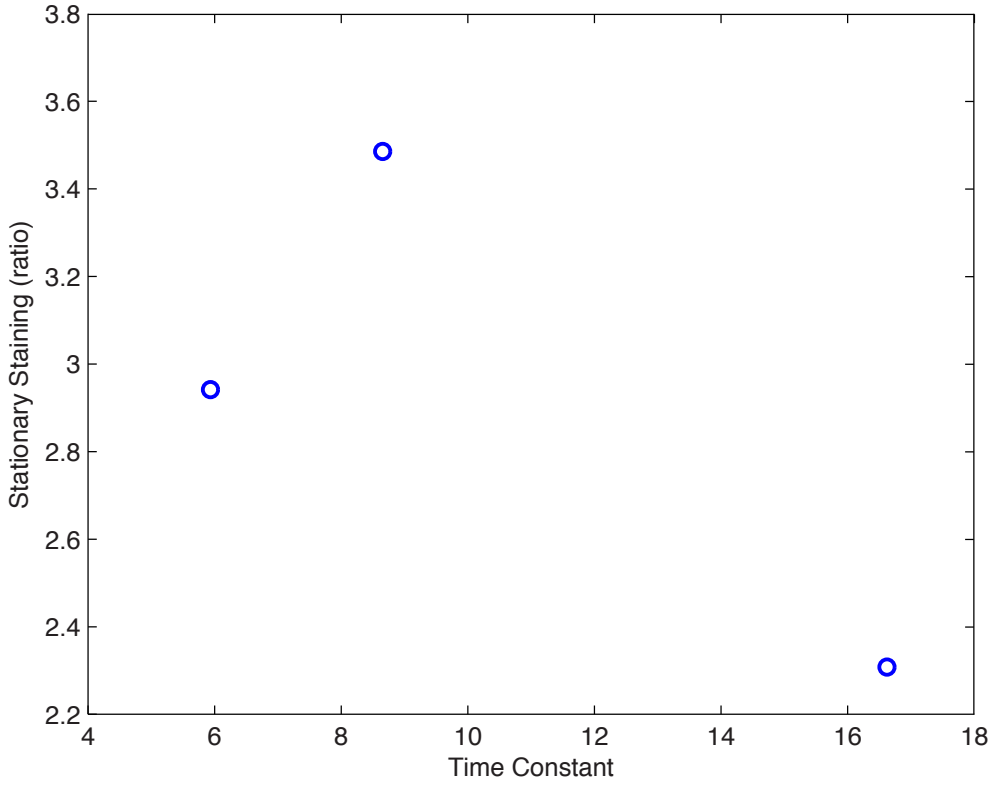

Figure 3-32 The relationship between τ_{MW} and the staining capacity for the various phosphate prodyes.

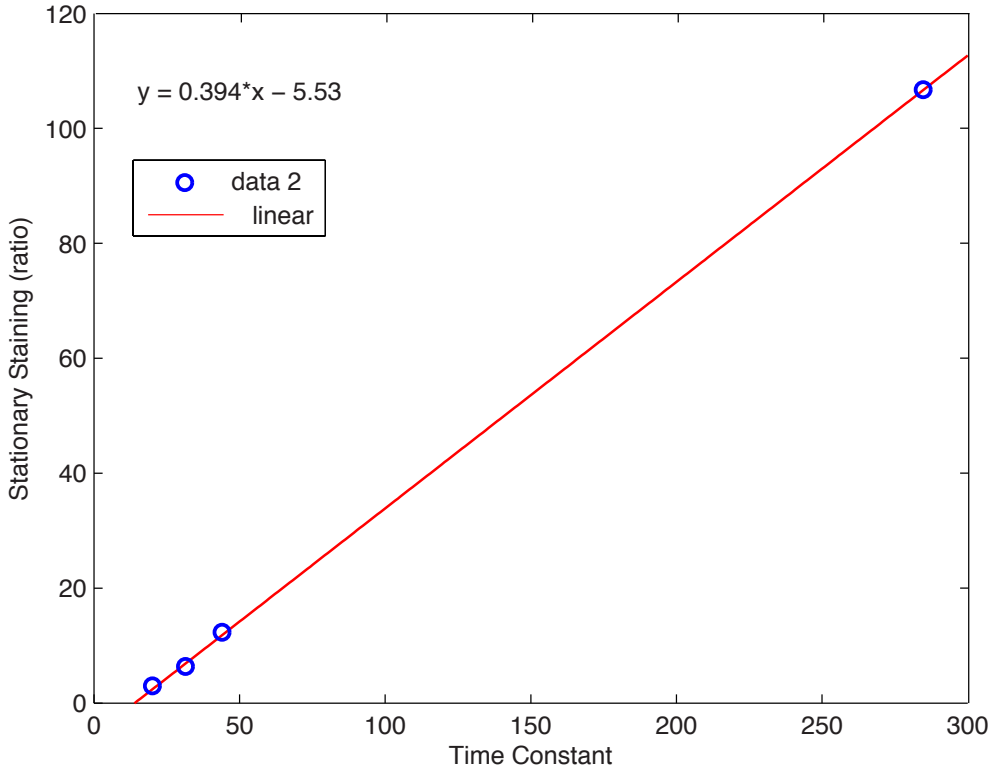

Figure 3-33 The relationship between τ_{MW} and the staining capacity for the various N-phosphonooxymethyl prodyes.

3.4 Future Directions

It is important to understand the factors that influence the selective staining capability of the newly developed prodyes. With this information, a more rational approach could be undertaken in the development of the next generation of dyes. In each of the prodye tails, there are 3 aliphatic carbon chains that can be varied in length; it is assumed that both the number of carbon atoms and the relative lengths of the chains can influence the binding ability of the dye, the first in terms of thermodynamics, and the second for the optimal conformation of the dye in the planar lipid bilayer.

As the lipid-vesicle titration method, employed in [11], is unsuitable for the N-phosphonooxymethyl prodyes, it is necessary to find a new method to determine the association and dissociation constants. One such method is surface plasmon resonance [116], a technique that can determine total bound mass of small organic molecules to a substrate-bound lipid bilayer. By measuring the rates of accumulation of the dye to the lipid at various concentrations, and its subsequent elution into buffer, models for the binding and dissociation mechanism can be built. This would allow for the development of the optimum tail composition for selective staining specificity.

Another option for measuring the binding constants would be to use the current apparatus to measure the diffusion time-course of the activated dye from transfected 'emitter' cells, as modeled by a Bessel function, to surrounding, non-transfected HEK293 cells, located at various distances from the emitter. Further work would be required to develop the model, and to modify the apparatus to prevent convection currents from spreading the activated dye.

The goal for the development of new, genetically targeted voltage sensitive dyes is the labeling of neurons *in vivo*. In pursuit of this target, HEK293 cells were used as a model cell type, due to the ease of culturing and transfection of this cell line. In parallel with HEK293 experimentation, preliminary work was undertaken to develop protocols with which to target dissociated E18 rat hippocampal neurons.

Neurons prepared using standard techniques [117], were subjected to transient transfection with the pcDNA5_FRT-IRES-PLAP-H2BGFP, using the procedure described in Appendix 7.4.5. This procedure was found to be difficult, and dissociated neurons undergo high mortality during transfection. However, neurons grown on glass coverslips were successfully transfected, and using a 1 μM Di-1,8P6-ANEPPS staining solution, neurons could be successfully selectively stained, as shown in Figure 3-34.

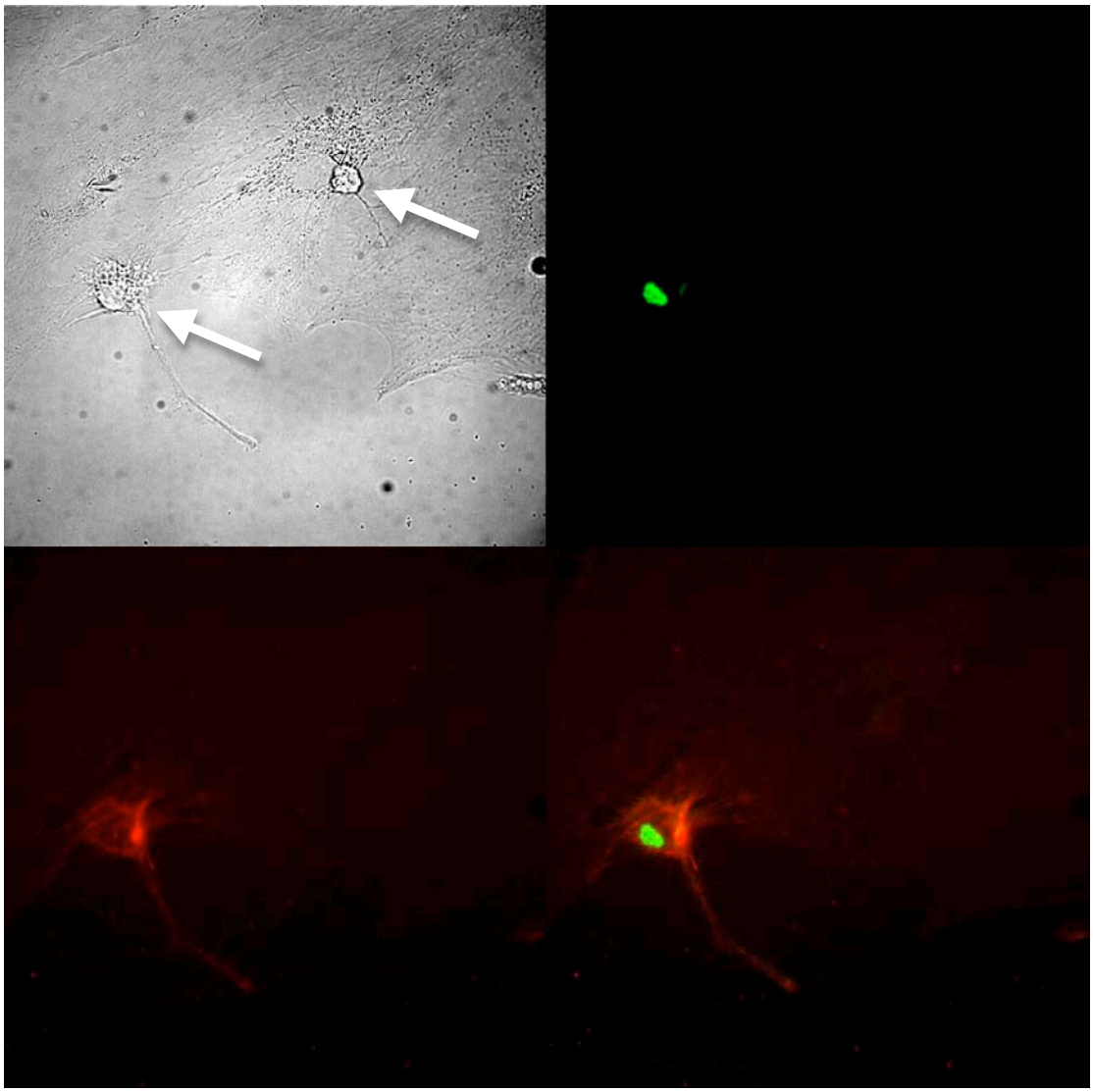

Figure 3-34 Two cultured hippocampal E18 rat neurons (marked by arrows). Selective staining is clearly observable in the neuron co-expressing H2BGFP and PLAP, with staining evident along the axon and dendrites.

Further work is required in improving cell culture techniques, transfection methodology and staining conditions. Co-culturing neurons with glial cells significantly increases dissociated neuron health, improving cell morphology and survival rates. Transfection options include biolistics, nucleofection and electroporation [118]. These techniques require complex equipment and reagents, and in the case of nucleofection and electroporation, can only be used to transfect freshly isolated neurons, however the cells that survive the transfection procedure are healthy, and do not suffer from adverse morphological changes that occur with Lipofectamine usage.

4 VOLTAGE SENSITIVE MEASUREMENTS

Fast voltage sensitive dyes are commonly used to measure the transmembrane voltage of neurons and myocardial cells, in a mechanism reliant on a combination of the molecular Stark effect, solvatochromism and photoisomerism. These effects rely on the correct position and orientation of the dye molecule in the hydrophobic domain of the cell membrane.

Although the new dyes demonstrate excellent selective staining, particularly with Di-1,8P6-ANEPPS, the placement of the tertiary amine moieties in the tail-region of the dyes may disrupt its positioning in the membrane, and hence reduce voltage sensitivity. Therefore, the aim of this chapter is to describe the design, development and application of the apparatus used to measure the voltage sensitivity of Di-1,8P6-ANEPPS in selectively stained cell membrane.

4.1 VSD mechanism

The Stark effect involves the interaction between the light-induced charge-redistribution that occurs in the body of the chromophore during excitation, and the charge's interaction with the electrical field that lies across the cell membrane. Due to the orientation of the amphiphilic voltage sensitive dyes in lipid membrane, the intramolecular charge translation from the pyridinium moiety to the excited-state aniline moiety has a charge displacement Δx of an elementary charge e_0, directed against a field $\bar{E} = V_M / d_M$, from the membrane voltage V_M across a membrane of thickness d_M. The spectral shift due to the charge displacement of a chromophore, oriented at angle ϑ to the membrane normal, is given in Equation 1 (Planck's constant h, velocity of light c).

$$hc\Delta\bar{\nu}_{ex}^{\max} = e_0 \Delta x \bar{E} \cos\vartheta \qquad (1)$$

From experimental studies on the ANEP chromophore of Di-4-ANEPBS [7], the measured shift in excitation $\Delta\bar{\nu}_{ex}^{\max}$ for ΔV_M = 100mV and d_M = 4 nm, gives the calculated charge displacement across the membrane as 0.43 nm. With the genetically targetable dyes sharing the same chromophore as Di-4-ANEPBS, the orientation angle ϑ of the chromophore in the lipid membrane is a critical factor in the Stark effect sensitivity achievable with these selectively staining dyes.

There are two effects that may interfere with a Stark-effect mechanism. Firstly, as the ANEP chromophore is not rigid, there can be both photoisomerism across the CC double bonds and photorotamerism around CC single bonds. These changes modify the dyes fluorescent properties and the intramolecular charge displacement during photoexcitation, and may be affected by the transmembrane electrical field. In particular, rotamerism has been shown to lead to a twisted internal charge-transfer state with a reduced fluorescence quantum yield [7].
Secondly, the hemicyanine voltage sensitive dyes are strongly solvatochromic; during photoexcitation and the subsequent emission of radiation, there is a rapid change in the dipole moment. This can interact with the solvent shell, with changes in solvent polarity leading to differential stabilization between the ground and excited states, and hence a change in the energy gap between these electronic states. As transmembrane voltage may influence the location of the charged dye at the interface of the extracellular media and the hydrophobic core of the plasma membrane, the dye can be subject to these effects. This voltage sensitive effect is present in many, but not all hemicyanine dyes, with the ANNINE dyes almost pure Stark effect probes, and ANEPPS relying on a mixture of the three mechanisms [7].

4.2 Experimental Apparatus

4.2.1 Optical Setup

The apparatus used to record voltage sensitivity in selectively stained cells is also required to image GFP localization and record the bright field images of the cells. All images were recorded with a Zeiss Plan-NEOFLUAR 40x/1.30 oil-immersion objective. For bright field imaging, the Axiovert 135T's integrated halogen lamp was used as the light source. For GFP imaging, the standard excitation and emission bandpass filters, and dichroic mirror set were used together, with an excitation at 470/40 nm, emission at 535/50 nm and the long-pass dichroic mirror at 495 nm. This is shown in Figure 4-1, together with the fluorescence spectra for GFP and Di-1,8P6-ANEPPS.
The emission profile of Di-4-ANEPBS in shown in Figure 4-1 (red), is quite broad and overlaps with red end of the GFP emission spectrum. With high levels of cell membrane staining, the fluorescence intensity of the dye measured in the 470/40 nm emission bandpass filter can be stronger than the signal generated by GFP, and therefore GFP imaging is made before the addition of the dye. The main emission profile for GFP is much narrower than the dye, however, the broad shoulder in the spectrum from 530-630 nm overlaps with the peak of the ANEP chromophore emission. The restriction of GFP to the cell nucleus, via its fusion to histone 2B, prevented plasma membrane overlap.

4.2 EXPERIMENTAL APPARATUS

The excitation of GFP through the standard 470/40 nm bandpass filter was accomplished with the use of a high intensity solid-state device, a 5 watt LED emitting at 470 nm with a spectral half-width of 25 nm. A high intensity of light is required for VSD measurements, as the signal (*S)* in a measurement will be proportional to the intensity of the light (*I)* and the noise (*N)* in that measurement will be proportional to square-root of *I*. Thus, the signal-to-noise ratio of each recording is given by $SNR = I/\sqrt{I}$. The intensity of LED illumination using this type of light source has been found to be sufficient for high-speed measurements of voltage sensitive dyes; the pixels of the most commonly used camera for voltage-sensitive dye research, the MiCAM Ultima (Brainvision Inc. Japan), were saturated with a sampling frequencies of 1kHz, at just ~60% of the maximum LED output [119] . Because a LED's emission is proportional to its current, the current was held constant with the Agilent Triple Output DC Power supply in current mode, and switched with an opto-isolator that was controlled by the TTL output of the camera system.

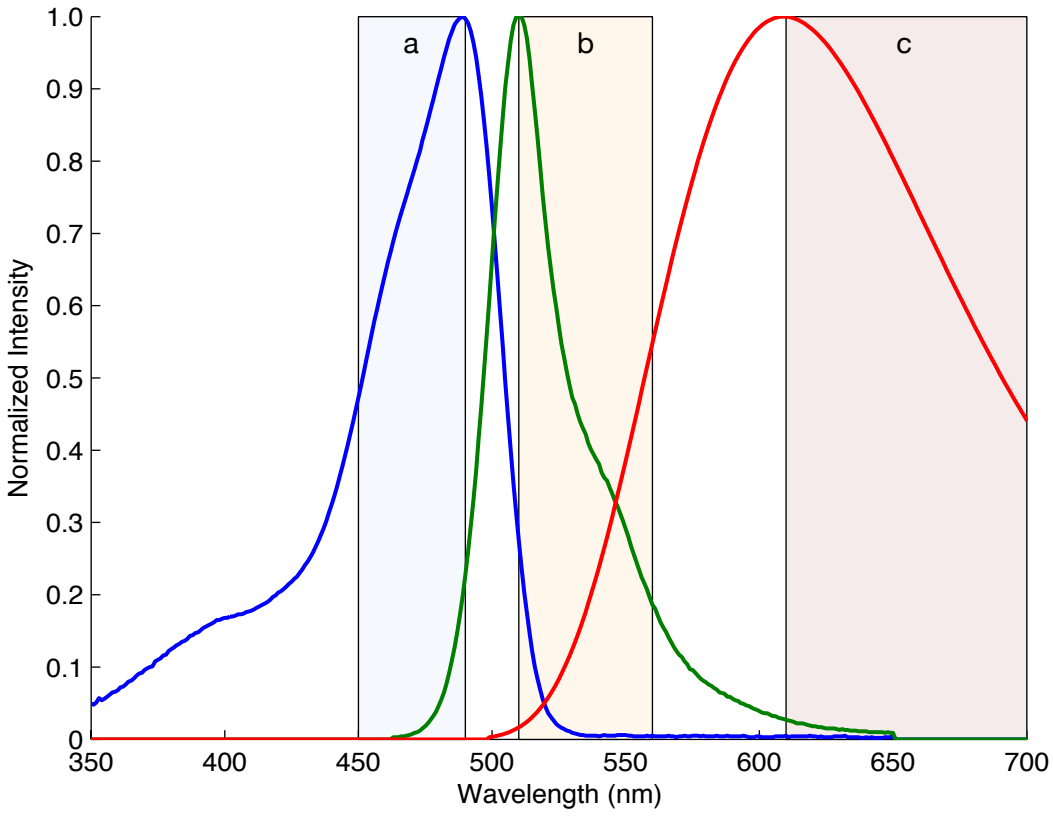

Figure 4-1 Fluorescent spectral data. The GFP excitation spectrum (blue), GFP emission spectrum (green), Di-1,8P6-ANEPPS emission spectrum (red), and the GFP filter set; a) excitation, b) emission and c) the long pass filter used for Di-1,8P6-ANEPPS voltage sensitivity recordings.

The LED used for fluorescence excitation also consumes far less power than other sources, at ~5 watts, compared to several hundred watts for the standard halogen and xenon lamp. This simplifies the apparatus, and eliminates the long warm-up times required by halogen lamps and the need for active cooling systems. The fast turn-on time (<100 ns) also eliminates the need for a mechanical shutter system, reducing vibration and increasing the maximum recording rate. The cheap plastic collimator lenses accompanying these LEDs was replaced with a precision collimator taken from a Zeiss mercury lamp, and the LEDs were mounted onto a heat-sink that attached to rails, allowing the easy adjustment of the focus and the exchange of LED modules (Figure 3-11). The excitation of the ANEP dye was made using a 530 nm LED with a spectral half width of 35 nm, and filtered with a bandpass of 525/30 nm. This excitation window is on the red edge of the excitation spectrum; the peak for Di-4-ANEPPS excitation in Retzius neuron membrane from *Hirudo medicinalis* ganglia was found at 484 nm [120]. The blue shift in the excitation spectrum that arises from increasing transmembrane potential generates the largest fractional changes from illumination in this region. Published works on a variety of cell and tissue types use excitation in this region, such as 520/40 nm for guinea pig ventricles [121] and chick spinal chord [122], 543 nm He-Ne laser light for dissociated cardiac tissue [123], and 530/20 nm for hippocampal slices [124].

For the emission spectrum, the maximum voltage sensitivity that could be found in cultures of cardiac myocytes was found to be obtainable with a long pass filter at 610 nm [125], and *Helix aspersa* neurons [126]. Figure 4-2-b shown the location of the long pass filter (610 nm, horizontal dashed line), and its relative location to the zones of maximum sensitivity. Shown in Figure 4-2-a is the parameterized spectral profile for Di-4-ANEPPS in Retzius cells, and in Figure 4-2-b is the sensitivity profile, showing the sensitivity achievable with the marked 530/30 nm filter [7]. The blue-shift in the emission spectrum of ANEP dyes induced by positive membrane potentials decreases the amount of light able to pass the 610 nm long pass filter, and so positive transmembrane voltages give negative fluorescent signals with this optical setup.

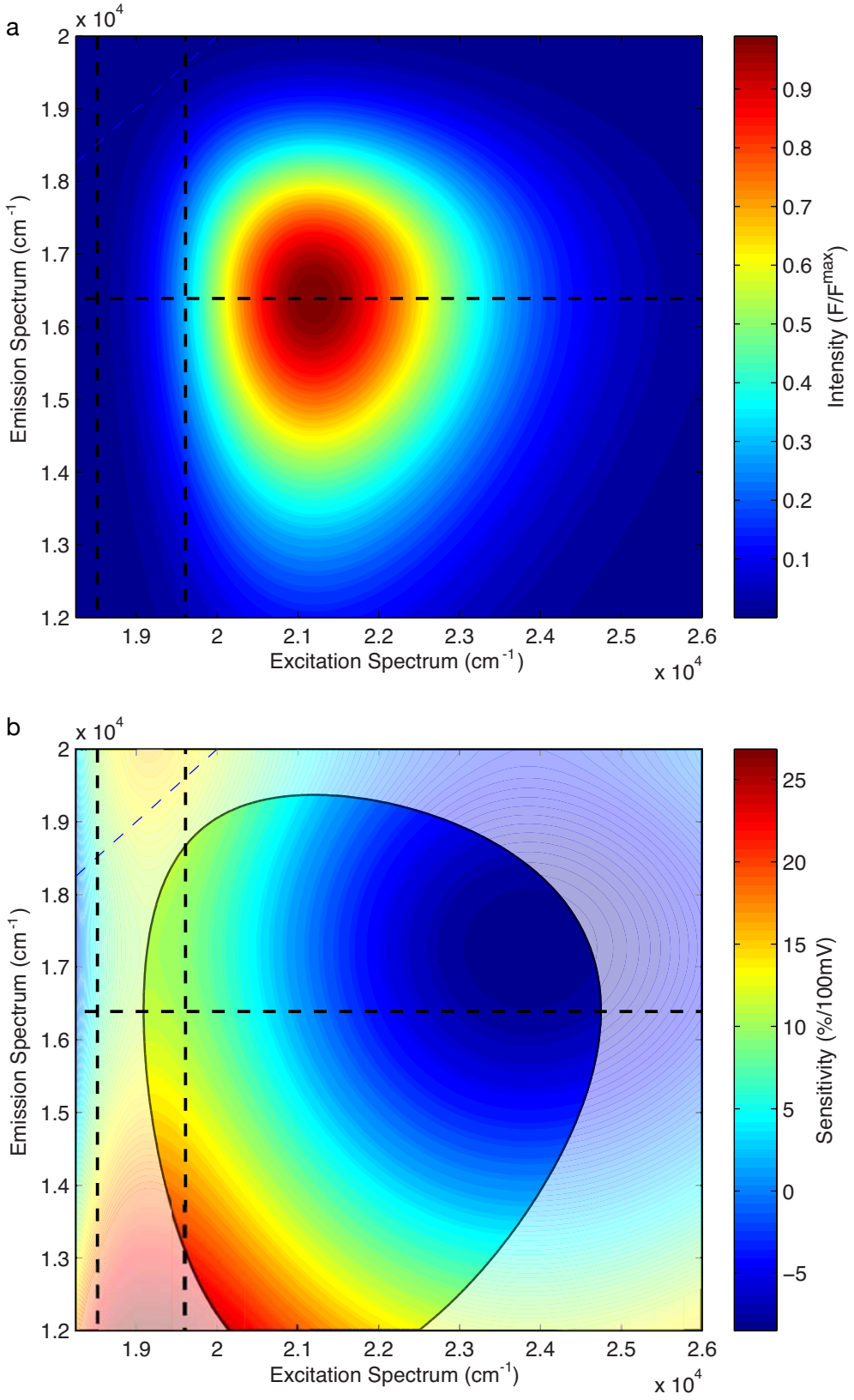

Figure 4-2 The parameterized spectral profiles for the ANEP chromophore, based on empirical data from [7]. a) the relative fluorescence spectra $F_{\bar{\nu}}(\bar{\nu}_{ex},\bar{\nu}_{em})/F_{\bar{\nu}}^{\max}$, b) the parameterized sensitivity $\Delta F_{\bar{\nu}}/F_{\bar{\nu}}\Delta V_M$ at V_M = -70 mV. The dashed vertical lines mark the width of the excitation bandpass filter, and the dashed horizontal line marks the emission long pass filter used.

4.2.2 Voltage Assay Apparatus

There are several techniques available to modulate the voltage across a cell's plasma membrane. For excitable cells, such as leg nerves from the lobster *Homarus americanus*, platinum electrodes can be used to stimulate the cells via direct external contact [21], or with a glass microelectrode for Guinea pig (*Cavia porcellus*) transverse hippocampal slices [127]. For other cell types, like *Xenopus* oocytes [128], or HEK293 cells [129], the patch-clamp technique can be used to very accurately control the transmembrane voltage of the cell. However, excitable tissue is difficult to culture *in vitro*, and its non-dividing cells require the use of transient transfection techniques that are extremely inefficient. Patch clamp techniques yield the highest levels of accuracy, but are limited to single cells. Thus, we chose to generate transmembrane voltages in transfected cell populations via the application of an extracellular electrical field with parallel platinum electrodes, as modified from previous literature [26,130]. This technique allows for the imaging of multiple cells in parallel, and the rapid replication of each experiment.

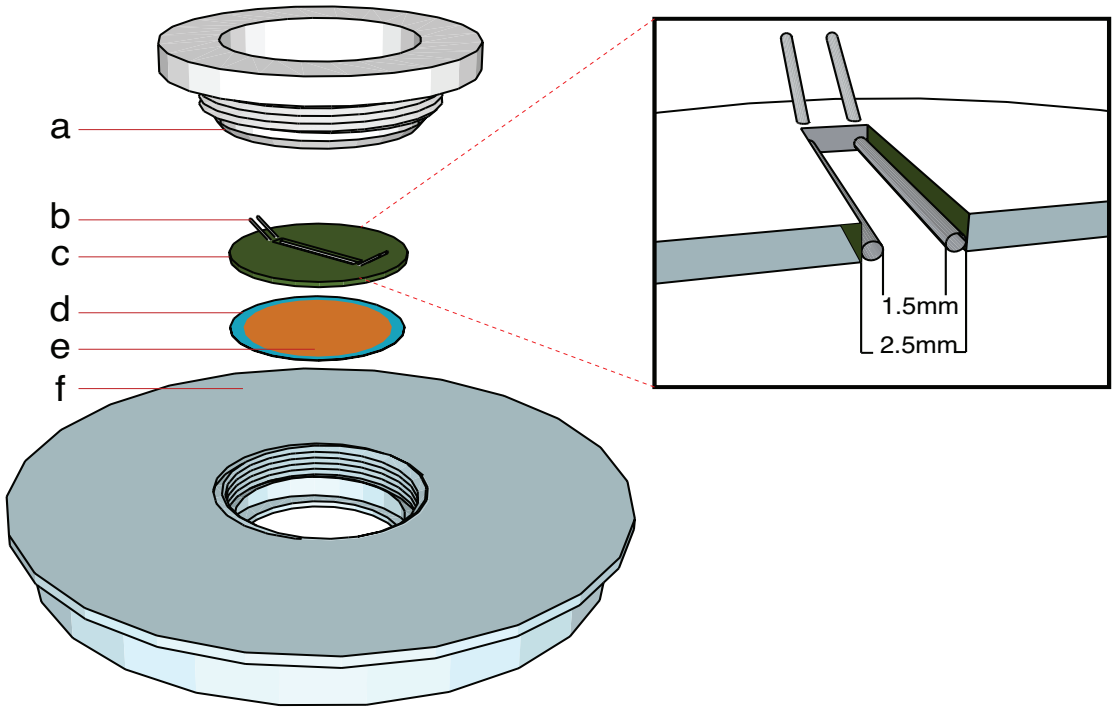

Figure 4-3 Electrical-Field apparatus; a) threaded mounting device, b) platinum electrodes, c) Plexiglas chamber, d) coverslip glass, e) HEK293 cell monolayer, f) Plexiglas mounting tray.

4.2 EXPERIMENTAL APPARATUS

The apparatus consisted of a large, removable Plexiglas mounting tray, as shown in Figure 4-3-f, which could be set into a frame on the microscope mounting plate. Into this disk, a monolayer of 40-60% confluent HEK293 cells (Figure 4-3-e), grown on 30mm round coverslip glass (Figure 4-3-d), could be mounted. A smaller Plexiglas disk, into which a slit 18mm long and 2.5 mm wide was cut (Figure 4-3-c), could then be pressed down onto the coverslip glass, forming a water-tight seal. In the slit in the Plexiglas disk were mounted two Platinum wire electrodes, as shown in Figure 4-3-b, lining the lower side of the long edges and passing though small channels drilled into the ends of the slit. A hollow threaded cylinder (Figure 4-3-a), was used to provide pressure on the disk and coverslip glass, to prevent movement and maintain the watertight seal while allowing access to the cells.

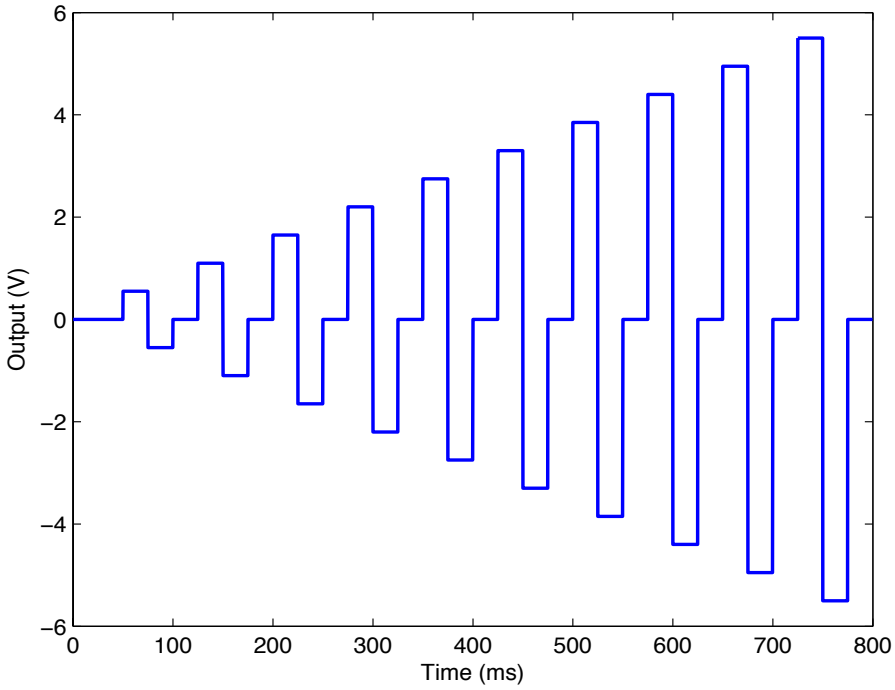

Figure 4-4 The ramping square wave signal generated by the Agilent 33120A arbitrary waveform generator.

The signal used for voltage sensitive measurements was generated on the 33120A Arbitrary Waveform Generator (Agilent), shown in Figure 4-4, and takes the form of a ramping square-wave pattern made up of 25 ms steps, ranging from 0 to ±5.5 V in 10 intervals.

In order to determine the transmembrane voltage induced in HEK293 cells by the platinum electrodes, the HEK293 cells were modeled as uniform, hemispherical shells enclosing a conductive cytoplasm within a uniform electrical field in a conductive medium. Assuming that there is no membrane conductance and that the interior of the cell is isopotential, then the voltage drop occurs across the plasma membrane, as shown in Figure 4-5.

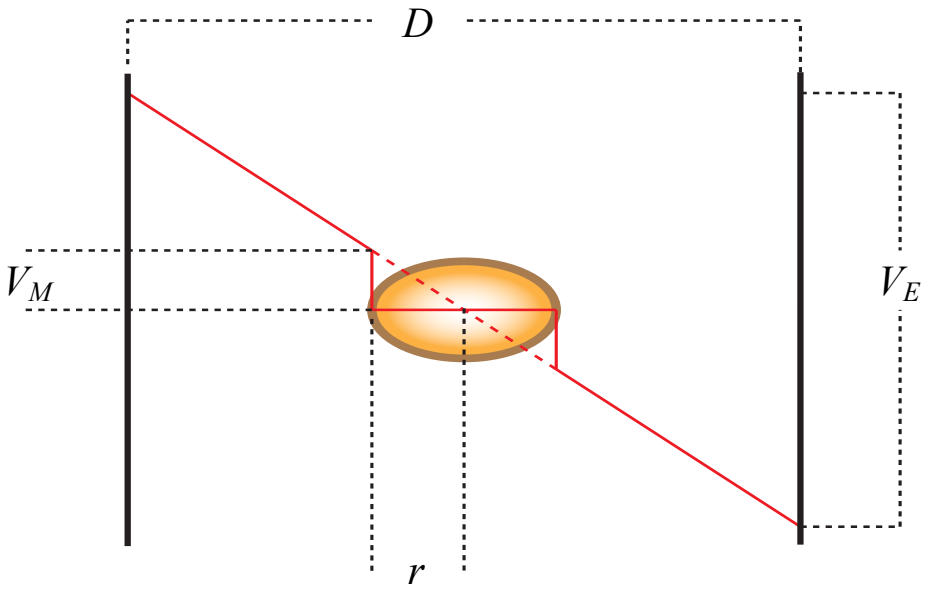

Figure 4-5 The induced transmembrane voltage in the plasma membrane of a cell. The electrical field drops across medium, as shown by the red line. The interior of the cell is isopotential; the linear drop in potential that would take place across the distance of the cell radius occurs over the membrane.

Thus, taking the voltage across the platinum electrodes V_E, and their separation D, we obtain the transmembrane voltage V_M at the pole of the cell from the solution to Laplace's equation in Equation 2, where r is the cell radius. The transmembrane voltage is enhanced by a factor of 1.5 over the voltage drop calculated by taking the product of the field strength and cell radius. This is due to the field lines being displaced by the insulating cell body [26,130] as opposed to running homogenously between the parallel electrodes.

$$V_M = -\frac{3}{2} \bullet \frac{V_E \bullet r}{D} \qquad (2)$$

The push-pull amplifier circuit, as shown in Figure 4-6-a, amplified the signal with a measured gain factor of 4.854x. This is ~3% less than the theoretical 5x gain, due to component tolerance. Neglecting the potential drop across the electrode/aqueous media interface, this generated a maximum of ±26.7 V between the electrodes (Figure 4-4-b), or 17.8 mV·μm^{-1} for the 1.5 mm gap between the platinum electrodes. For a cell of 10 μm diameter, and factoring in the 1.5 fold increase in transmembrane voltage due to the curvature of the field-lines induced by the cell morphology, this results in a maximum transmembrane voltage of 133.5 mV. This value is insufficient to induce electropermeabilization of the cell membrane, which occurs at ranges from 25-50 mV·μm^{-1}, as determined experimentally for Chinese hamster ovary cells (CHO) subjected to electrical fields in a similar apparatus [131].

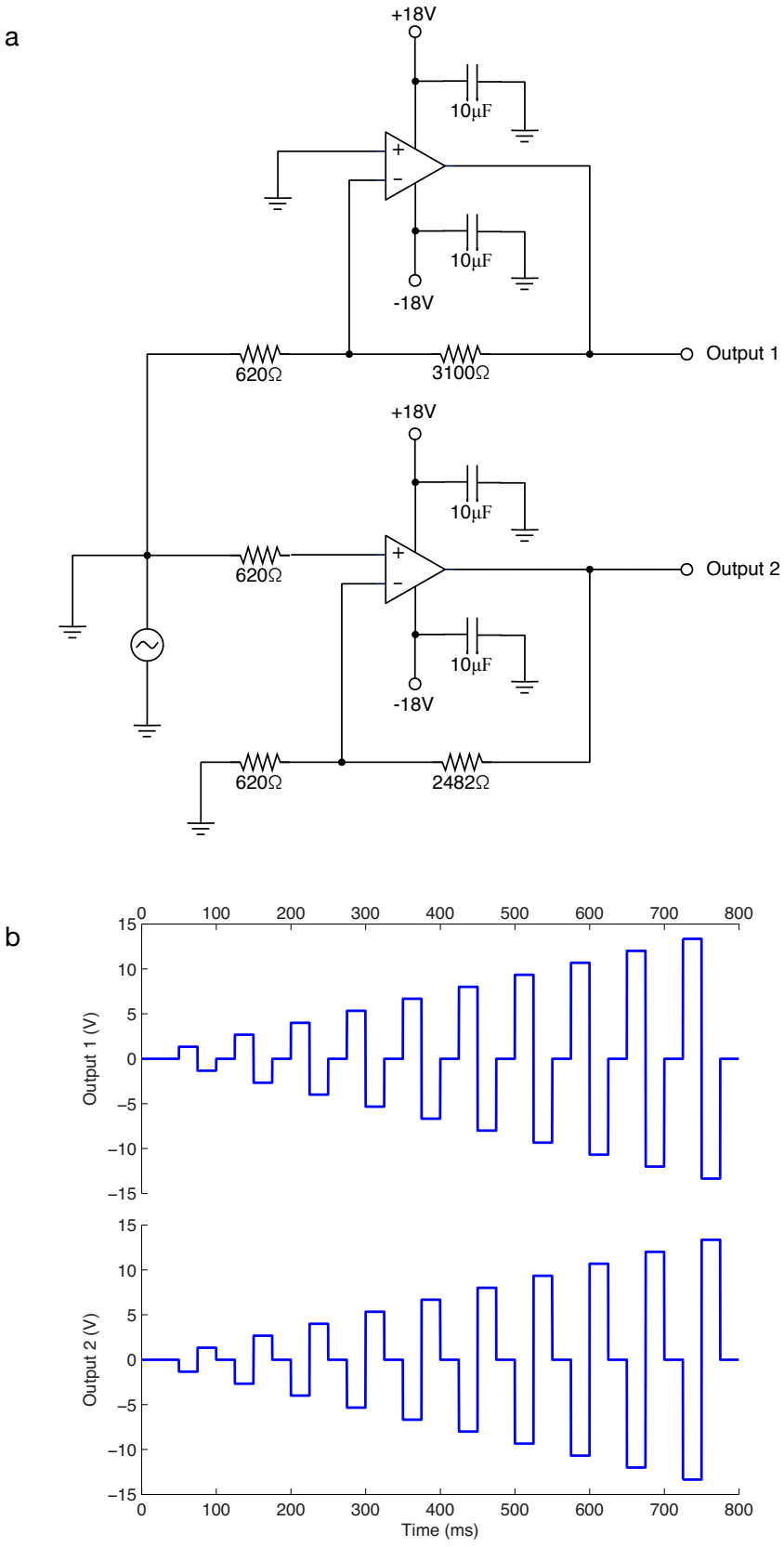

Figure 4-6 Custom push-pull amplifier, based on two OPA547 operational amplifiers, powered by the ±18 V rails of an Agilent Triple Output DC Power supply; a) circuit diagram, b) output of the amplifier.

4.2.3 Camera System

Images were taken with an iXonEM+ (Andor Technology) as shown in Figure 4-7-a, mounted on an Axiovert 135TV microscope (Carl Zeiss), with a Plan-NEOFLUAR 40x/1.30 oil-immersion objective. Fluorescence images were illuminated with Luxeon LEDs (Philips Lumileds) (Figure 4-7-d); GFP images used the Luxeon V LXHL-LB5C (peak 470 nm), with an excitation bandpass filter (470/40 nm), and an emission filter (535/50 nm). VSD sensitivity assays used the Luxeon V LXHL-LM5C (peak 530 nm), with an excitation filter (525/30 nm), and a long pass filter (610 nm) for emission. The camera was controlled via software on a PC, which in turn was used to record image sequence data, Figure 4-7-b.

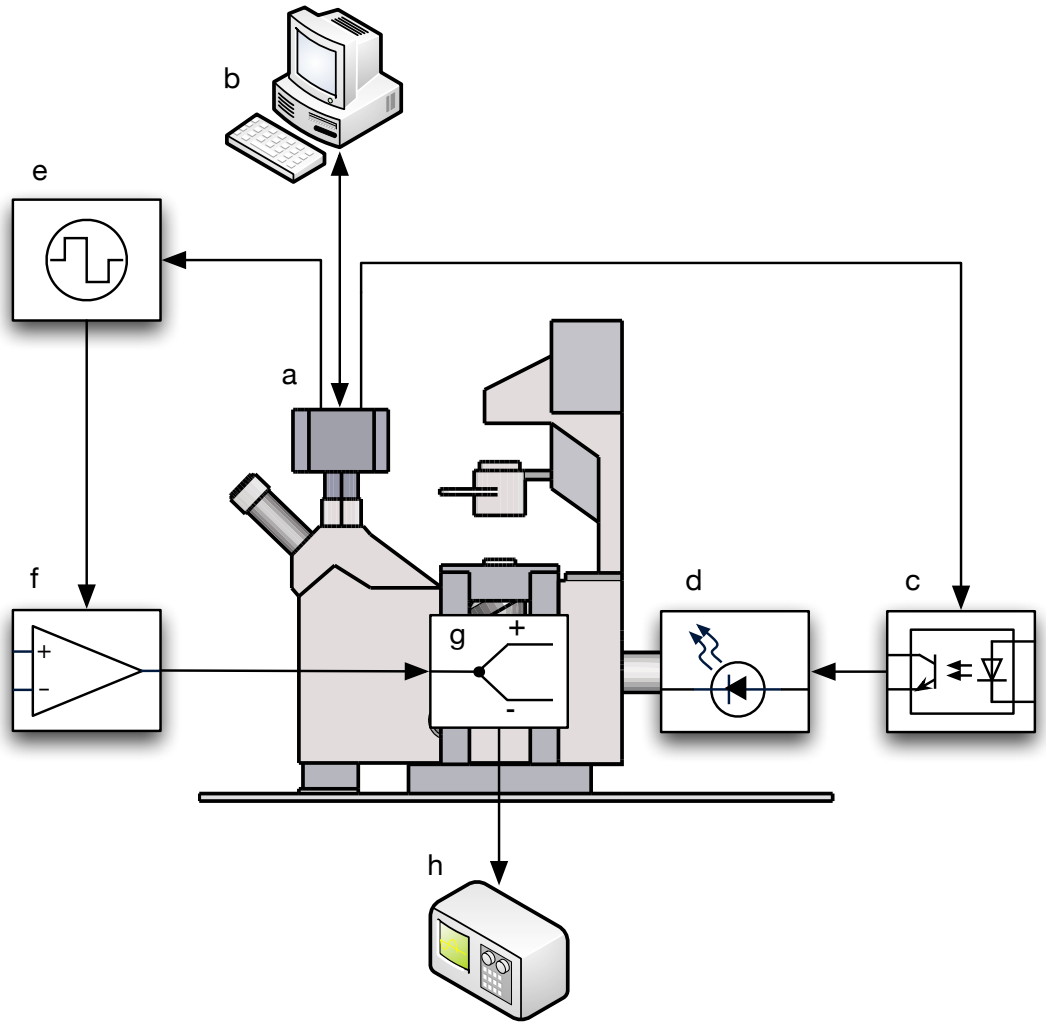

Figure 4-7 Schematic of the voltage apparatus; a) camera system, b) computer system, c) opto-isolator circuit, d) LED module, e) arbitrary waveform generator, f) push-pull amplifier circuit, g) electrical-field apparatus, h) oscilloscope.

The camera sensor was cooled to -80°C and set to Frame-Transfer mode, with 2x2 pixel binning mode for the faster readout speeds. The vertical shift speed was set to 1.9176 µs, with a pixel readout rate of 35 Mhz. With these settings, and an exposure time set to 23.06 ms, the image cycle time was exactly 25 ms, and thus matched to the square wave signal produced by the arbitrary waveform generator. To reduce noise, the EM gain level was set to 43, with a pre-amplifier gain set to 4; these levels were optimized experimentally to give the highest signal-to-noise ratios.

LED illumination was synchronized to camera acquisition timing to reduce bleaching, via an opto-isolated circuit (Figure 4-7-c) controlled by the camera's TTL output that also initiated the square wave signal produced by the arbitrary waveform generator (Figure 4-7-e). After the signal amplification by the push-pull circuit (Figure 4-7-f), the signal was applied to the platinum electrodes in the Perspex electrical-field apparatus (Figure 4-7-g), and monitored via an oscilloscope (Figure 4-7-h).

4.2.4 Measurement Protocol

The PLAP-IRES-H2BGFP stable cell line was co-cultured together with untransfected Flp-In-293 cells, each split 1:20 onto uncoated ⌀ 30 mm #1 glass coverslip (Thermo Scientific), in 35 mm polypropylene culture dishes (BD Biosciences), and grown to 40% confluency using standard protocols, in high glucose DMEM with 10% FBS, 2 mM L-glutamine and 1% pen-strep, at 37.0°C with 5% CO_2.

Just before voltage sensitivity experiments, the culture media was removed from the polypropylene dishes, and the cells gently rinsed once with buffer (100 mM NaCl, 70 mM D-Glucose, 20 mM AMPD, pH 8.6), followed by 2 ml of staining solution (1 µM Di-1,8P6-ANEPPS, 100 mM NaCl, 70 mM D-Glucose, 20 mM AMPD, pH 8.6) for 2 minutes. The staining solution was then gently removed, the moist coverslip containing the cells was transferred into the mounting tray (Figure 4-3-f), and the apparatus assembled as described above. The slit-chamber was filled with buffer, and the cells imaged under bright field and GFP fluorescence, with a merged example shown in Figure 4-8-a. This shows healthy HEK293 cells, ~50% of which are expressing GFP. There was some cell-detachment from the glass substrate, most likely due to the short culture time needed to reach 40% confluency, but this did not affect the measurements as these cell were removed with gentle washing.

A series of 32 images were then recorded, using the settings described above, with the sequence timing matching the amplified square wave signal applied to the platinum electrodes. The initial image in the sequence, with 0 V applied, is shown in Figure 4-8-b,

demonstrating the selective staining of cells expressing H2BGFP. The electrodes were aligned parallel to the vertical edges of the image, Output 1 on the right, and Output 2 on the left.

4.3 Results

The images were processed with Matlab (MathWorks Inc.), with the stacks of images converted into matrices. A region of interest (ROI) was defined over a cell that showed good levels of selective staining, as marked by the black box in Figure 4-8-b. Vertical columns of the ROI were averaged, to generate profiles across the cell, parallel to the applied electrical field. Figure 4-9 shows the fluorescent images of a cell exposed to the highest voltages, with positive and negative 26.7 V applied across the electrodes, in sub-images 'a' and 'b' respectively. There is a clearly visible difference in fluorescence intensity between the two images; stained cell membrane closest to the positive electrode on the right (Figure 4-9-a) shows increased fluorescence, whilst membrane on the opposite side of the cell shows decreased fluorescence. When the polarity is reversed, as shown in Figure 4-9-b, the pattern swaps, as expected. The ROI profiles are displayed in Figure 4-9-c and d.

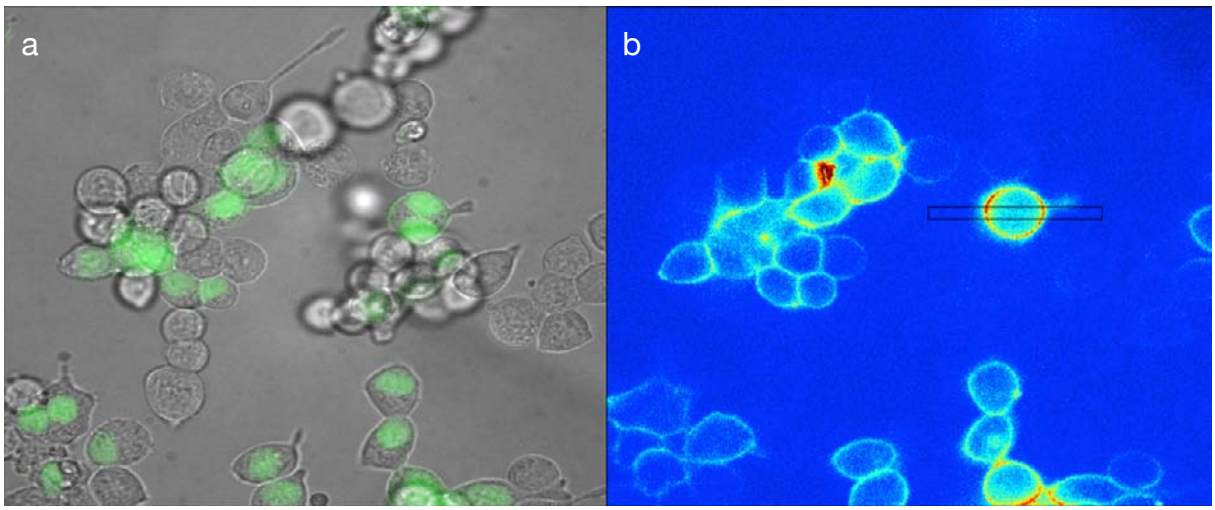

Figure 4-8 Images of HEK293 cells stably transfected with pcDNA5_FRT-IRES-PLAP-H2BGFP, co-cultured with normal HEK293 cells; a) overlaid GFP and bright field images, b) Selective staining levels.

The pattern of 32 images that aligns with the square wave signal can be broken down into overlapping 4-images sets. Each set begins and ends with an image recorded with zero applied voltage; these two control images were used to correct for bleaching that occurs during excitation of the dye. The bleaching of the dye was approximated as linear over the course of the 4-image set. After bleaching correction, the fluorescence intensity changes caused by the induced membrane potential was calculated, as shown visually in Figure 4-10-a

and as a profile in Figure 4-10-b, with the sensitivity of the dye found to be approximately symmetric across the cell. With each applied voltage, both the positive and negative response can be calculated.

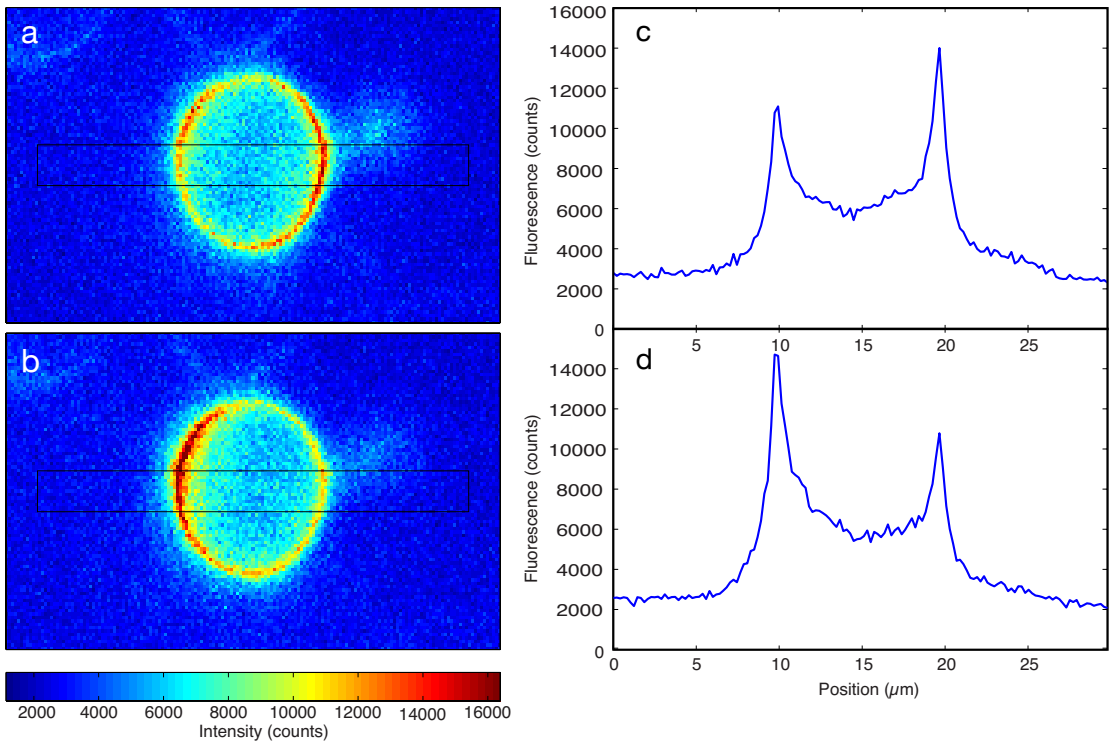

Figure 4-9 The profile of stained HEK293 cells subjected to an external electric field; a,c) show the field applied from the right to left, and b,d) from left to right.

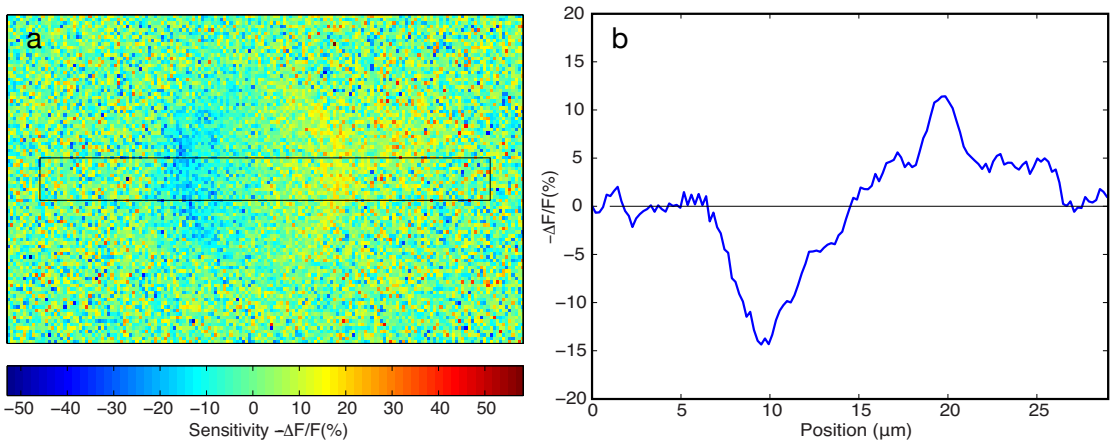

Figure 4-10 Sensitivity of the dye; a) the sensitivity image, calculated by subtracting fluorescence image of the cell from the applied-field cell image, b) the column-averaged ROI sensitivity profile.

The fluorescence profiles, shown in Figure 4-9-b and c, can be used to calculate the location of the cell membrane, and therefore to estimate the width of the cell. The camera was

calibrated by recording an image of transistors of known size. Using these locations, the image stack was processed to find the fluorescence response of the dye to each of the applied voltage steps, with the results shown in Figure 4-11-a. This shows the linear response between the dye fluorescence and the externally applied electrical field. Using the width of the cell, we can estimate the transmembrane voltages induced by the electrical field, the results of which are shown in Figure 4-11-b. Fitting the data, we find a sensitivity for the dye of 0.48%/V for the applied field, resulting in a sensitivity of -10.1%/100 mV for the induced transmembrane voltage. A range of measured sensitivities have been published for the voltage sensitive dye di-4-ANEPPS, as shown below in Table 6, with an average reported sensitivity of approximately -9.50%/100 mV. The values vary with cell type, and the selected excitation and emission filters.

Target	Ex (nm)	Em (nm)	-ΔF/F	Reference
Lipid bilayer	469	>620	8.0%/100 mV	[19]
Red blood cells	546	>590	12.0%/100 mV	[130]
Retzius cells	539*	639*	9.2%/100 mV	[24]
Red blood cells	492	>630	7.0%/100 mV	[121]
Neuroblastoma cell	530	>570	13%/100 mV	[132]

Table 6 Reported sensitivity of voltage sensitive dye di-4-ANEPPS in the literature. The average is a -ΔF/F of 9.5%/100 mV**. '*' -**maximum sensitivity as found via scanning with a continuous interference filter.

The calculated sensitivity of 10.10%/100 mV (with 95% confidence bounds of 9.61 to 10.6%), is slightly above the reported average, and this may be due to the 1.5x electrical field correction factor used to account for the curvature of the electrical field. As HEK293 cells have a morphology that is flatter than a hemisphere, the electrical field curvature should be reduced, generating a lower transmembrane potential.

The experiment was performed in triplicate, with cells widths of 9.7, 7.8 and 10.7 nm, normal for this cell type. The fit for the applied voltage, 0.48%/V, had a R-square value of 0.9615, with a RMSE 1.603. As expected, using cell widths to calculate the transmembrane potential yielded a better fit, increasing the R-square value to 0.9662, and lowering the RMSE to 1.502. The results appear to indicate that the introduction of the tertiary-amine functionality in the dye's tail, used by Di-1,8N6-ANEPPS to instill selective targeting ability via N-phosphonooxymethylation, does not adversely influence the binding orientation of the dye into HEK293 cell lipid membrane. The measured values are directly comparable to the widely used di-4-ANEPPS, and the levels of selective staining are more than sufficient to allow voltage sensitive recordings in this model system.

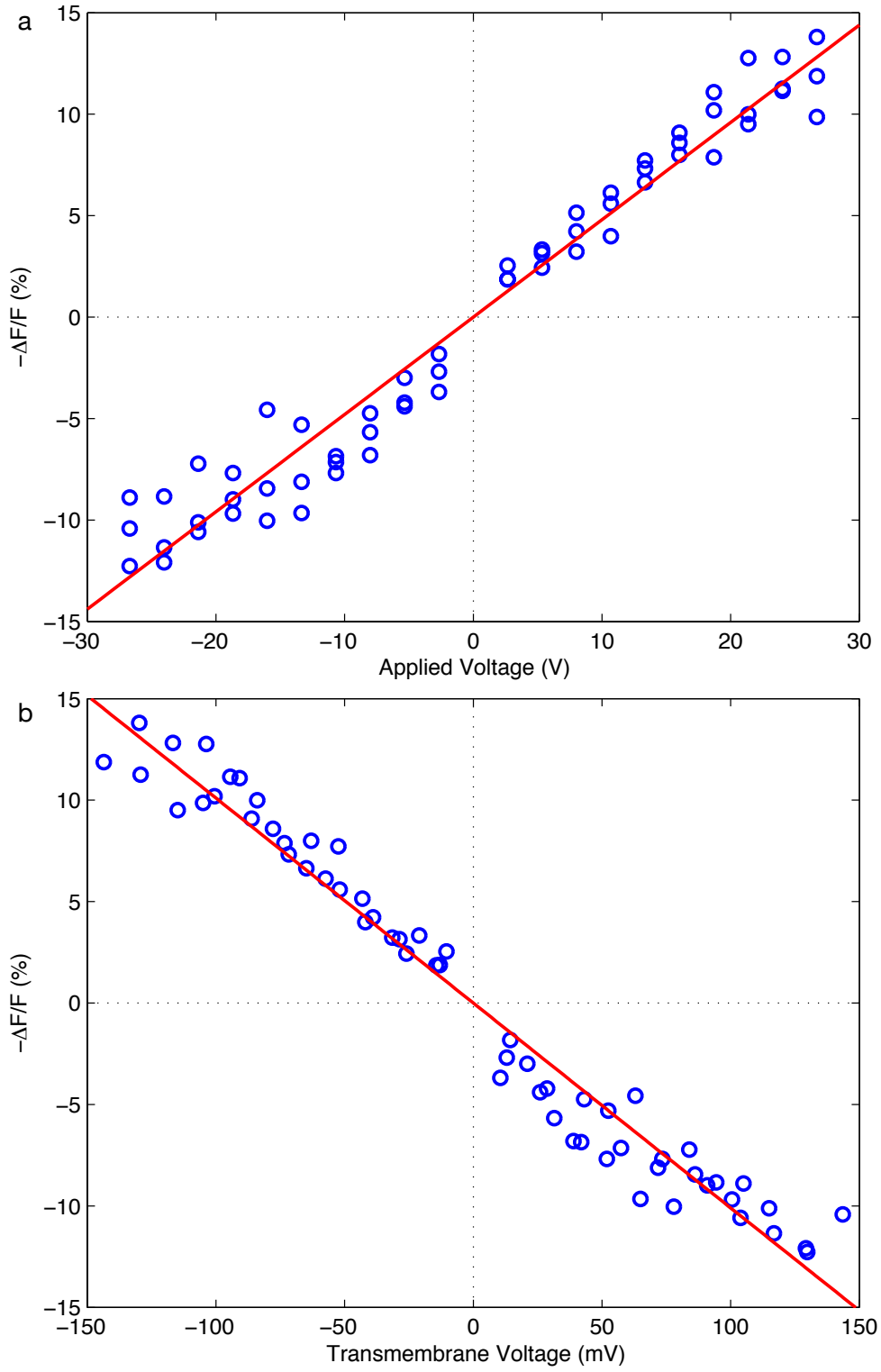

Figure 4-11 Voltage sensitive dye signals from selectively stained cells stimulated by an external electrical field; a) the measured sensitivity of stained cells, b) the sensitivity of the cells according to the calculated transmembrane voltage as derived from the measured cell width.

4.4 Future Directions

The apparatus used in this experiment applied an external electrical field across the cultured HEK293 cells. This allowed easy access to the cells for washing and staining purposes, as well as the analysis of a large number of cells in parallel. These criteria were very important in the initial development of these targetable VSD's. However, the transmembrane voltage induced in the cells is difficult to accurately calculate, as it relies on factors that are difficult to measure, such as cell morphology and the potential drop across the electrode/media interface during gas formation. Although the measured values are very much in line with the published values, and use published techniques for the experimental design and calculations, the sensitivity of the dye can only be estimated.

The application of the patch-clamp technique could be used to accurately measure the true voltage sensitivity of the dye [7], and would require only minimal reconfiguration of the current apparatus due to its open-access design. In addition, although Di-1,8P6-ANEPPS has shown both selective staining and voltage sensitivity in HEK293 cells, cell membrane composition is known to affect VSD sensitivity. The selective staining of dissociated rat hippocampal neurons has been performed, as mentioned in the future directions section of Chapter 3, and the patch-clamp technique would be required to test the dyes in this cell type.

Further testing could be performed via fluorescence interferometry [13], to determine the membrane orientation of the dye. Di-8-ANEPPS in lecithin membrane has an orientation of 37.8 ± 1.6°, and it would be interesting to see if this holds true for membrane-bound Di-1,8N6-ANEPPS, or whether the average orientation is maintained but has a greater variance.

5 DESIGN OF TRANS-SYNAPTIC TRACER

Unraveling the connectional neuroanatomy of the brain is a difficult undertaking, requiring methods that can identify single neurons or assemblies of neurons, and the connection of these cells to other neurons located elsewhere in the brain. Tracing the connections between the axons of neurons and their connections with the highly branched and complex dendritic tree of their target requires advanced microscopy and labeling techniques, together with complex algorithms to trace the morphology of the neurons in three dimensions.

In this chapter, the design and development of a new method for neuroanatomical tracing will be discussed, one that can be integrated with the genetically targeted voltage sensitive dye labeling described in the previous chapters. The goal of this set of methods, combined together, would be the ability to trace and label ensembles of functionally connected neurons, and monitor their electrophysiology with high spatial and temporal resolution.

5.1 Contemporary Tracing Techniques

The currently used methods for visualizing connected neurons can be broadly divided into two classes of mechanism. The first, the physico-chemical methods, rely on the diffusion or precipitation of chemical substances in neurons, whilst the second co-opts intrinsic biological processes involving the uptake and transport of biological compounds, and is used *in vivo* or *in vitro* on live tissue preparation with an appropriate tracing compound.

The physico-chemical methods began with the development of Golgi silver impregnation, a passive intracellular filling technique whereby a dark silver chromate precipitate is formed upon the reaction of silver nitrate and potassium dichromate within neurons, allowing visualization of the entire dendritic tree with light microscopy. The control over the staining process can be improved by applying a micropipette filled with the labeling compound either immediately against the cell membrane (termed ‘juxtacellular tracing’), or by impaling and filling the intracellular compartment with a diffusible dye. The later method can also be performed *in vivo* during electrophysiological experiments [14]. More recently, the fluorescent carbocyanine dyes DiI and DiO have been used as an anterograde and retrograde tracing agents; these dyes diffuse laterally through live and fixed neuron plasma membrane, including the distant projections of the dendritic tree [15]. The strongly lipophilic dyes are implanted into tissue, either as single crystals, or are ‘shot’ into the brain, in a method termed ‘DiOlistics’, analogous to the transfection technique of biolistics [133].

Techniques exploiting intrinsic biological processes can be further divided into two classes; anterograde methods involve the uptake and transport of tracer compounds from the dendrites or cell body in the direction of electrical signal propagation, whilst retrograde techniques are based on the endocytosis of tracer compounds at the axon terminals and their subsequent transport along the axon to the cell body, opposite of the direction of the electrical signal. The most commonly used anterograde and retrograde tracing compounds are horseradish peroxidase (HRP), wheat germ agglutinin (WGA), *Phaseolus vulgaris* leucoagglutinin (PHA-L), biocytin, Tetanus Neurotoxin (TeNT), and Cholera toxin subunit B (CTB) [134,135]. These tracers can be applied by injection or iontophoresis into the spinal column or brain, and are visualized histochemically or immunohistochemically after fixing [136]. These techniques are often combined, allowing distinct populations of neurons in close proximity to be identified [137], or the differing mechanisms of the tracer compounds used to label different regions of the neurons [138]. Transgenic techniques have been applied to generate the tracer proteins *in vivo*, giving stronger signals from genetically specified neurons [139-141].

The internalization of many of these protein tracers is based on receptor-mediated endocytosis, where they are then targeted for lysosomal degradation pathway. CTB binds to the cell surface ganglioside GM1 that resides in the caveolae, where it undergoes retrograde transport with the GM1-Trk-P75 complex to avoid degradation. WGA binds directly to P75, whilst TeNT binds to ganglioside GT1b in manner similar to CTB [142].

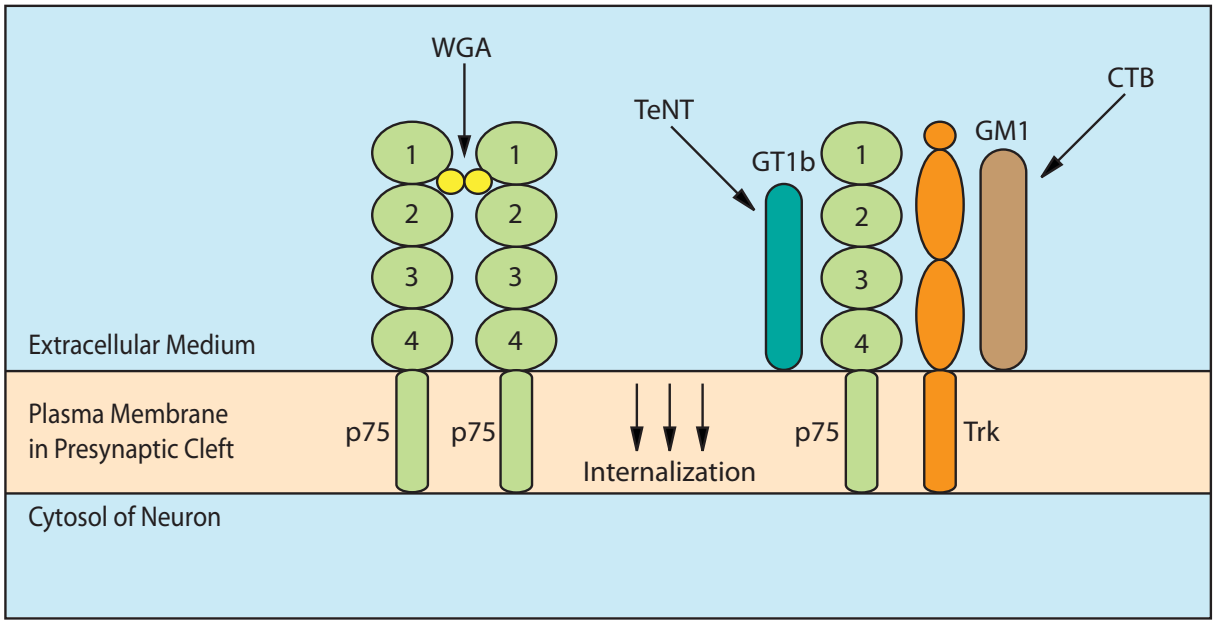

Figure 5-1 The utilization of the P75 trafficking system by retrograde trans-synaptic tracers. The commonly used tracers shown here bind either directly to P75, or one of its protein-complex subunits, such as GT1b, GM1 or Trk.

A third tracing technique in development is based on Rabies virus. This virus also binds to P75 where it is endocytosed, allowing it to infect the neuron [143]. The virus replicates in the cell, amplifying the signal, and allowing the infection of interconnected neurons, making it a sensitive retrograde marker of trans-synaptic pathways. It can be further improved with the recoding of the virus to incorporate fluorescent protein markers, such as green GFP [144], or red mRFP1 [17]. This system has been used to show the functional interconnection between the brain and retina [145], or retinal transplants [146].

The physico-chemical methods described above, although applicable to long-term experiment *in vivo* and demonstrating high spatial resolution, are limited by their inability to cross the trans-synaptic cleft. Thus, interconnected neuron labeled via DiOlistics must be identified manually from 3D scans, by tracing the paths of the axons and matching the connections to the target neurons dendritic tree, with no certainty as to the level of functional connection between physically connected neurons. The actively transported tracers, such as TeNT and WGA do have the ability to cross into connected neurons, and with the hijacking of the neurotransmitter recycling apparatus as the basis of their mechanism [143], the trans-synaptic transfer of the tracer is reliant on an active functional connection between the neurons. However, the signal generated in second or third-order interconnected neurons can be at the very limit of detection, requiring highly sensitive indirect immunohistochemical techniques on fixed brain slices. The viral methods have the benefit of high signal amplification, with second and third-order neuron expressing GFP at similar levels to the first infected neuron. These systems clearly define functional ensembles of neurons with high resolution, and can be adapted to express a variety protein-based marker. The disadvantages of using Rabies-based methods are the complexity of viral particle preparation, which is extremely time-consuming and requires specialized laboratory equipment; the toxicity of the virus to infected cell, which strongly limits the timeframe of the experiments and may alter the activity of the targeted neurons; and the biosecurity requirement for working with infectious transgenic particles, which limit its application to a minority of neurobiology laboratories.

What is required from a tracer system is the ability of the tracer to be genetically targeted to defined neurons or populations of neurons; the ability to cross the trans-synaptic cleft between only active, functionally connected neurons in a single direction, either anterograde or retrograde; the amplification of the reporter signal in each new layer of the neural network to equivalent levels; very low levels of cell toxicity or alteration of normal neuronal functioning; efficient and rapid methodology with a minimum of difficulty or reagents. Such a system must behave like a virus, propagating though a neural network, instigating the generation of new marker proteins in each newly activated neuron. The following work describes the basic

components and their integration to construct such a tracer system, based on a collection of molecular tools currently used in neuroscience. The proposed system utilizes a bacterial toxin, a bacteriophage recombinase, and a synthetic operon already present in transgenic mice.

5.2 Tetanus toxin in Trans-synaptic Tracing

Clostridium tetani is a common soil bacterium whose spores are extensively distributed in soil and in the intestine of wild and farmed animals. When introduced into necrotic or deep wounds, the low oxygen concentration and abundance of nutrients cause the spores germinate, and leading to the production of Tetanus neurotoxin (TeNT), a protein toxin that fills the bacterial cytosol and is released by autolysis [147]. The toxin binds specifically to the end terminals of motor neurons in the neuromuscular junction, attaching to the ganglioside GT1b [148]. Although the internalization of TeNT does not affect motor neurons, it enters a retrograde transport pathway, and is delivered to the spinal cord where it is then released and internalized again by inhibitory interneurons [149-151]. In these cells, TeNT causes an irreversible block of the release of GABA and glycine, which is responsible for the spastic paralysis [152]. Fragments of the TeNT have been used to map the primary visual pathways connecting the retina with the visual cortex via immunohistochemistry[150], and show the wiring of the paravertebral sympathetic ganglion of the pigeon, *Columbia livia* [151].

5.2.1 Tetanus toxin Structure and Function

Tetanus toxin was first cloned and expressed in *Escherichia coli* in 1986 [153], with the nucleotide sequence publish in the same year [154]. The 150 kDa protein is synthesized as a single chain, and undergoes several post translational modifications; the N-terminal methionine residue is cleaved, the peptide is cut into two fragments, and the two peptides are joined via disulfide bridge [155]. Each of the two peptides performs a different role in inducing spastic paralysis. The longer peptide, termed the Heavy Chain (HC), has been found to bind to the GT1b ganglioside, whilst the Light Chain (LC) is a zinc-endopeptidase, and causes proteolysis of VAMP and synaptobrevin in hippocampal neurons, where they are cleaved at a single Gln-Phe peptide bond [156]. These proteins are involved in the release of synaptic vesicles containing GABA and glycine, and their cleavage prevents the release of the two inhibitory neurotransmitters at the chemical synapse [157].

The 100 kDa TeNT HC can be further subdivided into the N-terminal (HCN), and C-terminal (HCC) fragments, derived from the digestion of the HC with papain [153]. Crystallography studies of the HC [158,159] show that the N-terminal domain of HCN contains a jelly roll fold similar to the carbohydrate binding domain of plant lectins, and conserved with Cholera

toxin subunit B. The C-terminal of HCN adopts a modified ß-trefoil, a structure known to mediate protein–protein interactions, and this domain binds to GT1b [152,160]. After the binding induced by the HCC fragment, TeNT is endocytosed, with the toxin trapped in the lumen of the endocytic vesicle, unable to pass through the lipid bilayer. Vesicles targeted for the lysosomal degradation pathway are acidified, and the acidic pH induces a conformational change in the TeNT HCN, causing its transition from a water-soluble neutral form to an acidic form with surface-exposed hydrophobic areas. Acidification of membrane-bound TeNT has been shown to form ion channels in planar lipid bilayers, and also in spinal cord neurons, with the channels opening at high frequency at pH 5.0 but not at neutral pH. Although the exact mechanism is unknown, it is believed that this pore-formation allows the escape of the TeNT LC into the neuronal cytosol, where it acts against VAMP and synaptobrevin to induce its toxic effects [156,157,161,162].

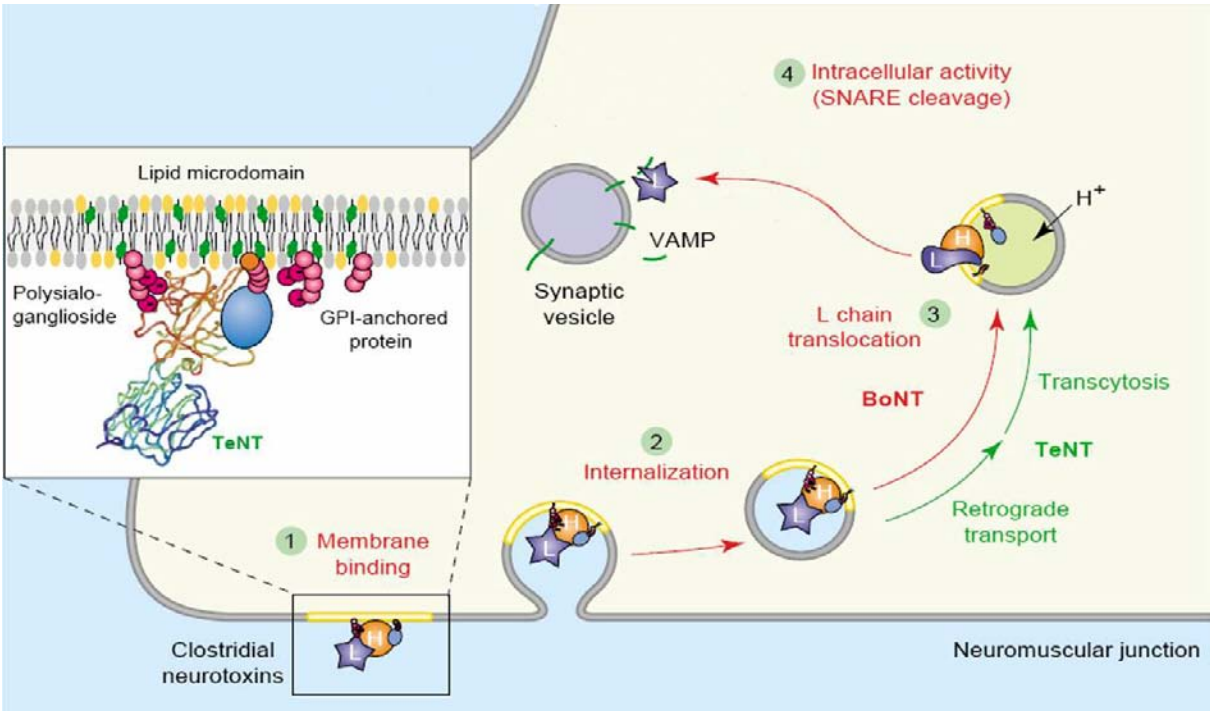

Figure 5-2 The mechanism of Tetanus Neurotoxin action.

The light chain is a 50 kDa protein that contains a His-Glu-Xaa-Xaa-His + Glu zinc-binding zinc-endopeptidase motif [163]. Further studies utilizing X-ray crystallography [164,165] and active-site mutagenesis [166] detail the active site of the metalloprotease. It consists of a primary sphere of residues coordinating a Zn^{2+} (His232, His236 and Glu270), surrounded by a secondary sphere of residues that determine enzymatic specificity and activity. A fourth Zn^{2+} ligand is a nucleophilic water molecule that also forms a strong hydrogen bond with Glu233.

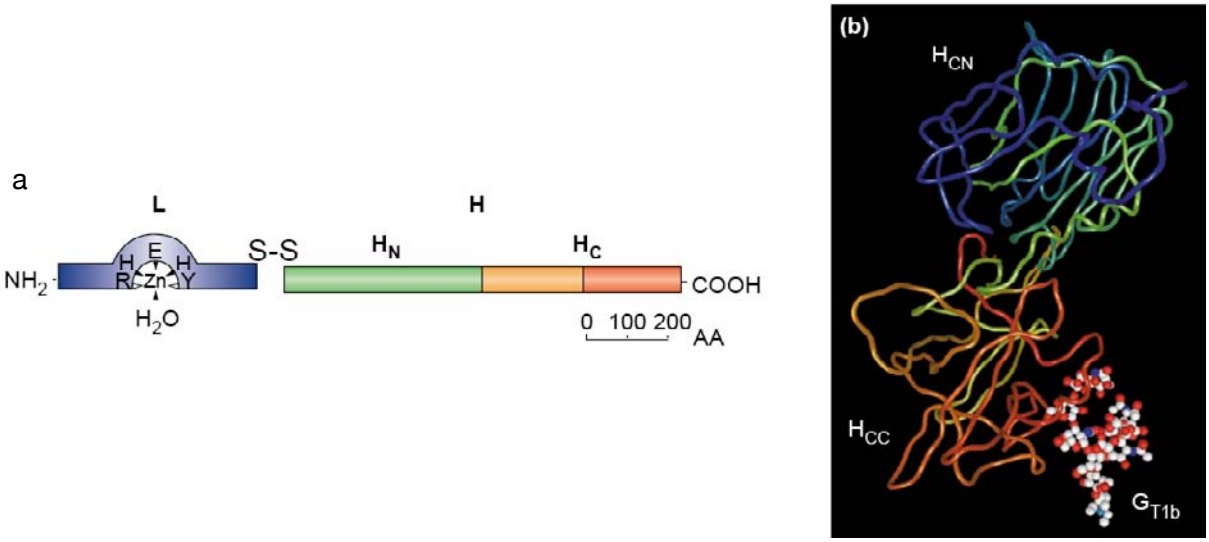

Figure 5-3 Tetanus Neurotoxin; a) a schematic of the domains of the toxin, b) the crystal structure of the heavy chain bound to GT1b.

5.2.2 Tetanus Toxin Fusion Proteins

Tetanus neurotoxins ability to traffic across synapses has made it a valuable tool in mapping neural networks. In particular, the HCC fragment has found use in a variety of fusion proteins, where it has been attached to therapeutic proteins, markers and DNA binding motifs as a neuron-specific delivery system. The enzyme superoxide dismutase (SOD) has been shown to provide protection to neurons in experimental models of stroke and Parkinson's disease, and mutations in SOD shown to cause motor neuron disease. A fusion of SOD with TeNT HCC, expressed and purified from *Escherichia coli,* and injected into the tongue and hind leg of mice can be detected in the brainstem at similar levels to HCC alone [167,168]. Other therapeutic proteins targeted to the central nervous system (CNS) include the survival motor neuron (SMN) gene, defects in which causes spinal muscular atrophy [169], and the lysosomal enzyme ß-glucuronidase, defects in which cause the accumulation and storage of its partially degraded substrate, and give rise to lysosomal storage diseases [170].

To avoid complex histochemical techniques required to trace the retrograde transport of HCC, it has been fused with marker proteins such as ß-galactosidase [171,172] or GFP [173] for direct injection of the purified protein *in vivo*. The *in vivo* transfection of cells with plasmids encoding these fusion proteins, or the use of transgenics has also been used to directly express and deliver the fusion protein to the CNS in mice [173-175]. As shown in Figure 5-4-B, when the GFP-HCC fusion protein is expressed in the CA1 region of the hippocampus, it can be clearly detected with fluorescence microscopy [173]. The CA1 region is innervated with the

Schaffer collaterals, the axons of the CA3 pyramidal neurons. The CA3 neurons are in turn innervated by the granule cells in the dentate gyrus via their mossy fibers (Figure 5-4-A). The fusion protein can be detected in the CA3 region with confocal imaging, and via X-gal immunohistochemistry in the dentate gyrus (DG). Analysis for mRNA via in situ hybridization shows that expression of the fusion protein occurs in the CA1 region and cortex, but not in the CA3 region and dentate gyrus, confirming the trans-synaptic transfer of the GFP-HCC fusion protein into these two hippocampal sub-regions.

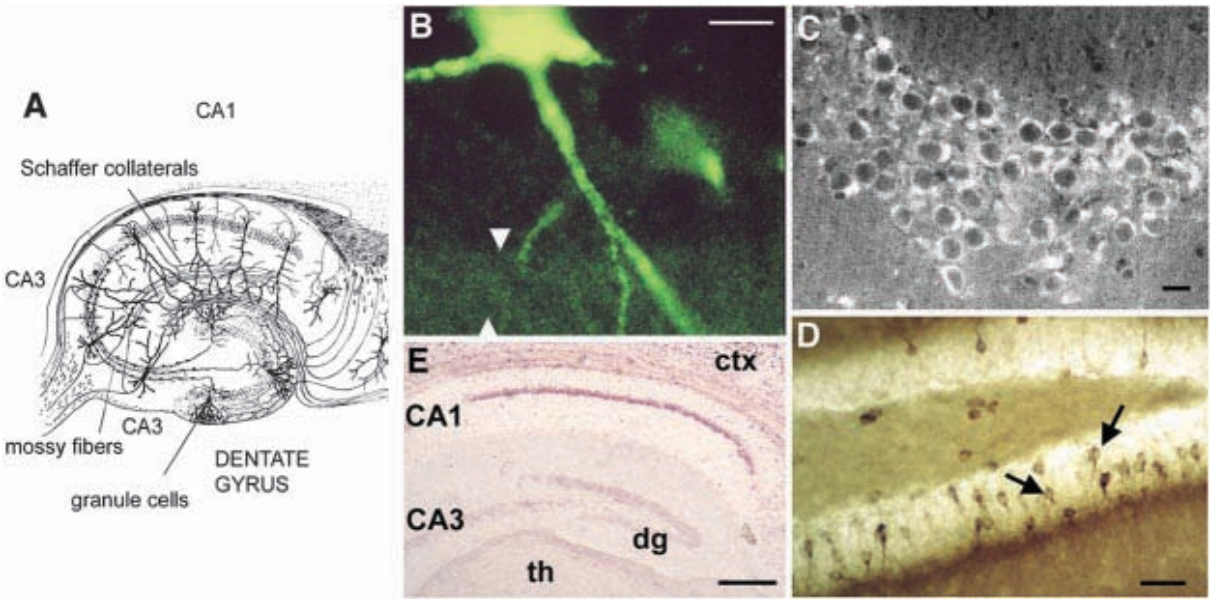

Figure 5-4 Trans-synaptic tracing with a GFP-HCC fusion protein; a) the structure of the mouse hippocampus, b) CA1 showing GFP fluorescence, c) confocal imaging of GFP, d) Immuno-histochemical staining of GFP, e) in situ hybridization showing mRNA in the CA1 and cortex (ctx), but not in the CA3 and DG. Images taken from [173].

In the TeNT fusion proteins described above, only the HCC fragment was utilized, enabling the trans-synaptic transfer of the fusion protein. However, in the case of the therapeutic fusion proteins, although they were clearly detected in the CNS, there was little to no activity shown, presumably due to the proteins inability to escape the endocytic vesicle into the cytosol. The Type-D Botulinum neurotoxin (BoNT/D) is structurally highly similar to TeNT, and operates via the same mechanism of trans-synaptic transfer followed by light chain translocation and peptidase activity. Fusion proteins comprising of full-length BoNT/D, fused at the LC N-terminal with GFP, firefly luciferase or dihydrofolate reductase (DHFR), showed that the LC fusion fragment could remain active while delivering the fused marker proteins [176]. Interestingly, the fusion protein incorporating globular DHFR showed higher toxicity than

that which used GFP; GFP has an extremely stable ß-barrel structure, and its unfolding seems to inhibit membrane translocation even more than the larger globular DHFR protein.

5.3 Cre recombinase

This 38 kDa type I topoisomerase from the P1 bacteriophage catalyzes site-specific recombination of DNA between loxP sites. The enzyme does not require any cofactors or extra sequence elements, and Cre-mediated recombination quickly reaches equilibrium between substrate and reaction products [177]. The targets of Cre are the loxP sequence elements, 34-base pair (bp) elements composed of an 8-bp spacer region flanked by two 13-bp inverted repeats [178]. As the recombinase requires this specific 34-bp sequence, the probability of finding such a sequence at random would be one in $\sim 10^{18}$. As the entire mammalian genome is only $\sim 3 \times 10^{9}$-bp, it is highly unlikely that an exact loxP site is represented outside of the phage genome. The products of the recombination are dependent on the location and relative orientation of the loxP elements. Two DNA molecules, each containing a single loxP site, will be crossed together. In a single DNA molecule, the fragment between loxP sites in the same orientation will be excised in circular form, and the DNA between loxP sites in opposing directions will be inverted with respect to the rest of the DNA [110].

5.3.1 Recombination in Molecular Biology

Cre recombinase plays an important role as a tool for modifying genes and chromosomes. Genes can be selectively and reliably deactivated in a process termed ‘Floxing’, by the insertion of two LoxP sequences into sites that flank the targeted gene. Cre recombinase can then be expressed in the target cells to delete the segment of DNA flanked by LoxP sites in experimental animals [179]. It has been used to generate animals with genetic deletions restricted to specific cell types (tissue-specific knockout) or enable genetic deletions to be performed upon the administration of a Cre-activating drug (inducible knockout) in a number of transgenic species. There are many transgenic mouse lines with tissue specific or inducible Cre expression systems, and these allow the inactivation of a gene of interest simply by breeding a floxed animal with a pre-existing Cre line.

The second major application of Cre is the activation of repressed genes. Similar to the Floxing method, a circular segment of DNA is excised in a Cre catalyzed reaction; however, this segment lies directly after a promoter element and contains either the coding for a marker protein, or a stop codon. Thus, before the application of Cre, the promoter induces the transcription of the marker or stop codon, and after excision the gene of interest is transcribed

[180]. Mouse transgenic lines using this system to express GFP, YFP, CFP and LacZ upon recombination are commonly used tools to test new transgenic tissue-specific Cre lines [181-183]. The Cre-inducible, dendrite-targeted MAP2-GFP fusion protein allows the visualization of specific types of neurons [184].

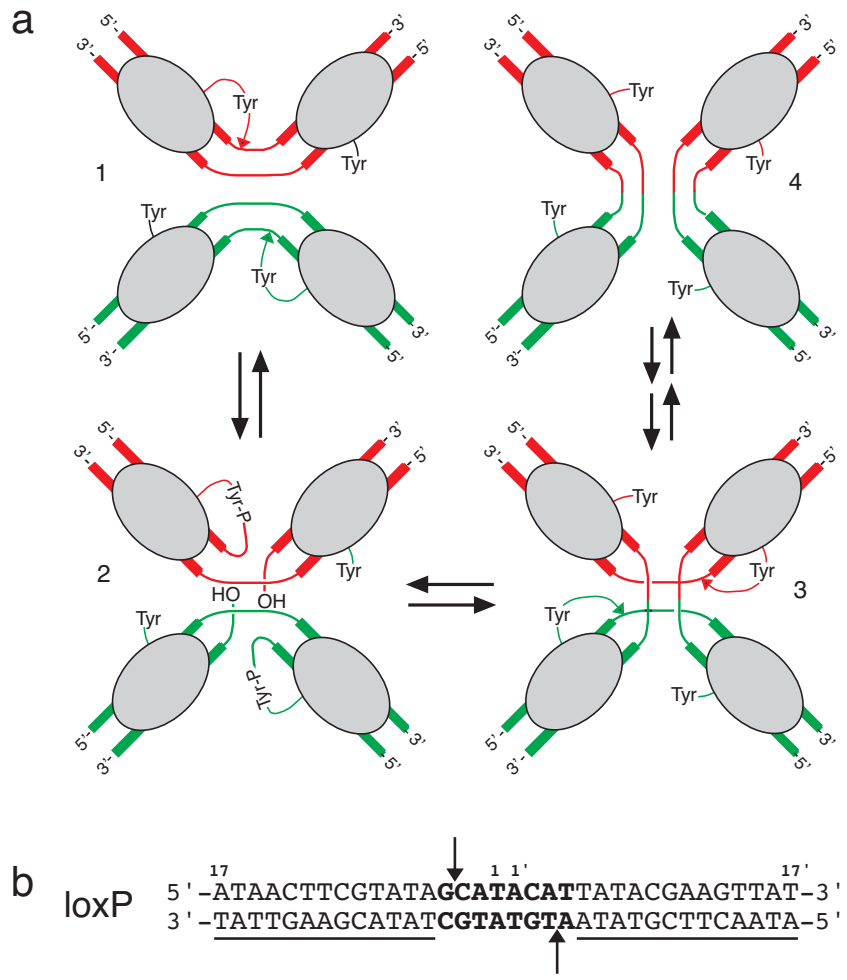

Figure 5-5 The molecular mechanism of Cre recombinase; a) the sequence taken during the reaction, b) the 34-bp loxP site, with the cleavage site shown in bold.

5.3.2 Structure and Mechanism

The molecular mechanism of Cre recombination involves the binding of single recombinase molecule to each palindromic half of a loxP site. The recombinase molecules then form a tetramer, and in doing so bringing the two loxP sites together, as shown in Figure 5-5-a-1 [177]. Crystallographic studies on Cre/mutant LoxP element complexes have captured the intermediate states in the recombination reaction [185]. The recombination occurs within the directional spacer area of the loxP sites.

The conserved Tyr324 then cleaves each substrate to form covalent phosphotyrosine intermediates in an antiparallel arrangement, Figure 5-5-a-2. The cleavage of the

phosphodiester linkages leaves two nucleophilic 5-hydroxyl groups, which in turn then attack the phosphotyrosine of their partner substrate, yielding a Holliday-junction intermediate, Figure 5-5-a-3. This process occurs a second time, and the next two cleavage and strand-exchange reactions yield the final recombinant products, shown in Figure 5-5-a-4.

5.3.3 Cre Recombinase Fusion Proteins

The tetramer structure formed by Cre and two strands of DNA is vital for the correct functioning of the recombinase, and fusion proteins incorporating Cre must not distort this structure. Fusions with GFP, at both the C- and N-terminal of Cre have yielded active proteins [186,187], demonstrating both fluorescence and recombinase activity. Another, more extreme modification to Cre, involved the splitting of the protein into two inactive fragments. The two fragments were fused to FKBP12 and FRB respectively; these two protein domains are know to form a dimer in the presence of rapamycin [188]. Co-expression of the two fusion proteins show no recombinase activity, but the addition of rapamycin rapidly induces the formation of dimer pairs of active Cre recombinase, demonstrating that the system is robust in terms of allosteric interference.

A fusion protein combining Cre recombinase and the secretion and translocation signal from the *Salmonella enterica* secreted protein SopE [189], has shown that Cre is able to unwind and pass though a transmembrane pore, where it can reform its active tertiary structure in the cytosol. This system was used as a highly sensitive test of protein translocation, and activated the expression of luciferase or GFP via the stop-codon excision technique described above.

5.4 Proposed system

Utilizing these two proteins, together with the technique described above for the induced expression of repressed genes, we have all the required components for construction of a trans-synaptic tracing system that fulfils the criteria listed at the end of section 5.2. A fusion protein that links Cre recombinase to the N-terminal of the TeNT LC could migrate in a retrograde direction though the central nervous system by virtue of the properties of the TeNT HCC. In each neuron through which the fusion protein is trafficked, a portion of the vesicles containing the fusion protein will be processed through the lysosomal degradation pathway, and acidification of the vesicles will induce the TeNT HCN to reconfigure into a pore structure that will release the LC into the neuron's cytoplasm. The Cre recombinase, which is fused to the LC and known to be able to pass though bacteria pores, could enter the cytoplasm. After entering the nucleus it could catalyze the deletion of a LoxP flanked stop-codon that represses the expression of a marker gene such as LacZ, GFP or PLAP. Thus, only

four molecules of the fusion protein would be required to induce the high level expression of a marker gene, and unambiguously indicate connected neurons in a functional network. Utilizing the PLAP-expressing transgenic mouse Cre-reporter line, the trans-synaptic tracing system described could be directly employed for use with the Di-1,8P6-ANEPPS described in Chapters 2,3 and 4. In this way, for the first time functional networks could be clearly labeled with a voltage sensitive dye, allowing real-time and high-resolution electrophysiological measurements.

In order to create this system, a number of steps must be completed. The tetanus toxin must be codon optimized for expression in mammalian cells lines and modified to eliminate toxicity. The fusion protein with Cre recombinase must be created, with the peptide linker region between the two proteins optimized for enzyme activity. Finally, the fusion protein must be tested for firstly Cre activity in a model cell line, and then for trans-synaptic transfer between functionally connected neurons.

5.5 Vector Design

The fusion protein is designed to be expressed in mouse neurons; as the coding sequences for the two proteins are derived from a bacteria and a bacteriophage, the codon usage employed is quite different to that which would yield high levels of translation in mammalian cell lines [190]. It is believed that the selection of codon triplet is based on the tRNA concentrations, which vary between organisms, and also on GC concentration [191]. Tables comparing the comparative codon usage for a large number of organisms has been published, and they include both the mouse, *Mus musculus,* and *Clostridium tetani* [192]. The comparison in codon usage between these two organisms is shown in Appendix 7.5.

Re-encoding a gene to use a new codon table involves the translation of the DNA into an amino acid sequence, and then selecting a new set of codons that match the frequency of use in the genome of the target organism. Whilst doing so, it is important to avoid incorporating ‘slow pairs’, which are sets of codons known to interfere with and slow the rate of translation, possibly used to generate for pauses during protein synthesis, during which the protein can fold correctly [190,193-195].

A large number of proteins have been codon optimized for expression in new organisms, often yielding a large increase in expression [196]. These include Human Type 1 Neurofibromin Protein in *Escherichia coli*, for a 3-fold improvement [197]; human chorionic gonadotropin in *Dictyostelium discoideum*, giving a 4- to 5-fold improvement [198]; the *Caenorhabditis elegans* GluCla1 and GluClb ion channel genes in *Xenopus* oocytes, for a 6- to 9-fold increase [199]; and Cre recombinase for Mus musculus, showing a 2-fold

improvement [200]. The last re-encoded gene, named iCre, was used for this project, and was obtained in the pBlueScript plasmid pBS SK-iCre, shown in Appendix 7.7.2.3 with the GenBank accession number AY056050.

Tetanus neurotoxin has also been codon optimized for two organisms; the HCC fragment has been codon optimized for *Escherichia coli* [201], to be expressed and purified for use as a trans-synaptic tracer, and also codon optimized for *Mus musculus*, for use as DNA vaccine [202]. However, although both of these studies demonstrated significantly improved expression levels of the HCC fragment, this project requires the full-length sequence of TeNT. During the re-encoding, it is important to maintain the correct GC-percentage [203], a value of ~46% in mammalian genomes [204].

An important issue in dealing with TeNT is its toxicity. Dealing with an active version of the toxin requires high biosafety levels, and a much stricter and more complicated set of experimental procedures. Based on the mutagenesis and x-ray crystallography studies on the TeNT LC, it is possible to produce a mutant protein with no remaining peptidase activity [205]. This was performed via the substitution of Glutamic Acid^{234}, a residue that together with Zn^{2+} is known to coordinate a water molecule that is vital in the proteolysis reaction, with neutral Alanine. This disruption of the catalytic site renders TeNT non-toxic. The second substitution was of Tyrosine^{375} with Phenylalanine. This amino acid is part of the secondary sphere of residues around the Zn^{2+} that determines substrate specificity, and its disruption also deactivates peptidase activity, further ensuring the safety of the fusion-protein [166].

Lastly, the native coding sequence of TeNT contains various restriction sites, some of which are used in the molecular biology laboratory for cloning. Thus, during the re-encoding of the protein sequence to make use of the mouse codon usage patterns, codons were chosen so as to remove these restriction sites, and also to add new restriction sites to key locations in the protein. These new restriction sites divide the heavy chain into the HCC and HCN fragment, and also divide up the LC. This would allow future experimentation to determine the minimum required fragment of the LC that still confers vesicle membrane translocation to the fusion proteins.

5.5.1 Gene Synthesis

The sequence for TeNT was obtained from GenBank, accession number X04436 (http://www.ncbi.nlm.nih.gov/nuccore/40769), from the paper [206]. The raw sequence data was translated into a peptide sequence with the LaserGene software package (DNASTAR Inc.), where the two peptide-substitutions to eliminate the peptidase-induce toxicity were then made. The peptide sequence was then entered into the GeneDesigner software package

(DNA2.0 Inc.), where the sequence was back-translated into a DNA sequence using *Mus musculus* codon pattern usage. A comparison of the codon usage by the two organisms is shown in Appendix 7.5, together with the wild-type and re-encoded TeNT sequences. The 5' untranslated region from ß-globin, together with the Kozak sequence were added to the beginning of the sequence, and triple Stop codons were added to the 3' end, shown in Figure 5-6, so as to increase expression levels of the protein [207]. The blunt-end EcoRV restriction site was added to the DNA sequence directly after the Start codon, to allow the fusion of Cre recombinase and other marker genes via PCR cloning.

Figure 5-6 Elements of the synthesized TeNT fragment (sTeNT).

The sequence of the final construct, sTeNT, is shown in Appendix 7.6.1. During the re-encoding, common restriction sites that would interfere for cloning techniques were removed, and new sites added, their locations marked in Appendix 7.6.2 and listed Appendix 7.6.3. The gene was then constructed by DNA2.0 Inc, via the ligase chain reaction (LCR) on the set of synthetic oligonucleotides listed in Appendix 7.6.4 and 7.6.5. The fragment was blunt-cloned into the EcoRV site of the plasmid pBluescript, destroying this restriction site, and leaving the single EcoRV in the coding sequence of the gene, Appendix 7.7.2.1.

5.5.2 Spacer Design

The fusion of Cre, GFP and the luciferase genes to sTeNT was performed with blunt-end cloning of the PCR amplified fragments. The PCR primer was designed to amplify out the coding domain, either with or without a flexible spacer. The role of the spacer is to separate the proteins, reducing the chance unfavorable interaction between the marker and the light chain.

Length	Peptide Sequence
11	SGGGGSGGGGS
11	ASGGGGSGGGS
14	ASGGGSGGGSGGGS
15	$(GGGGS)_3$
17	ASGGSGGGSGGGSGGGS
23	AS-$(GGSG)_3$-GSGGSGGGS

Table 7 Common spacer domains for linking fusion proteins. The first listed spacer was used link Cre recombinase, GFP or Luciferase with sTeNT.

A variety of suitable spacers have been published, [12], including a variety of linkers used to improve Cre recombinase fusion-protein activities [188], as listed in Table 7. These spacers use a repeated poly-Glycine domain, separated by Serine residues. Codon optimization of the flexible linker is important in providing good expression of the fusion protein [208]. The nucleotide sequence published in this paper was used directly in the design of a PCR amplification primer, encoding the peptide sequence 'SGGGGSGGGGS', and shown the first entry in Table 7.

5.5.3 Vector Construction

The iCre gene was obtained from pBS SK-iCre, Appendix 7.7.2.3; the EGFP gene from the plasmid pcDNA3-EGFP, Appendix 7.7.2.5; and the Luciferase gene from pGL3-CMVe-PDGFb-Luc, Appendix 7.7.2.6. Oligonucleotide primers for amplifying out the coding sequences were ordered from Eurofins MWG GmbH. The forward primer for amplifying out each gene skipped the ATG start signal, as the cloning plasmid pBS-sTeNT already contains this codon. The reverse primer skipped the stop codon so as to produce a fusion with TeNT; a second reverse primer for each gene also added the DNA sequence for the double poly-Glycine flexible spacer. Amplified sequences were cleaned up via gel electrophoresis, and blunt-end ligated into the pre-cut and cleaned pBS-sTeNT plasmid at the EcoRV restriction site, using the PCR and cloning protocols are described in the Appendix 7.4, with the resulting plasmids shown in Appendix 7.7.2.10 to 7.7.2.12. Each of the plasmids was then amplified in transformed One Shot Top10 *E. coli* cells, as outlined in Appendix 7.4.3.

For expression in mammalian cells, the coding sequences were cut from the pBlueScript cloning plasmids using the incorporated EcoRI and the NotI restriction site that was added during gene synthesis. The fragments were then cleaned up via gel electrophoresis, and cloned into the precut pcDNA3 expression vector, using the standard protocols described in Appendix 7.4. Gene sequencing was performed using the amplification primers, together with new primers designed to amplify overlapping regions of the coding sequences within each plasmid; no mutations detected for any of the constructs.

Protein	Origin	Cloning Plasmid	Expression Vector
Cre	pBS SK-iCre	pBS KS-iCre-sTeNT	pcDNA-iCre-sTeNT
		pBS KS-iCre-spacer-sTeNT	pcDNA-iCre-spacer-sTeNT
eGFP	pcDNA3-EGFP	pBS KS-EGFP-sTeNT	pcDNA-EGFP-sTeNT
		pBS KS-EGFP-spacer-sTeNT	pcDNA-EGFP-spacer-sTeNT
Luciferase	pGL3-CMVe-PDGFb-Luc	pBS KS-Luc-sTeNT	pcDNA-Luc-sTeNT
		pBS KS-Luc-spacer-sTeNT	pcDNA-Luc-spacer-sTeNT

Table 8 Constructs of the synthetic Tetanus Neurotoxin (sTeNT)

5.6 Fusion Protein Testing

The initial tests of the fusion protein were of the Cre recombinase and marker activity. The tests for GFP expression were performed in HEK293 cells via fluorescence microscopy, using the same apparatus as described in Chapter 3.3. Using the calcium phosphate transfection protocol, Appendix 7.4.3, cells were transfected with either pcDNA-GFP-sTeNT or pcDNA-GFP-spacer-sTeNT, with GFP expression tested for after 24 hours. With positive results recorded for both fusion-proteins, it was decided to move directly on to test for Cre recombinase activity.

5.6.1 Stoplight system

A vector designed for the testing of Cre recombinase activity has been developed, such that recombinase activity changes the transiently expressed protein from DsRed to GFP [209]. This plasmid, pYY12-Stoplight and shown in Appendix 7.7.2.21, was developed to monitor the translocation of Cre recombinase fused to the *Salmonella enterica* secretion and translocation signals [189].

To act as a positive control for the Stoplight system, the codon optimized Cre recombinase from the cloning vector pBS SK-iCre was cut out with restriction enzymes HindIII and KpnI, cleaned up via gel electrophoresis, and the fragment cloned into the mammalian expression vector pcDNA3 (Appendix 7.7.2.2), to generate the plasmid pcDNA3-iCre, shown in Appendix 7.7.2.4.

This Stoplight vector was co-transfected with pcDNA3-iCre, pcDNA-iCre-sTeNT or pcDNA-iCre-spacer-sTeNT in HEK295 cells with the calcium phosphate protocol, and the cells imaged after 48 hours. The results are shown below, with Figure 5-7a and Figure 5-7b showing the negative and positive controls respectively. The plasmid pcDNA-iCre-sTeNT in Figure 5-7c shows no evidence of GFP expression, indicating that the Cre recombinase is unable to catalyze the recombination of the Stoplight plasmid. The vector that included the flexible spacer, pcDNA-iCre-spacer-sTeNT, shows both GFP and DsRed expression. This indicates that the recombination event has occurred, but that more time was required when using the fusion protein than with the iCre alone, as DsRed was expressed for a time long enough for it to accumulate in the cells before the recombination of pYY12-Stoplight. The efficiency of the fusion protein appears to be very good though, with almost all of the DsRed expressing cells shown to express GFP after 48 hours. For the aims of this project, the longer amount of time required by the sTeNT and iCre fusion protein to catalyze recombination is not a critical parameter.

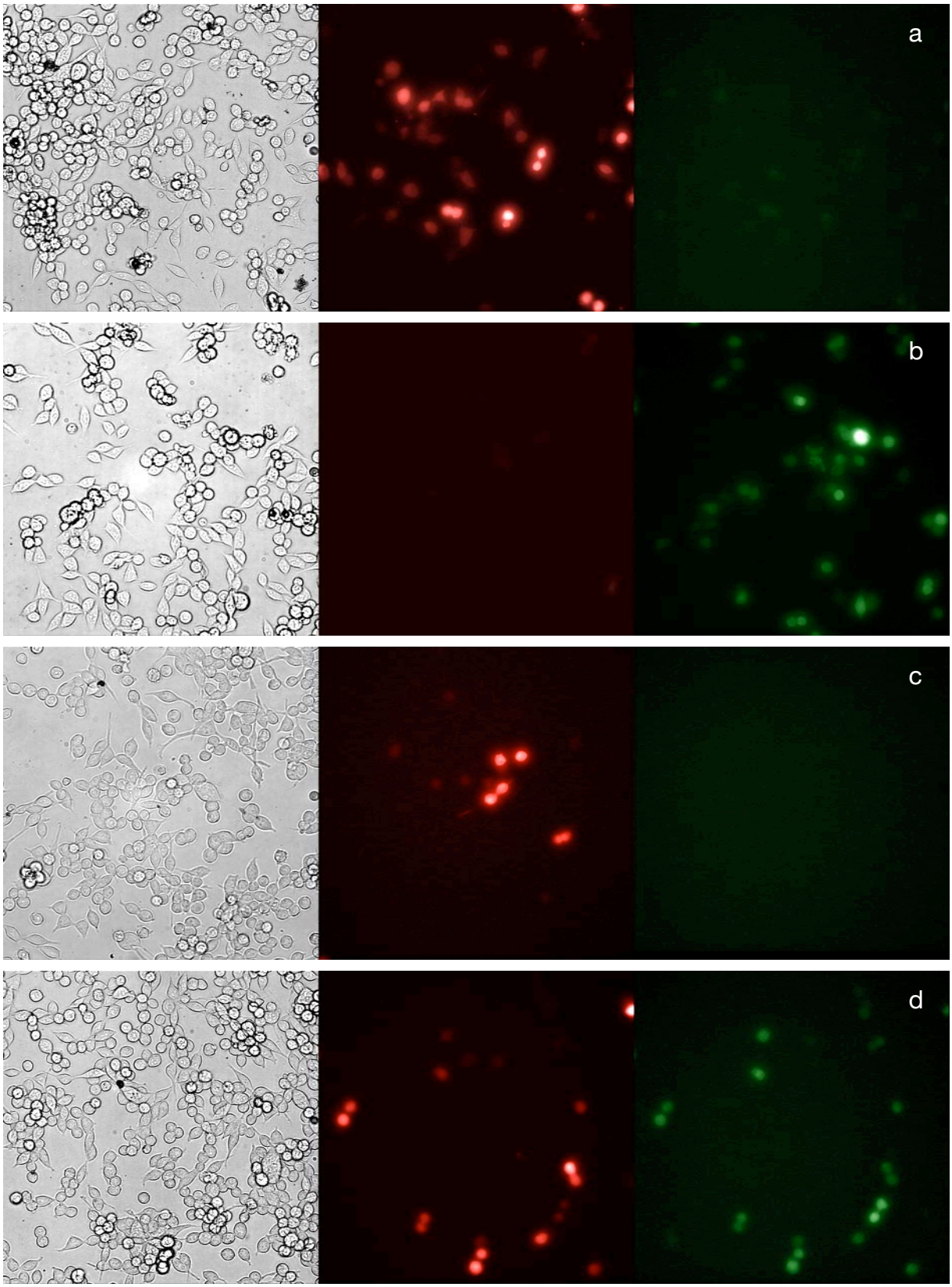

Figure 5-7 Cre-TeNT fusion-protein testing, showing bright field, red and green fluorescence images; a) Negative control, pYY12-Stoplight, b) Positive control, pYY12-Stoplight and pcDNA3-iCre, c) pYY12-Stoplight and pcDNA3-iCre-sTeNT, d) pYY12-Stoplight and pcDNA3-iCre-spacer-sTeNT

5.6.2 FACS testing

For a more quantitative analysis of the activity of the Cre recombinase fusion proteins, Fluorescence-activated cell sorting (FACS) was used to analyze the expression levels of GFP and DsRed in transiently transfected cells. Using the same transfection protocols as described above, HEK293 cells were transfected, and following 48 hours in culture the cell were trypsinized, and the suspension passed through the FACSCalibur machine (BD Biosciences Inc.). Using the Forward Scattering (FSC), which correlates with the cell volume, and Side Scattering (SSC), which depends on the inner complexity of the cell, healthy cells were gated on the FlowJo software package (Tree Star Inc.). These healthy cells were then analyzed for fluorescence, with GFP detection at 530/30 on channel FL1-H, and DsRed detection at 585/42 on channel FL2-H, with the results shown in Figure 5-8. The FACSCalibur apparatus is equipped with an air-cooled 15mW 488 nm Ar Ion laser and a 9mW 635 nm Diode Laser; the 488 nm laser was used to excite both fluorescent proteins, and although not optimal for DsRed's excitation maxima at 556 nm, provides sufficient illumination for measurements involving this marker [210].

The negative and positive controls (Figure 5-8-a and Figure 5-8-b), show that the majority of cells do not show fluorescence, at 83.2% and 75.6% respectively. The transfect with pcDNA3-iCre-sTeNT shows a similar distribution as the negative control, with 2.52% of cells showing some slight signal in the 585/42 nm channel in the control, and 2.51% with the iCre-sTeNT fusion (Figure 5-8-c), using the cutoff shown in the diagram. As DsRed is known to pass though a green-emission phase during maturation [211], this small overlap may be unavoidable with this vector. The positive control shows GFP expression in 24.2% of the cells, compared with 16.62% of the iCre-spacer-sTeNT fusion (Figure 5-8-d). As with the fluorescence images, the cells also show the expression of DsRed, with 20.79% above the cutoff.

Plasmid	DsRed Expression (%)	GFP Expression (%)
Negative Control	16.57	2.52
pcDNA3-iCre	3.48	21.2
pcDNA3-iCre-sTeNT	16.43	2.64
pcDNA3-iCre-spacer-sTeNT	20.79	16.62

Table 9 Results for the FACS analysis of pYY12-Stoplight recombination.

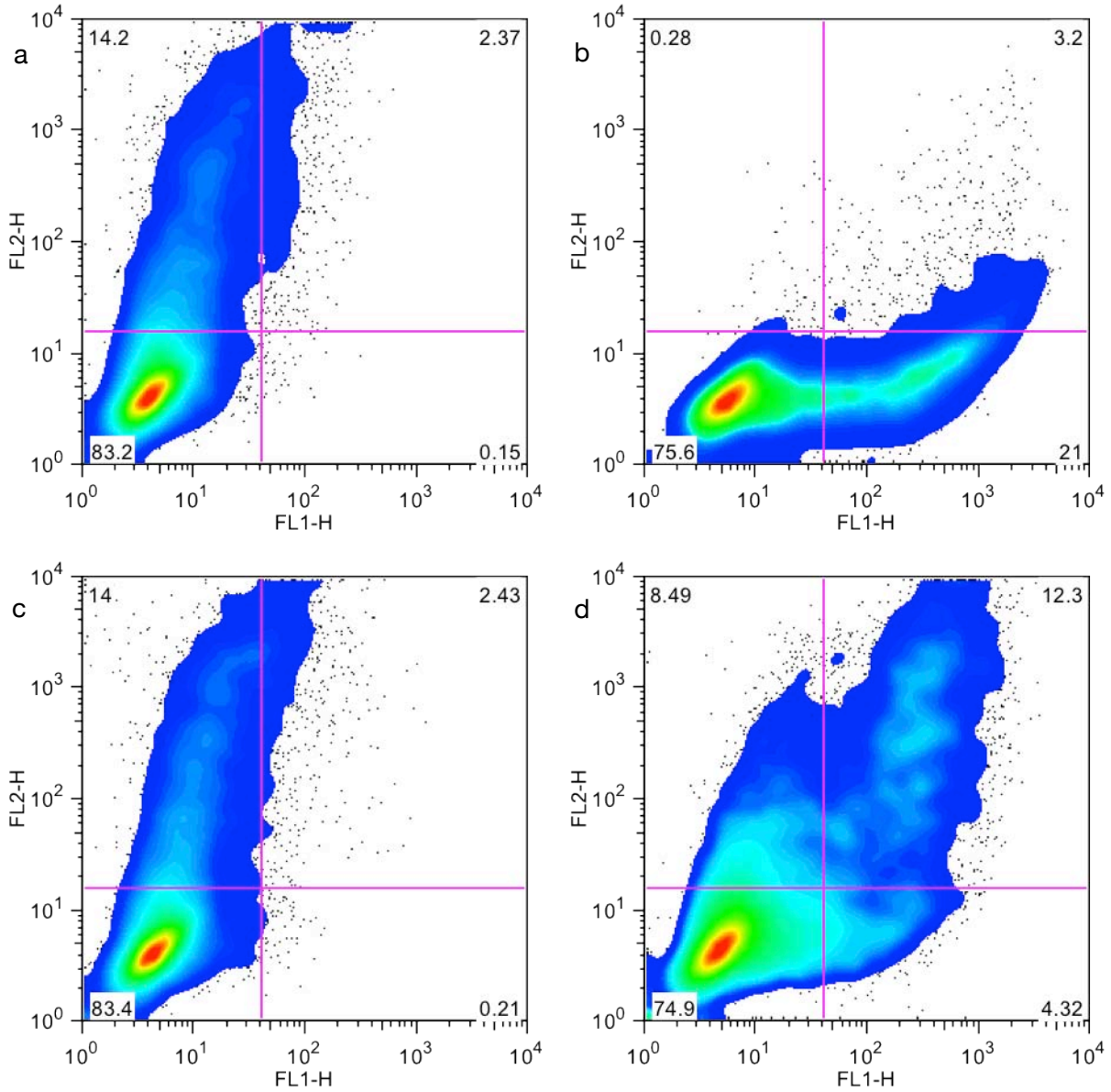

Figure 5-8 FACS analysis of the iCre/sTeNT fusion proteins with the Stoplight system; a) Negative control, pYY12-Stoplight, b) Positive control, pYY12-Stoplight and pcDNA3-iCre, c) pYY12-Stoplight and pcDNA3-iCre-sTeNT, d) pYY12-Stoplight and pcDNA3-iCre-spacer-sTeNT

The low transfection rate, as determined by the low percentage for fluorescing cells, would be improved with the use of Lipofectamine transfection instead of calcium phosphate. It would also be interesting to postpone the FACS analysis for a further 24 hours to see whether the DsRed expression falls further, or if the percentages of cells expressing GFP increases; however, HEK293 cells grow rapidly, and the plasmid-copy number per cell would not be maintained upon cell division. The iCre protein clearly demonstrates rapid DNA recombination. After the translation of the enzyme, the recombinase could either migrate into the nucleus and act on the pYY12-Stoplight plasmid, or it could remain in the cytosol with

the plasmid migrating back and forth from the nucleus. With the iCre-spacer-sTeNT fusion, the lower and slower recombination of pYY12-Stoplight may be due to a number of possible mechanisms. The fusion itself may interfere with the enzyme; this is clearly a strong possibility noting the complete lack of activity in the spacer-free fusion. This, the most likely possibility, would be overcome with the modification of the spacer domain, as there are a variety of structural motifs available for separating fusion proteins. Such a modified fusion protein would show improved efficiency; however this would not necessarily improve the overall system, as recombination is the key event, not the length of time that recombination requires. A second possibility is that the protein does not undergo the required post-translational cleavage that separates the heavy and light chain, and that the sterically bulky heavy chain prevents or impedes the transfer of the protein into the nucleus. This possibilty could be solved via the modification of the peptide sequence so as to contain a more applicable cleavage site between the sTeNT HC and LC, one for a peptidase known to operate in the post-translational machinery of the neuronal ribosome. A third possibility is that although the protein is correctly processed, the presence of just the sTeNT LC is enough to prevent the fusion protein's access to the nucleus. In the final two cases, the fusion would still be able to operate on pYY12-Stoplight plasmids in the cytosol. Thus, it is not possible to make further tests on the function of the iCre-spacer-sTeNT fusion protein, without utilizing a reporter system that is integrated into the cell genome via stable transfection, and is thus not dependant on cytosolic Cre activity.

5.6.3 Stable Cell Line Testing

A second cell line was obtained for Cre analysis, immortalized mouse fibroblasts from the transgenic mouse line ROSA26-LacZ, which are used for the detection of tissue-specific promoter-controlled Cre recombinase activity [181], expressing ß-galactosidase upon the recombinase-induced excision of a "stop" sequence placed between the start codon and DNA sequence for the marker gene. As this construct is integrated into the mouse genome, Cre recombinase must enter the cell nucleus to activate the expression of the marker. The fibroblasts were transiently transfected with pcDNA3-iCre, pcDNA3-iCre-sTeNT and pcDNA3-iCre-spacer-sTeNT, using the calcium phosphate method (Appendix 7.4.3), and stained with X-Gal after 24 hours with the results shown in Figure 5-9 (Appendix 7.4.7). Although the levels of Cre recombinase activity are extremely low for the iCre-spacer-sTeNT fusion (Figure 5-9-c), this is conclusive evidence that the fusion works as designed.

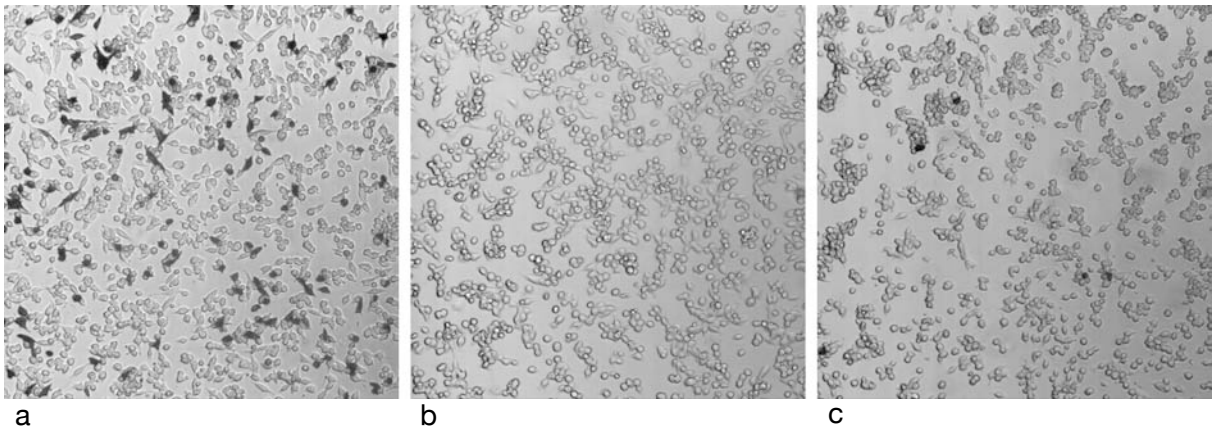

Figure 5-9 X-Gal staining for Cre-reporter activity after fusion-protein transfection into mouse fibroblast cells; a) positive control, pcDNA3-iCre, showing Cre activity in ~10% of cells, b) pcDNA3-iCre-sTeNT, showing no evidence of ß-galactosidase activity, c) pcDNA3-iCre-spacer-sTeNT, giving very low rates of recombinase activity, >0.5%.

5.7 Development of a Testing Protocol

With the iCre-spacer-sTeNT fusion protein having been demonstrated to retain recombinase activity, no further tests are possible on HEK293 or other non-neuronal cell systems, as the TeNT protein requires active synaptic connections in order to undergo trans-synaptic transmission. Although in previous chapters dissociated hippocampal neurons were used to test for selective staining with the new voltage sensitive dyes, the neurons were found to be very fragile, and best transfected within 48 hours of harvesting [94]. As it takes tens of days for active connections to develop between neurons *in vitro*, late transfection would lead to the death of the majority of neurons, and early transfection would show only very low levels of expression after this amount of time had elapsed. The most efficient method would be the use of acute hippocampal brain slices. Such cultured brain tissue contains healthy neurons, well supported by their surrounding glial cells, and when taken from mice ~1 week old, reproduce most anatomical and functional properties of the corresponding *in vivo* hippocampal structure for ~6 months *in vitro* [212,213]. However, there is concomitant loss of vascular and hormone regulation, shearing of dendritic process and axons, and tissue debris along the cutting surface. However, the direct visualization and the ability to access all regions of the slice make this the most efficient technique for testing trans-synaptic transfer of the fusion protein.
The ROSA26-LacZ mouse line would offer hippocampal slices that would detect Cre recombinase activity with high sensitivity using X-gal staining. Although GFP or YFP marker lines would offer better localization in live cultures, the LacZ staining method allows for a slow and detailed analysis of neuron connectivity using fixed and preserved slices.

5.7 DEVELOPMENT OF A TESTING PROTOCOL

5.7.1 Transfection Options

The transfection of primary cell lines, especially neurons, is difficult and shows low efficiency coupled with high cell mortality [214]. Layers of dead cell debris and glial cells, which surround the slice and neurons respectively, hinder the transfection of neurons in slice-culture; this barrier excludes the use of standard transfection techniques, which are unable to penetrate into the hippocampal slice efficiently [215]. Three techniques have been developed to overcome this problem; pseudovirus transfection, where complex and highly efficient viral machinery is used to deliver genes into the slice [216-218]; biolistics, a technique that utilizes the high mass and velocity of gold particles to penetrate the slice, where they carry the plasmid DNA [219,220]; and electroporation-mediated transfection, where single neurons in slice-culture are transfected using micropipettes loaded with plasmid DNA [221].

For the analysis of neural networks, micro-electroporation mediated transfection would be the optimal technique, allowing for the dissection of individual neural circuits. However, for testing purposes, it is the least useful technique as it requires the most difficult handling procedures, and has low efficiency. The biolistics technique and pseudovirus techniques can both be used to transfect neurons from a small sub-region of the brain; biolistics 'bullets' can be targeted to a small region with the use of a mask to block the off-target transfection of cells, and small pseudovirus aliquots can be microinjected into desired regions of the brain (Figure 5-10). With the end goal of this research the *in vivo* tracing of neural circuitry, the pseudovirus methods were investigated.

The most developed viral systems for the transfection of neurons are the Human immunodeficiency virus (HIV-1) derived Lentiviral vectors [222]. The viruses, members of the *Retroviridae* family, are named after the slow progression of their clinical symptoms (*lenti* is Latin for slow), taking months or years to progress, and often leading to the wasting and death of their hosts [218]. HIV-1 is an enveloped and spherical virus, ~120 nm in diameter, comprised of plasma membrane of host-cell origin and containing a conical capsid. This protein-based capsid contains a diploid RNA genome of ~9.3 kb which encodes nine open reading frames. Three of these genes are the Gag, Pol, and Env poly-proteins, which are subsequently cleaved into functional subunits. Gag is processed during maturation to form the structural proteins matrix, capsid, nucleocapsid, and spacer peptides P6, P2, and P1. Pol is cleaved into reverse transcriptase, integrase, and HIV protease. Env is cleaved to form the transmembrane and surface glycoproteins required for viral binding and entry into the cells [223].

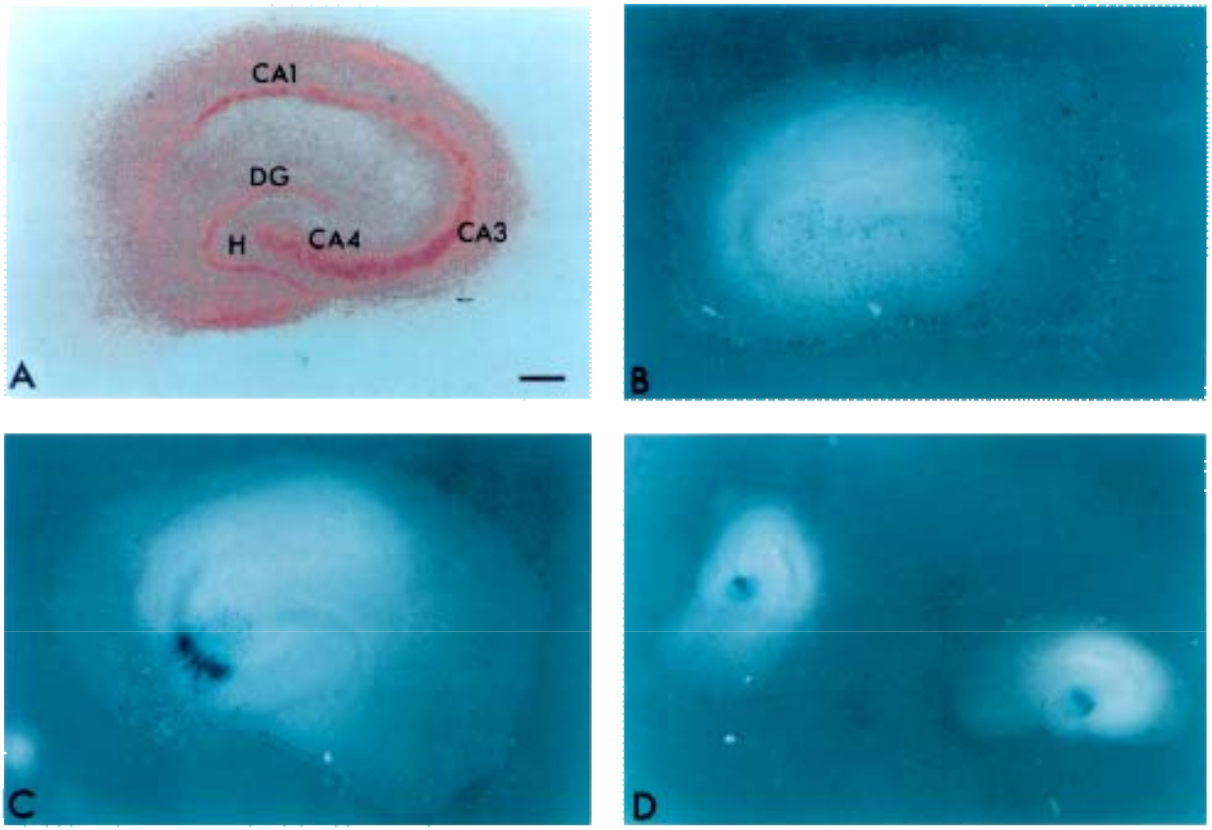

Figure 5-10 Pseudoviral transfection with a ß-galactosidase encoding vector of cultured organotypic hippocampal slices; a) the structure of the hippocampus, b) surface transfection with viral stock solution, d) CA3 region microinjection, d) hilus region microinjection, taken from [224].

Two of the remaining 6 genes are transactivators, to enhance the gene expression of the other HIV-1 proteins, and the last four genes are the virulence factors. These encode proteins that are not essential for viral replication, but modulate HIV-1 virulence and pathogenesis *in vivo*, and are comprised of virion infectivity factor, the viral protein R, the viral protein U, and the negative factor.

Other structures in the viral genome include the 5' and 3' long terminal repeats (LTR) at either end of the RNA molecule, which are themselves acted on by the integrase protein during the insertion of the HIV-1 genome into host genome, and also as promoter/enhancers to induce the transcription of new copies of the HIV-1 genome. The packaging signal ψ is an RNA element that forms secondary and tertiary structures in which purine-rich loops appear to be critical for Gag binding [225], and allows copies of the genome to be correctly packaged into newly synthesized viral capsids.

The HIV-1 virus has been adapted into a pseudoviral vector to carry transgenes into target cells via the separation of the genome into useful components, with the mutation and deletion of elements giving rise to virulence and replication capability. The most important step in the development of 'safe' pseudoviral vectors was the engineering of self-inactivating vectors

(SIN), involving the deletion of most of the U3 region of the LTR, which renders the LTR largely transcriptionally inactive [226]. Thus, once integrated into the transduced target cell genome, the lentiviral genome is no longer capable of producing packageable copies of the RNA viral genome [227]. Also, the viral genome has been reduced to just three essential structural and functional genes; Gag, Pol and Env, with each of the encoding genes located on separate plasmids from the transgene of interest. Thus, four separate plasmids are required to create pseudoviral particles, with only the transgene plasmid containing the packaging signal ψ, so none of the HIV-1 structural genes are actually present in the packaged pseudoviral genome. To prevent undesirable recombination events that could generate a replication-competent virus from the four plasmids, they have also been engineered not to contain any regions of homology. Finally, the Rev and Pol genes have been rendered Rev dependent, preventing their expression in the absence of Rev, which act on the RRE structure in the Gag/Pol mRNA transcript, allowing it access to the host cell's translational machinery [228-232].

5.7.2 Promoter Selection

As standard lentiviral vectors will transduce all cell types present in organotypic hippocampal slices, the signal generated by neuronal labeling with fluorescent proteins or LacZ would be contaminated by the signals produced from glial and other cell types. Pseudoviral vectors based on lentivirus can be pseudotyped to display higher tropism for neurons than glial cells [216,233], however low yields and a complicated methodology make this an unattractive route. Lentivirus vectors commonly use unspecific promoters, but the use of a neuron-specific promoter would confine marker expression to neurons, regardless of the breadth of cell types transduced. The platelet-derived growth factor ß-chain (PDGF-ß) promoter is such a neuron-specific promoter, but suffers from low expression rates compared to the CMV enhancer/promoter pair, one of the strongest drivers of protein expression discovered. Research has shown that a hybrid promoter, constructed by appending a 380-bp fragment of CMV enhancer upstream of the 1.5-kb PDGF-ß promoter, has both neuronal-specificity coupled with CMV promoter levels of expression [234]. This hybrid promoter has been used in adeno-associated pseudoviral vectors for neuron-specific transgene expression in rat striatum [235]. The hybrid promoter was selected for neuron-specific use, and the CMV promoter for initial testing purposes in this project.

5.7.3 Lentiviral Vector Construction

The ViraPower Promoterless Lentiviral Gateway Kit (Invitrogen), was used to generate pseudoviral particles. This system generates a lentiviral expression plasmid from three separate plasmids, containing the promoter, gene of interest and viral packaging elements in a single recombination step [236]. The CMV enhancer/human PDGF-ß promoter (CMVe-PDGFb) was amplified out of the plasmid pGL3-CMVe-PDGFb-Luc with PCR with the primer pair 5'-CCCTGGGTCGACATTGAT-3' and 5'-TTTCAGTTCCTCGACTCT-3', and topo cloned into pENTR5-TOPO, to give the plasmid pENTR5'-CMVe-PDGFb (Appendix 7.7.3.1). In a similar manner, the CMV promoter was amplified from pcDNA3-EGFP with the primer pair 5'-CGATGTACGGGCCAGATAT-3' and 5'-AATTTCGATAAGCCAGTA-AG-3', to yield pENTR5'-CMV (Appendix 7.7.3.2).

From the plasmid pcDNA3-iCre, using the primer pair 5'-GTGCCCAAGAAG-AAGAGGAAAGTCTC-3' and 5'-GTCCCCATCCTCGAGCAGCC-3', the gene for codon-optimized Cre was amplified and topo cloned into the pENTR/D-TOPO plasmid, giving pENTR/D-iCre, as shown in Appendix 7.7.3.3. The iCre-spacer-sTeNT gene from pBS KS-iCre-spacer-sTeNT was PCR amplified using the primer pair 5'-GTGCCCAAGAA-GAAGAGGAAAGTCTC-3' and 5'-GGGATGGACAAATGACTGATA-ATAG-3', yielding pENTR/D-iCre-spacer-sTeNT (Appendix 7.7.3.4), after cloning the fragment into the pENTR/D-TOPO plasmid.

The Multisite Gateway reaction was performed using the clonase recombination enzyme mix, to generate expression vectors using both the CMV promoter, and the iCre and iCre-spacer-sTeNT fusion protein, together with the pLenti6/R4R2/V5-DEST expression vector, as shown in Figure 5-11. This yielded plasmids pLenti6-CMV-iCre and pLenti6-CMV-iCre-spacer-sTeNT, as shown in Appendix 7.7.3.7 and 7.7.3.5.

5.7.4 Lentiviral Particle Production and Testing

The expression plasmids described above, together with lentiviral packaging plasmids, were used to transfect 293FT cells grown in a 10 cm tissue culture plate to 90-95% confluency in standard HEK293 cell media (D-MEM containing 10% FBS, 2 mM L-glutamine, 0.1 mM MEM Non-Essential Amino Acids, 1% penicillin/streptomycin, and 1 mM MEM Sodium Pyruvate). During transfection, the cells were kept in antibiotic free media together with the DNA-Lipofectamine2000 complexes overnight. After this period, the transfection media was replaced with standard HEK293 cell media, and after 48 hours, the virus-containing supernatant was collected in 15 ml sterile, capped, conical tubes. These were placed in a

centrifuge at 3000 rpm for 15 minutes at +4°C to pellet cell debris, and the remaining viral supernatant was stored in 1 ml aliquots in cryovials at -80°C.

The infectious supernatant was used to transfect the mouse fibroblast Cre-reporter cell line. 24 hours after infection, the cells were assayed for ß-galactosidase activity with X-Gal, with the results shown in Figure 5-12. The results show that although the iCre viral particles correctly induce the expression of functional Cre recombinase, the iCre-spacer-sTeNT shows no activity.

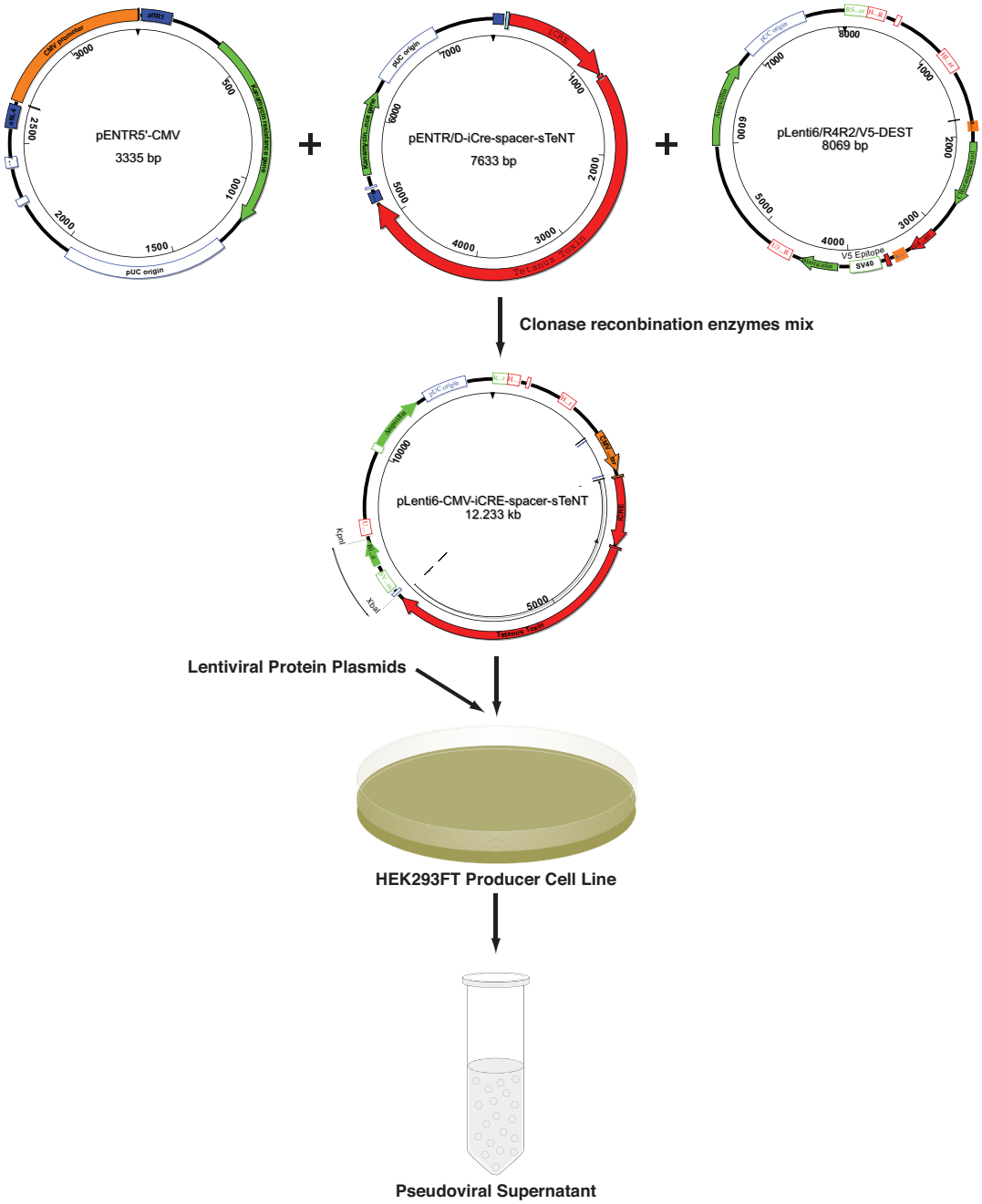

Figure 5-11 Recombination of the Promoter, Gene and Expression vectors to produce vector for the generation of pseudoviral particles in HEK293 cells.

As the fusion protein is known to be expressed in this cell type, as demonstrated in Chapter 5.6.3, further analysis of the viral particle production is required. It is known that genome size is an important factor in the production of functional viral particles [237], with larger inserts showing reduced viral titre, although inserts in excess of 18 kb have been demonstrated. For large inserts, reduced centrifuge speeds during concentration give improved yields, but show reduced viability with increase insert length [238], as shown in Figure 5-13. The iCre insert has a packaging insert of 4780 bp, in a vector of 8254 bp, whereas the packaging insert for iCre-spacer-sTeNT has a length of 8759 bp, in a vector of 12,233 bp. Assuming that both of these vectors followed the same pattern as those described in Figure 5-13, we could expect approximately 3 orders of magnitude more infectious particles with the iCre compared to the iCre-spacer-sTeNT fusion virus.

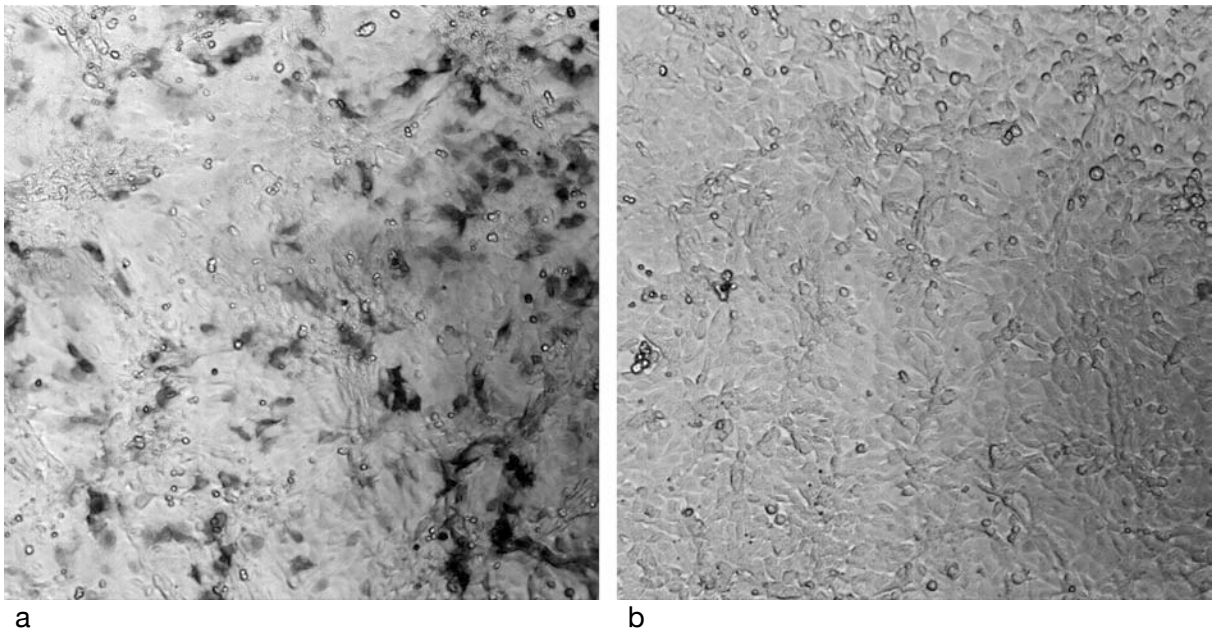

Figure 5-12 The expression of ß-galactosidase in the mouse fibroblast Cre-reporter cell line, 24 hours after the infection of the cultures with Cre fusion protein pseudoviral particles; a) iCre encoding lentivirus, b) iCre-spacer-sTeNT fusion encoding lentivirus.

The pLenti6/R4R2/V5-DEST expression vector contains the encoding and promoter for the Blasticidin resistance gene, which is used to ensure the generation of stable cell lines. This gene is unnecessary for this project, and so the 966 bp stretch of DNA holding the sequence and flanked by the XbaI and KpnI restriction sites was cut from the pLenti6/R4R2/V5-DEST plasmid, and cleaned up with agarose gel electrophoresis, before blunt end processing with the Klenow fragment and blunt-end ligation. The new vector, pLenti6/R4R2/V5-DEST-cut, was used in the Multisite Gateway reaction to generate pLenti6-CMV-iCre-spacer-sTeNT-cut and pLenti6-CMV-iCre-cut, and viral particles were produced as described above. The results

of the infection of Cre-reporter mouse fibroblasts are shown in Figure 5-14.

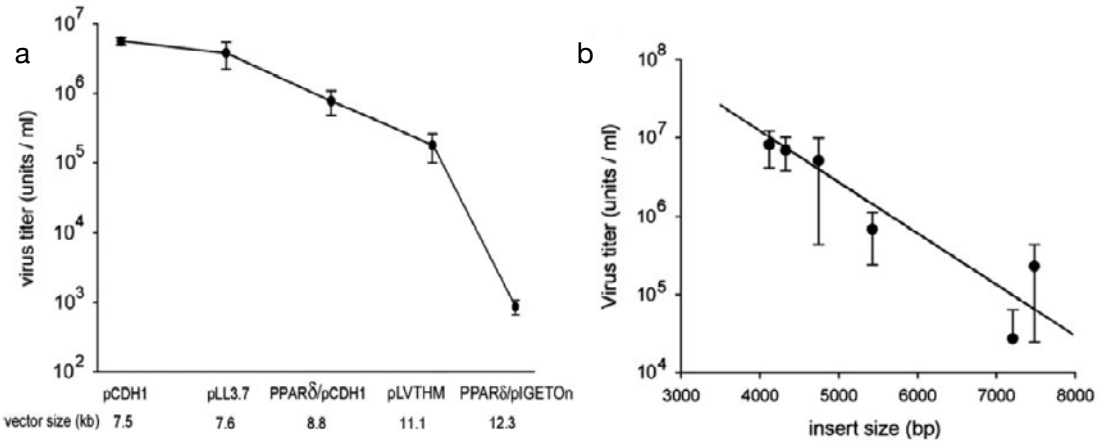

Figure 5-13 The production of active viral particles as compared to vector and packaging insert length; a) the size of the plasmid containing the transgene, b) the length of the packaging insert, from 5' LTR to 3' LTR.

A higher rate of recombination has occurred using the pLenti6-CMV-iCre-cut control vector compared to the uncut version, however the desired CMV-iCre-spacer-sTeNT-cut fusion proteins still shows no signs of Cre recombinase activity. The new vector has a length of 11,267 bp, with a packaging insert of 7793 bp, a size that leads to poor viral titre according to the study described above [238]. This fact, together with the low enzymatic activity of the fusion protein, could explain the negative results for this experiment.

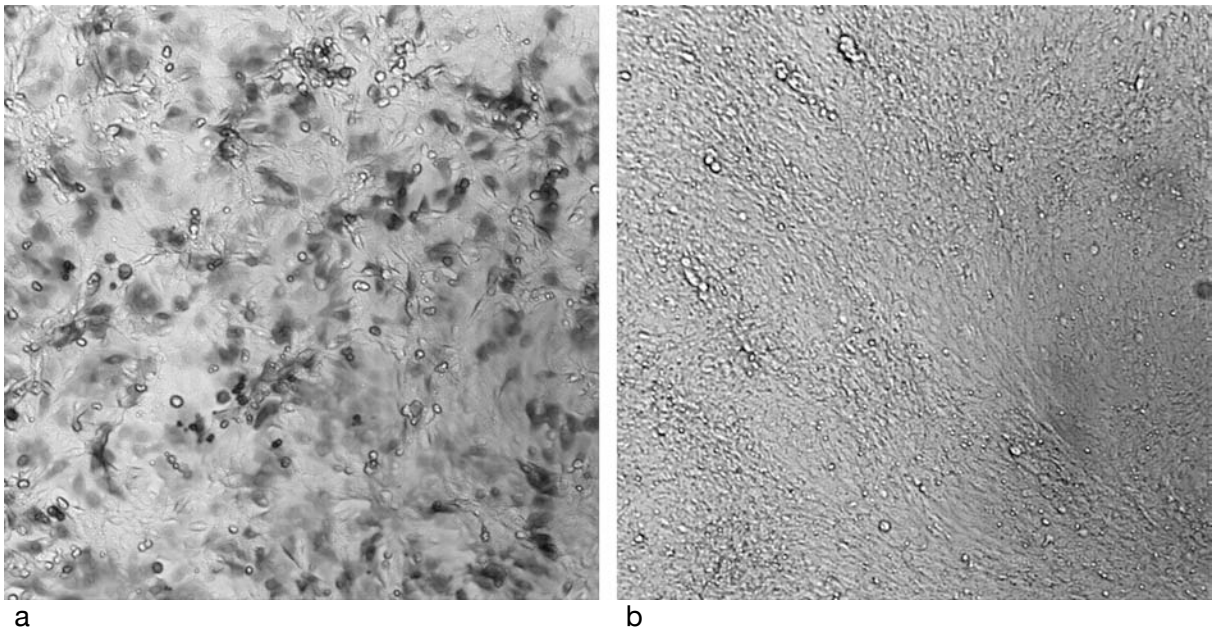

Figure 5-14 The expression of ß-galactosidase in the mouse fibroblast Cre-reporter cell line, 24 hours after the infection of the cultures with Cre fusion protein pseudoviral particles; a) iCre-CUT encoding lentivirus, b) iCre-spacer-sTeNT-CUT fusion encoding lentivirus.

5.8 Conclusion

Fusion proteins of Cre recombinase and Tetanus Neurotoxin were successfully constructed, fulfilling the criteria of good expression in mammalian cells and a lack of toxicity. The proteins were expressed in both transiently and stably transfected cell lines that encoded a marker system for Cre recombinase activity, with the construct pcDNA3-iCre-spacer-sTeNT that utilized an eleven amino acid flexible spacer demonstrating acceptable levels of activity.

With this successful result, the construct was used in a lentiviral delivery system, with the aim of transfecting neurons in cultured organotypic hippocampal slices. However, the delivery system was found to show no detectable activity for the construct, although the positive control using codon optimized Cre recombinase showed normal activity. This negative result is most probably due to the poor packaging of large constructs into the lentiviral particle.

Although the development of a lentiviral delivery system was not completed, this in no way compromises the goal of the project, as there are a variety of other delivery systems available with which to introduce genetic material to neurons *in vivo*. However, time constraints prevented further exploration into these alternatives.

5.9 Future Directions

The flexible spacer that links the recombinase to the sTeNT LC has an important impact on the protein's enzymatic activity. The current fusion proteins shows degraded activity compared to native Cre, and optimization of the flexible linker may increase the activity to near wild-type levels. Two new linker elements have been synthesized; a flexible linker with the sequence LPPPPDPPPPLPPPPDPPPPLPPPPLPPPP, and a linker that takes on a more ridged helical secondary structure LAEAAAKEAAAKEAAAKEAAAKEAAAKAAA, useful for keeping subunits of a fusion protein separated [239-241]. These new fusion proteins have yet to be fully tested, but initial studies suggest improved Cre recombinase activity in both constructs.

Further work on improving the lentiviral system may result in the production of functional viral particle. There are two main routes available. The first involves the further reduction of the packaging insert and expression plasmid length, to increase viral titre by building more stable infectious particles. This could be performed via the excision of further unneeded DNA elements, or the replacement of CMV with a smaller promoter. The second option involves the application of various techniques to concentrate the viral particles, such as ultracentrifugation, dialysis, ion exchange chromatography, or by precipitation using polyethylene glycol [242,243], to give an ~1000 fold increase in viral titre. With both options

combined, a functional, high titre stock of infectious particles could be produced for microinjections into slices.

Although this method is the most direct route for future *in vivo* work, two alternative methods may offer a faster route to the successful application if the fusion *in vitro*. The first, mentioned in section 5.7.1, is biolistics. Taking the already prepared pcDNA3 expression vectors for the various fusion proteins, and using the plasmid DNA to coat gold 'bullets', the vectors could be used directly on organotypic hippocampal slices. This would eliminate the need for further molecular biology, and the need for an S2 biosafety laboratory. However, the low level of transfection efficiency, coupled with poor Cre recombinase activity would require large numbers of slices to be transfected. Furthermore, biolistics is not readily applicable to *in vivo* research, the ultimate goal of the project, as it requires open access to the regions of tissue of interest.

A second possibility is the expression of the protein in *E. coli*, followed by purification and the direct injection of the protein into Cre-reporter mouse lines. This technique is often use in tetanus neurotoxin research [244,245], and would require the cloning of the fusion protein sequence into a bacteria expression vector, together with an N-terminal purification tag [246]. This would eliminate the problems of low levels of expression demonstrated so far, and furthermore, post-translational modification could be performed on the purified protein, such as adding fluorescent labels like the biarsenical labels FlAsH and ReAsH [247,248], that have already been used to trace bacterial toxin translocation across cell membranes [249].

In each of the three possible future directions the goal would be the introduction of the fusion protein into the CA1 region of cultured hippocampal slices. The would allow the tracing of Schaffer collaterals back to the CA3 neurons cell bodies, and then back through the mossy fibers to the granule cells in the dentate gyrus, with the entire connected neural network clearly visualized with ß-galactosidase X-gal histochemistry.

The synthetic Tetanus Neurotoxin has much potential, apart from the uses described in Chapter 5. The ability of the toxin to transport proteins into the cytosol could be applied to the delivery of plasmid DNA for neuron specific transfection, or for the directed delivery of therapeutic proteins to the central nervous system [250]. Also, more complex methods to unravel neural network connectivity are possible with the development of new fusion proteins. The Flp recombinase could be used as a replacement for Cre, and with the right Flp/Cre reporter transgenic mouse lines, multiple circuits, and their interconnections could be mapped. One particularly interesting possibility would be the generation of two new sTeNT fusions, each binding to one fragment of a split Cre protein. Such split Cre enzyme fragments have been fused to the rapamycin-binding elements FKBP12 and FRB respectively [188].

Alone, these fragments show no recombinase activity, but in the presence of rapamycin, the two fragments are brought together, activating the hybrid Cre recombinase. If two new sTeNT fusions were constructed with these hybrid fragments, and introduced into different regions of the central nervous system, the introduction of rapamycin would cause the activation and selective labeling of neurons where the two neural pathways meet. Such experiments are not possible with the current tools available in neurobiology, and developments in this area may serve to elucidate the hidden complexity of the brain.

6 CONCLUSION

In this project, several important steps have been completed in the development of genetically targeted voltage sensitive dyes. Seven new voltage sensitive prodyes have been synthesized, with each shown to be an alkaline phosphatase substrate, all based on the sensitive ANEP chromophore. Three phosphate prodyes, based on model dyes created by Hinner, were initially created [12]. However, these were found to lack sufficient selectivity, and so a new group of prodyes was designed, using recent advances in medicinal prodrug chemistry to overcome this limitation. Four target compounds were synthesized and tested, based on the phosphonooxymethylation of the dyes tertiary amine tail, with one of the new compounds, di-1,8P6-ANEPPS, exhibiting excellent cell membrane targeting.

Based on this success, an apparatus used to externally apply electrical fields to *in vitro* cell cultures was then designed and constructed, and the new compound, di-1,8P6-ANEPPS, was then shown to possess comparable levels of voltage sensitivity to the widely used voltage sensitive dye, di-4-ANEPPS.

In parallel with this project, a new technique for tracing connected neural circuits has been proposed. The initial steps of design and planning have lead to the construction of a variety of new fusion proteins, based on the non-toxic, synthetic *Clostridium tetani* neurotoxin. The Cre recombinase based fusion proteins have been shown to function correctly, and the construct is now ready for testing in brain slices, potentially offering the most straightforward and accurate method for the analysis of brain connectivity obtainable.

If the fusion protein is found to function as it was designed, the successful application of these two new techniques applied together could open up new areas of research in neurobiology, allowing the first analysis of the electrophysiology of connected neural circuits.

7 APPENDIX

7.1 Abbreviations

Abbreviation	Expansion
aa	amino acid
AMPD	2-amino-methyl-1,3-propanediol
ANEP	amino naphthyl ethenyl pyridinium
ANNINE	anellated hemicyanine (dye)
AP	alkaline phosphatase
APMA	artificial plasma membrane anchor
ASP	amino styryl pyridinium
BCIP	5-bromo-4-chloro-3-indolyl-phosphate
bp	base pair
CFP	cyan fluorescent protein
CHO	Chinese hamster ovary (mammalian cell line)
CMV	cytomegalovirus
CNS	central nervous system
DMEM	dulbecco´s modified eagle medium
DNA	deoxyribonucleic acid
EGFP	enhanced green fluorescent protein
FACS	fluorescence-activated cell sorting
GFP	green fluorescent protein
GPI	glycosyl phosphatidylinositol
H2B	histone 2b
HC	heavy chain
HCC	heavy chain c-terminal fragment
HCN	heavy chain n-terminal fragment
HEK293	human embryonic kidney (mammalian cell line)
HIV	human immunodeficiency virus
HRP	horse radish peroxidase
IRES	internal ribosome entry site
kb	kilo bases
kDa	kilo Daltons
LacZ	β-galactosidase
LC	light chain
LCR	ligase chain reaction
LED	light-emitting diode
LTR	long terminal repeat
MCS	multiple cloning site
mRNA	messenger ribonucleic acid
NBT	nitro-blue tetrazolium chloride
NMR	nuclear magnetic resonance
PAGE	polyacrylamide gel electrophoresis
PCR	polymerase chain reaction
PDGF-ß	platelet-derived growth factor ß-chain

PLAP	placental alkaline phosphatase
RBF	round bottom flask
RFP	red fluorescent protein
ROI	region of interest
SDS	sodium dodecyl sulfate
SIN	self-inactivating
SOD	superoxide dismutase
sTeNT	synthetic tetanus neurotoxin
TeNT	tetanus neurotoxin
TLC	thin layer chromatography
TTL	transistor-transistor logic
VSD	voltage sensitive dye
WGA	wheat-germ agglutinin
YFP	yellow fluorescent protein

7.2 Equipment and Materials

7.2.1 Dye Synthesis Solvents

Solvent	**Supplier**	**Article Number**
Acetonitrile	YMC	2856
Ammonia soln. 25%	Merck	1054402500
t-Butanol	VWR	1019902500
Chloroform	VWR	1024456025
Chloroform, high purity	VMC	4443-30L
Dichloromethane	VWR	1060506025
Diethylether	VWR	1009546025
Diethylether, dry	VWR	1009291000
Dimethylformamide	VWR	1030532500
Dimethylsulfoxide	Merck	1029521000
1,2-Dimethoxyethan	Fluka	38569
Ethanol, absolute	VWR	1009832500
Ethanol, denatured	VWR	1009746025
Ethylacetate	VWR	1096236025
n-Heptane	VWR	1043796025
Methanol	VWR	1060096025
Methanol, high purity	YMC	3041-30L
Nitromethane	VWR	8208941000
Pyridine	Merck	1097281000
HCl, fuming 37%	VWR	1003141000
Tetrahydrofuran	VWR	1081071000
Triethylamine	VWR	8083521000

7.2.2 Dye Synthesis Reagents

Chemical	Supplier	Article Number
Ammonium acetate	Merck	1011160500
(2-Biphenyl)die-tert-butylphosphine	Aldrich	638439
6-Bromohexan-1-ol	Aldrich	186481
6-Bromonaphtalene-2-ol	Aldrich	B73406-100G
3-Bromopropanesulfonic acid sodium salt	Sigma	32912-25G
3-Bromopropyltrimethylammonium bromide	Aldrich	3779-42-8
1-Bromoundecane	Sigma-Aldrich	245038-100G
4-Chloro-1-butanol	Lancaster	4042
6-Chloro-1-hexanol	Lancaster	X06055G0100
Cs_2CO_3	VWR	102040
2-(Dicyclohexylphosphino) biphenyl	Alfa Aesar	H27019
Di-8-ANNEPS	Invitrogen	D3167
Dibutylamine	Lancaster	24920
Diethylamine	Fluka	31730-250ML
Dimethyl chlorophosphate	Aldrich	437891-25ml
Glacial Acetic Acid	VWR	1000421000
1-Hexanol	VWR	804393
1-Iodobutane	VWR	8047860250
1-Iodooctane	Aldrich	238295-100G
1-Iododecane	Aldrich	238252-100G
3-Iodo-1-propanol	Aldrich	451061-10G
K_2CO_3	Merck	1049281000
K_3PO_4	VWR	105102
Methane sulfonic acid	Fluka	64280
Methane sulfonyl anhydride	Sigma-Aldrich	269190-25G
Methyloctylamine	Alfa Aesar	L18639
N,N-Dimethylbutylamine	Aldrich	369527-250ml
Na_2SO_4	VWR	8222845000
NaI	Fluka	71712
NaOt-Bu	VWR	818374
N-Butylmethylamine	Fluka	20251
N-Methylbutylamine	VWR	818639
N-Methyloctane-1-amine	Alfa Aesar	18639
Nonafluorobutane-1-sulfonylfluoride	Alfa Aesar	B21322
1,2,2,6,6-Pentamethylpiperidine	Sigma-Aldrich	76850-5ml
$Pd(OAc)_2$	VWR	818056
Pd_2dba_2	VWR	807103
$POCl_3$	Alfa Aesar	10525
1,3-Propanesultone	Fluka	81815
Silica gel	YMC	SL06575
Silica gel Prontosil 120-20-C18-AQ	Bischoff	0010F184PS200
Tosyl chloride	Fluka	89732
Tri(Dibenzylideneacetone) Di-palladium(O)	Aldrich	328774
tri-(o-tolyl)phosphine	Fluka	93415-5G
Triflic anhydride	Fluka	91720
Trifluoro-methanesulfonic acid chloride	VWR	818292
Trifluoroacetate	VWR	808260
Vinylpyridine	Aldrich	V320-4

7.2.3 Molecular Biology Reagents

Chemical	Supplier	Article Number
Agar	Serva	11396
AMPD	Aldrich	A9754-25G
Ampicillin	Gibco	11593-027
$CaCl_2$	Aldrich	C-7902
D-Glucose	Gibco	20251
D-PBS	Gibco	14040-091
DMEM	Gibco	21885-025
Ethidium bromide	Serva	21251
FBS	Gibco	10091-130
G-418	Gibco	11811-064
Gentamicin	Aldrich	G 3632
Hygromycin	BD Bioscience	631309
KCl	Aldrich	P-4504
Klenow Fragment	Fermantas	EP0051
L-Glutamine	Aldrich	G-3126
$MgCl_2$	Aldrich	M-2393
Na_2HPO_4	Aldrich	S-5136
NaCl	Aldrich	S-5886
Tris	Roth	4855.2
Trypsin-EDTA	Gibco	12400-054

7.2.4 Molecular Biology Kits

Kit Name	Supplier	Article Number
Flp-In System	Invitrogen	K6010-01
NucleoBond Xtra Midi kit	Macherey-Nagel	740410.100
pENTR5'TOPO TA Cloning Kit	Invitrogen	K591-20
QIAprep Miniprep Kit (250)	Qiagen	27106
QIAquick Gel Extraction Kit	Qiagen	28704
QIAquick PCR Purification Kit (50)	Qiagen	28104
ß-Gal Staining Kit	Invitrogen	K45-0450
ViraPower Promoterless Lentiviral Kit	Invitrogen	K591-10

7.2.5 Restriction Enzymes

Enzyme	Supplier	Article Number
AflI	Biolabs	R0520L
EcoRI	Fermentas	ER0271
EcoRV	Fermentas	ER0301
HindIII	Fermentas	ER0501
KpnI	Biolabs	R0142S
MluI	Fermentas	ER0562
NotI	Fermentas	ER0592
SalI	Biolabs	R0138L
XbaI	Fermentas	ER0681
XhoI	Fermentas	ER0691

7.2.6 Microscope Apparatus

Item	Supplier	Article Number
⌀ 35 mm polypropylene culture dishes	BD Bioscience	351008
⌀ 30 mm #1 Glass coverslips	Thermo Sci.	004710289
iXonEM+ Camera system	Andor Tech.	DU885KCS
Axiovert microscope	Carl Zeiss	135TV
Plan-NEOFLUAR 40x/1.30	Carl Zeiss	440451-9903-000
Luxeon V Blue	Philips	LXHL-LB5C
Luxeon V Green	Philips	LXHL-LM5C
Arbitrary Waveform Generator	Agilent	33120A
Platinum Wire 0.50 mm diameter	WPI	PTP201
30 MHz Oscilloscope	Grundig	CO30
Triple Output DC Power supply	Agilent	E3631A
Operational Amplifier	TI Inc.	OPA547

7.2.7 Other Apparatus

Item	Supplier	Article Number
Cell Biology Microscope	Zeiss	Axiolab
Cell Incubator	Heraeus	Cell
Flow Box	Heraeus	Herasafe
Neuronal Cell Incubator	Thermo	Cell 150
PCR Robo-cycler	Stratagene	Gradient 40
pH Meter	Knick	646

7.3 PCR amplification protocols

7.3.1 PCR Programs

Product	Start	Denature	Anneal	Elongation	Cycles	Holding
PLAP	94°C, 4 m	94°C, 45 s	65°C, 45 s	72°C, 4 m	25	6°C, ∞
APMA-AP	94°C, 4 m	94°C, 45 s	51°C, 45 s	72°C, 4 m	25	6°C, ∞
APMA-AP-IRES-H2BGFP	94°C, 4 m	94°C, 45 s	62°C, 45 s	73°C, 6 m	25	6°C, ∞
PLAP-IRES-H2BGFP	94°C, 4 m	94°C, 45 s	62°C, 45 s	72°C, 6 m	25	6°C, ∞
EGFP	94°C, 4 m	94°C, 45 s	55°C, 45 s	73°C, 6 m	25	6°C, ∞
EGFP-spacer	94°C, 4 m	94°C, 45 s	55°C, 45 s	73°C, 5 m	25	6°C, ∞
Luc	94°C, 4 m	94°C, 45 s	65°C, 45 s	73°C, 5 m	25	6°C, ∞
Luc-spacer	94°C, 4 m	94°C, 45 s	65°C, 45 s	73°C, 5 m	25	6°C, ∞
iCre	94°C, 4 m	94°C, 45 s	65°C, 45 s	73°C, 5 m	25	6°C, ∞
iCre-spacer	94°C, 4 m	94°C, 45 s	65°C, 45 s	73°C, 5 m	25	6°C, ∞
CMVe-PDGFb	94°C, 4 m	94°C, 45 s	60°C, 45 s	73°C, 5 m	25	6°C, ∞
CMV	94°C, 4 m	94°C, 45 s	60°C, 45 s	73°C, 5 m	25	6°C, ∞
iCre_s_sTeNT	94°C, 4 m	94°C, 45 s	60°C, 45 s	73°C, 5 m	25	6°C, ∞

7.3.2 PCR Primers

DNA Oligo were supplied by Eurofins MWG GmbH.

Fragment	Primer	Sequence
PLAP	PLAP_XhoI_for	5'-TTGACCTCGAGATGATTCTGGGGCCCTGCA-3'
	PLAP_MluI_rev	5'-TTACGACGCGTTCAGGGAGCAGTGGCCGTCTC-3'
PLAP-IRES-H2BGFP	PLAP_GFP_Afl2_for	5'-TCTACTTAAGGCCACCATGATTCTGGGGCCCTGC-3'
	PLAP_GFP_NotI_rev	5'-CTGCTCGAAGCATTAACCCTCAC-3'
APMA-AP	APMA-AP_XhoI_for	5'-TTGACCTCGAGATGGGCCACCATCACCACCATC-3'
	APMA-AP_MluI_rev	5'-TTACGACGCGTTATTATCACAGGTCCTCCTCGC-3'
APMA-AP-IRES-H2BGFP	A_ap_GFP_Afl2_for	5'-TCTACTTAAGGCCACCATGGGCCACCATCACCAC-3'
	A_ap_GFP_NotI_rev	5'-CTGCTCGAAGCATTAACCCTCAC-3'
EGFP	EGFP_for	5'-ATGGTGAGCAAGGGCGAG-3'
	EGFP_rev	5'-CTTGTACAGCTCGTCCATGC-3'
EGFP+spacer	EGFP_for	5'-ATGGTGAGCAAGGGCGAG-3'
	EGFP_rev_sp	5'-CGACCCACCTCCGCCCGAGCCACCGCCAC CAGACTTGTACAGCTCGTCCATGC-3'
Luciferase	luc_for	5'-GAAGACGCCAAAAACATAAAGAAAG-3'
	luc_rev	5'-CACGGCGATCTTTCCGCC-3'
Luciferase+ spacer	luc_for	5'-GAAGACGCCAAAAACATAAAGAAAG-3'
	luc_rev_sp	5'-CGACCCACCTCCGCCCGAGCCACCG CCACCAGACACGGCGACTTTCCGCC-3'
iCre	iCre_for	5'-GTGCCCAAGAAGAAGAGGAAAGTCTC-3'
	iCRE_rev	5'-GTCCCCATCCTCGAGCAGCC-3'
iCre+spacer	iCre_for	5'-GTGCCCAAGAAGAAGAGGAAAGTCTC-3'
	iCRE_rev_sp	5'-CGACCCACCTCCGCCCGAGCCACCG CCACCAGAGTCCCCATCCTCGAGCAGCC-3'
CMVe-PDGFb promoter	CMVe-PDGFb _for	5'-CCCTGGGTCGACATTGAT-3'
	CMVe-PDGFb _rev	5'-TTTCAGTTCCTCGACTCT-3'
CMV promoter	CMV_for	5'-CGATGTACGGGCCAGATAT-3'
	CMV_rev	5'-AATTTCGATAAGCCAGTAAG-3'
iCre+spacer +sTeNT	iCre_s_sTeNT_for	5'-GTGCCCAAGAAGAAGAGGAAAGTCTC-3'
	iCre_s_sTeNT_rev	5'-GGGATGGACAAATGACTGATAATAG-3'

7.4 Protocols

7.4.1 PCR Amplification

This procedure was used to amplify fragments of DNA from plasmids, using the PCR primers and programs listed above in Appendix 7.3.

Procedure:

1) Prepare the following reaction mixture using the primers from Appendix 7.3.2:

2.5 µl	10X *Pfu* Buffer
5 µl	$MgSO_4$ (25 mM)
2 µl	dNTPs (25mM)
2 µl	Forward Primer
2 µl	Reverse Primer
1 µl	Template DNA
1 µl	Pfu-Polymerase (recombinant)
34.5 µl	Water, nuclease-free

2) Follow the timing program from Appendix 7.3.1, using 25 cycles.
3) Analyze via agarose electrophoresis, (0.8% agarose, TBE, EthBr, 90V).

7.4.2 Klenow Polishing

The Klenow Fragment is the large fragment from DNA Polymerase I, and was used to create blunt-end dsDNA from restriction-enzyme excised sequences of plasmid DNA. It fills in the recessed 3' ends of DNA fragment, whilst digesting away protruding 3' overhang.

Procedure:

1) Prepare the following reaction mixture:

17 µl	Digested DNA (aqueous solution)
2 µl	10X reaction buffer for Klenow Fragment
0.5 µl	dNTPs (25mM)
0.5 µl	Klenow Fragment (10U/µl)

2) Incubate the mixture at 37°C for 20 minutes.
3) Stop the reaction by heating at 75°C for 20 minutes.

7.4.3 Transformation of Chemically Competent *E. coli*

This procedure was used to amplify plasmid DNA, and used One Shot TOP10 cells from Invitrogen. The transformed cells were then used for maxi, midi or mini plasmid preparation.

Procedure:

1) Thaw, on ice, one 50 µl vial of *E. coli* cells.
2) Pipette 3 µl of each ligation reaction directly into the vial of competent cells and mix by tapping gently.
3) Incubate the vial on ice for 15 minutes.
4) Heatshock for exactly 30 seconds in the 42°C water bath.
5) Add 250 µl of pre-warmed S.O.C medium to each vial.
6) Incubate for 1h at 37°C.
7) Spread 100 µl from the vial on separate, labeled LB agar plates. Invert the plates and incubate at 37°C overnight.
8) Select colonies and analyze by restriction digest.

7.4.4 HEK293 cells Transient Transfection

7.4.4.1 $CaCl_2$ Transfection

This was the standard procedure for transiently transfecting HEK293 cells.

Procedure:

1) The day before transfection, trypsinize and count the cells. Plate ~4 x 10^5 cells per well in 2.0 ml of complete growth medium. Cell density should be 40-50% confluent on the day of transfection.
2) On the day of transfection, remove growth medium from cells and replace with 2.0 ml of complete growth medium.
3) In a 2 ml tube, prepare the following solution:

4 µg	Plasmid DNA
7.6 µl	2 M $CaCl_2$ solution
62 µl	Tris buffer (pH 7.6)

4) In a second tube, add 62 µl HBS buffer, consisting of:

50 mM	HEPES (pH 7.13)
1.5 mM	Na_2HPO_4
280 mM	NaCl

5) Add the DNA solution dropwise to the HBS buffer and incubate at room temperature for 30 min.
6) Transfer the calcium-phosphate-DNA suspension into the Petri dish. Add the suspension drop by (1 drop/sec) and gently mix by rocking the dish.
7) Incubate the cells at 37 °C for 4 hours.
8) Wash the cells with PBS, and then add pre-warmed complete growth medium.
9) Incubate the cells at 37°C in a CO_2 incubator for 24 hours post-transfection before assaying for transgene expression.

7.4.4.2 Lipofectamine Transfection

The transient transfection of HEK293 cells for dye staining used this procedure, as non-selective staining of the glass substrate was decreased compared to $CaCl_2$ Transfection.

Procedure:

1) The day before transfection, trypsinize and count the cells. Plate ~6.25 x 10^5 cells per well in 2.0 ml of complete growth medium. Cell density should be 50-80% confluent on the day of transfection.
2) On the day of transfection, remove growth medium from cells and replace with 2.0 ml of complete growth medium.
3) In a 2 ml tube, dilute 2.5 µg of DNA in 500 µl of serum free growth medium.
4) Add 5.0 µl of Lipofectamine 2000 reagent into the DNA solution, mix gently and incubate 30 minutes at room temperature to form DNA-Lipofectamine reagent complexes.
5) After 30 minute incubation, add 100 µl of the DNA-Lipofectamine 2000 reagent complexes directly to each well containing cells and mix gently by rocking the plate back and forth.
6) Incubate the cells at 37°C in a CO_2 incubator for 24 hours post-transfection before assaying for transgene expression.

7.4.5 Hippocampal Neuron Transient Transfection

Rat hippocampal neurons were prepared using standard protocols [117], from embryos at day 18 (E-18). The cells were cultured for 24 hours before transfection in B27-supplemented Neurobasal A (NBA) medium, on poly-lysine coated glass coverslips held in 6-well plates.

Procedure:

1) Replace media in each well with 2 ml NBA, and keep conditioned media
2) In a 1.5 ml tube, dilute 4 µg of DNA in 400 µl of NBA.
3) Add 8.0 µl of Lipofectamine reagent into the DNA solution, mix gently and incubate 30 minutes at room temperature to form DNA-Lipofectamine Reagent complexes.
4) Add 400ul of mix to each well, incubate 30-45 min
5) Replace media with conditioned media saved from step #1.

7.4.6 BCIP/NBT Staining

These compounds are used to identify cells expressing an alkaline phosphatase, producing a purple precipitation on enzymatic activation of the substrate.

Procedure:

1) The growth media should be gently removed via suction.
2) Detection buffer was prepared, consisting of:

100mM	Tris, pH 9.5
100mM	NaCl
50mM	$MgCl_2$

3) Cells are then rinsed with PBS containing 2mM $MgCl_2$
4) Fix cells with PBS containing 2mM $MgCl_2$ and 4% formaldehyde for 10 seconds on ice.
5) Remove the fixing buffer, and rinse the cells once with detection buffer, then incubate the cells with 2 ml of detection buffer for 15 minutes.
6) While the cells are in the detection buffer, prepare the following reaction buffer:

50 µl	BCIP Stock (10 mg/ml)
100 µl	NBT Stock (50mg/ml in 70% DMF)
5 ml	Detection Buffer

7) The detection buffer is exchanged with 1 ml of reaction buffer, and the reaction allowed to process until dark purple precipitation on the cells is visible by eye, ~30-60 minutes.

7.4.7 X-Gal Staining

This technique is used to histochemically identify cells that express ß-galactosidase.

Procedure:

1) The growth media should be gently removed via suction.
2) Cells are then rinsed with 2.5 ml PBS containing 2mM.
3) Fix the cells with 3 ml 1X Fixative Solution for 10 minutes at room temperature.
4) While the plate is in the Fixative Solution, prepare the following Staining Solution in a polypropylene plastic tube:

25 µl	Solution A
25 µl	Solution B
25 µl	Solution C
125 µl	20 mg/ml X-gal in DMF
2.3 ml	PBS

5) Rinse the plate twice with 2.5 ml 1X PBS.
6) Add 2.5 ml Staining Solution to the plate. Incubate at 37°C for 1 hour, with a dark blue precipitate generated on ß-galactosidase expressing cells.

7.5 Codon Usage Tables

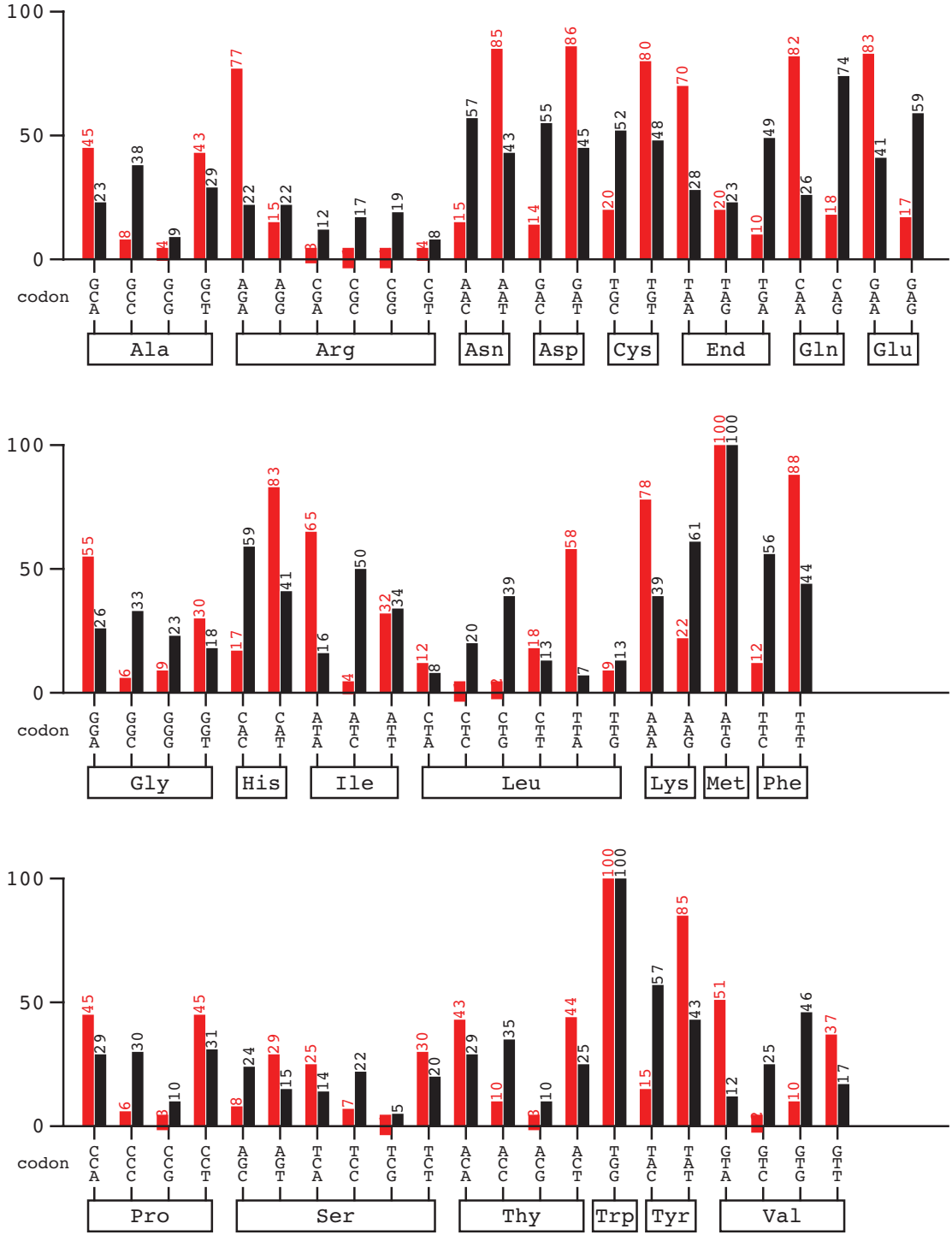

Codon Table 1: *Clostridium tetani* Genome

Codon Table 2: *Mus musculus* Genome

Mean difference: 25.58%

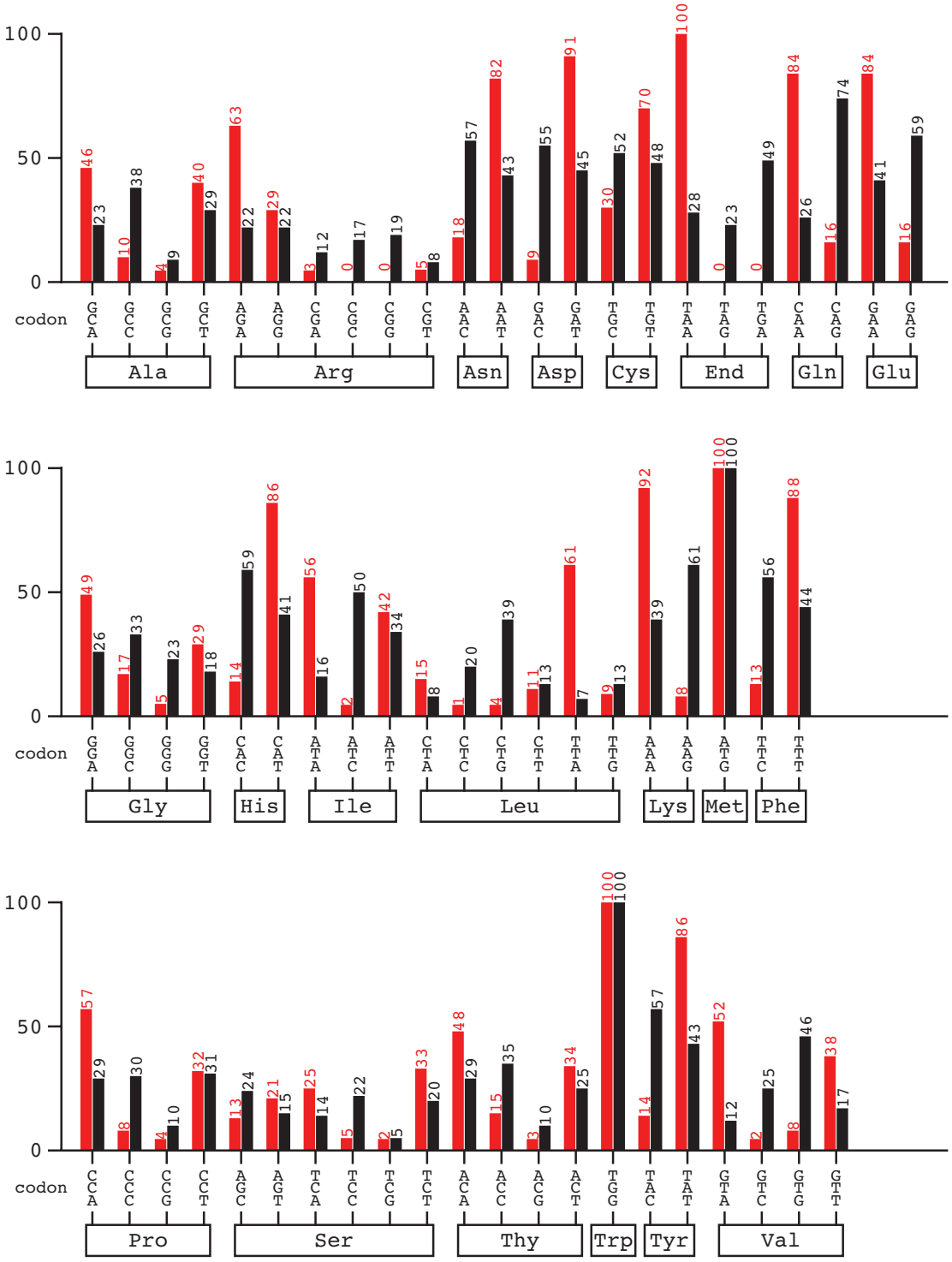

Codon Table 1: Tetanus Neurotoxin

Codon Table 2: *Mus musculus* Genome

Mean difference: 26.13%

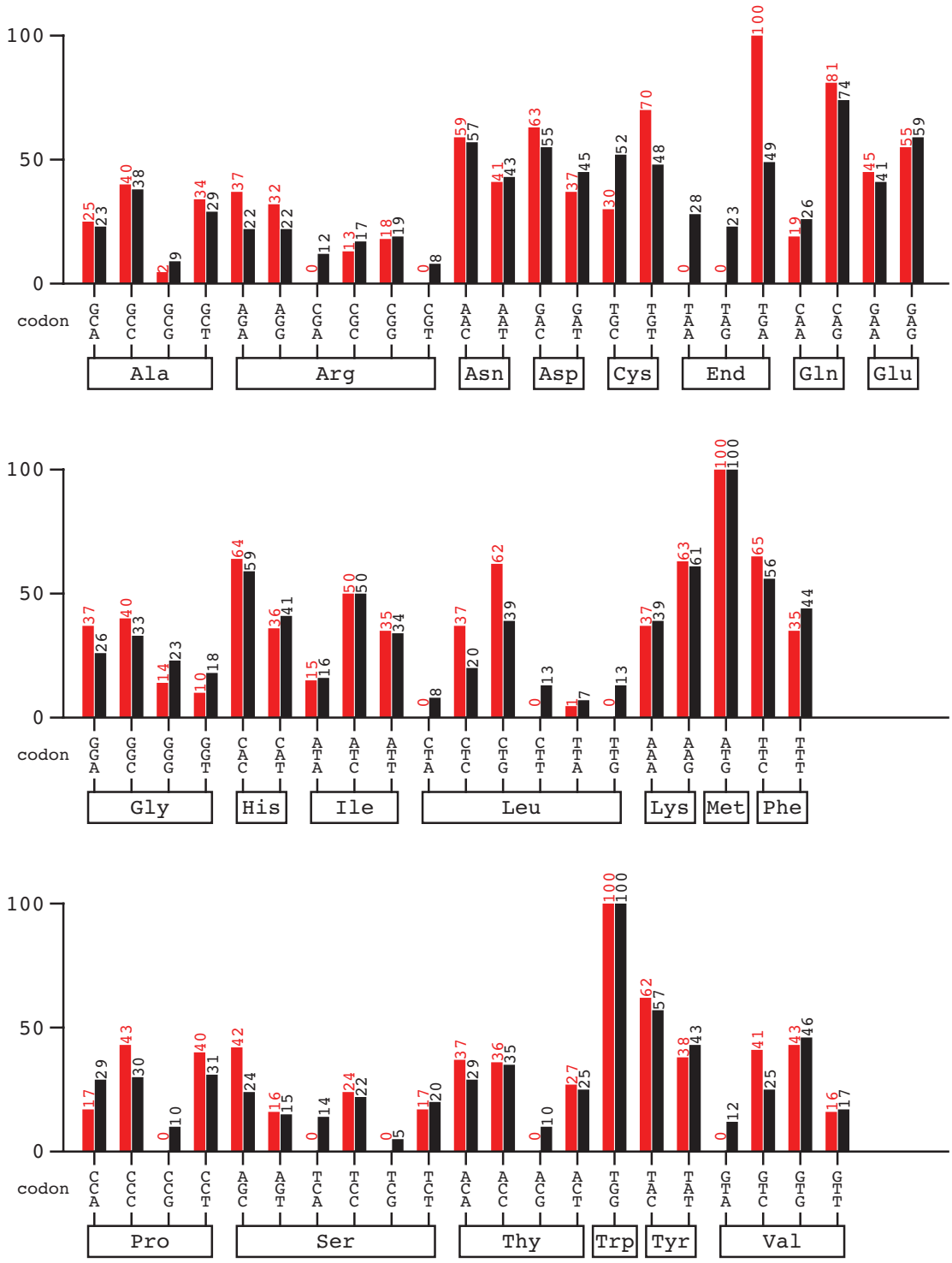

Codon Table 1: Codon Optimized and Modified Tetanus Neurotoxin

Codon Table 2: *Mus musculus* Genome

Mean difference: 8.64%

7.6 Codon Optimized TeNT

7.6.1 Synthesized Sequence

GAATACAAGCTACTTGTTCTTTTTGCAACCATGGATATCCCCATCACCATCAACAACTTCAGGTACAGCGACCCCGTGAACAACGACACCATCA
TCATGATGGAGCCTCCCTATTGTAAGGGCCTGGATATTTACTACAAAGCCTTCAAGATAACAGACAGGATTTGGATTGTGCCTGAAAGATATGA
ATTTGGCACCAAGCCAGAAGACTTCAACCCACCCAGCTCCCTCATCGAGGGTGCCAGCGAGTACTACGATCCCAACTACCTGAGGACAGACTCT
GACAAGGATAGGTTCCTGCAGACCATGGTGAAGCTCTTCAATAGAATCAAGAACAATGTCGCTGGGGAGGCCCTGCTCGACAAAATTATCAACG
CCATTCCTTATCTCGGCAATTCTTATAGTCTCCTGGACAAATTCGATACAAATAGTAATAGTGTGTCTTTCAATCTGCTCGAACAGGACCCCAG
TGGGGCCACTACTAAAAGTGCTATGCTGACTAATCTCATCATCTTCGGGCCTGGCCCCGTGCTCAACAAGAATGAAGTTAGGGGCATTGTCTTA
AGGGTGGACAATAAGAATTATTTCCCTTGCAGGGACGGGTTTGGTTCTATCATGCAGATGGCCTTTTGTCCTGAGTACGTGCCAACATTTGATA
ATGTGATTGAAAACATCACCAGCCTCACAATCGGGAAGAGCAAATACTTCCAAGATCCCGCACTGCTCCTGATGCACGCACTGATTCATGTCCT
GCACGGACTGTATGGAATGCAAGTGTCTAGTCACGAGATCATTCCTTCTAAGCAGGAAATTTACATGCAACACACTTATCCTATTAGCGCTGAA
GAACTGTTTACCTTCGGAGGCCAGGACGCTAATCTGATCAGCATCGACATCAAGAACGACCTGTATGAGAAGACACTGAACGACTACAAAGCAA
TCGCCAATAAGCTCAGCCAGGTCACAAGCTGTAACGACCCTAATATTGACATCGACAGCTATAAACAAATCTACCAGCAGAAATACCAGTTTGA
TAAAGACAGCAACGGACAGTACATAGTTAACGAAGATAAGTTCCAGATTCTCTACAACAGTATCATGTATGGATTCACTGAAATTGAGCTCGGA
AAGAAGTTCAATATCAAAACAAGGCTGAGCTTCTTTTCCATGAACCACGACCCTGTGAAGATCCCCAACCTCCTCGATGACACAATTTACAACG
ACACTGAAGGCTTTAACATCGAGTCCAAAGACCTGAAAAGCGAGTATAAGGGACAGAACATGCGGGTCAACACTAACGCGTTCAGGAATGTCGA
CGGAAGCGGACTGGTGAGCAAACTGATCGGCCTCTGTAAGAAGATCATCCCTCCCACTAACATTAGAGAGAATCTCTACAATAGAACAGCCAGC
CTGACAGACCTGGGCGGCGAGCTGTGTATCAAGATTAAAAACGAAGATCTGACCTTCATCGCCGAGAAAAACTCCTTCAGTGAGGAACCTTTCC
AGGATGAGATTGTGTCTTATAACACTAAGAATAAACCTCTGAACTTCAACTACAGCCTGGATAAGATTATCGTGGATTACAACCTCCAGAGTAA
AATCACTCTGCCCAACGATAGAACAACACCCGTGACCAAGGGGATACCCTACGCTCCCGAGTATAAGAGCAACGCAGCCAGCACAATCGAAATC
CATAACATTGACGACAACACTATCTACCAGTATCTCTACGCTCAGAAGTCTCCTACTACTCTCCAGAGAATAACAATGACAAACAGCGTGGATG
ATGCACTCATTAATAGCACAAAAATCTACAGCTACTTTCCATCCGTGATCTCCAAGGTTAACCAAGGAGCTCAGGGCATTCTCTTCCTGCAGTG
GGTTAGAGACATCATCGACGATTTTACAAACGAATCCTCCCAGAAGACAACCATCGACAAGATAAGCGACGTTTCTACCATTGTGCCCTACATC
GGTCCAGCCCTCAACATAGTTAAGCAGGGATACGAGGGAAATTTCATAGGCGCTCTCGAAACCACCGGGGTTGTCCTGCTGCTGGAATACATCC
CCGAGATAACACTGCCAGTGATCGCAGCACTGTCCATCGCCGAGAGCAGCACCCAGAAAGAGAAAATCATTAAAACTATTGACAATTTTCTGGA
AAAGCGCTATGAGAAGTGGATAGAGGTTTATAAGCTGGTCAAGGCTAAATGGCTGGGCACCGTGAATACCCAGTTCCAGAAAAGAAGTTATCAG
ATGTACAGATCCCTGGAGTATCAAGTCGATGCTATTAAGAAAATCATAGACTATGAATACAAGATTTATTCCGGGCCTGACAAAGAACAGATCG
CCGACGAGATTAACAATCTCAAGAATAAACTGGAAGAGAAGGCCAACAAGGCCATGATTAACATCAACATATTCATGCGGGAGTCCAGCAGATC
CTTTCTCGTGAACCAAATGATTAACGAAGCAAAGAAACAGCTGCTGGAATTTGACACTCAAAGTAAGAACATCCTCATGCAGTACATCAAGGCT
AATTCCAAGTTCATAGGCATAACTGAGCTGAAGAAGCTCGAATCCAAGATCAATAAAGTCTTCAGCACTCCCATTCCTTTTTCCTACAGCAAAA
ATCTGGACTGCTGGGTCGATAACGAAGAGGATATAGATGTTATTCTCAAGAAGTCCACAATCCTGAATCTCGACATTAATAACGACATCATCAG
CGATATATCTGGCTTCAACTCTTCCGTCATTACCTATCCCGACGCACAGCTGGTCCCTGGAATCAACGGTAAGGCTATCCACCTCGTCAACAAC
GAAAGCAGCGAAGTGATTGTGCACAAGGCTATGGACATAGAGTACAACGACATGTTCAATAATTTCACCGTCAGTTTTTGGCTGAGGGTGCCTA
AGGTCAGCGCAAGCCACCTCGAACAGTATGGCACAAACGAGTATTCCATCATCAGCTCTATGAAGAAGCATTCCCTGAGCATCGGAAGCGGCTG
GAGCGTCAGCCTCAAGGGTAACAATCTCATATGGACCCTGAAGGACTCCGCTGGAGAGGTCCGCCAGATTACTTTTCGGGATCTGCCCGATAAG
TTCAATGCTTACCTGGCCAACAAGTGGGTGTTCATCACTATCACAAACGACAGGCTGTCTTCTGCCAACCTGTATATTAACGGAGTCCTGATGG
GCAGTGCAGAGATTACCGGCCTGGGAGCTATCCGGGAGGACAATAACATTACACTGAAGCTGGATAGATGTAATAACAATAATCAGTACGTCAG
TATCGACAAATTTAGAATCTTTTGCAAAGCCCTGAATCCTAAAGAGATAGAGAAACTGTACACCTCTTACCTCAGCATCACCTTTCTCCGCGAT
TTTTGGGGCAATCCCCTGAGGTACGACACAGAGTACTATCTCATCCCCGTCGCTAGCTCCTCTAAAGACGTCCAGCTCAAAAACATTACCGACT
ACATGTATCTGACCAATGCACCTAGTTATACAAATGGCAAGCTGAACATTTACTACCGCAGACTGTACAACGGCCTGAAATTCATTATCAAACG
GTACACCCCCAATAACGAAATTGATTCTTTCGTGAAATCCGGAGACTTCATTAAGCTGTACGTCAGCTACAACAATAACGAGCACATTGTTGGA
TACCCCAAGGATGGAAATGCTTTCAACAATCTGGACAGAATCCTGCGGGTCGGGTACAATGCCCCAGGCATTCCACTCTATAAGAAGATGGAAG
CCGTCAAGCTGCGGGACCTGAAAACCTATAGTGTGCAGCTGAAGCTGTACGACGATAAAAATGCATCCCTGGGACTCGTCGGCACTCATAACGG
ACAGATCGGCAACGACCCAAACCGCGATATACTCATAGCCAGCAACTGGTACTTCAATCATCTCAAGGACAAGATTCTGGGTTGTGATTGGTAT
TTCGTGCCTACCGATGAGGGATGGACAAATGACTGATAATAGGCGGCCGC

e5'UTR-bG	Untranslated region from b-globin.
eT-Kozak	Kozak sequence, also including the G immediately after the start codon.
Start	ATG start codon, Methionine
EcoRV	GATATC Used to insert in-frame blunt-cut DNA for fusion proteins.
Stop	TGA, TAA AND TAG. All three are used for improved protein expression.
NotI	GCGGCCGC Used to cut out the vector for cloning.

GC percentage: 45.67%

7.6.2 Restriction Site Modifications I

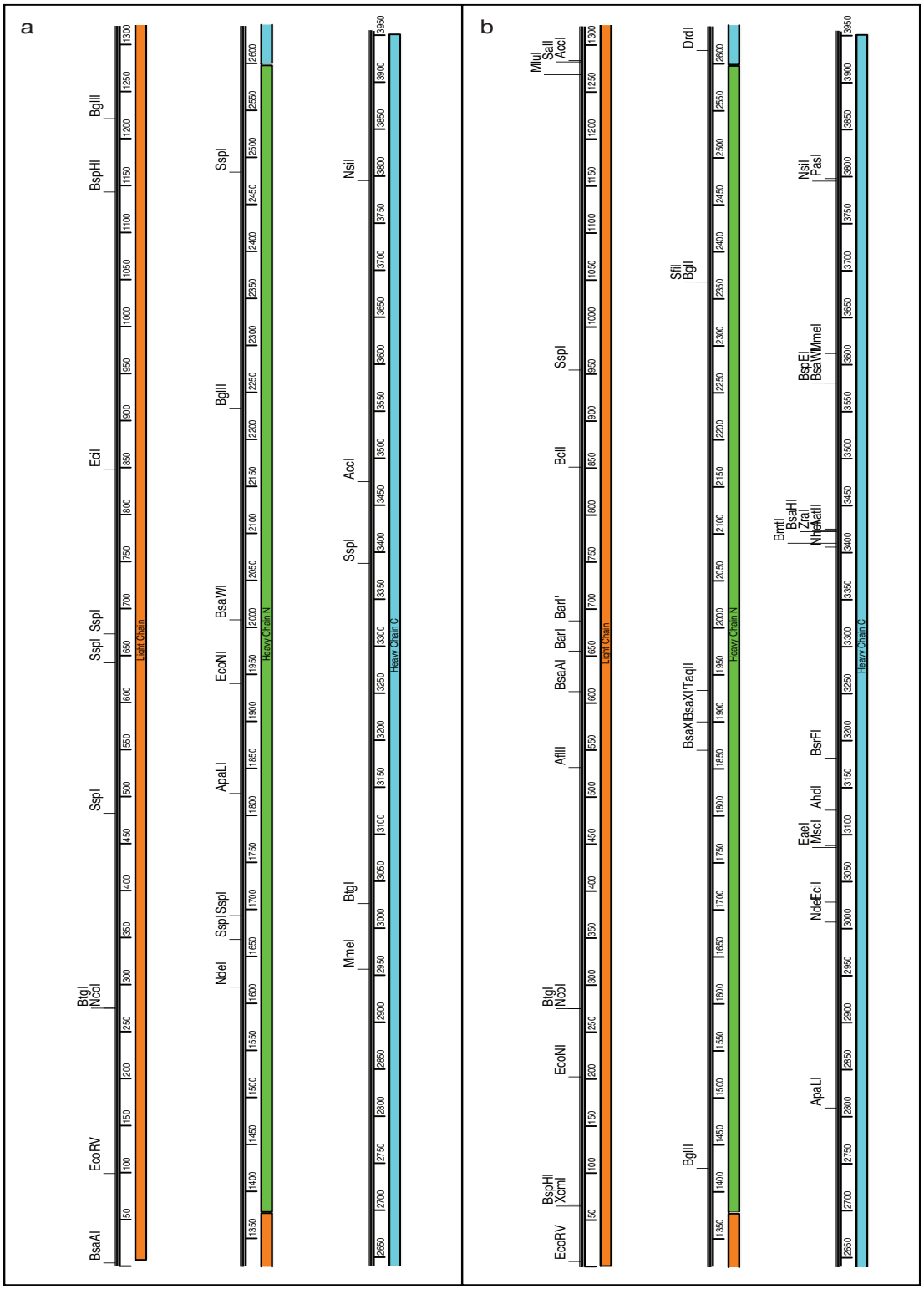

a) Wild-type Tetanus Neurotoxin, b) Codon optimized, non-toxic Tetanus Neurotoxin

7.6.3 Restriction Site Modifications II

Wild-Type TeNT		Codon Optimized TeNT	
Name	**Position**	**Name**	**Position**
AarI	305	AatII	3426
Acc65I	3812	AflII	532
AccI	3476	AhdI	3127
AflIII	715	ApaLI	2810
AjuI	2604	BarI	656
AjuI'	2572	BarI'	688
AlwNI	2303	BclI	852
ApaLI	1824	BglI	2369
BpmI	1608	BglII	1426
BsaAI	5	BmtI	3411
BsaWI	2009	BsaAI	613
BseMII	207	BsaHI	3423
BseRI	1410	BsaWI	3581
BsgI	3192	BsaXI	1871
BsmAI	3345	BsaXI'	1901
BsmFI	178	BspEI	3581
BsmI	744	BspHI	66
BspCNI	208	BsrFI	3182
BspHI	1144	BtgI	276
BsrGI	3763	DrdI	2615
BstUI	3029	EaeI	3087
BstZ17I	3477	EciI	3029
Cac8I	3865	EcoNI	203
EciI	849	EcoRV	7
EcoNI	1941	MluI	1269
EcoRV	100	MmeI	3613
HaeII	1998	MscI	3089
HgaI	1766	NcoI	276
HincII	1816	NdeI	3008
HpaI	1816	NheI	3407
Hpy99I	2327	NsiI	3796
KpnI	3816	PasI	3799
MmeI	2957	SfiI	2369
MspA1I	3029	SspI	955
NciI	2754	TaqII	1934
NcoI	276	XcmI	67
NdeI	1618	ZraI	3424
NsiI	3796		
NspI	719		
PpiI	2421		
PpiI'	2389		
SacII	3030		
ScaI	3159		
StuI	1296		
TaqI	1002		
TaqII'	1840		
TstI	1918		

7.6.4 Synthesis Primers Forward

Primer Name	Sequence
B053-1-1	GAGACGAATTCGATGAATACAAGCTACT
B053-1-2	CATGGTTGCAAAAAGAACAAGTAGCTTGTATTCATCGAAT
B053-1-3	TGTTCTTTTTGCAACCATGGATATCCCCATCACCATCAAC
B053-1-4	CACGGGGTCGCTGTACCTGAAGTTGTTGATGGTGATGGGG
B053-1-5	AGCGACCCCGTGAACAACGACACCATCATCATGATGGAGC
B053-1-6	TCCAGGCCCTTACAATAGGGAGGCTCCATCATGATGATGG
B053-1-7	TATTGTAAGGGCCTGGATATTTACTACAAAGCCTTCAAGA
B053-1-8	AATCCAAATCCTGTCTGTTATCTTGAAGGCTTTGTAGTAA
B053-1-9	TAACAGACAGGATTTGGATTGTGCCTGAAAGATATGAATT
B053-1-10	AGTCTTCTGGCTTGGTGCCAAATTCATATCTTTCAGGCAC
B053-1-11	ACCAAGCCAGAAGACTTCAACCCACCCAGCTCCCTCATCG
B053-1-12	GGATCGTAGTACTCGCTGGCACCCTCGATGAGGGAGCTGG
B053-1-13	GCGAGTACTACGATCCCAACTACCTGAGGACAGACTCTGA
B053-1-14	TGGTCTGCAGGAACCTATCCTTGTCAGAGTCTGTCCTCAG
B053-1-15	GGTTCCTGCAGACCATGGTGAAGCTCTTCAATAGAATCAA
B053-1-16	CTCCCCAGCGACATTGTTCTTGATTCTATTGAAGAGCTTC
B053-1-17	TGTCGCTGGGGAGGCCCTGCTCGACAAAATTATCAACGCC
B053-1-18	AGAATTGCCGAGATAAGGAATGGCGTTGATAATTTTGTCG
B053-1-19	CCTTATCTCGGCAATTCTTATAGTCTCCTGGACAAATTCG
B053-1-20	AAAGACACACTATTACTATTTGTATCGAATTTGTCCAGGAGA
B053-1-21	ATACAAATAGTAATAGTGTGTCTTTCAATCTGCTCGAACAG
B053-1-22	TTTAGTAGTGGCCCCACTGGGGTCCTGTTCGAGCAGATTG
B053-1-23	TGGGGCCACTACTAAAAGTGCTATGCTGACTAATCTCATC
B053-1-24	ACGGGGCCAGGCCCGAAGATGATGAGATTAGTCAGCATAG
B053-1-25	CCTGGCCCCGTGCTCAACAAGAATGAAGTTAGGGGCATTG
B053-1-26	ATTCTTATTGTCCACCCTTAAGACAATGCCCCTAACTTCA
B053-1-27	TTAAGGGTGGACAATAAGAATTATTTCCCTTGCAGGGACG
B053-1-28	GGCCATCTGCATGATAGAACCAAACCCGTCCCTGCAAGGG
B053-1-29	CTATCATGCAGATGGCCTTTTGTCCTGAGTACGTGCCAAC
B053-1-30	ATGTTTTCAATCACATTATCAAATGTTGGCACGTACTCAG
B053-1-31	ATTTGATAATGTGATTGAAAACATCACCAGCCTCACAATC
B053-1-32	ATCTTGGAAGTATTTGCTCTTCCCGATTGTGAGGCTGGTG
B053-1-33	AGAGCAAATACTTCCAAGATCCCGCACTGCTCCTGATGCA
B053-1-34	TCCGTGCAGGACATGAATCAGTGCGTGCATCAGGAGCAGT
B053-1-35	ATGTCCTGCACGGACTGTATGGAATGCAAGTGTCTAGTCA
B053-1-36	CTGCTTAGAAGGAATGATCTCGTGACTAGACACTTGCATT
B053-1-37	AGATCATTCCTTCTAAGCAGGAAATTTACATGCAACACAC
B053-1-38	CTTCAGCGCTAATAGGATAAGTGTGTTGCATGTAAATTTC
B053-1-39	TCCTATTAGCGCTGAAGAACTGTTTACCTTCGGAGGCCAG
B053-1-40	ATGTCGATGCTGATCAGATTAGCGTCCTGGCCTCCGAAGG
B053-1-41	CTGATCAGCATCGACATCAAGAACGACCTGTATGAGAAGA
B053-1-42	ATTGCTTTGTAGTCGTTCAGTGTCTTCTCATACAGGTCGT
B053-1-43	GAACGACTACAAAGCAATCGCCAATAAGCTCAGCCAGGTC
B053-1-44	TCAATATTAGGGTCGTTACAGCTTGTGACCTGGCTGAGCT
B053-1-45	CTGTAACGACCCTAATATTGACATCGACAGCTATAAACAAAT
B053-1-46	CTGGTATTTCTGCTGGTAGATTTGTTTATAGCTGTCGATG
B053-1-47	ACCAGCAGAAATACCAGTTTGATAAAGACAGCAACGGACA
B053-1-48	GAACTTATCTTCGTTAACTATGTACTGTCCGTTGCTGTCT
B053-1-49	ACATAGTTAACGAAGATAAGTTCCAGATTCTCTACAACAGTATC

B053-1-50	AATTTCAGTGAATCCATACATGATACTGTTGTAGAGAATCTG
B053-1-51	ATGTATGGATTCACTGAAATTGAGCTCGGAAAGAAGTTCA
B053-1-52	GAAGCTCAGCCTTGTTTTGATATTGAACTTCTTTCCGAGC
B053-1-53	AAACAAGGCTGAGCTTCTTTTCCATGAACCACGACCCTGT
B053-1-54	TGTCATCGAGGAGGTTGGGGATCTTCACAGGGTCGTGGTT
B053-1-55	AACCTCCTCGATGACACAATTTACAACGACACTGAAGGCT
B053-1-56	TTCAGGTCTTTGGACTCGATGTTAAAGCCTTCAGTGTCGT
B053-1-57	CGAGTCCAAAGACCTGAAAAGCGAGTATAAGGGACAGAAC
B053-1-58	CGCGTTAGTGTTGACCCGCATGTTCTGTCCCTTATACTCG
B053-1-59	GGTCAACACTAACGCGTTCAGGAATGTCGACGGAAGCGGA
B053-1-60	ACAGAGGCCGATCAGTTTGCTCACCAGTCCGCTTCCGTCG
B053-1-61	CTGATCGGCCTCTGTAAGAAGATCATCCCTCCCACTAACA
B053-1-62	TTCTATTGTAGAGATTCTCTCTAATGTTAGTGGGAGGGAT
B053-1-63	TTAGAGAGAATCTCTACAATAGAACAGCCAGCCTGACAGA
B053-1-64	TCTTGATACACAGCTCGCCGCCCAGGTCTGTCAGGCTGGC
B053-1-65	CGAGCTGTGTATCAAGATTAAAAACGAAGATCTGACCTTC
B053-1-66	CGATGAAGGTCAGATCTTCGTT

7.6.5 Synthesis Primers Reverse

Primer Name	**Sequence**
B053-2-1	AACGAAGATCTGACCTTCATCGCCGAGAAAAAC
B053-2-2	CTGGAAAGGTTCCTCACTGAAGGAGTTTTTCTCGGCGATG
B053-2-3	GTGAGGAACCTTTCCAGGATGAGATTGTGTCTTATAACAC
B053-2-4	GAAGTTCAGAGGTTTATTCTTAGTGTTATAAGACACAATCTCA
B053-2-5	TAAGAATAAACCTCTGAACTTCAACTACAGCCTGGATAAG
B053-2-6	GGAGGTTGTAATCCACGATAATCTTATCCAGGCTGTAGTT
B053-2-7	CGTGGATTACAACCTCCAGAGTAAAATCACTCTGCCCAAC
B053-2-8	TTGGTCACGGGTGTTGTTCTATCGTTGGGCAGAGTGATTT
B053-2-9	ACACCCGTGACCAAGGGGATACCCTACGCTCCCGAGTATA
B053-2-10	GATTGTGCTGGCTGCGTTGCTCTTATACTCGGGAGCGTAG
B053-2-11	GCAGCCAGCACAATCGAAATCCATAACATTGACGACAACA
B053-2-12	CGTAGAGATACTGGTAGATAGTGTTGTCGTCAATGTTATG
B053-2-13	CTATCTACCAGTATCTCTACGCTCAGAAGTCTCCTACTAC
B053-2-14	GTCATTGTTATTCTCTGGAGAGTAGTAGGAGACTTCTGAG
B053-2-15	CTCCAGAGAATAACAATGACAAACAGCGTGGATGATGCAC
B053-2-16	CTGTAGATTTTTGTGCTATTAATGAGTGCATCATCCACGC
B053-2-17	CATTAATAGCACAAAAATCTACAGCTACTTTCCATCCGTG
B053-2-18	AGCTCCTTGGTTAACCTTGGAGATCACGGATGGAAAGTAG
B053-2-19	AGGTTAACCAAGGAGCTCAGGGCATTCTCTTCCTGCAGTG
B053-2-20	AATCGTCGATGATGTCTCTAACCCACTGCAGGAAGAGAAT
B053-2-21	GAGACATCATCGACGATTTTACAAACGAATCCTCCCAGAA
B053-2-22	CGCTTATCTTGTCGATGGTTGTCTTCTGGGAGGATTCGTT
B053-2-23	CCATCGACAAGATAAGCGACGTTTCTACCATTGTGCCCTA
B053-2-24	CTATGTTGAGGGCTGGACCGATGTAGGGCACAATGGTAGA
B053-2-25	CCAGCCCTCAACATAGTTAAGCAGGGATACGAGGGAAATT
B053-2-26	GGTGGTTTCGAGAGCGCCTATGAAATTTCCCTCGTATCCC
B053-2-27	GCTCTCGAAACCACCGGGGTTGTCCTGCTGCTGGAATACA
B053-2-28	TCACTGGCAGTGTTATCTCGGGGATGTATTCCAGCAGCAG
B053-2-29	GATAACACTGCCAGTGATCGCAGCACTGTCCATCGCCGAG

B053-2-30	ATGATTTTCTCTTTCTGGGTGCTGCTCTCGGCGATGGACA
B053-2-31	ACCCAGAAAGAGAAAATCATTAAAACTATTGACAATTTTCTGG
B053-2-32	ACTTCTCATAGCGCTTTTCCAGAAAATTGTCAATAGTTTTA
B053-2-33	AAAAGCGCTATGAGAAGTGGATAGAGGTTTATAAGCTGGT
B053-2-34	GCCCAGCCATTTAGCCTTGACCAGCTTATAAACCTCTATC
B053-2-35	GCTAAATGGCTGGGCACCGTGAATACCCAGTTCCAGAAAA
B053-2-36	GATCTGTACATCTGATAACTTCTTTTCTGGAACTGGGTATT
B053-2-37	GAAGTTATCAGATGTACAGATCCCTGGAGTATCAAGTCGA
B053-2-38	ATAGTCTATGATTTTCTTAATAGCATCGACTTGATACTCCAGG
B053-2-39	TGCTATTAAGAAAATCATAGACTATGAATACAAGATTTATTCCGGG
B053-2-40	CGATCTGTTCTTTGTCAGGCCCGGAATAAATCTTGTATTC
B053-2-41	CTGACAAAGAACAGATCGCCGACGAGATTAACAATCTCAA
B053-2-42	CCTTCTCTTCCAGTTTATTCTTGAGATTGTTAATCTCGTC
B053-2-43	GAATAAACTGGAAGAGAAGGCCAACAAGGCCATGATTAAC
B053-2-44	CTCCCGCATGAATATGTTGATGTTAATCATGGCCTTGTTG
B053-2-45	ACATATTCATGCGGGAGTCCAGCAGATCCTTTCTCGTGAA
B053-2-46	CTTTGCTTCGTTAATCATTTGGTTCACGAGAAAGGATCTG
B053-2-47	CAAATGATTAACGAAGCAAAGAAACAGCTGCTGGAATTTG
B053-2-48	TGAGGATGTTCTTACTTTGAGTGTCAAATTCCAGCAGCTG
B053-2-49	TCAAAGTAAGAACATCCTCATGCAGTACATCAAGGCTAAT
B053-2-50	AGTTATGCCTATGAACTTGGAATTAGCCTTGATGTACTGC
B053-2-51	CCAAGTTCATAGGCATAACTGAGCTGAAGAAGCTCGAATC
B053-2-52	GCTGAAGACTTTATTGATCTTGGATTCGAGCTTCTTCAGC
B053-2-53	AAGATCAATAAAGTCTTCAGCACTCCCATTCCTTTTTCCT
B053-2-54	CAGCAGTCCAGATTTTTGCTGTAGGAAAAAGGAATGGGAG
B053-2-55	CAAAAATCTGGACTGCTGGGTCGATAACGAAGAGGATATA
B053-2-56	GGACTTCTTGAGAATAACATCTATATCCTCTTCGTTATCGAC
B053-2-57	GATGTTATTCTCAAGAAGTCCACAATCCTGAATCTCGACA
B053-2-58	TCGCTGATGATGTCGTTATTAATGTCGAGATTCAGGATTG
B053-2-59	CGACATCATCAGCGATATATCTGGCTTCAACTCTTCCGTC
B053-2-60	CAGCTGTGCGTCGGGATAGGTAATGACGGAAGAGTTGAAG
B053-2-61	CGACGCACAGCTGGTCCCTGGAATCAACGGTAAGGCTATC
B053-2-62	CTGCTTTCGTTGTTGACGAGGTGGATAGCCTTACCGTTGA
B053-2-63	GTCAACAACGAAAGCAGCGAAGTGATTGTGCACAAGGCTA
B053-2-64	CATGTCGTTGTACTCTATGTCCATAGCCTTGTGCACAATC
B053-2-65	ACATAGAGTACAACGACATGTTCAATAATTTCACCGTCAG
B053-2-66	TAGGCACCCTCAGCCAAAAACTGACGGTGAAATTATTGAA
B053-2-67	GCTGAGGGTGCCTAAGGTCAGCGCAAGCCACCTCGAACAG
B053-2-68	ATGATGGAATACTCGTTTGTGCCATACTGTTCGAGGTGGC
B053-2-69	ACAAACGAGTATTCCATCATCAGCTCTATGAAGAAGCATT
B053-2-70	AGCCGCTTCCGATGCTCAGGGAATGCTTCTTCATAGAGCT
B053-2-71	ATCGGAAGCGGCTGGAGCGTCAGCCTCAAGGGTAACAATC
B053-2-72	GAGTCCTTCAGGGTCCATATGAGATTGTTACCCTTGAGGC
B053-2-73	GGACCCTGAAGGACTCCGCTGGAGAGGTCCGCCAGATTAC
B053-2-74	GAACTTATCGGGCAGATCCCGAAAAGTAATCTGGCGGACC
B053-2-75	ATCTGCCCGATAAGTTCAATGCTTACCTGGCCAACAAGTG
B053-2-76	GTCGTTTGTGATAGTGATGAACACCCACTTGTTGGCCAGG
B053-2-77	CATCACTATCACAAACGACAGGCTGTCTTCTGCCAACCTG
B053-2-78	GCCCATCAGGACTCCGTTAATATACAGGTTGGCAGAAGAC
B053-2-79	GGAGTCCTGATGGGCAGTGCAGAGATTACCGGCCTGGGAG
B053-2-80	AGTGTAATGTTATTGTCCTCCCGGATAGCTCCCAGGCCGG
B053-2-81	GAGGACAATAACATTACACTGAAGCTGGATAGATGTAATAAC

B053-2-82	CGATACTGACGTACTGATTATTGTTATTACATCTATCCAGCTTC
B053-2-83	AATAATCAGTACGTCAGTATCGACAAATTTAGAATCTTTTGCAAA
B053-2-84	CTCTTTAGGATTCAGGGCTTTGCAAAAGATTCTAAATTTGT
B053-2-85	GCCCTGAATCCTAAAGAGATAGAGAAACTGTACACCTCTT
B053-2-86	GGAGAAAGGTGATGCTGAGGTAAGAGGTGTACAGTTTCTC
B053-2-87	CAGCATCACCTTTCTCCGCGATTTTTGGGGCAATCCCCTG
B053-2-88	ATGAGATAGTACTCTGTGTCGTACCTCAGGGGATTGCCCC
B053-2-89	GACACAGAGTACTATCTCATCCCCGTCGCTAGCTCCTCTA
B053-2-90	TAATGTTTTTGAGCTGGACGTCTTTAGAGGAGCTAGCGAC
B053-2-91	GTCCAGCTCAAAAACATTACCGACTACATGTATCTGACCA
B053-2-92	CATTTGTATAACTAGGTGCATTGGTCAGATACATGTAGTC
B053-2-93	ATGCACCTAGTTATACAAATGGCAAGCTGAACATTTACTA
B053-2-94	AGGCCGTTGTACAGTCTGCGGTAGTAAATGTTCAGCTTGC
B053-2-95	ACTGTACAACGGCCTGAAATTCATTATCAAACGGTACACC
B053-2-96	AGAATCAATTTCGTTATTGGGGGTGTACCGTTTGATAATG
B053-2-97	CCCAATAACGAAATTGATTCTTTCGTGAAATCCGGAGACT
B053-2-98	TGTAGCTGACGTACAGCTTAATGAAGTCTCCGGATTTCAC
B053-2-99	CTGTACGTCAGCTACAACAATAACGAGCACATTGTTGGAT
B053-2-100	TGAAAGCATTTCCATCCTTGGGGTATCCAACAATGTGCTC
B053-2-101	AGGATGGAAATGCTTTCAACAATCTGGACAGAATCCTGCG
B053-2-102	AATGCCTGGGGCATTGTACCCGACCCGCAGGATTCTGTCC
B053-2-103	TGCCCCAGGCATTCCACTCTATAAGAAGATGGAAGCCGTC
B053-2-104	ATAGGTTTTCAGGTCCCGCAGCTTGACGGCTTCCATCTTC
B053-2-105	CGGGACCTGAAAACCTATAGTGTGCAGCTGAAGCTGTACG
B053-2-106	GTCCCAGGGATGCATTTTTATCGTCGTACAGCTTCAGCTG
B053-2-107	TGCATCCCTGGGACTCGTCGGCACTCATAACGGACAGATC
B053-2-108	TATCGCGGTTTGGGTCGTTGCCGATCTGTCCGTTATGAGT
B053-2-109	ACCCAAACCGCGATATACTCATAGCCAGCAACTGGTACTT
B053-2-110	AGAATCTTGTCCTTGAGATGATTGAAGTACCAGTTGCTGG
B053-2-111	CATCTCAAGGACAAGATTCTGGGTTGTGATTGGTATTTCG
B053-2-112	TCCATCCCTCATCGGTAGGCACGAAATACCAATCACAACC
B053-2-113	CCGATGAGGGATGGACAAATGACTGATAATAGGCGGCCGC
B053-2-114	GAGACAAGCTTGATGCGGCCGCCTA

7.7 Plasmid Maps

7.7.1 Marker Plasmid Project

7.7.1.1 pIRES

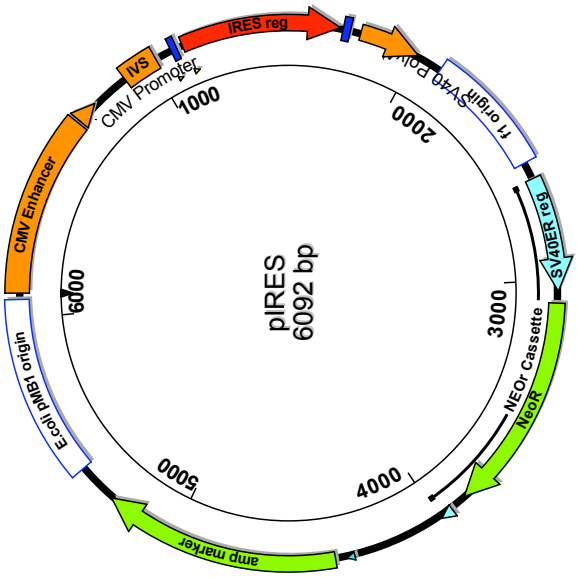

MCS A: bases 1085..1107
MCS B: bases 1722..1748
f1 origin: bases 2103..2558
SV40ER reg: bases 2622..3039
SV40 origin: bases 2938..3003
synth_PolyA term: bases 3941..3989
SV40 PolyA: bases 1787..2008
NEOr Cassette: bases 2622..3989
E.coli pMB1 origin: bases 5408..6069

7.7.1.2 pBOS-H2BGFP

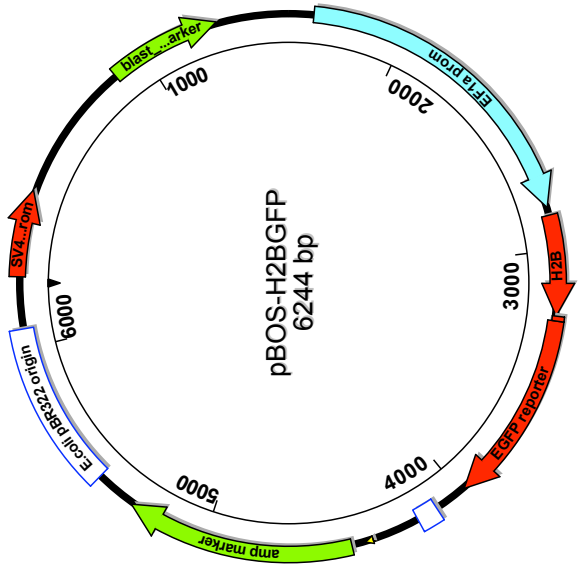

SV40 prom: bases 145..347
SV40 origin: bases 192..269
blast_S marker: bases 869..1291
EF1a prom: bases 1656..2840
EGFP reporter: bases 3263..3979
amp prom: bases 4367..4395
amp marker: bases 4448..5298
E.coli pBR322 origin: bases 5453..6074
H2B: bases 2870..3244
Linker: bases 3245..3262
EGFP: bases 4367..4395

7.7.1.3 pcDNA5/FRT

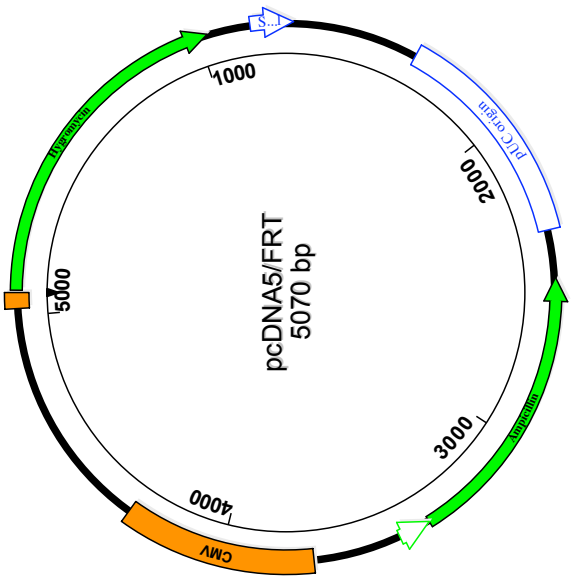

Hygromycin: bases 8..1028
SV40 early polyadenylation signal: bases 1160..1290
pUC origin: bases complement(1673..2346)
bla promoter: bases complement(3352..3450)
Ampicillin (bla) resistance gene: bases (2491..3351)

7.7.1.4 pcDNA3-APMA-ap

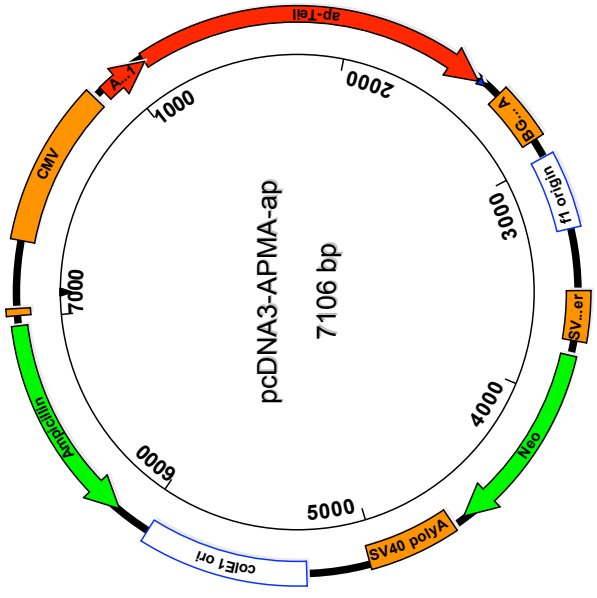

APMA: bases 907..2614
BGH poly A: bases 2678..2909
SV 40 origin: bases 3644..3729
Neo : bases 3811..4605
SV40 polyA: bases 4660..5032
colE1 origin: bases 5292..5965
Ampicillin: bases complement(6110..6970)
f1 origin: bases 2989..3295
SV40 Promoter: bases 3548..3749
Ampicillin promoter: bases 7012..7040

7.7.1.5 pcDNA5_FRT-IRES-PLAP-H2BGFP

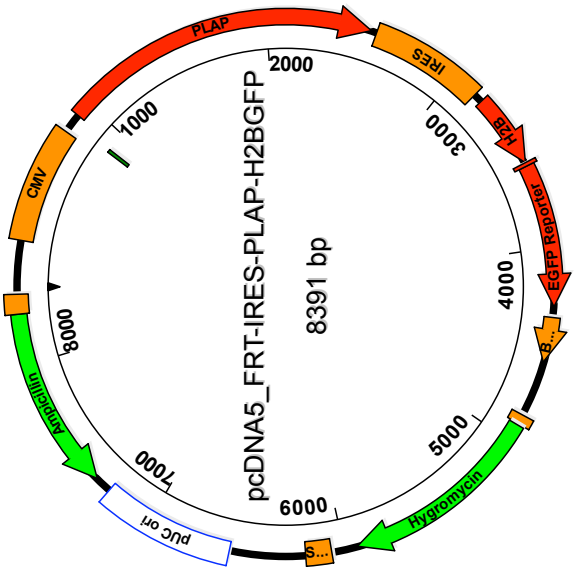

FRT: bases 4857..4904
Hygromycin: bases 4912..5932
SV40pA: bases 6064..6194
pUC origin: bases 6577..7250
Ampicillin: bases complement(7335..8255)
Pbla: bases 8256..8354
EGFP Reporter: bases 3578..4294
H2B: bases 3185..3559
CMV: bases 232..819
T7: bases 863..882
PLAP: bases 920..2530
IRES: bases 2559..3139

7.7.1.6 pcDNA5_FRT-IRES-APMA-ap-H2BGFP

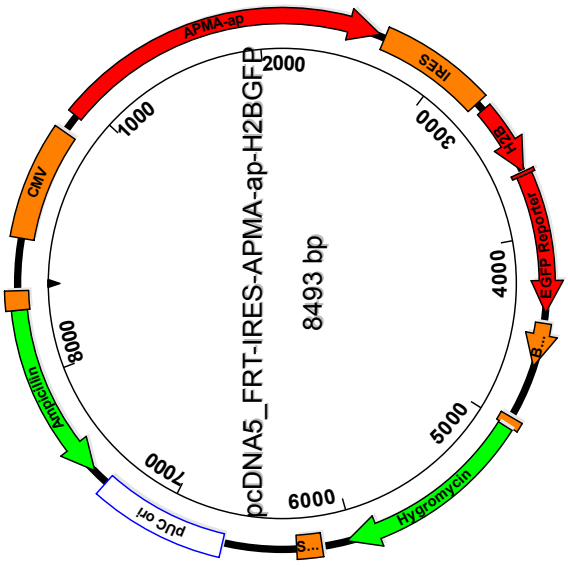

IRES: bases 2661..3241
H2B-EGFP: bases 3287..4402
BGH: bases 4451..4675
FRT: bases 4959..5006
Hygromycin: bases 5014..6034
SV40pA: bases 6166..6296
pUC origin: bases 6679..7352
Ampicillin: bases complement(7437..8357)
Pbla: bases 8358..8456
EGFP Reporter: bases 3680..4396
H2B: bases 3287..3661

7.7.2 Synthetic Tetanus Neurotoxin Project

7.7.2.1 pBS-sTeNT

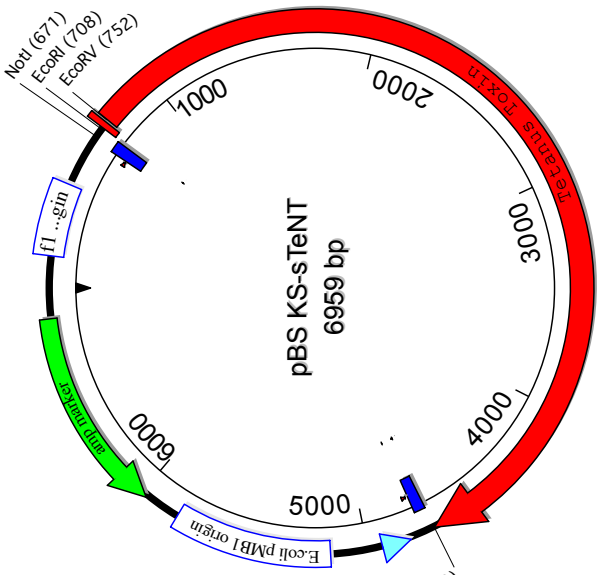

f1 origin: bases complement(135..441)
E.coli pMB1 origin: bases 5156..5823
lac promoter: bases complement(4815..4936)
PRO bacteriophage T3: bases 4772..4772
PRO bacteriophage T7: bases 643..643
amp marker: bases complement(5974..6831)
T7 promoter: bases 625..646
T3 promoter: bases complement(4770..4789)
T3212-1.1(B053F)M13+.scf(1>716): bases 633..1348
Untranslated region from b-globin: bases 716..742
triple stop codons: bases 4697..4705

7.7.2.2 pcDNA3

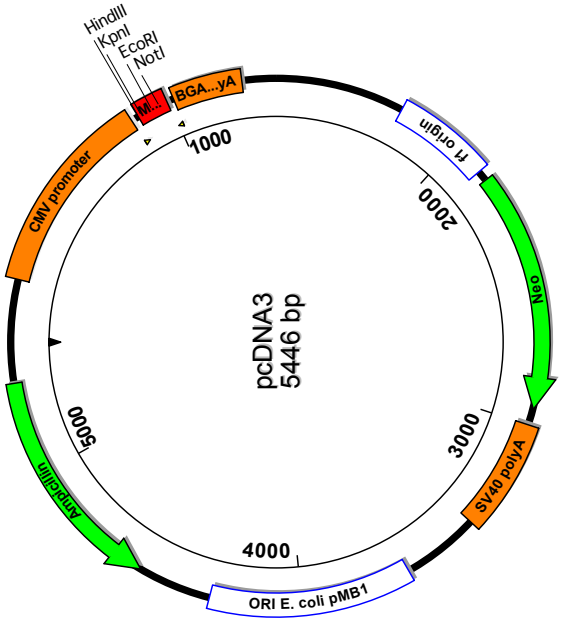

PRO bacteriophage T7: bases 864..882
MCS: bases 889..994
PRO bacteriophage Sp6: bases complement(999..1016)
ORIGIN E. coli pMB1: bases 3632..4305
f1 origin: bases 1790..2115
BGA polyA: bases 1018..1249
CMV promoter: bases 209..863
SV40 polyA: bases 3000..3372
SV40 origin: bases 1984..2069

7.7.2.3 pBS SK-iCre

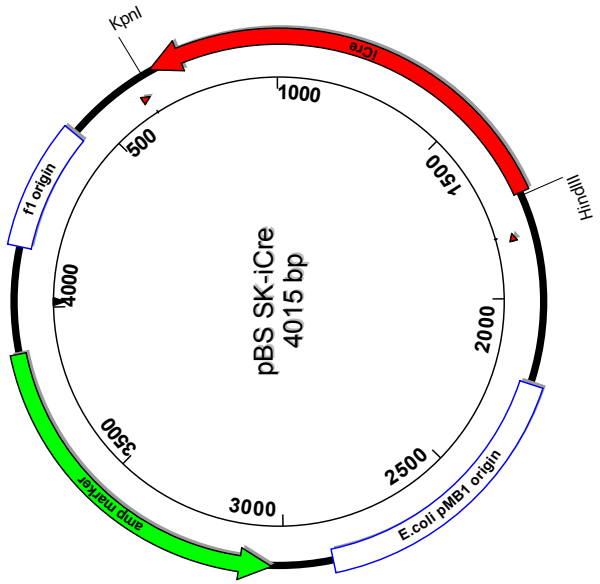

PRO bacteriophage T3: bases complement(1828..1828)
PRO bacteriophage T7: bases 643..643
E.coli pMB1 origin: bases 2212..2879
amp marker: bases complement(3030..3887)
T7 promoter: bases 625..646
T3 promoter: bases complement(1826..1845)
iCre: bases complement(680..1735)

7.7.2.4 pcDNA3-iCre

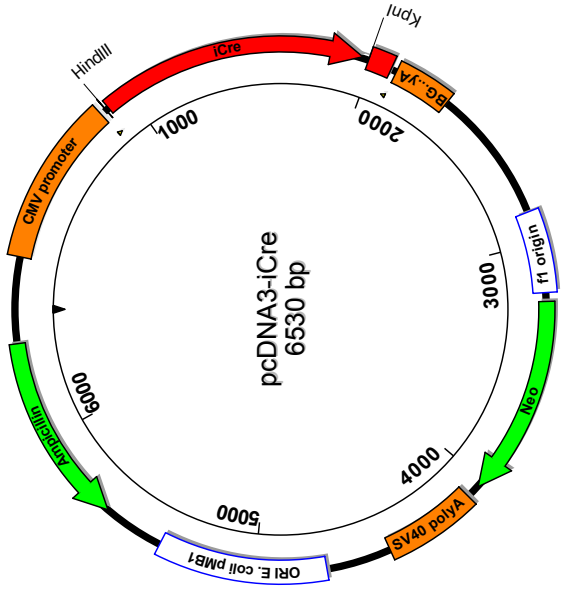

ORIGIN E. coli pMB1: bases 4716..5389
f1 origin: bases 2874..3199
BGA polyA: bases 2102..2333
CMV promoter: bases 209..863
SV40 polyA: bases 4084..4456
SV40 origin: bases 3068..3153
iCre: bases 902..1957

7.7.2.5 pcDNA3-EGFP

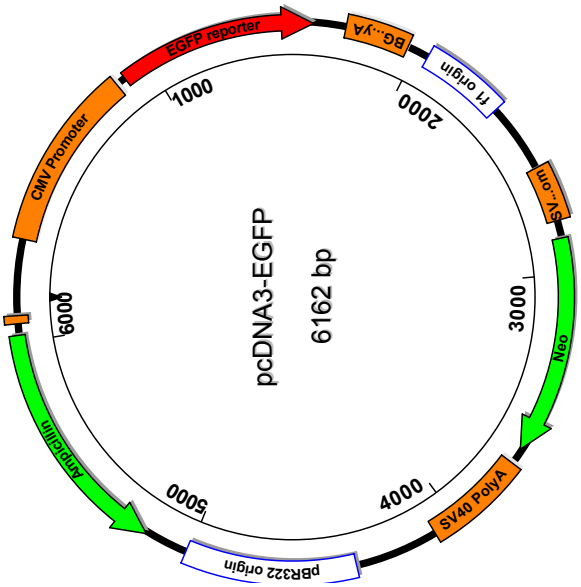

CMV Promoter: bases 209..863
BGA polyA: bases 1734..1965
EGFP reporter: bases 900..1616
Sp6 prom: bases 1716..1733
f1 origin: bases 2045..2351
SV40ER reg: bases 2461..2697
SV40 origin: bases 2651..2728
Neo: bases 2870..3658
lac prom: bases 4054..4083
pBR322 origin: bases 4392..5011
Ampicillin: bases 5166..6026
SV40 PolyA: bases 3716..4088

7.7.2.6 pGL3-CMVe-PDGFb-Luc

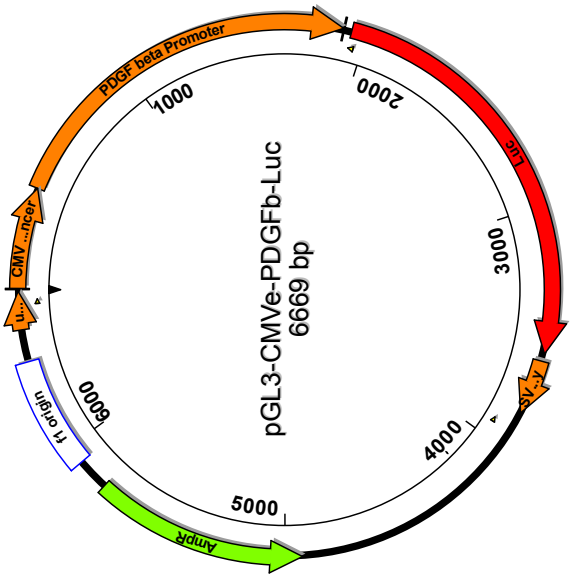

GL primer2: bases complement(1940..1962)
SV40 late poly(A) signal: bases 3623..3844
ColE1 origin: bases complement(4169..4169)
f1 origin: bases 5923..6378
upstream poly(A) signal: bases 6509..6662
RV primer3 sequencing primer binding site: bases 6611..6630
RVprimer4 binding site: bases complement(3912..3931)
CMV Enhancer: bases 6..413
PDGF beta Promoter: bases 414..1904

7.7.2.7 pBS KS-iCre-sTeNT

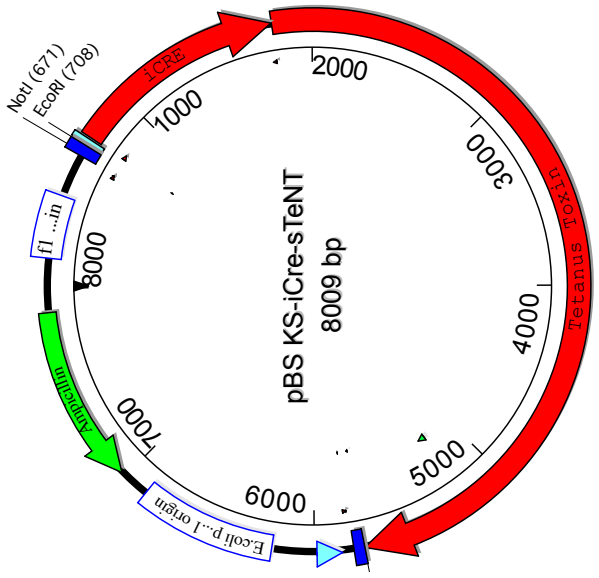

f1 origin: bases complement(135..441)
E.coli pMB1 origin: bases 6206..6873
lac promoter: bases complement(5865..5986)
PRO bacteriophage T3: bases 5822..5822
PRO bacteriophage T7: bases 643..643
Untranslated region from b-globin: bases 716..742
triple stop codons: bases 5747..5755
MCS: bases 5756..5808
iCRE: bases 752..1801

7.7.2.8 pBS KS-iCre-spacer-sTeNT

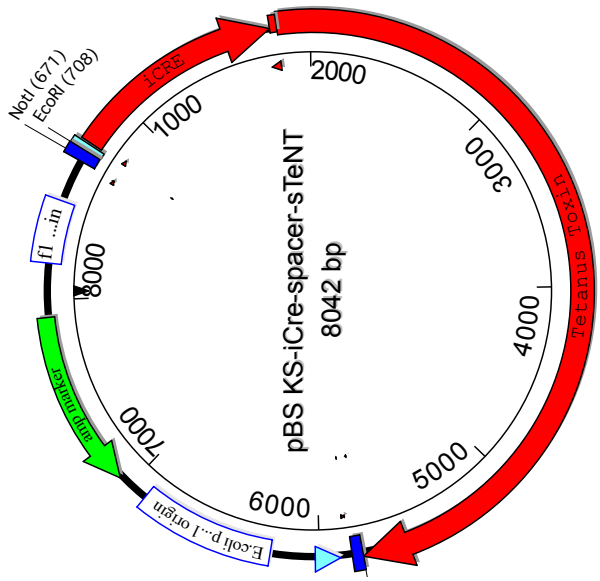

f1 origin: bases complement(135..441)
E.coli pMB1 origin: bases 6239..6906
lac promoter: bases complement(5898..6019)
PRO bacteriophage T3: bases 5855..5855
PRO bacteriophage T7: bases 643..643
amp marker: bases complement(7057..7914)
Untranslated region from b-globin: bases 716..742
triple stop codons: bases 5780..5788
iCRE: bases 752..1801
spacer: bases 1802..1834

7.7.2.9 pBS KS-Luc-sTeNT

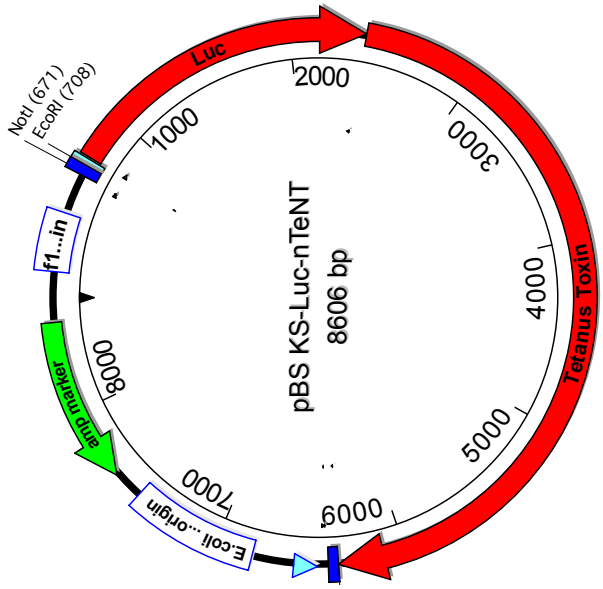

f1 origin: bases complement(135..441)
E.coli pMB1 origin: bases 6803..7470
lac promoter: bases complement(6462..6583)
PRO bacteriophage T3: bases 6419..6419
PRO bacteriophage T7: bases 643..643
amp marker: bases complement(7621..8478)
Untranslated region from b-globin: bases 716..742
triple stop codons: bases 6344..6352
Luc: bases 752..2398

7.7.2.10 pBS KS-Luc-spacer-sTeNT

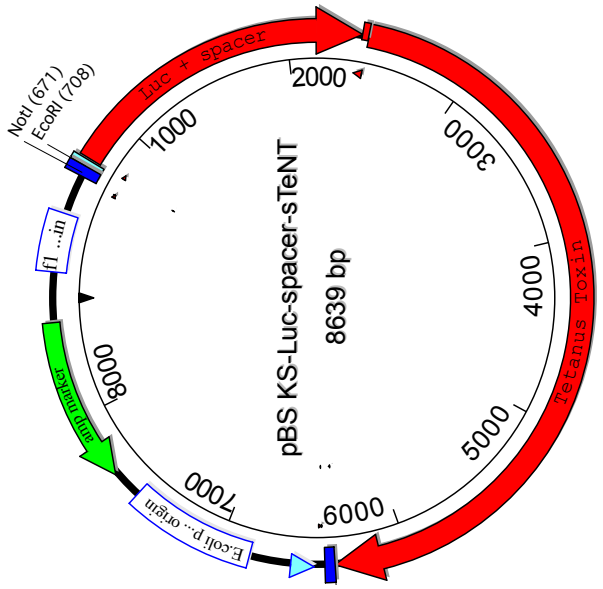

f1 origin: bases complement(135..441)
E.coli pMB1 origin: bases 6836..7503
lac promoter: bases complement(6495..6616)
PRO bacteriophage T3: bases 6452..6452
PRO bacteriophage T7: bases 643..643
amp marker: bases complement(7654..8511)
Untranslated region from b-globin: bases 716..742
triple stop codons: bases 6377..6385
Luc + spacer: bases 752..2398
spacer: bases 2399..2431

7.7.2.11 pBS KS-EGFP-sTeNT

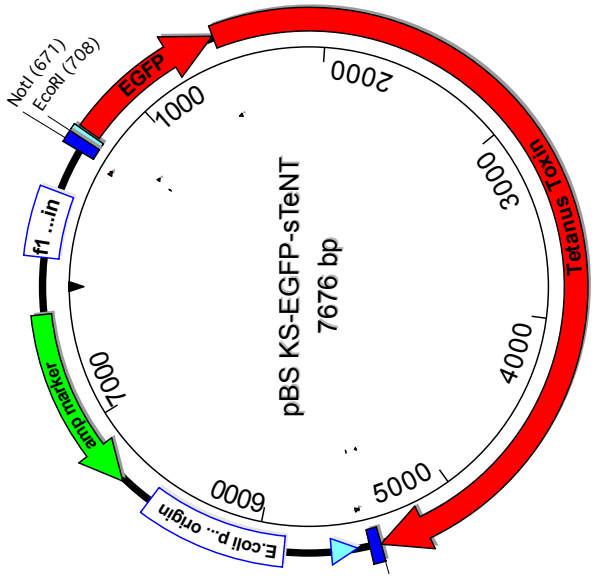

f1 origin: bases complement(135..441)
E.coli pMB1 origin: bases 5873..6540
lac promoter: bases complement(5532..5653)
PRO bacteriophage T3: bases 5489..5489
PRO bacteriophage T7: bases 643..643
amp marker: bases complement(6691..7548)
Untranslated region from b-globin: bases 716..742
triple stop codons: bases 5414..5422
EGFP: bases 752..1468

7.7.2.12 pBS KS-EGFP-spacer-sTeNT

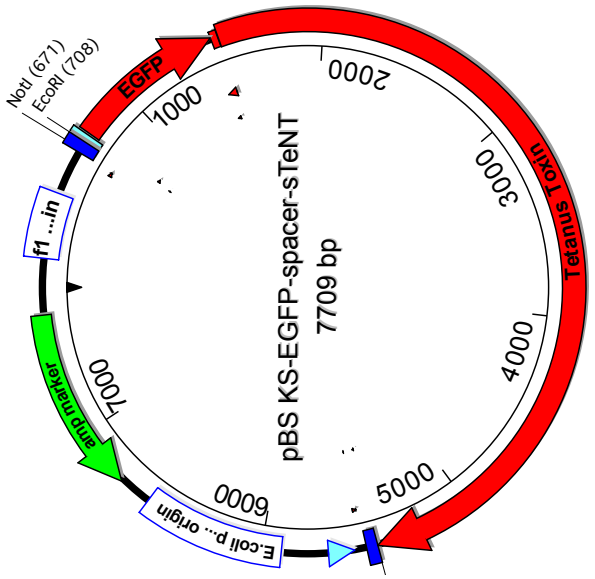

f1 origin: bases complement(135..441)
E.coli pMB1 origin: bases 5906..6573
lac promoter: bases complement(5565..5686)
PRO bacteriophage T3: bases 5522..5522
PRO bacteriophage T7: bases 643..643
amp marker: bases complement(6724..7581)
Untranslated region from b-globin: bases 716..742
triple stop codons: bases 5447..5455
EGFP: bases 752..1468
spacer: bases 1469..1501

7.7.2.13 pBS KS-iCre-FLEX-sTeNT

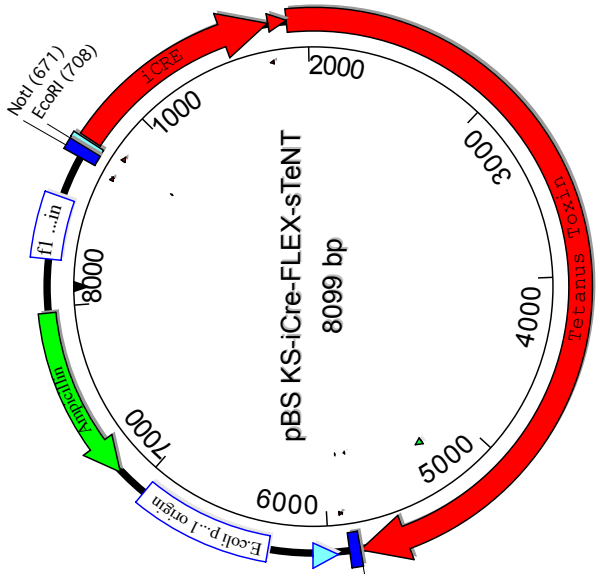

f1 origin: bases complement(135..441)
E.coli pMB1 origin: bases 6296..6963
lac promoter: bases complement(5955..6076)
PRO bacteriophage T3: bases 5912..5912
PRO bacteriophage T7: bases 643..643
Untranslated region from b-globin: bases 716..742
triple stop codons: bases 5837..5845
iCRE: bases 752..1801

7.7.2.14 pBS KS-iCre-HELI-sTeNT

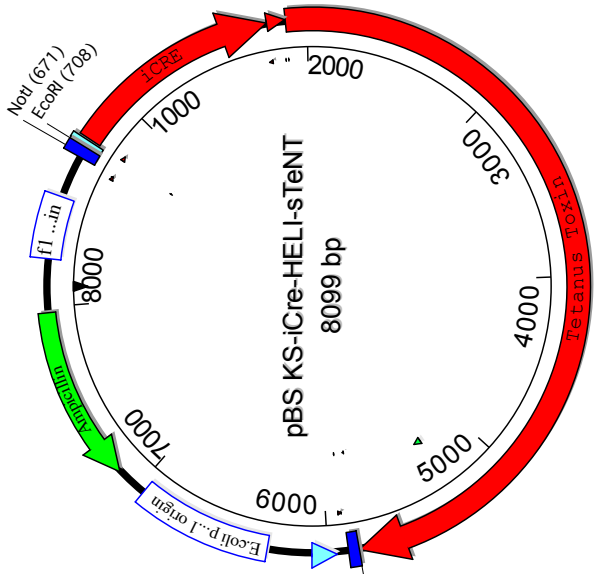

f1 origin: bases complement(135..441)
E.coli pMB1 origin: bases 6296..6963
lac promoter: bases complement(5955..6076)
PRO bacteriophage T3: bases 5912..5912
PRO bacteriophage T7: bases 643..643
Untranslated region from b-globin: bases 716..742
triple stop codons: bases 5837..5845
MCS: bases 5846..5898
iCRE: bases 752..1801

7.7.2.15 pcDNA3-iCre-sTeNT

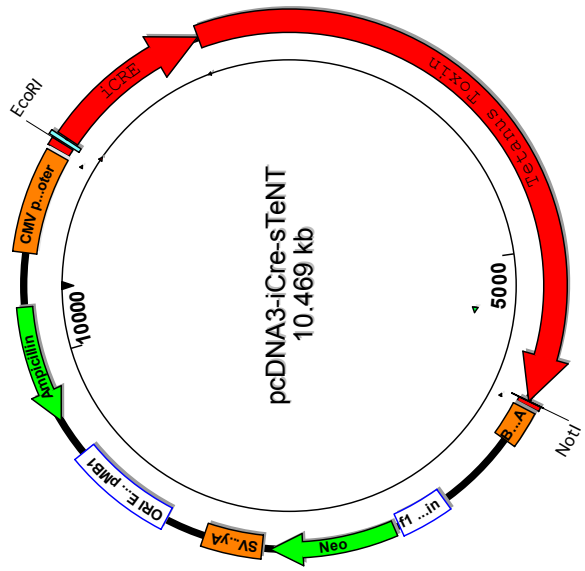

PRO bacteriophage T7: bases 864..882
PRO bacteriophage Sp6: bases complement(6022..6039)
ORIGIN E. coli pMB1 (ColE1 and pBR322): bases 8655..9328
f1 origin: bases 6813..7138
BGA polyA: bases 6041..6272
CMV promoter: bases 209..863
SV40 polyA: bases 8023..8395
SV40 origin: bases 7007..7092
Untranslated region from b-globin: bases 947..973
iCRE: bases 983..2032
triple stop codons: bases 5978..5986

7.7.2.16 pcDNA3-iCre-spacer-sTeNT

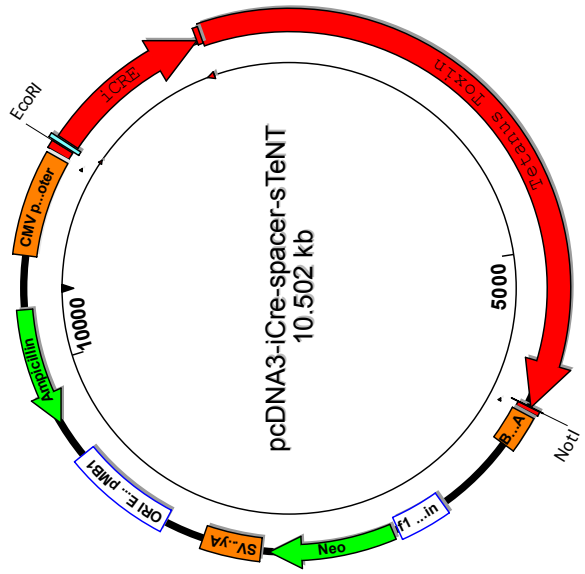

PRO bacteriophage T7: bases 864..882
PRO bacteriophage Sp6: bases complement(6055..6072)
ORIGIN E. coli pMB1 (ColE1 and pBR322): bases 8688..9361
f1 origin: bases 6846..7171
BGA polyA: bases 6074..6305
CMV promoter: bases 209..863
SV40 polyA: bases 8056..8428
SV40 origin: bases 7040..7125
Untranslated region from b-globin: bases 947..973
iCRE: bases 983..2032
spacer: bases 2033..2065
triple stop codons: bases 6011..6019

7.7.2.17 pcDNA3-Luc-sTeNT

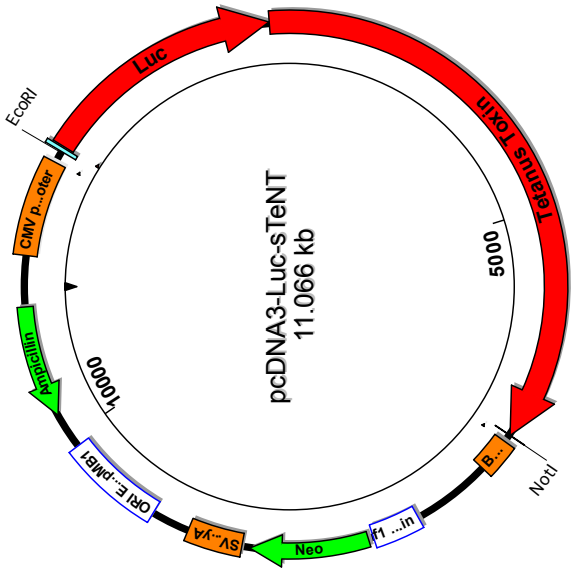

PRO bacteriophage T7: bases 864..882
PRO bacteriophage Sp6: bases complement(6619..6636)
ORIGIN E. coli pMB1 (ColE1 and pBR322): bases 9252..9925
f1 origin: bases 7410..7735
BGA polyA: bases 6638..6869
CMV promoter: bases 209..863
SV40 polyA: bases 8620..8992
SV40 origin: bases 7604..7689
Untranslated region from b-globin: bases 947..973
Luc: bases 983..2629
triple stop codons: bases 6575..6583

7.7.2.18 pcDNA3-Luc-spacer-sTeNT

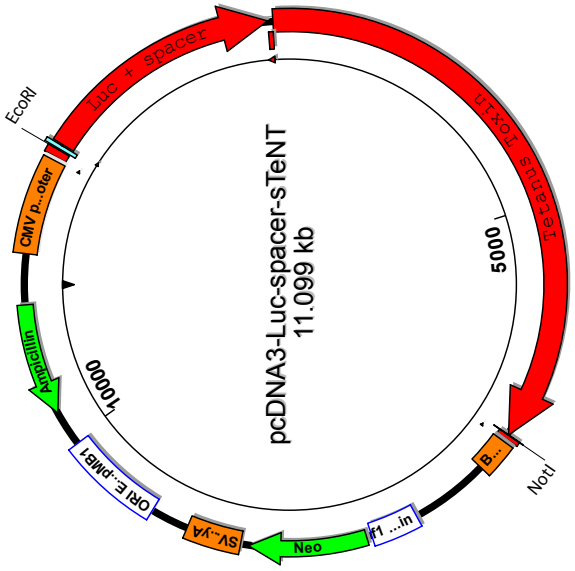

PRO bacteriophage T7: bases 864..882
PRO bacteriophage Sp6: bases complement(6652..6669)
ORIGIN E. coli pMB1 (ColE1 and pBR322): bases 9285..9958
f1 origin: bases 7443..7768
BGA polyA: bases 6671..6902
CMV promoter: bases 209..863
SV40 polyA: bases 8653..9025
SV40 origin: bases 7637..7722
Untranslated region from b-globin: bases 947..973
Luc + spacer: bases 983..2629
spacer: bases 2630..2662
triple stop codons: bases 6608..6616

7.7.2.19 pcDNA3-EGFP-sTeNT

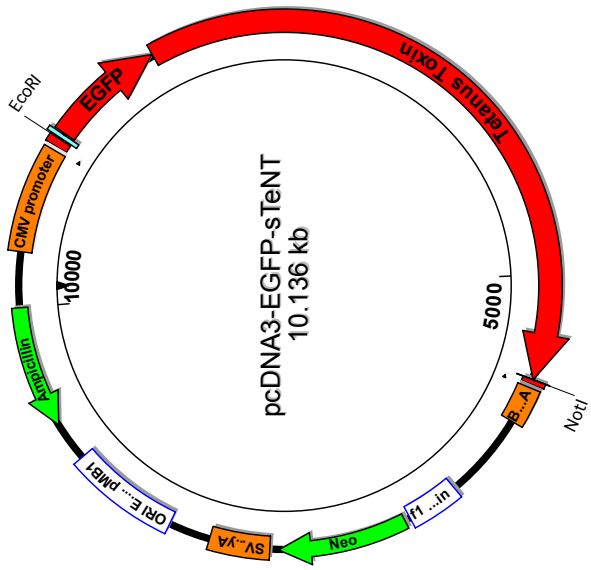

PRO bacteriophage T7: bases 864..882
PRO bacteriophage Sp6: bases complement(5689..5706)
E. coli pMB1 (ColE1 and pBR322): bases 8322..8995
f1 origin: bases 6480..6805
BGA polyA: bases 5708..5939
CMV promoter: bases 209..863
SV40 polyA: bases 7690..8062
SV40 origin: bases 6674..6759
Untranslated region from b-globin: bases 947..973
EGFP: bases 983..1699
triple stop codons: bases 5645..5653

7.7.2.20 pcDNA3-EGFP-spacer-sTeNT

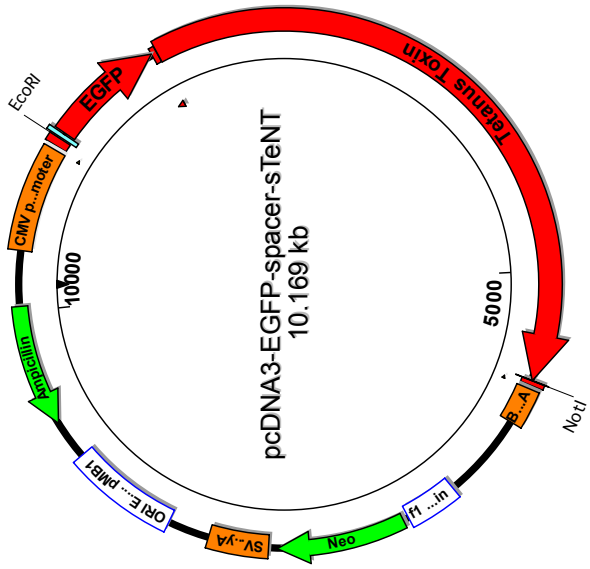

PRO bacteriophage T7: bases 864..882
MCS: bases join(889..938,5689..5717)
PRO bacteriophage Sp6: bases complement(5722..5739)
E. coli pMB1 (ColE1 and pBR322): bases 8355..9028
f1 origin: bases 6513..6838
BGA polyA: bases 5741..5972
CMV promoter: bases 209..863
SV40 polyA: bases 7723..8095
SV40 origin: bases 6707..6792
Untranslated region from b-globin: bases 947..973
EGFP: bases 983..1699
spacer: bases 1700..1732
triple stop codons: bases 5678..5686

7.7.2.21 pYY12-Stoplight

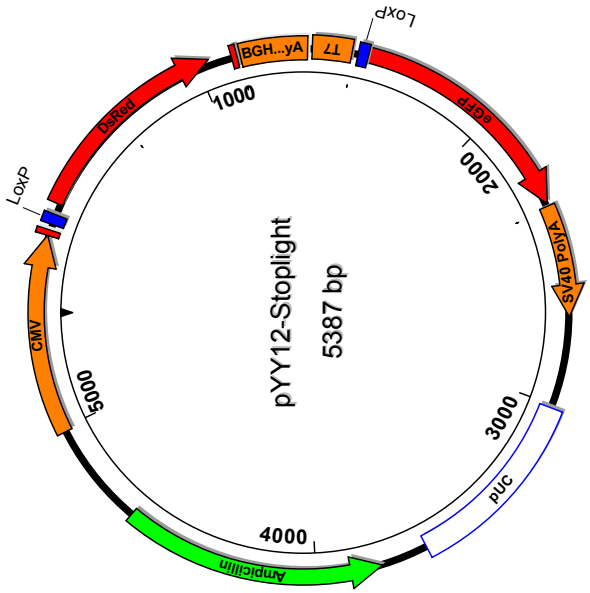

CMV: bases 5010..254
Ampicillin: bases 3805..4665
BGH PolyA: bases 1166..1385
SV40 PolyA: bases 2363..2730
pUC: bases 3034..3650
DsRed: bases 384..1064
eGFP: bases 1581..2354

7.7.3 Lentiviral Project Plasmids

7.7.3.1 pENTR5'-CMVe-PDGFb

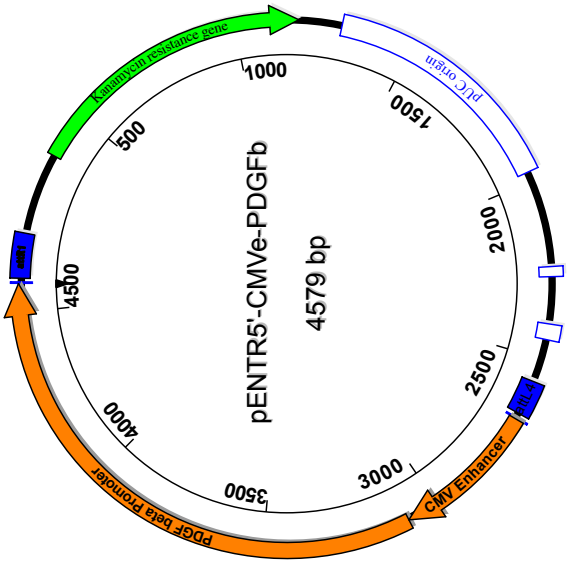

TOPO recognition site 2: bases 2..5
attR1: bases 16..140
GW3 priming site: bases 47..76
M13 reverse priming site: bases 240..256
Kanamycin resistance gene: bases 369..1178
pUC origin: bases 1299..1972
M13 forward (-20) priming site: bases 2512..2527
attL4: bases 2567..2663
GW1 priming site: bases 2605..2629
TOPO recognition site 1: bases 2676..2679
CMV Enhancer: bases 2681..3088
PDGF beta Promoter: bases 3089..4579

7.7.3.2 pENTR5'-CMV

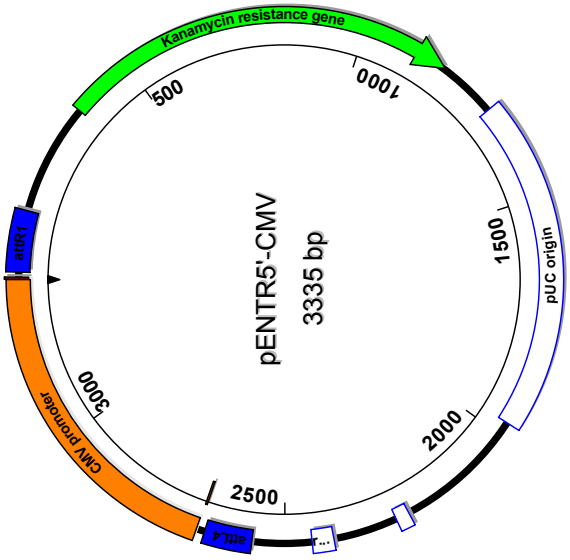

TOPO recognition site 2: bases 2..5
attR1: bases 16..140
GW3 priming site: bases 47..76
M13 reverse priming site: bases 240..256
Kanamycin resistance gene: bases 369..1178
pUC origin: bases 1299..1972
rrnB T2 transcription terminator: bases complement(2243..2270)
rrnB T1 transcription terminator: bases complement(2402..2445)
M13 forward (-20) priming site: bases 2512..2527
GW1 priming site: bases 2605..2629
TOPO recognition site 1: bases 2676..2679
CMV promoter: bases 2681..3335

7.7.3.3 pENTR/D-iCre

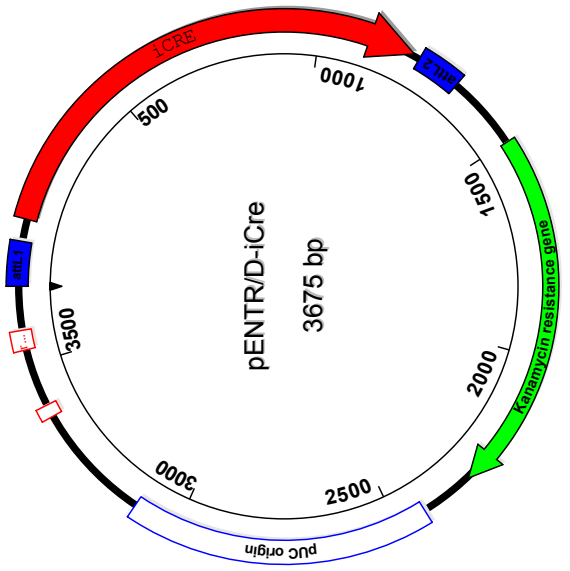

TOPO recognition site 1: bases 112..116
Untranslated region from b-globin: bases 121..147
iCRE: bases 151..1216
M13 forward (-20) priming site: bases 3644..3659
TOPO recognition site 2: bases 1207..1220
attL2: bases 1232..1331
T7 Promoter/priming site: bases complement(1348..1367)
M13 reverse priming site: bases 1372..1388
Kanamycin resistance gene: bases 1501..2310
pUC origin: bases 2431..3104

7.7.3.4 pENTR/D-iCre-spacer-sTeNT

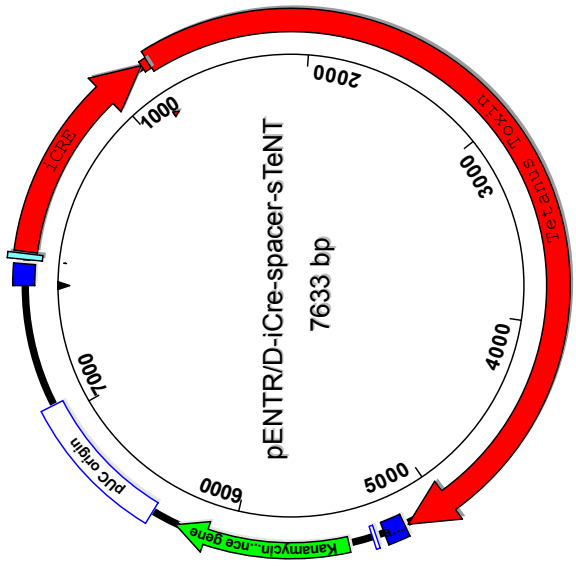

TOPO recognition site 1: bases 112..116
Untranslated region from b-globin: bases 121..147
iCRE: bases 157..1186
triple stop codons: bases 5165..5173
rrnB T2 transcription termination sequence: bases 7333..7360
rrnB T1 transcription termination sequence: bases 7492..7535
M13 forward (-20) priming site: bases 7602..7617
TOPO%AE recognition site 2: bases 5174..5178
attL2: bases 5190..5289
T7 Promoter/priming site: bases complement(5306..5325)
M13 reverse priming site: bases 5330..5346
Kanamycin resistance gene: bases 5459..6268
pUC origin: bases 6389..7062
spacer: bases complement(1187..1219)

7.7.3.5 pLENTI6-CMV-iCre-spacer-sTeNT

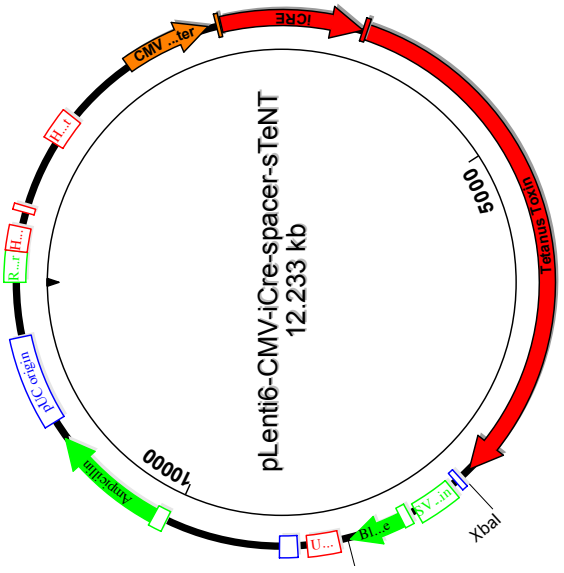

RSV promoter: bases 1..229
HIV-1 5' LTR: bases 230..410
HIV-1 psi () packaging signal: bases 521..565
HIV-1 Rev response element (RRE): bases 1075..1308
attR2 site: bases 2539..7690
V5 epitope: bases 7743..7784
SV40 early promoter and origin: bases 7839..8148
EM7 promoter: bases 8203..8269
Blasticidin resistance gene: bases 8270..8668
U3/3' LTR: bases 8754..8988
U3: bases 8754..8807
3' LTR: bases 8808..8988
SV40 polyadenylation signal: bases 9060..9191
bla promoter: bases 10050..10148
Ampicillin (bla) resistance gene: bases 10149..11009
pUC origin: bases 11154..11827
TOPO recognition site 1: bases 1856..1859
CMV: bases 1861..2515
TOPO recognition site 2: bases 2517..2520
TOPO recognition site 1: bases 2567..2571
Untranslated region from b-globin: bases 2576..2602
iCRE: bases 2612..3662
triple stop codons: bases 7640..7648
TOPO recognition site 2: bases 7650..7654

7.7.3.6 pLENTI6-CMV-iCre-spacer-sTeNT-cut

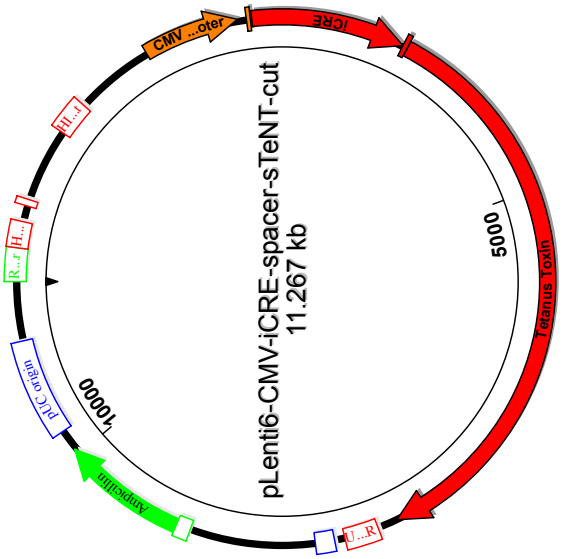

RSV promoter: bases 1..229
HIV-1 5' LTR: bases 230..410
HIV-1 psi () packaging signal: bases 521..565
HIV-1 Rev response element (RRE): bases 1075..1308
attR2 site: bases 2539..7690
U3/3' LTR: bases 7788..8022
U3: bases 7788..7841
3' LTR: bases 7842..8022
SV40 polyadenylation signal: bases 8094..8225
bla promoter: bases 9084..9182
Ampicillin (bla) resistance gene: bases 9183..10043
pUC origin: bases 10188..10861
TOPO recognition site 1: bases 1856..1859
CMV promoter: bases 1861..2515
TOPO recognition site 2: bases 2517..2520
TOPO recognition site 1: bases 2567..2571
Untranslated region from b-globin: bases 2576..2602
iCRE: bases 2612..3662
triple stop codons: bases 7640..7648
TOPO recognition site 2: bases 7650..7654
spacer: bases 3662..3694

7.7.3.7 pLENTI6-CMV-iCre-cut

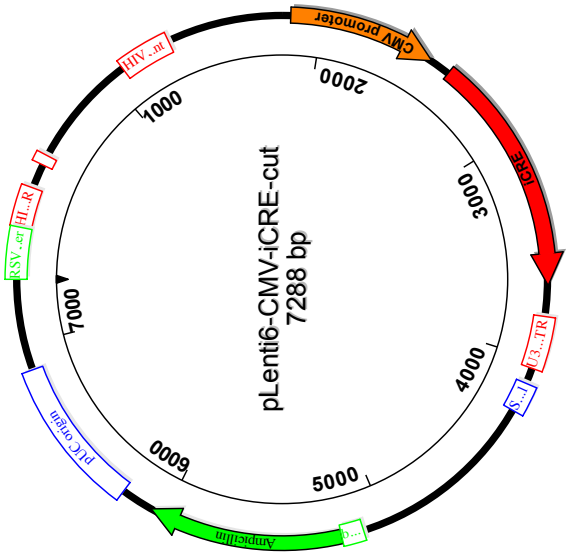

RSV/5' LTR hybrid promoter: bases 1..410
RSV promoter: bases 1..229
HIV-1 5' LTR: bases 230..410
HIV-1 psi () packaging signal: bases 521..565
HIV-1 Rev response element (RRE): bases 1075..1308
attR2 site: bases 3704..3711
U3/3' LTR: bases 3809..4043
U3: bases 3809..3862
3' LTR: bases 3863..4043
SV40 polyadenylation signal: bases 4115..4246
bla promoter: bases 5105..5203
Ampicillin (bla) resistance gene: bases 5204..6064
pUC origin: bases 6209..6882
TOPO recognition site 1: bases 1856..1859
CMV promoter: bases 1861..2515
TOPO recognition site 2: bases 2517..2520
TOPO recognition site 1: bases 2567..2571
Untranslated region from b-globin: bases 2576..2602
iCRE: bases 2606..3671
TOPO recognition site 2: bases 3662..3675

8 LITERATURE

1 Churchland, P. S. & Sejnowski, T. J. Perspectives on cognitive neuroscience. *Science* 242, 741-745 (1988).

2 Grinvald, A. & Hildesheim, R. VSDI: a new era in functional imaging of cortical dynamics. *Nature Reviews Neuroscience* 5, 874-885 (2004).

3 Knöpfel, T., Díez-García, J. & Akemann, W. Optical probing of neuronal circuit dynamics: genetically encoded versus classical fluorescent sensors. *Trends in Neurosciences* 29, 160-166 (2006).

4 Baker, B. *et al.* Genetically encoded fluorescent sensors of membrane potential. *Brain Cell Biology* 36, 53-67 (2008).

5 Hendel, T. *et al.* Fluorescence changes of genetic calcium indicators and OGB-1 correlated with neural activity and calcium in vivo and in vitro. *Journal of Neuroscience* 28, 7399-7411 (2008).

6 Stosiek, C., Garaschuk, O., Holthoff, K. & Konnerth, A. In vivo two-photon calcium imaging of neuronal networks. *Proc. Natl. Acad. Sci. U.S.A.* 100, 7319-7324 (2003).

7 Kuhn, B. & Fromherz, P. Anellated hemicyanine dyes in a neuron membrane: Molecular Stark effect and optical voltage recording. *The Journal of Organic Chemistry B* 107, 7903-7913 (2003).

8 Antic, S., Major, G. & Zecevic, D. Fast optical recordings of membrane potential changes from dendrites of pyramidal neurons. *Journal of Neurophysiology* 82, 1615-1621 (1999).

9 Grinvald, A., Fine, A., Farber, I. & Hildesheim, R. Fluorescence monitoring of electrical responses from small neurons and their processes. *Biophysical Journal* 42, 195-198 (1983).

10 Fromherz, P. & Vetter, T. Cable properties of arborized Retzius cells of the leech in culture as probed by a voltage-sensitive dye. *Proc. Natl. Acad. Sci. U.S.A.* 89, 2041-2045 (1992).

11 Hinner, M. J., Hübener, G. & Fromherz, P. Enzyme-Induced Staining of Biomembranes with Voltage-Sensitive Fluorescent Dyes. *The Journal of Organic Chemistry B* 108, 2445-2453 (2004).

12 Hinner, M. J., Hübener, G. & Fromherz, P. Genetic targeting of individual cells with a voltage-sensitive dye through enzymatic activation of membrane binding. *ChemBioChem* 7, 495-505 (2006).

13 Lambacher, A. & Fromherz, P. Orientation of hemicyanine dye in lipid membrane measured by fluorescence interferometry on a silicon chip. *The Journal of Physical Chemistry B* 105, 343-346 (2001).

14 Wouterlood, F. G., Vinkenoog, M. & van den Oever, M. Tracing tools to resolve neural circuits. *Network (Bristol, England)* 13, 327-342 (2002).

15 Callahan, C. A., Yoshikawa, S. & Thomas, J. B. Tracing axons. *Current Opinion in Neurobiology* 8, 582-586 (1998).

16 Rockland, K. S. Connectional neuroanatomy: the changing scene. *Brain Research* 1000, 60-63 (2004).

17 Banfield, B. W., Kaufman, J. D., Randall, J. A. & Pickard, G. E. Development of pseudorabies virus strains expressing red fluorescent proteins: new tools for multisynaptic labeling applications. *Journal of Virology* 77, 10106-10112 (2003).

18 Boldogköi, Z. *et al.* Novel tracing paradigms--genetically engineered herpesviruses as tools for mapping functional circuits within the CNS: present status and future prospects. *Progress in Neurobiology* 72, 417-445 (2004).

19 Fluhler, E. N., Burnham, V. G. & Loew, L. M. Spectra, membrane binding, and potentiometric responses of new charge shift probes. *Biochemistry* 24, 5749-5755 (1985).

20 Hassner, A., Birnbaum, D. & Loew, L. M. Charge-shift probes of membrane-potential. *The Journal of Organic Chemistry* 49, 2546-2551 (1984).

21 Wuskell, J. P. *et al.* Synthesis, spectra, delivery and potentiometric responses of new styryl dyes with extended spectral ranges. *Journal of Neuroscience Methods* 151, 200-215 (2006).

22 Obaid, A. L., Loew, L. M., Wuskell, J. P. & Salzberg, B. M. Novel naphthylstyryl-pyridium potentiometric dyes offer advantages for neural network analysis. *Journal of Neuroscience Methods* 134, 179-190 (2004).

23 Hübener, G., Lambacher, A. & Fromherz, P. Anellated hemicyanine dyes with large symmetrical solvatochromism of absorption and fluorescence. *The Journal of Physical Chemistry B* 107, 7896-7902 (2003).

24 Zhou, Yan, Wuskell, J. P., Loew, L. M. & Antic, S. Intracellular long-wavelength voltage-sensitive dyes for studying the dynamics of action potentials in axons and thin dendrites. *Journal of Neuroscience Methods* 164, 225–239 (2007).

25 Ephardt, H. & Fromherz, P. Fluorescence of amphiphilic hemicyanine dyes without free double-bonds. *The Journal of Physical Chemistry* 97, 4540-4547 (1993).

26 Kuhn, B., Fromherz, P. & Denk, W. High sensitivity of Stark-shift voltage-sensing dyes by one- or two-photon excitation near the red spectral edge. *Biophysical Journal* 87, 631-639 (2004).

27 Fromherz, P., Hübener, G., Kuhn, B. & Hinner, M. J. ANNINE-6plus, a voltage-sensitive dye with good solubility, strong membrane binding and high sensitivity. *European Biophysics Journal* 37, 509-514 (2007).

28 Hinner, M., Marrink, S. & de Vries, A. Location, Tilt, and Binding: A Molecular Dynamics Study of Voltage-Sensitive Dyes in Biomembranes. *The Journal of Physical Chemistry B* 113, 15807–15819 (2009).

29 Orbach, H. & Vanessen, D. In-vivo tracing of pathways and spatiotemporal activity patterns in rat visual-cortex using voltage-sensitive dyes. *Experimental Brain Research* 94, 371-392 (1993).

30 Wallace, P. M. & Senter, P. D. In vitro and in vivo activities of monoclonal antibody-alkaline phosphatase conjugates in combination with phenol mustard phosphate. *Bioconjugate Chemistry* 2, 349-352 (1991).

31 Yagi, S. *et al.* Development of anti-influenza virus drugs I: Improvement of oral absorption and in vivo anti-influenza activity of stachyflin and its derivatives. *Pharmaceutical Research* 16, 1041-1046 (1999).

32 Baker, W. *et al.* A prodrug approach toward the development of water soluble fluoroquinolones and structure-activity relationships of quinoline-3-carboxylic acids. *Journal of Medicinal Chemistry* 47, 4693-4709 (2004).

33 Heimbach, T. *et al.* Absorption rate limit considerations for oral phosphate prodrugs. *Pharmaceutical Research* 20, 848-856 (2003).

34 Stella, V. J. & Nti-Addae, K. W. Prodrug strategies to overcome poor water solubility. *Advanced Drug Delivery Reviews* 59, 677-694 (2007).
35 Krise, J. P., Zygmunt, J., Georg, G. I. & Stella, V. J. Novel prodrug approach for tertiary amines: synthesis and preliminary evaluation of N-phosphonooxymethyl prodrugs. *Journal of Medicinal Chemistry* 42, 3094-3100 (1999).
36 Krise, J. P., Narisawa, S. & Stella, V. J. A novel prodrug approach for tertiary amines. 2. Physicochemical and in vitro enzymatic evaluation of selected N-phosphonooxymethyl prodrugs. *Journal of Pharmaceutical Sciences* 88, 922-927 (1999).
37 Krise, J. P., Charman, W. N., Charman, S. A. & Stella, V. J. A novel prodrug approach for tertiary amines. 3. In vivo evaluation of two N-phosphonooxymethyl prodrugs in rats and dogs. *Journal of Pharmaceutical Sciences* 88, 928-932 (1999).
38 Ueda, Y. *et al.* Phosphonooxymethyl prodrugs of the broad spectrum antifungal azole, ravuconazole: synthesis and biological properties. *Bioorganic & Medicinal Chemistry Letters* 13, 3669-3672 (2003).
39 Kumpulainen, H. *et al.* Synthesis, in vitro and in vivo characterization of novel ethyl dioxy phosphate prodrug of propofol. *European Journal of Pharmaceutical Sciences* 34, 110-117 (2008).
40 Simplicio, A. L., Clancy, J. M. & Gilmer, J. F. Prodrugs for Amines. *Molecules* 13, 519-547 (2008).
41 Csizmadia, F., Tsantili-Kakoulidou, A., Panderi, I. & Darvas, F. Prediction of distribution coefficient from structure. 1. Estimation method. *Journal of Pharmaceutical Sciences* 86, 865-871 (1997).
42 Klopman, G., Li, J., Wang, S. & Dimayuga, M. Computer automated log P calculations based on an extended group-contribution approach. *Journal of Chemical Information and Modeling* 34, 752-781 (1994).
43 Bouchard, G., Carrupt, P. A., Testa, B., Gobry, V. & Girault, H. H. The apparent lipophilicity of quaternary ammonium ions is influenced by galvani potential difference, not ion-pairing: a cyclic voltammetry study. *Pharmaceutical Research* 18, 702-708 (2001).
44 Bouchard, G., Carrupt, P.-A., Testa, B., Gobry, V. & Girault, H. H. Lipophilicity and solvation of anionic drugs. *Chemistry (Weinheim an der Bergstrasse, Germany)* 8, 3478-3484 (2002).
45 McComb, R. B. & Bowers, G. N. Study of optimum buffer conditions for measuring alkaline phosphatase activity in human serum. *Clinical Chemistry* 18, 97-104 (1972).
46 Cruz, O. & Kuffler, D. P. Neuroprotection of adult rat dorsal root ganglion neurons by combined hypothermia and alkalinization against prolonged ischemia. *Neuroscience* 132, 115-122 (2005).
47 Newman, M. & Galt, R. The syntheses of 3'-fluoro- and 4-fluoro-10-methyl-1,2-benzanthracenes. *The Journal of Organic Chemistry* 25, 214-215 (1960).
48 De Meijere, A. & Meyer, F. Fine feathers make fine birds: the Heck reaction in modern garb. *Angewandte Chemie* 33, 2379-2411 (1994).
49 Wolfe, J. & Buchwald, S. L. Palladium-Catalyzed Amination of Aryl Triflates. *The Journal of Organic Chemistry* 62, 1264-1267 (1997).
50 Tundel, R. E., Anderson, K. W. & Buchwald, S. L. Expedited palladium-catalyzed amination of aryl nonaflates through the use of microwave-irradiation and soluble organic amine bases. *The Journal of Organic Chemistry* 71, 430-433 (2006).

51 Louie, J., Driver, M., Hamann, B. & Hartwig, J. Palladium-Catalyzed Amination of Aryl Triflates and Importance of Triflate Addition Rate. *The Journal of Organic Chemistry* 62, 1268-1273 (1997).

52 Anderson, K. W., Mendez-Perez, M., Priego, J. & Buchwald, S. L. Palladium-catalyzed amination of aryl nonaflates. *The Journal of Organic Chemistry* 68, 9563-9573 (2003).

53 Woo, H. Y. *et al.* Solvent effects on the two-photon absorption of distyrylbenzene chromophores. *Journal of the American Chemical Society* 127, 14721-14729 (2005).

54 Guo, Q., WU, J., Jiang, C. & Wang, Z. A Novel Palladium-Catalyzed Reaction and Its Application in Preparation of Derivatives of Stilbazols. *Chinese Chemical Letters* 12, 339-402 (2001).

55 Lattuada, L. & Uberti, F. Convenient Synthesis of Di (n-octadecyl) amine and Di (n-hexadecyl) amine. *Organic Preparations and Procedures International* 34, 643-646 (2002).

56 Juntunen, J., Vepsäläinen, J., Niemi, R., Laine, K. & Järvinen, T. Synthesis, in vitro evaluation, and intraocular pressure effects of water-soluble prodrugs of endocannabinoid noladin ether. *Journal of Medicinal Chemistry* 46, 5083-5086 (2003).

57 Sakakura, A., Katsukawa, M. & Ishihara, K. Selective synthesis of phosphate monoesters by dehydrative condensation of phosphoric acid and alcohols promoted by nucleophilic bases. *Organic Letters* 7, 1999-2002 (2005).

58 Jablonkai, I. & Oroszlan, P. Preparation of ω -functionalized eicosane-phosphate building blocks. *Chemistry and Physics of Lipids* 133, 103-112 (2005).

59 Wu, W., Bergstrom, D. E. & Davisson, V. J. A combination chemical and enzymatic approach for the preparation of azole carboxamide nucleoside triphosphate. *The Journal of Organic Chemistry* 68, 3860-3865 (2003).

60 Davis, S. C. & Szoka, F. C. Cholesterol phosphate derivatives: synthesis and incorporation into a phosphatase and calcium-sensitive triggered release liposome. *Bioconjugate Chemistry* 9, 783-792 (1998).

61 Davisson, V. J., DAVIS, D., Dixit, V. & Poulter, C. Synthesis of nucleotide 5'-diphosphates from 5'-o-tosyl nucleosides. *The Journal of Organic Chemistry* 52, 1794-1801 (1987).

62 Abe, K., Kato, K., Arai, T., Rahim, M. & Sultana, I. Synthetic studies on apoptolidin: synthesis of the C12–C28 fragment via a highly stereoselective …. *Tetrahedron Letters* 45, 8843-8853 (2004).

63 Giannessi, F., Misiti, D., Muck, S. & Scafetta, N. Totally Enantioselective Inversion of Configuration of (5)-(+)-Carnithe Derivatives. *Angewandte Chemie* 33, 2076 - 2078 (1994).

64 Akiyama, Y., Fukuhara, T. & Hara, S. Regioselective synthesis of fluorohydrines via S(N)2-type ring-opening of epoxides with TBABF-KHF2. *Synlett* 10, 1530-1532 (2003).

65 Berger, J., Howard, A. D., Gerber, L., Cullen, B. R. & Udenfriend, S. Expression of active, membrane-bound human placental alkaline phosphatase by transfected simian cells. *Proc. Natl. Acad. Sci. U.S.A.* 84, 4885-4889 (1987).

66 Ogata, S., Hayashi, Y., Takami, N. & Ikehara, Y. Chemical characterization of the membrane-anchoring domain of human placental alkaline phosphatase. *Journal of Biological Chemistry* 263, 10489-10494 (1988).

67 Berger, J., Micanovic, R., Greenspan, R. J. & Udenfriend, S. Conversion of placental alkaline phosphatase from a phosphatidylinositol-glycan-anchored protein to an integral transmembrane protein. *Proc. Natl. Acad. Sci. U.S.A.* 86, 1457-1460 (1989).
68 Englund, P. T. The structure and biosynthesis of glycosyl phosphatidylinositol protein anchors. *Annual Review Biochemistry* 62, 121-138 (1993).
69 Fields-Berry, S. C., Halliday, A. L. & Cepko, C. L. A recombinant retrovirus encoding alkaline phosphatase confirms clonal boundary assignment in lineage analysis of murine retina. *Proc. Natl. Acad. Sci. U.S.A.* 89, 693-697 (1992).
70 Gustincich, S., Feigenspan, A., Wu, D. K., Koopman, L. J. & Raviola, E. Control of dopamine release in the retina: a transgenic approach to neural networks. *Neuron* 18, 723-736 (1997).
71 Raviola, E. A molecular approach to retinal neural networks. *Functional Neurology* 17, 115-119 (2003).
72 Kollins, K. M., Powell, S. K. & Rivas, R. J. GPI-anchored human placental alkaline phosphatase has a nonpolarized distribution on the cell surface of mouse cerebellar granule neurons in vitro. *Journal of Neurobiology* 39, 119-141 (1999).
73 Mujtaba, T., Han, S. S. W., Fischer, I., Sandgren, E. P. & Rao, M. S. Stable expression of the alkaline phosphatase marker gene by neural cells in culture and after transplantation into the CNS using cells derived from a transgenic rat. *Experimental Neurology* 174, 48-57 (2002).
74 Skynner, M. J. *et al.* Transgenic mice ubiquitously expressing human placental alkaline phosphatase (PLAP): an additional reporter gene for use in tandem with beta-galactosidase (lacZ). *International Journal of Developmental Biology* 43, 85-90 (1999).
75 Georgatsos, J. G. Specificity and phosphotransferase activity of purified placental alkaline phosphatase. *Archives of Biochemistry and Biophysics* 121, 619-624 (1967).
76 Cox, W. G. & Singer, V. L. A high-resolution, fluorescence-based method for localization of endogenous alkaline phosphatase activity. *Journal of Histochemistry and Cytochemistry* 47, 1443-1456 (1999).
77 Le Du, M.-H., Stigbrand, T., Taussig, M. J., Menez, A. & Stura, E. A. Crystal structure of alkaline phosphatase from human placenta at 1.8 A resolution. Implication for a substrate specificity. *Journal of Biological Chemistry* 276, 9158-9165 (2001).
78 O'Brien, P. J. & Herschlag, D. Alkaline phosphatase revisited: hydrolysis of alkyl phosphates. *Biochemistry* 41, 3207-3225 (2002).
79 Chen, R., Knez, J. J., Merrick, W. C. & Medof, M. E. Comparative efficiencies of C-terminal signals of native glycophosphatidylinositol (GPI)-anchored proproteins in conferring GPI-anchoring. *Journal of Cellular Biochemistry* 84, 68-83 (2001).
80 Munro, S. Localization of proteins to the Golgi apparatus. *Trends in Cell Biology* 8, 11-15 (1998).
81 von Heijne, G. Recent advances in the understanding of membrane protein assembly and structure. *Quarterly Reviews of Biophysics* 32, 285-307 (2001).
82 Cubitt, A. B. *et al.* Understanding, improving and using green fluorescent proteins. *Trends in Biochemical Sciences* 20, 448-455 (1995).
83 Cormack, B. P., Valdivia, R. H. & Falkow, S. FACS-optimized mutants of the green fluorescent protein (GFP). *Gene* 173, 33-38 (1996).
84 Tsien, R. Y. Building and breeding molecules to spy on cells and tumors. *FEBS Letters* 579, 927-932 (2005).

85 Shaner, N. C. *et al.* Improved monomeric red, orange and yellow fluorescent proteins derived from Discosoma sp. red fluorescent protein. *Nature Biotechnology* 22, 1567-1572 (2004).
86 Merzlyak, E. M. *et al.* Bright monomeric red fluorescent protein with an extended fluorescence lifetime. *Nature Methods* 4, 555-557 (2007).
87 Patterson, G. H. A new harvest of fluorescent proteins. *Nature Biotechnology* 22, 1524-1525 (2004).
88 Shaner, N. C., Steinbach, P. A. & Tsien, R. Y. A guide to choosing fluorescent proteins. *Nature Methods* 2, 905-909 (2005).
89 Rizzo, M. A., Springer, G. H., Granada, B. & Piston, D. W. An improved cyan fluorescent protein variant useful for FRET. *Nature Biotechnology* 22, 445-449 (2004).
90 Zamyatnin, A. A. *et al.* Dual-colour imaging of membrane protein targeting directed by poa semilatent virus movement protein TGBp3 in plant and mammalian cells. *Journal of General Virology* 83, 651-662 (2002).
91 Bhattacharya, D., Mazumder, A., Miriam, S. A. & Shivashankar, G. V. EGFP-tagged core and linker histones diffuse via distinct mechanisms within living cells. *Biophysical Journal* 91, 2326-2336 (2006).
92 Kanda, T., Sullivan, K. F. & Wahl, G. M. Histone-GFP fusion protein enables sensitive analysis of chromosome dynamics in living mammalian cells. *Current Biology* 8, 377-385 (1998).
93 Ohki, E. C., Tilkins, M. L., Ciccarone, V. C. & Price, P. J. Improving the transfection efficiency of post-mitotic neurons. *Journal of Neuroscience Methods* 112, 95-99 (2001).
94 Dalby, B. *et al.* Advanced transfection with Lipofectamine 2000 reagent: primary neurons, siRNA, and high-throughput applications. *Methods* 33, 95-103 (2004).
95 Martínez-Salas, E. Internal ribosome entry site biology and its use in expression vectors. *Current Opinion in Biotechnology* 10, 458-464 (1999).
96 Komar, A. & Hatzoglou, M. Internal ribosome entry sites in cellular mRNAs: Mystery of their existence. *Journal of Biological Chemistry* 280, 23425-23428 (2005).
97 Blumenthal, T. Operons in eukaryotes. *Briefings in Functional Genomics & Proteomics* 3, 199-211 (2005).
98 Ritchie, H. & Wang, L. A mammalian bicistronic transcript encoding two dentin-specific proteins. *Biochemical and Biophysical Research Communications* 231, 425-428 (1997).
99 Gingras, A. C., Raught, B. & Sonenberg, N. eIF4 initiation factors: effectors of mRNA recruitment to ribosomes and regulators of translation. *Annual Review Biochemistry* 68, 913-963 (1999).
100 Chappell, S., Edelman, G. M. & Mauro, V. P. A 9-nt segment of a cellular mRNA can function as an internal ribosome entry site (IRES) and when present in linked multiple copies greatly enhances IRES activity. *Proc. Natl. Acad. Sci. U.S.A.* 97, 1536-1541 (2000).
101 Oh, S. K., Scott, M. P. & Sarnow, P. Homeotic gene Antennapedia mRNA contains 5'-noncoding sequences that confer translational initiation by internal ribosome binding. *Genes & Development* 6, 1643-1653 (1992).
102 Pestova, T. V. *et al.* Molecular mechanisms of translation initiation in eukaryotes. *Proc. Natl. Acad. Sci. U.S.A.* 98, 7029-7036 (2001).

103 Stoneley, M. & Willis, A. E. Cellular internal ribosome entry segments: structures, trans-acting factors and regulation of gene expression. *Oncogene* 23, 3200-3207 (2004).
104 Jackson, R., Howell, M. & Kaminski, A. The novel mechanism of initiation of Picornavirus RNA translation. *Trends in Biochemical Sciences* 15, 477-483 (1990).
105 Gorski, J. A. & Jones, K. R. Efficient bicistronic expression of cre in mammalian cells. *Nucleic Acids Research* 27, 2059-2061 (1999).
106 Zhu, Y., Feuer, G., Day, S. L., Wrzesinski, S. & Planelles, V. Multigene lentiviral vectors based on differential splicing and translational control. *Molecular Therapy* 4, 375-382 (2001).
107 Douin, V. *et al.* Use and comparison of different internal ribosomal entry sites (IRES) in tricistronic retroviral vectors. *BMC Biotechnology* 4, 16-28 (2004).
108 Kolupaeva, V., Pestova, T., Hellen, C. & Shatsky, I. Translation eukaryotic initiation factor 4G recognizes a specific structural element within the internal ribosome entry site of encephalomyocarditis virus RNA. *Journal of Biological Chemistry* 273, 18599-18604 (1998).
109 Craig, N. L. The mechanism of conservative site-specific recombination. *Annual Review of Genetics* 22, 77-105 (1988).
110 Branda, C. S. & Dymecki, S. M. Talking about a revolution: The impact of site-specific recombinases on genetic analyses in mice. *Developmental Cell* 6, 7-28 (2004).
111 Saini, D., Kala, M., Jain, V. & Sinha, S. Targeting the active site of the placental isozyme of alkaline phosphatase by phage-displayed scFv antibodies selected by a specific uncompetitive inhibitor. *BMC Biotechnology* 5, 33-46 (2005).
112 Guizar-Sicairos, M., Thurman, S. T. & Fienup, J. R. Efficient subpixel image registration algorithms. *Optics Letters* 33, 156-158 (2008).
113 Fienup, J. & Kowalczyk, A. Phase retrieval for a complex-valued object by using a low-resolution image. *Journal of the Optical Society of America A: Optics and Image Science* 7, 450-458 (1990).
114 Zhang, F., Kamp, F. & Hamilton, J. A. Dissociation of long and very long chain fatty acids from phospholipid bilayers. *Biochemistry* 35, 16055-16060 (1996).
115 Hoyrup, P., Davidsen, J. & Jorgensen, K. Lipid membrane partitioning of lysolipids and fatty acids: Effects of membrane phase structure and detergent chain length. *The Journal of Physical Chemistry B* 105, 2649-2657 (2001).
116 Heyse, S., Stora, T., Schmid, E., Lakey, J. H. & Vogel, H. Emerging techniques for investigating molecular interactions at lipid membranes. *Biochimica et Biophysica Acta* 1376, 319-338 (1998).
117 Vicario-Abejón, C. Long-term culture of hippocampal neurons. *Current Protocols in Neuroscience* Chapter 3, Unit 3.2 (2004).
118 Zeitelhofer, M. *et al.* High-efficiency transfection of mammalian neurons via nucleofection. *Nature Protocols* 2, 1692-1704 (2007).
119 Nishimura, M., Shirasawa, H. & Song, W.-J. A light-emitting diode light source for imaging of neural activities with voltage-sensitive dyes. *Neuroscience Research* 54, 230-234 (2006).
120 Fromherz, P. & Lambacher, A. Spectra of voltage-sensitive fluorescence of styryl-dye in neuron membrane. *Biochimica et Biophysica Acta* 1068, 149-156 (1991).
121 Loew, L. M. *et al.* A naphthyl analog of the aminostyryl pyridinium class of potentiometric membrane dyes shows consistent sensitivity in a variety of tissue, cell, and model membrane preparations. *Journal of Membrane Biology* 130, 1-10 (1992).

122 Tsau, Y. *et al.* Dye screening and signal-to-noise ratio for retrogradely transported voltage-sensitive dyes. *Journal of Neuroscience Methods* 70, 121-129 (1996).
123 Cheng, D. K., Tung, L. & Sobie, E. A. Nonuniform responses of transmembrane potential during electric field stimulation of single cardiac cells. *American Journal of Physiology* 277, 351-362 (1999).
124 Tominaga, T., Tominaga, Y., Yamada, H., Matsumoto, G. & Ichikawa, M. Quantification of optical signals with electrophysiological signals in neural activities of Di-4-ANEPPS stained rat hippocampal slices. *Journal of Neuroscience Methods* 102, 11-23 (2000).
125 Rohr, S. & Salzberg, B. M. Multiple site optical recording of transmembrane voltage (MSORTV) in patterned growth heart cell cultures: assessing electrical behavior, with microsecond resolution, on a cellular and subcellular scale. *Biophysical Journal* 67, 1301-1315 (1994).
126 Zecevic, D. & Antic, S. Fast optical measurement of membrane potential changes at multiple sites on an individual nerve cell. *Histochemical Journal* 30, 197-216 (1999).
127 Sinha, S. R. & Saggau, P. Simultaneous optical recording of membrane potential and intracellular calcium from brain slices. *Methods* 18, 204-214, 175 (1999).
128 Asamoah, O. K., Wuskell, J. P., Loew, L. M. & Bezanilla, F. A fluorometric approach to local electric field measurements in a voltage-gated ion channel. *Neuron* 37, 85-97 (2003).
129 Sakai, R., Repunte-Canonigo, V., Raj, C. D. & Knöpfel, T. Design and characterization of a DNA-encoded, voltage-sensitive fluorescent protein. *European Journal of Neuroscience* 13, 2314-2318 (2001).
130 Gross, D., Loew, L. M. & Webb, W. W. Optical imaging of cell membrane potential changes induced by applied electric fields. *Biophysical Journal* 50, 339-348 (1986).
131 Valic, B. *et al.* Effect of electric field induced transmembrane potential on spheroidal cells: theory and experiment. *European Biophysics Journal* 32, 519-528 (2003).
132 Xu, C. & Loew, L. M. The effect of asymmetric surface potentials on the intramembrane electric field measured with voltage-sensitive dyes. *Biophysical Journal* 84, 2768-2780 (2003).
133 Benediktsson, A. M., Schachtele, S. J., Green, S. H. & Dailey, M. E. Ballistic labeling and dynamic imaging of astrocytes in organotypic hippocampal slice cultures. *Journal of Neuroscience Methods* 141, 41-53 (2004).
134 Wang, H. F., Shortland, P., Park, M. J. & Grant, G. Retrograde and transganglionic transport of horseradish peroxidase-conjugated cholera toxin B subunit, wheatgerm agglutinin and isolectin B4 from Griffonia simplicifolia I in primary afferent neurons innervating the rat urinary bladder. *Neuroscience* 87, 275-288 (1998).
135 Angelucci, A., Clascá, F. & Sur, M. Anterograde axonal tracing with the subunit B of cholera toxin: a highly sensitive immunohistochemical protocol for revealing fine axonal morphology in adult and neonatal brains. *Journal of Neuroscience Methods* 65, 101-112 (1996).
136 Vercelli, A., Repici, M., Garbossa, D. & Grimaldi, A. Recent techniques for tracing pathways in the central nervous system of developing and adult mammals. *Brain Research Bulletin* 51, 11-28 (2000).
137 Ojima, H. & Takayanagi, M. Use of two anterograde axon tracers to label distinct cortical neuronal populations located in close proximity. *Journal of Neuroscience Methods* 104, 177-182 (2001).

138 Novikov, L. N. Labeling of central projections of primary afferents in adult rats: a comparison between biotinylated dextran amine, neurobiotin and Phaseolus vulgaris-leucoagglutinin. *Journal of Neuroscience Methods* 112, 145-154 (2001).
139 Yoshihara, Y. *et al.* A genetic approach to visualization of multisynaptic neural pathways using plant lectin transgene. *Neuron* 22, 33-41 (1999).
140 Yoshihara, Y. Visualizing selective neural pathways with WGA transgene: combination of neuroanatomy with gene technology. *Neuroscience Research* 44, 133-140 (2002).
141 Hanno, Y., Nakahira, M., Jishage, K.-i., Noda, T. & Yoshihara, Y. Tracking mouse visual pathways with WGA transgene. *European Journal of Neuroscience* 18, 2910-2914 (2003).
142 Butowt, R. & von Bartheld, C. S. Connecting the dots: trafficking of neurotrophins, lectins and diverse pathogens by binding to the neurotrophin receptor p75NTR. *European Journal of Neuroscience* 17, 673-680 (2003).
143 von Bartheld, C. S. Axonal transport and neuronal transcytosis of trophic factors, tracers, and pathogens. *Journal of Neurobiology* 58, 295-314 (2004).
144 DeFalco, J. *et al.* Virus-assisted mapping of neural inputs to a feeding center in the hypothalamus. *Science* 291, 2608-2613 (2001).
145 Smeraski, C. A., Sollars, P. J., Ogilvie, M. D., Enquist, L. W. & Pickard, G. E. Suprachiasmatic nucleus input to autonomic circuits identified by retrograde transsynaptic transport of pseudorabies virus from the eye. *Journal of Comparative Neurology* 471, 298-313 (2004).
146 Seiler, M. J., Sagdullaev, B. T., Woch, G., Thomas, B. B. & Aramant, R. B. Transsynaptic virus tracing from host brain to subretinal transplants. *European Journal of Neuroscience* 21, 161-172 (2005).
147 Schiavo, G., Matteoli, M. & Montecucco, C. Neurotoxins affecting neuroexocytosis. *Physiological Reviews* 80, 717-766 (2000).
148 Emsley, P. *et al.* The structures of the H(C) fragment of tetanus toxin with carbohydrate subunit complexes provide insight into ganglioside binding. *Journal of Biological Chemistry* 275, 8889-8894 (2000).
149 Schwab, M. E., Suda, K. & Thoenen, H. Selective retrograde transsynaptic transfer of a protein, tetanus toxin, subsequent to its retrograde axonal transport. *Journal of Cell Biology* 82, 798-810 (1979).
150 Manning, K. A., Erichsen, J. T. & Evinger, C. Retrograde transneuronal transport properties of fragment C of tetanus toxin. *Neuroscience* 34, 251-263 (1990).
151 Cabot, J. B. *et al.* Retrograde, trans-synaptic and transneuronal transport of fragment C of tetanus toxin by sympathetic preganglionic neurons. *Neuroscience* 40, 805-823 (1991).
152 Verastegui, C., Lalli, G., Bohnert, S. & Meunier, F. Clostridial Neurotoxins. *Journal of Toxicology* 21, 203–227 (2002).
153 Fairweather, N. F., Lyness, V. A., Pickard, D. J., Allen, G. & Thomson, R. O. Cloning, nucleotide sequencing, and expression of tetanus toxin fragment C in Escherichia coli. *Journal of Bacteriology* 165, 21-27 (1986).
154 Fairweather, N. F. & Lyness, V. A. The complete nucleotide sequence of tetanus toxin. *Nucleic Acids Research* 14, 7809-7812 (1986).
155 Krieglstein, K., Henschen, A., Weller, U. & Habermann, E. Arrangement of disulfide bridges and positions of sulfhydryl groups in tetanus toxin. *European Journal of Biochemistry* 188, 39-45 (1990).

156 Matteoli, M. *et al.* Synaptic vesicle endocytosis mediates the entry of tetanus neurotoxin into hippocampal neurons. *Proc. Natl. Acad. Sci. U.S.A.* 93, 13310-13315 (1996).
157 Rossetto, O., Seveso, M., Caccin, P., Schiavo, G. & Montecucco, C. Tetanus and botulinum neurotoxins: turning bad guys into good by research. *Toxicon* 39, 27-41 (2000).
158 Anderson, M. D. *et al.* Crystallographic characterization of tetanus toxin fragment C. *Journal of Molecular Biology* 230, 673-674 (1993).
159 Umland, T. C. *et al.* Structure of the receptor binding fragment HC of tetanus neurotoxin. *Nature Structural Biology* 4, 788-792 (1997).
160 Sinha, K. *et al.* Analysis of mutants of tetanus toxin Hc fragment: ganglioside binding, cell binding and retrograde axonal transport properties. *Molecular Microbiology* 37, 1041-1051 (2000).
161 Lalli, G., Bohnert, S., Deinhardt, K., Verastegui, C. & Schiavo, G. The journey of tetanus and botulinum neurotoxins in neurons. *Trends in Microbiology* 11, 431-437 (2003).
162 Neale, E. A. Moving across membranes. *Nature Structural Biology* 10, 2-3 (2002).
163 Montecucco, C. & Schiavo, G. Tetanus and botulism neurotoxins: a new group of zinc proteases. *Trends in Biochemical Sciences* 18, 324-327 (1993).
164 Breidenbach, M. A. & Brunger, A. T. 2.3 A crystal structure of tetanus neurotoxin light chain. *Biochemistry* 44, 7450-7457 (2005).
165 Rao, K. N., Kumaran, D., Binz, T. & Swaminathan, S. Structural analysis of the catalytic domain of tetanus neurotoxin. *Toxicon* 45, 929-939 (2005).
166 Rossetto, O. *et al.* Active-site mutagenesis of tetanus neurotoxin implicates TYR-375 and GLU-271 in metalloproteolytic activity. *Toxicon* 39, 1151-1159 (2001).
167 Figueiredo, D. M. *et al.* Delivery of recombinant tetanus-superoxide dismutase proteins to central nervous system neurons by retrograde axonal transport. *Experimental Neurology* 145, 546-554 (1997).
168 Francis, J. W. *et al.* Tetanus toxin fragment C as a vector to enhance delivery of proteins to the CNS. *Brain Research* 1011, 7-13 (2004).
169 Francis, J. W. *et al.* A survival motor neuron:tetanus toxin fragment C fusion protein for the targeted delivery of SMN protein to neurons. *Brain Research* 995, 84-96 (2003).
170 Jiang, K., Watson, D. J. & Wolfe, J. H. A genetic fusion construct between the tetanus toxin C fragment and the lysosomal acid hydrolase beta-glucuronidase expresses a bifunctional protein with enhanced secretion and neuronal uptake. *Journal of Neurochemistry* 93, 1334-1344 (2005).
171 Coen, L., Osta, R., Maury, M. & Brûlet, P. Construction of hybrid proteins that migrate retrogradely and transynaptically into the central nervous system. *Proc. Natl. Acad. Sci. U.S.A.* 94, 9400-9405 (1997).
172 Miana-Mena, F. J. *et al.* Fragment C tetanus toxin: a putative activity-dependent neuroanatomical tracer. *Acta Neurobiologiae Experimentalis* 63, 211-218 (2003).
173 Maskos, U., Kissa, K., St Cloment, C. & Brûlet, P. Retrograde trans-synaptic transfer of green fluorescent protein allows the genetic mapping of neuronal circuits in transgenic mice. *Proc. Natl. Acad. Sci. U.S.A.* 99, 10120-10125 (2002).
174 Miana-Mena, F. J. *et al.* A non-viral vector for targeting gene therapy to motoneurons in the CNS. *Neuro-Degenerative Diseases* 1, 101-108 (2006).
175 Sano, H., Nagai, Y. & Yokoi, M. Inducible expression of retrograde transynaptic genetic tracer in mice. *Genesis* 45, 123-128 (2007).

176 Bade, S. *et al.* Botulinum neurotoxin type D enables cytosolic delivery of enzymatically active cargo proteins to neurones via unfolded translocation intermediates. *Journal of Neurochemistry* 91, 1461-1472 (2004).
177 Nagy, A. Cre recombinase: the universal reagent for genome tailoring. *Genesis* 26, 99-109 (2000).
178 Lee, G. & Saito, I. Role of nucleotide sequences of loxP spacer region in Cre-mediated recombination. *Gene* 216, 55-65 (1998).
179 Brocard, J., Feil, R., Chambon, P. & Metzger, D. A chimeric Cre recombinase inducible by synthetic,but not by natural ligands of the glucocorticoid receptor. *Nucleic Acids Research* 26, 4086-4090 (1998).
180 Lakso, M. *et al.* Targeted oncogene activation by site-specific recombination in transgenic mice. *Proc. Natl. Acad. Sci. U.S.A.* 89, 6232-6236 (1992).
181 Soriano, P. Generalized lacZ expression with the ROSA26 Cre reporter strain. *Nature Genetics* 21, 70-71 (1999).
182 Lobe, C. G. *et al.* Z/AP, a double reporter for cre-mediated recombination. *Developmental Biology* 208, 281-292 (1999).
183 Srinivas, S. *et al.* Cre reporter strains produced by targeted insertion of EYFP and ECFP into the ROSA26 locus. *BMC Developmental Biology* 1, 4-12 (2001).
184 Huang, Z. J., Yu, W., Lovett, C. & Tonegawa, S. Cre/loxP recombination-activated neuronal markers in mouse neocortex and hippocampus. *Genesis* 32, 209-217 (2002).
185 Guo, F., Gopaul, D. N. & van Duyne, G. D. Structure of Cre recombinase complexed with DNA in a site-specific recombination synapse. *Nature* 389, 40-46 (1997).
186 Le, Y., Miller, J. L. & Sauer, B. GFPcre fusion vectors with enhanced expression. *Analytical Biochemistry* 270, 334-336 (1999).
187 Gagneten, S., Le, Y., Miller, J. & Sauer, B. Brief expression of a GFP cre fusion gene in embryonic stem cells allows rapid retrieval of site-specific genomic deletions. *Nucleic Acids Research* 25, 3326-3331 (1997).
188 Jullien, N., Sampieri, F., Enjalbert, A. & Herman, J.-P. Regulation of Cre recombinase by ligand-induced complementation of inactive fragments. *Nucleic Acids Research* 31, 131-140 (2003).
189 Briones, G., Hofreuter, D. & Galán, J. E. Cre reporter system to monitor the translocation of type III secreted proteins into host cells. *Infection and Immunity* 74, 1084-1090 (2006).
190 Irwin, B., Heck, J. D. & Hatfield, G. W. Codon pair utilization biases influence translational elongation step times. *Journal of Biological Chemistry* 270, 22801-22806 (1995).
191 Nagata, T., Uchijima, M., Yoshida, A., Kawashima, M. & Koide, Y. Codon optimization effect on translational efficiency of DNA vaccine in mammalian cells: analysis of plasmid DNA encoding a CTL epitope derived from microorganisms. *Biochemical and Biophysical Research Communications* 261, 445-451 (1999).
192 Nakamura, Y., Gojobori, T. & Ikemura, T. Codon usage tabulated from international DNA sequence databases: status for the year 2000. *Nucleic Acids Research* 28, 292 (1999).
193 Gustafsson, C., Govindarajan, S. & Minshull, J. Codon bias and heterologous protein expression. *Trends in Biotechnology* 22, 346-353 (2004).
194 Friberg, M., von Rohr, P. & Gonnet, G. Limitations of codon adaptation index and other coding DNA-based features for prediction of protein expression in Saccharomyces cerevisiae. *Yeast* 21, 1083-1093 (2004).

195 Moura, G. *et al.* Comparative context analysis of codon pairs on an ORFeome scale. *Genome Biology* 6, R28 (2005).
196 Kim, C. H., Oh, Y. & Lee, T. H. Codon optimization for high-level expression of human erythropoietin (EPO) in mammalian cells. *Gene* 199, 293-301 (1997).
197 Hale, R. S. & Thompson, G. Codon optimization of the gene encoding a domain from human type 1 neurofibromin protein results in a threefold improvement in expression level in Escherichia coli. *Protein Expression and Purification* 12, 185-188 (1998).
198 Vervoort, E. B. *et al.* Optimizing heterologous expression in dictyostelium: importance of 5' codon adaptation. *Nucleic Acids Research* 28, 2069-2074 (2000).
199 Slimko, E. M. & Lester, H. A. Codon optimization of Caenorhabditis elegans GluCl ion channel genes for mammalian cells dramatically improves expression levels. *Journal of Neuroscience Methods* 124, 75-81 (2003).
200 Shimshek, D. R. *et al.* Codon-improved Cre recombinase (iCre) expression in the mouse. *Genesis* 32, 19-26 (2002).
201 Makoff, A. J., Oxer, M. D., Romanos, M. A., Fairweather, N. F. & Ballantine, S. Expression of tetanus toxin fragment C in E. coli: high level expression by removing rare codons. *Nucleic Acids Research* 17, 10191-10202 (1989).
202 Stratford, R. *et al.* Influence of codon usage on the immunogenicity of a DNA vaccine against tetanus. *Vaccine* 19, 810-815 (2000).
203 Lavner, Y. & Kotlar, D. Codon bias as a factor in regulating expression via translation rate in the human genome. *Gene* 345, 127-138 (2005).
204 Vinogradov, A. E. Genome size and GC-percent in vertebrates as determined by flow cytometry: the triangular relationship. *Cytometry* 31, 100-109 (1998).
205 Li, Y. *et al.* Recombinant forms of tetanus toxin engineered for examining and exploiting neuronal trafficking pathways. *Journal of Biological Chemistry* 276, 31394-31401 (2001).
206 Eisel, U. *et al.* Tetanus toxin: primary structure, expression in E. coli, and homology with botulinum toxins. *EMBO Journal* 5, 2495-2502 (1986).
207 Makrides, S. C. Strategies for achieving high-level expression of genes in Escherichia coli. *Microbiological Reviews* 60, 512-538 (1996).
208 Trinh, R., Gurbaxani, B., Morrison, S. L. & Seyfzadeh, M. Optimization of codon pair use within the (GGGGS)3 linker sequence results in enhanced protein expression. *Molecular Immunology* 40, 717-722 (2003).
209 Yang, Y. S. & Hughes, T. E. Cre stoplight: a red/green fluorescent reporter of Cre recombinase expression in living cells. *BioTechniques* 31, 1036-1041 (2001).
210 Klasen, M. & Wabl, M. Silent point mutation in DsRed resulting in enhanced relative fluorescence intensity. *BioTechniques* 36, 236-238 (2004).
211 Sacchetti, A., Subramaniam, V., Jovin, T. M. & Alberti, S. Oligomerization of DsRed is required for the generation of a functional red fluorescent chromophore. *FEBS Letters* 525, 13-19 (2002).
212 Gogolla, N., Galimberti, I., DePaola, V. & Caroni, P. Preparation of organotypic hippocampal slice cultures for long-term live imaging. *Nature Protocols* 1, 1165-1171 (2006).
213 Gogolla, N., Galimberti, I., DePaola, V. & Caroni, P. Long-term live imaging of neuronal circuits in organotypic hippocampal slice cultures. *Nature Protocols* 1, 1223-1226 (2006).
214 Watanabe, S. Y. *et al.* Calcium phosphate-mediated transfection of primary cultured brain neurons using GFP expression as a marker: application for single neuron electrophysiology. *Neuroscience Research* 33, 71-78 (1999).

215 Murphy, R. C. & Messer, A. Gene transfer methods for CNS organotypic cultures: a comparison of three nonviral methods. *Molecular Therapy* 3, 113-121 (2001).
216 Teschemacher, A. G. *et al.* Targeting specific neuronal populations using adeno- and lentiviral vectors: applications for imaging and studies of cell function. *Experimental Physiology* 90, 61-69 (2004).
217 Dittgen, T. *et al.* Lentivirus-based genetic manipulations of cortical neurons and their optical and electrophysiological monitoring in vivo. *Proc. Natl. Acad. Sci. U.S.A.* 101, 18206-18211 (2004).
218 Kremer, E. Gene transfer to the central nervous system: Current state of the art of the viral vectors. *Current Genomics* 6, 13-37 (2005).
219 Wirth, M. J. & Wahle, P. Biolistic transfection of organotypic cultures of rat visual cortex using a handheld device. *Journal of Neuroscience Methods* 125, 45-54 (2003).
220 Zhang, G. & Selzer, M. E. In vivo transfection of lamprey brain neurons by gene gun delivery of DNA. *Experimental Neurology* 167, 304-311 (2001).
221 Rathenberg, J., Nevian, T. & Witzemann, V. High-efficiency transfection of individual neurons using modified electrophysiology techniques. *Journal of Neuroscience Methods* 126, 91-98 (2003).
222 Wong, L.-F. *et al.* Lentivirus-mediated gene transfer to the central nervous system: therapeutic and research applications. *Human Gene Therapy* 17, 1-9 (2006).
223 Ramezani, A. & Hawley, R. G. Overview of the HIV-1 Lentiviral Vector System. *Current Protocols in Neuroscience* Chapter 16, Unit 16.21 (2002).
224 Ridoux, V., Robert, J., Perricaudet, M., Mallet, J. & Le Gal La Salle, G. Adenovirus mediated gene transfer in organotypic brain slices. *Neurobiology of Disease* 2, 49-54 (1995).
225 Lever, A. M. L., Strappe, P. M. & Zhao, J. Lentiviral vectors. *Journal of Biomedical Science* 11, 439-449 (2004).
226 Miyoshi, H., Blömer, U., Takahashi, M., Gage, F. H. & Verma, I. M. Development of a self-inactivating lentivirus vector. *Journal of Virology* 72, 8150-8157 (1998).
227 Logan, A. C., Lutzko, C. & Kohn, D. B. Advances in lentiviral vector design for gene-modification of hematopoietic stem cells. *Current Opinion in Biotechnology* 13, 429-436 (2002).
228 Dull, T. *et al.* A third-generation lentivirus vector with a conditional packaging system. *Journal of Virology* 72, 8463-8471 (1998).
229 Trono, D. Lentiviral vectors: turning a deadly foe into a therapeutic agent. *Gene Therapy* 7, 20-23 (2000).
230 Mitta, B. *et al.* Advanced modular self-inactivating lentiviral expression vectors for multigene interventions in mammalian cells and in vivo transduction. *Nucleic Acids Research* 30, 113-131 (2002).
231 Anson, D. S. & Fuller, M. Rational development of a HIV-1 gene therapy vector. *The Journal of Gene Medicine* 5, 829-838 (2003).
232 Delenda, C. Lentiviral vectors: optimization of packaging, transduction and gene expression. *The Journal of Gene Medicine* 6, 125-138 (2004).
233 Yang, L., Bailey, L., Baltimore, D. & Wang, P. Targeting lentiviral vectors to specific cell types in vivo. *Proc. Natl. Acad. Sci. U.S.A.* 103, 11479-11484 (2006).
234 Liu, B. H., Wang, X., Ma, Y. X. & Wang, S. CMV enhancer/human PDGF-beta promoter for neuron-specific transgene expression. *Gene Therapy* 11, 52-60 (2003).
235 Wang, C. Y. *et al.* Improved neuronal transgene expression from an AAV-2 vector with a hybrid CMV enhancer/PDGF-beta promoter. *The Journal of Gene Medicine* 7, 945-955 (2005).

236 Sasaki *et al.* Multi-gene gateway clone design for expression of multiple heterologous genes in living cells: Eukaryotic clones containing two and three ORF multi-gene cassettes expressed from a single promoter. *Journal of Biotechnology* 136, 103-112 (2005).
237 Kumar, M., Keller, B., Makalou, N. & Sutton, R. E. Systematic determination of the packaging limit of lentiviral vectors. *Human Gene Therapy* 12, 1893-1905 (2001).
238 al Yacoub, N., Romanowska, M., Haritonova, N. & Foerster, J. Optimized production and concentration of lentiviral vectors containing large inserts. *The Journal of Gene Medicine* 9, 579-584 (2007).
239 Arai, R., Ueda, H., Kitayama, A., Kamiya, N. & Nagamune, T. Design of the linkers which effectively separate domains of a bifunctional fusion protein. *Protein Engineering* 14, 529-532 (2001).
240 Arai, R., Wriggers, W., Nishikawa, Y., Nagamune, T. & Fujisawa, T. Conformations of variably linked chimeric proteins evaluated by synchrotron X-ray small-angle scattering. *Proteins* 57, 829-838 (2004).
241 Bai, Y. & Shen, W.-C. Improving the oral efficacy of recombinant granulocyte colony-stimulating factor and transferrin fusion protein by spacer optimization. *Pharmaceutical Research* 23, 2116-2121 (2006).
242 Tiscornia, G., Singer, O. & Verma, I. Production and purification of lentiviral vectors. *Nature Protocols* 1, 241-245 (2006).
243 Kutner, R. H., Zhang, X. Y. & Reiser, J. Production, concentration and titration of pseudotyped HIV-1-based lentiviral vectors. *Nature Protocols* 4, 495-505 (2009).
244 Deinhardt, K., Berninghausen, O., Willison, H. J., Hopkins, C. R. & Schiavo, G. Tetanus toxin is internalized by a sequential clathrin-dependent mechanism initiated within lipid microdomains and independent of epsin1. *Journal of Cell Biology* 174, 459-471 (2006).
245 Perreault, M.-C., Bernier, A. P., Renaud, J.-S., Roux, S. & Glover, J. C. C fragment of tetanus toxin hybrid proteins evaluated for muscle-specific transsynaptic mapping of spinal motor circuitry in the newborn mouse. *Neuroscience* 141, 803-816 (2006).
246 Lichty, J. J., Malecki, J. L., Agnew, H. D., Michelson-Horowitz, D. J. & Tan, S. Comparison of affinity tags for protein purification. *Protein Expression and Purification* 41, 98-105 (2005).
247 Cao, H. *et al.* A red cy3-based biarsenical fluorescent probe targeted to a complementary binding Peptide. *Journal of the American Chemical Society* 129, 8672-8673 (2007).
248 Martin, B. R., Giepmans, B. N. G., Adams, S. R. & Tsien, R. Y. Mammalian cell-based optimization of the biarsenical-binding tetracysteine motif for improved fluorescence and affinity. *Nature Biotechnology* 23, 1308-1314 (2005).
249 Mota, L. J. & Holden, D. W. FlAsHlights on bacterial virulence proteins. *Nature Methods* 2, 898-899 (2005).
250 Dietz, G. P. H. & Bähr, M. Delivery of bioactive molecules into the cell: the Trojan horse approach. *Molecular and Cellular Neuroscience* 27, 85-131 (2004).

ACKNOWLEDGMENTS

I would firstly like to thank Prof. Dr. Peter Fromherz for bringing me into his group, and for his support and advise throughout the past few years.

With out the help of the team of people around me, the successes of this project would never have been achieved.

Dr. Alexander Kaul for his advice and critical reading of this manuscript.

Alexander Kunze for design and construction of the stimulation apparatus.

Dr. Armin Lambacher for his help in all things scientific and excellent advice in microscopy, fluorescence and photography.

Doris Eckerlein for her help in cell culture and neuron preparation.

Elisabeth Weyher-Stingl for her advice and help in mass spectroscopy.

Dr. Gerd Hübener for his help in the planning of the synthesis of the prodyes.

Dr. Ingmar Peitz for his advice and zerg rushes.

Dr. Marlon Hinner for his warm help in bringing me though the bureaucracy and starting me off in this project.

Max Eickenscheidt for his input on the application of electrical fields and Go.

Michaela Morawetz for her help in all matters in the molecular biology lab.

Robert Pabst for the fine construction of the laboratory apparatus.

Sonja Golla for her help in the synthesis of the fluorinated dyes and for her care of Pepper.

Stephanie Stumhofer for her excellent work in the chemical synthesis of the prodyes.

And of course for the love and support of my wife, Alexandra Witzke-Ng, who has always been at my side and given me the motivation to succeed throughout this long but rewarding endeavor.

Finally, thanks to my loving parents, Eddie and Jan, who instilled in me a passion for understanding and discovery as a child; together, these are the true spirit of science.